The role of MAP4K4 in cardiac muscle cell death

Micaela M. Jenkins

CID: 00855768

National Heart and Lung Institute

Faculty of Medicine

Imperial College London

A Thesis submitted to

Imperial College London for Doctor of Philosophy

Imperial College London

National Heart and Lung Institute

Word count: 65,028

Acknowledgements

I express my sincerest thanks to Professor Michael Schneider and Professor Sian Harding for enabling the opportunity to work on this exciting project as well as for all their help, support and advice during course of my studies. I am also very grateful to the British Heart Foundation for awarding me the studentship to undertake this research.

I would like to acknowledge the extensive work carried out by the MAP4K4 team past and present, which provided the foundations for this study. I am especially grateful to Lorna Fiedler for all her scientific and moral support all the way through from my MRes days to this day. Lorna's insight into the project has been absolutely invaluable to me as has her guidance and support.

I am extremely grateful to Dr Michela Noseda for imparting to me the research and technical skills necessary to complete the work hereby presented as well as for the daily support and guidance on every respect. I am indebted to Tom Owen, Eleanor Humphrey and Carolina Pinto Ricardo not only for their generous technical and academic assistance but also for accompanying me in the happy as well as hard moments during these three years.

I would also like to thank all the members of the Schneider and Harding laboratories for their support and advice and for generally making my days at work so enjoyable. I would also like to acknowledge the Carling group for having provided me with training on the Seahorse platform and kindly allowed me to use their equipment on a regular basis.

Special thanks to my family, friends and particularly Quin. It was your encouragement and support that took me through these years and always made me see the light at the end of the tunnel.

Finally, I would like to dedicate this thesis to my mother and grandfather, my everlasting sources of inspiration and strength.

Declaration of Originality

I declare that the work hereby presented was conducted by the author, except where indicated by special reference in the text, and that no part of the dissertation has been submitted for any other degree.

Some of the results contained in this thesis have been presented at conferences and seminars.

Micaela M. Jenkins

Copyright Declaration

‘The copyright of this thesis rests with the author and is made available under a Creative Commons Attribution Non-Commercial No Derivatives licence. Researchers are free to copy, distribute or transmit the thesis on the condition that they attribute it, that they do not use it for commercial purposes and that they do not alter, transform or build upon it. For any reuse or redistribution, researchers must make clear to others the licence terms of this work’

Table of contents

Acknowledgements 3
Declaration of Originality 4
Copyright Declaration 5
Table of contents 6
List of Figures 10
List of Tables 14
List of abbreviations 15
Abstract 19
1. Introduction 20
1.1 Heart failure as a socio-economic problem 21
1.2 Pathobiology of heart failure 24
1.3 Cell death signalling pathways 28
1.3.1 Apoptosis 29
1.3.2 Necrosis 33
1.3.3 Autophagy 38
1.4 Cell death in myocardial infarction and heart failure 39
1.4.1 Apoptosis in myocardial infarction and heart failure 41
1.4.2 Necrosis in myocardial infarction and heart failure 44
1.4.3 Autophagy in myocardial infarction and heart failure 45
1.5 Metabolism 49
1.6 Metabolism in myocardial infarction and heart failure 51
1.7 The protein kinase complement of the human genome 55
1.7.1 Classification and mode of action 55
1.7.2 Structure 58
1.7.3 Mitogen-activated protein kinases (MAPKs) 59
1.8 MAPKs in heart failure 63
1.8.1 MAP kinases in heart failure 63
1.8.2 MAP3 kinases in heart failure 67
1.8.3 MAP4K kinases in heart failure 70
1.9 Induced pluripotent stem cells (iPSCs) as a tool for drug discovery 75
1.9.1 Characterisation of iPSC-derived cardiomyocytes 77
1.9.2 Engineered heart tissue (EHT) as a platform for drug evaluation 78
2. The aim 81
2. Methods 84

2.1 hiPSC-CM culture 85
2.2 MAP4K4 pharmacological inhibition 86
2.3 Cell death induction 89
2.4 Cell death assays 89
2.5 Immunocytostaining (2D) 90
2.6 Mitochondrial respiration analysis 92
2.7 Protein quantification 93
2.8 hiPSC-CMs thawing for human engineered heart tissue (hEHTs) generation 93
2.9 EHT generation 94
2.10 EHT solutions 94
2.11 Force calculation in EHTs and contractile assessment 96
2.12 Immunocytochemistry 98
2.13 Calcium dynamics assessment 99
2.14 Statistical Analysis 100
3. Results 101
Effects of MAP4K4 inhibition on cell death in 2-dimensional human iPSC-CM culture. 102
3.1 Optimisation of conditions for human cardiac muscle cell death induced by H_2O_2 104
3.2 Effect of the MAP4K4 inhibitor IC4-001 on plasma membrane disruption induced by H_2O_2 106
3.3 Effect of the MAP4K4inhibitor IC4-001 on caspase-3 activation induced by H_2O_2 108
3.4 Effect of the MAP4K4 inhibitor IC4-001 on BID cleavage induced by H_2O_2 111
3.5 Effect of H_2O_2 and IC4-001 on downstream MAPK activation 113
3.6 Synopsis of main findings 116
3.7 Discussion 117
4. Results 123
Assessment of the effects of MAP4K4 inhibitors on cardiac mitochondrial function 124
4.1 The effects of H_2O_2 on mitochondrial function in iCell cardiomyocytes. 127
4.2 Effect of the MAP4K4 inhibitor IC4-001 on mitochondrial function in iCell cardiomyocytes. 129
4.3 The effects of menadione on mitochondrial function in iCell cardiomyocytes. 136
4.4 Effect of MAP4K4 inhibitor GNE-495 on mitochondrial function in iCell cardiomyocytes. 138
4.5 Effect of MAP4K4 inhibitor DMX-5804 on mitochondrial function in iCell cardiomyocytes. 142
4.6 Optimisation of seeding density, oligomycin and FCCP concentration for assessment of mitochondrial respiration in CorV.4U cardiomyocytes. 145
4.7 Effect of MAP4K4 inhibitor DMX-5804 on mitochondrial function in CorV.4U cardiomyocytes. 148

4. 8 Synopsis of main findings 153
4.9 Discussion 154
5. Results 159
The effects of MAP4K4 inhibitor DMX-5804 on calcium handling 160
5.1 Effects of the MAP4K4 inhibitor DMX-5804 on menadione-induced calcium handling impairment in CorV.4U hiPSC-CMs 161
5.2 Effects of MAP4K4 inhibitor DMX-5804 on menadione-induced cleaved caspase-3 induction, membrane integrity and mitochondrial membrane potential in CorV.4U cardiomyocytes 164
5.3 Summary 167
Discussion 168
6. Results 171
3-dimensional human engineered heart tissue as a testbed for assessing effects of MAP4K4 inhibitors on cardiac cell death and contractility 172
6.1 Effect of MAP4K4 inhibitor IC4-001 on force of contraction and beating rate in iCell-derived hEHT. 173
6.2 Effect of pharmacological inhibition of MAP4K4 by IC4-001 on long term contractile function in hEHT including systolic and diastolic function 176
6.3 Generation of hEHT using CorV.4U CMs 179
6.4 Effect of MAP4K4 inhibitor GNE-495 on force and beating rate in CorV4U-derived hEHT treated with doxorubicin 181
6.5 Cytotoxic and contractile screening of DMX-5804 in iCell-derived hEHT 185
6.6 Optimisation of hEHT without fibroblast co-culture and the use menadione as the death signal for the cytotoxic and contractile assessment of DMX-5804 in CorV4U-derived hEHT 188
6.7 Synopsis of main findings 195
6.8 Discussion 196
7. Discussion 203
7.1 The role of MAP4K4 in human cardiomyocyte cell death 206
7.2 The role of MAP4K4 in function in 2D culture 212
7.3 Human engineered heart tissue as a platform for dissecting the role of MAP4K4 in the heart 215
7.4 Technical limitations 218
7.5 Future directions 222
7. 6 Concluding remarks 224
8. References 226
9. Supplement 302
Knockdown strategies as a tool to explore the role of MAP4K4 in cell death and contractility in hEHT 303
9.1 Optimisation of Lentiviral trandsduction in 293 FT HEKS 304

9.2 Optimisation of Lentiviral transduction in hiPSC-CMs 305
9.3 Optimisation of Lentiviral transduction in hEHT 307
9.4 MAP4K4 knockdown followed by menadione treatment – cell death and contractile response 310
9.5 MAP4K4 knockdown followed by DMX-5804 and menadione treatment – cell death and contractile response 314
9.6 Synopsis of main findings 319
9.7 Discussion 320
9.8 Methods 323
9.8.1 HEK293T culture 323
9.8.2 Lentiviral vector production, transduction and titration 323
9.8. 2.1 Bacterial Culture and DNA purification 324
9.8.2.2 Lentiviral vector production and concentration 326
9.8.2.3 Lentiviral vector titration 326
9.8.2.4 Viral transduction of hEHTs 327
9.8.3 RNA Extraction (EHTs) 328
9.8.4 Gene expression analysis 328

List of Figures

Figure 1.1 Cardiovascular disease statistics

Figure 1.2 Heart failure continues to increase.

Figure 1.3 Potential approaches to increase cardiomyocyte number as a therapy.

Figure 1.4 Image depicting the intrinsic and extrinsic signalling pathways in apoptosis.

Figure 1.5 Image depicting the molecular pathways leading to necrosis after cardiac I/R injury.

Figure 1.6 Schematic representation of impaired mitochondrial capacity and function in heart failure.

Figure 1.7 Abnormal mitochondrial energy production along the inner membrane.

Figure 1.8 Dendogram showing the protein kinase families as per protein sequence homology.

Figure 1.9 Scheme showing signal transduction pathways activated by various kinases.

Figure 2.1 Schematic illustration of the EHT generation process and contractile assessment.

Figure 3.1 Induction of cell death by H_2O_2 measured after 4-24 hr treatment at indicated concentrations.

Figure 3.2 Loss of plasma membrane integrity in the presence of MAP4K4 inhibitor in response to H_2O_2 in hiPSC-CMs.

Figure 3.3 Cleaved caspase-3 in the presence of MAP4K4 inhibitor in response to H_2O_2 in hiPSC-CMs.

Figure 3.4 BID cleavage in the presence of MAP4K4 inhibitor in response to H_2O_2 in hiPSC-CMs.

Figure 3.5 Assessment of p-38 phosphorylation in the presence of MAP4K4 inhibitor in response to H_2O_2 in hiPSC-CMs.

Figure 3.6 Assessment of ERK phosphorylation in the presence of MAP4K4 inhibitor in response to H_2O_2 in hiPSC-CMs.

Figure 4.1 Mitochondrial respiration in iCell hiPSC-CMs after 12 days in culture as measured by oxygen consumption rate (OCR).

Figure 4.2 The effect of H_2O_2 on mitochondrial respiration in iCell hiPSC-CMs.

Figure 4.3 The effect of 10μM MAP4K4 inhibitor IC4-001 following H_2O_2 treatment on mitochondrial respiration in hiPSC-CMs.

Figure 4.4 Individual components of mitochondrial respiration on MAP4K4 inhibitor IC4-001 following 25 μM H_2O_2 treatment in iCell hiPSC-CMs.

Figure 4.5 Individual components of mitochondrial respiration on MAP4K4 inhibitor IC4-001 following 12.5 μM H_2O_2 treatment in iCell hiPSC-CMs.

Figure 4.6 The effect of MAP4K4 inhibitor IC4-001 following H_2O_2–induced mitochondrial dysfunction on glycolysis and total protein in iCell hiPSC-CMs.

Figure 4.7 The effect of menadione on mitochondrial respiration in iCell hiPSC-CMs.

Figure 4.8 The effect of 10μM MAP4K4 inhibitor GNE-495 following menadione treatment on mitochondrial respiration in iCell hiPSC-CMs.

Figure 4.9 Individual components of mitochondrial respiration in response to MAP4K4 inhibitor GNE-495 following menadione treatment.

Figure 4.10 The effect of MAP4K4 inhibitor GNE-495 on menadione-induced mitochondrial dysfunction as measured by ECAR.

Figure 4.11 The effect of 10μM MAP4K4 inhibitor DMX-5804 following menadione treatment on mitochondrial respiration in iCell hiPSC-CMs.

Figure 4.12 Individual components of mitochondrial respiration in response to MAP4K4 inhibitor DMX-5804 (5804) following menadione treatment in iCell hiPSC-CMs.

Figure 4.13 Assessment of plasma membrane integrity in DMX-5804-treated iCell hiPSC-CMs in response to menadione.

Figure 4.14 Cell seeding number optimisation for CorV.4U hiPSC-CMs.

Figure 4.15 Oligomycin and FCCP concentration optimisation in CorV.4U hiPSC-CMs.

Figure 4.16 The effect of 10μM MAP4K4 inhibitor DMX-5804 following menadione treatment on mitochondrial respiration in CorV.4U hiPSC-CMs.

Figure 4.17 Individual components of mitochondrial respiration in response to MAP4K4 inhibitor DMX-5804 (5804) following menadione treatment in CorV.4U hiPSC-CMs.

Figure 4.18 The effect of MAP4K4 inhibitor DMX-5804 on menadione-induced mitochondrial dysfunction as measured by ECAR in CorV.4U hiPSC-CMs.

Figure 4.19 Assessment of plasma membrane integrity in DMX-5804-treated CorV.4U hiPSC-CMs in response to menadione.

Figure 5.1 The effect of DMX-5804 on calcium handling for menadione-treated CorV.4U hiPSC-CMs.

Figure 5.2 The effect of MAP4K4 inhibitor DMX-5804 on calcium dynamics in menadione-treated CorV.4U hiPSC-CMs.

Figure 5.3 Cell death in MAP4K4 pharmacologically inhibited CorV.4U hiPSC-CMs in response to menadione in 2D.

Figure 6.1 The effect of MAP4K4 inhibitor IC4-001 on contraction measurements in hEHT.

Figure 6.2 Long term effect on contraction measurements after pharmacological inhibition of MAP4K4 in hEHT.

Figure 6.3 Systolic and diastolic assessment after pharmacological inhibition of MAP4K4 in hEHT.

Figure 6.4 Contractile profile of human EHT generated from CorV.4U and iCell hiPSC-CMs measured by force and BPM over 14 days.

Figure 6.5 Induction of cell death by doxorubicin in CorV.4U-derived EHTs.

Figure 6.6 Plasma membrane integrity and contractility assessment of MAP4K4 inhibitor GNE-495-treated CorV.4U-derived hEHT subjected to doxorubicin.

Figure 6.7 Plasma membrane integrity and contractility assessment of MAP4K4 inhibitor DMX-5804-treated iCell-derived hEHT subjected to doxorubicin.

Figure 6.8 Cleaved caspase-3 levels after DMX-5804 treatment subjected to doxorubicin in iCell hEHT.

Figure 6.9 Contractile profile of CorV.4U-derived hEHT generated in the presence or absence of fibroblasts

Figure 6.10 Induction of cell death by menadione in CorV.4U EHTs as measured by loss of plasma membrane integrity.

Figure 6.11 The contractile effect of menadione in CorV.4U-derived hEHT.

Figure 6.12 Plasma membrane integrity assessment of MAP4K4 inhibitor DMX-5804-treated CorV.4U-derived hEHT subjected to menadione.

Figure 6.13 Contractility assessment of MAP4K4 inhibitor DMX-5804-treated CorV.4U-derived hEHT subjected to menadione.

Figure 9.5 Plasma membrane integrity assessment of MAP4K4 shRNA-treated CorV.4U-derived hEHT subjected to menadione.

Figure 9.6 Contractility assessment of MAP4K4 shRNA-treated CorV.4U-derived hEHT subjected to menadione.

Figure 9.7 Assessment of systolic and diastolic function in MAP4K4 shRNA-treated CorV.4U-derived hEHT subjected to menadione.

Figure 9.8 Plasma membrane integrity assessment of MAP4K4 shRNA-treated CorV.4U-derived hEHT subjected to 10μM menadione in conjunction with 10μM DMX-5804.

Figure 9.9 Preliminary assessment of force in MAP4K4 shRNA-treated CorV.4U-derived hEHT subjected to 10μM menadione in conjunction with 10μM DMX-5804.

Figure 9.10 Preliminary assessment of BPM in MAP4K4 shRNA-treated CorV.4U-derived hEHT subjected to 10μM menadione in conjunction with 10μM DMX-5804.

Figure 9.12 Schematic representation of the pZIP lentiviral shRNA vector, its features and elements.

List of Tables

Table 2.1 Comparison of IC4-001 and DMX-5804 compound potency (IC_{50}) against human MAP4K4, other MAP4Ks, and selected other protein kinases.

Table 2.2 In vitro IC_{50} values for GNE-495.

Table 2.3. Pharmacokinetic (PK) properties of in-house MAP4K4 inhibitors.

Table 2.4. Pharmacokinetic properties of GNE-495 in three preclinical species: mouse, rat, and dog.

Table 2.5 Antibodies.

Table 2.6 Seahorse assay reagents and instrumentation.

Table 2.7 EHT reagents and instrumentation.

Table 2.8 Antibodies used for EHT immunocytochemistry.

Table 9.1 pZIP shRNA sequences.

Table 9.2 qRT-PCR primers.

List of abbreviations

α-MHC, alpha myosin heavy chain
ACE, angiotensin-converting enzyme
AIF, Apoptosis Inducing Factor
AK, Adenylate Kinase
AKDR, AK Detection Reagent
AMPK, AMP-activated protein kinase
ARC, Apoptosis Repressor protein with a CARD domain
ASK1, apoptosis signal-regulating kinase 1
Atg, Autophagy related
ATP, adenosine triphosphate
β-AR, β-adrenergic receptors
Bid, BH3-interacting Domain Death
β-MHC, beta myosin heavy chain
BMP, bone morphogenic proteins
BPM, beats per minute
c-FLIP, FLICE-(FADD-Like IL-1β-converting enzyme)
c-raf, v-raf-1 murine leukemia viral oncogene homolog
CaMKII, Ca2+/calmodulin-dependent protein kinase II
Caspases, cysteine-dependent aspartate-specific proteases
CSQ, calsequestrin
CHD, coronary heart disease
CHD, C-terminal citron homology domain
CK1, casein kinase 1
CMV, cytomegalovirus
Cn, calcineurin
CsA, cyclosporine A
CVD, cardiovascular disease
CYLD, cylindromatosis D
CypD, Cyclophilin D
Cyt-c, Cytochrome c
DAMPs, Danger-associated Molecular Patterns
DCM, dilated cardiomyopathy

DDs, Death Domains

DISC, Death Inducing Signalling Complex

Dox, doxorubicin

EB, Embryonic Body

ECAR, Extracellular Acidification Rate

EGF, epidermal growth factor

EndoG, Endonuclease G

EHT, engineered heart tissue

ER, Endoplasmic Reticulum

ERK1/2 (or MAPK3), Extracellular Signal-Related Kinase 1

ERK5 (or MAPK7), Extracellular Signal-Regulated Kinase 5

ESC, Embryonic Stem Cells

FADD, Fas (TNFRSF6)-associated via Death Domain

FasL (or CD95), Fas Ligand

FGF-2, fibroblast growth factor-2

GATA4, GATA binding protein 4

GCK, Germinal centre kinase

GPCRs, G-protein-coupled receptors

HCM, hypertrophic cardiomyopathy

hEHT, human engineered heart tissue

hESCs, human embryonic stem cells

HF, heart failure

HGK, hepatocyte progenitor kinase-like/germinal centre kinase-like kinase

H_2O_2, Hydrogen Peroxide

I/R, ischaemia/reperfusion

IAP, Inhibitor of Apoptosis

IKK, IκB kinase

IL-1β, interleukin-1β

hiPSC-CMs, human induced pluripotent stem cell-derived cardiomyocytes

iPSCs, induced-pluripotent stem cells

JNK, Jun N-terminal kinase

KO, knockout

LDH, lactase dehydrogenase

LTCC, L-type Ca2+ channel

LV, left ventricle or ventricular

MAP2K, mitogen-activated protein kinase kinase

MAP3K, mitogen-activated protein kinase kinase kinase

MAP4K, mitogen-activated protein kinase kinase kinase kinase

MAP4K4, HGK/GCK-like kinase, Nck-interacting kinase

MAPK, mitogen-activated protein kinase

MAPKKs or MAP2Ks, MAP Kinase Kinases

MAPKAPK, MAP Kinase-activating Protein Kinases

MAPKKK or MAP3K, MAP Kinase Kinase Kinase

MAPKKKK or MAP4K, MAPKKK Kinase

MAPK(s), mitogen-activated protein kinase(s)

MEFs, Mouse Embryonic Fibroblasts

MEK (or MKK), MAPK kinase

MEKK (or MAPKKK), MAPK kinase kinase

MEKK1, MAPK/ERK Kinase Kinase-1

MI, Myocardial Infarction

MINK, Mishappen-like Kinase 1

MKP, Mitogen-Activated Protein Kinase Phosphatase

MLC2v, Myosin, Light Chain 2 (or Cardiac Ventricular Myosin Light Chain 2)

MLK2/3, Mixed Lineage Kinase 2/3

MLKL, Mixed Lineage Kinase Domain Like

mPTP, Mitochondrial Permeability Transition Pore

mRNA, Messenger RNA

mtDNA, mitochondrial DNA

mTOR, Mechanistic Target of Rapamycin

N/A, Not Applicable

Nec-1, Necrostatin-1

NF- κB, Nuclear Factor Kappa B

NRVCs, Neonatal Rat Ventricular Cardiomyocytes

OCR, Oxygen Consumption Rate

p38, MAPK14

P53 (or TP53), Tumour Protein p53

PAK, C-terminals, p21-activated Kinases

PAMPs, Pathogens-associated Molecular Patterns

PCI, Percutaneous Coronary Intervention(s)

PKC, Protein Kinase C

PKG, cGMP-dependent Protein Kinase

PLC, Phospholipase C

PRRs, Recruit Pattern Recognition Receptors

P/S, Penicillin/Streptomycin

PYK2, Proline-rich Tyrosine Kinase 2

RIP1 (or RIPK1), Receptor Interacting Protein 1 serine/threonine kinase

RIP3 (or RIPK3), Receptor Interacting Protein 3 serine/threonine kinase

RISK, Reperfusion Injury Salvage Kinase

RNAi, RNA interference

ROCK, Rho-associated kinase

ROS, Reactive Oxygen Species

RT, Room Temperature

SAPK(s), Stress-activated Protein Kinase(s)

shRNA, Short-hairpin RNA

sNix, Nix/Bnip3L

STE20, S. cerevisiae Sterile 20

STEMI, ST-Elevation Myocardial Infarction

TAB1, TAK1-binding protein

TAB2/3, TAK-1 Binding Protein

TAC, Transverse Aortic Constriction

TAK1 (or MAP3K7), TGFβ-Activated Kinase-1

TCA , Tricarboxylic Acid

TFGβ, Transforming Growth Factor b

TKL, Tyrosine Kinase-like

TKs, Tyrosine Kinases

TMRE, Potentiometric Mitochondrial Dye

TNFα, Tumour Necrosis Factor α

TNFR, TNF Receptor

TNIK, NCK-Interacting Protein Kinase

TRADD (or TNFRSF1A), TNF Receptor superfamily 1A-associated via Death Domain

TRAF2, TNF Receptor-Associated Factor

TRAIL, TNF-Related Apoptosis Inducing Ligand

TUNEL, Terminal Uridine Nick-End Labeling

UV, Ultraviolet

VDAC1/3, Voltage-dependent Anion Channel

VEGF, Vascular Endothelial Growth Factor

VPS34, Vacuolar Protein Sorting gene34

WT, Wild Type

XIAP, X-linked IAP

YM, Young's Modulus

Abstract

Mitogen-activated protein kinase kinase-kinase-kinase-4 (MAP4K4) is activated in failing human hearts and by apoptotic triggers in cultured cardiomyocytes and mouse hearts. Potent, highly selective inhibitors of human MAP4K4 were previously identified that protect against hydrogen peroxide (H_2O_2)-induced cell death in rat cardiomyocytes and human iPSC-derived cardiomyocytes (hiPSC-CMs), a newly emerging platform for improved target validation and cardiac drug development. Here, we investigate whether MAP4K4 activity influences mitochondrial function, contractility and calcium cycling in hiPSC-CMs using H_2O_2, menadione or doxorubicin as three inducers of reactive oxygen species (ROS).

Human iPSC-CM metabolism was assessed using a Seahorse XF24 analyser to monitor oxygen consumption rate (OCR). Both exogenous (H_2O_2) and endogenous ROS (menadione) reduced mitochondrial respiration levels as measured by OCR. Pharmacological inhibition of MAP4K4 using three complementary inhibitors did not by itself affect mitochondrial function, demonstrating the lack of any potential adverse effect, and was at least partially protective against decreased mitochondrial function induced by H_2O_2 or menadione. Likewise, MAP4K4 inhibition protected against calcium cycling impairment by menadione, as measured by the % of wells with detectable calcium transients.

To circumvent the limitations of using 2D cultures alone, human engineered heart tissue (hEHT) was also used, providing greater biochemical and functional maturity. None of the 3 MAP4K4 inhibitors altered spontaneous contraction frequency (beats per min, BPM) or force in hEHT. MAP4K4 inhibition was protective against menadione-induced cell death 24 after treatment, as measured by adenylate kinase (AK) release. Force, beating rate, time to peak contraction and time from peak to 80% relaxation were preserved for 24 hrs.

These results identify MAP4K4 as a mediator of oxidative stress-induced cell death whose pharmacological inhibition preserves cell death, mitochondrial function and contractility in a human setting.

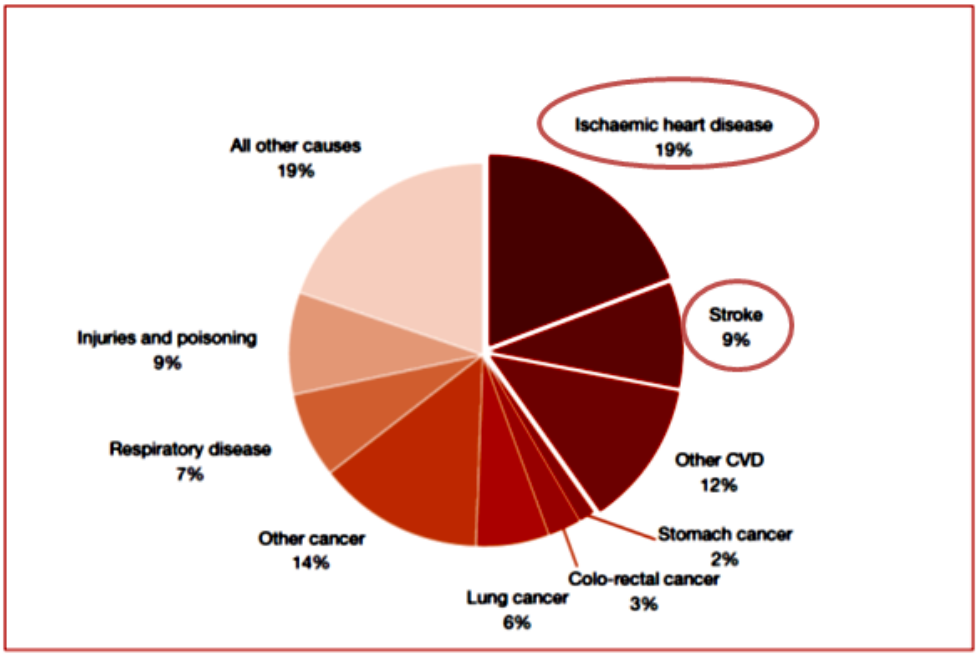
281 words

1. Introduction

1.1 Heart failure as a socio-economic problem

Cardiovascular disease is the biggest killer worldwide, and ischaemic heart disease is the most common, with an incidence of 8 million per year globally (Wang et al. 2016). The most frequent form of ischaemic heart disease is myocardial infarction (MI), an acute ischemic injury resulting in widespread cardiac muscle cell death with an incidence of 7 million per year worldwide (White & Chew 2008) and over 70,000 per year in the UK (Wilkins et al. 2017). In recent years, Europe has seen cardiovascular disease account for 3.9 million deaths per year and the European Union (EU) 1.8 million, accounting for 45% and 37% of all deaths in Europe and the EU respectively (Wilkins et al. 2017). In non-EU countries, cardiovascular disease accounts for an even larger proportion of total deaths recorded, 54% (Townsend et al. 2016). Related costs in the EU are split between health care (53%, €111 billion), productivity losses (26%, €54 billion) and the informal care of people with cardiovascular disease (21%, €45 billion) (Wilkins et al. 2017). Thus, cardiovascular disease imposes a high economic burden worldwide.

Ischaemic heart disease and cerebrovascular disease are the most common causes of cardiovascular related deaths (**Fig. 1.1**), and this accounts for 1.8 million and 1.0 million deaths respectively (Wilkins et al. 2017; Benjamin et al. 2017). More women (2.2 million) die from cardiovascular disease than men (1.8 million), accounting for 49% of all deaths in women and 40% of all deaths in men (Benjamin et al. 2017). These gender differences may relate to higher incidence of cerebrovascular disease and 'other cardiovascular diseases' in women as the numbers for men and women in terms of ischaemic heart disease are similar (Benjamin et al. 2017). Further, this year approximately 695,000 Americans will have a coronary event, 325,000 will have a recurrent one and 165,000 will have silent myocardial infarction (Benjamin et al. 2017).



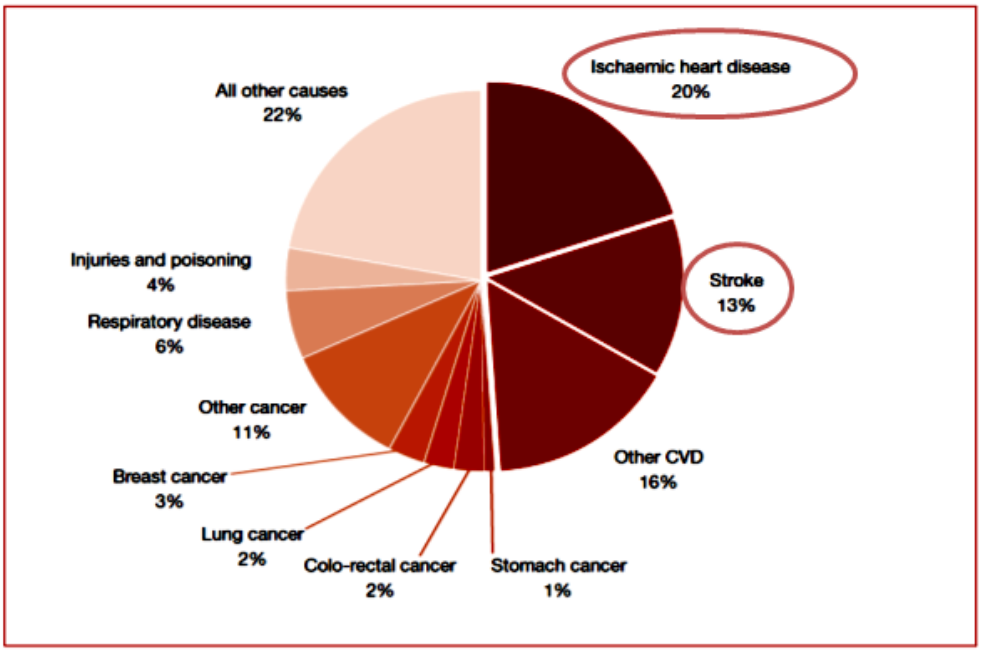


Figure 1.1 Cardiovascular disease statistics. Causes of death for men (top) and women (bottom) in Europe (Wilkins et al. 2017). Modified from Wilkins et al. 2017.

An aging population translates into increased prevalence of heart failure due to higher incidence of common risk factors such as hypertension and coronary disease coupled with these conditions appearing at younger ages; this brings about issues both in terms of life expectancy and quality of life as well as medical costs, including chronic disability post heart failure in MI survivors (Heidenreich et al. 2013; Selker et al. 2017; Stone et al. 2016). Despite the decrease in mortality in developed countries over the last 20 years due to improved prevention and control measures, which resulted in a decrease in risk factors due to better secondary prevention, heart failure and hypertension treatments, mortality remains high, with 50% of hospitalised patients not surviving past 3 years (Heidenreich et al. 2013). During the 1990-2003 period there was an increase in percutaneous coronary interventions (PCI) **(Fig. 1.2A)** however the number of patients hospitalised for heart failure was unchanged **(Fig. 1.2B)** and almost half (44-45%) died within a year (Chen et al. 2013), suggesting that current treatment has not been able to improve hospitalisation figures. Germany was shown to have performed the largest number of PCIs during this period, possibly as a result of a more developed healthcare system or a stronger emphasis on cardiovascular medicine. The use of systemic therapies (such as statins) after PCIs, has been associated with mortality reduction in patients. Often, patients survive MI but then undergo other cardiovascular events (Strömbäck et al. 2017; Stein et al. 2014), which in turn, translate into higher risk of a second MI causing extra burden on the healthcare system.

Furthermore, cardiovascular disease is expected to globally increase from 17.1 million in 2004 to 23.4 million in 2030 with heart failure set to increase from 2012 to 2030 by 23% as a result of increased life expectancy (Heidenreich et al. 2013). This highlights the need to understand human heart failure and its processes – in particular, heart failure following myocardial infarction – to identify new therapeutic approaches.

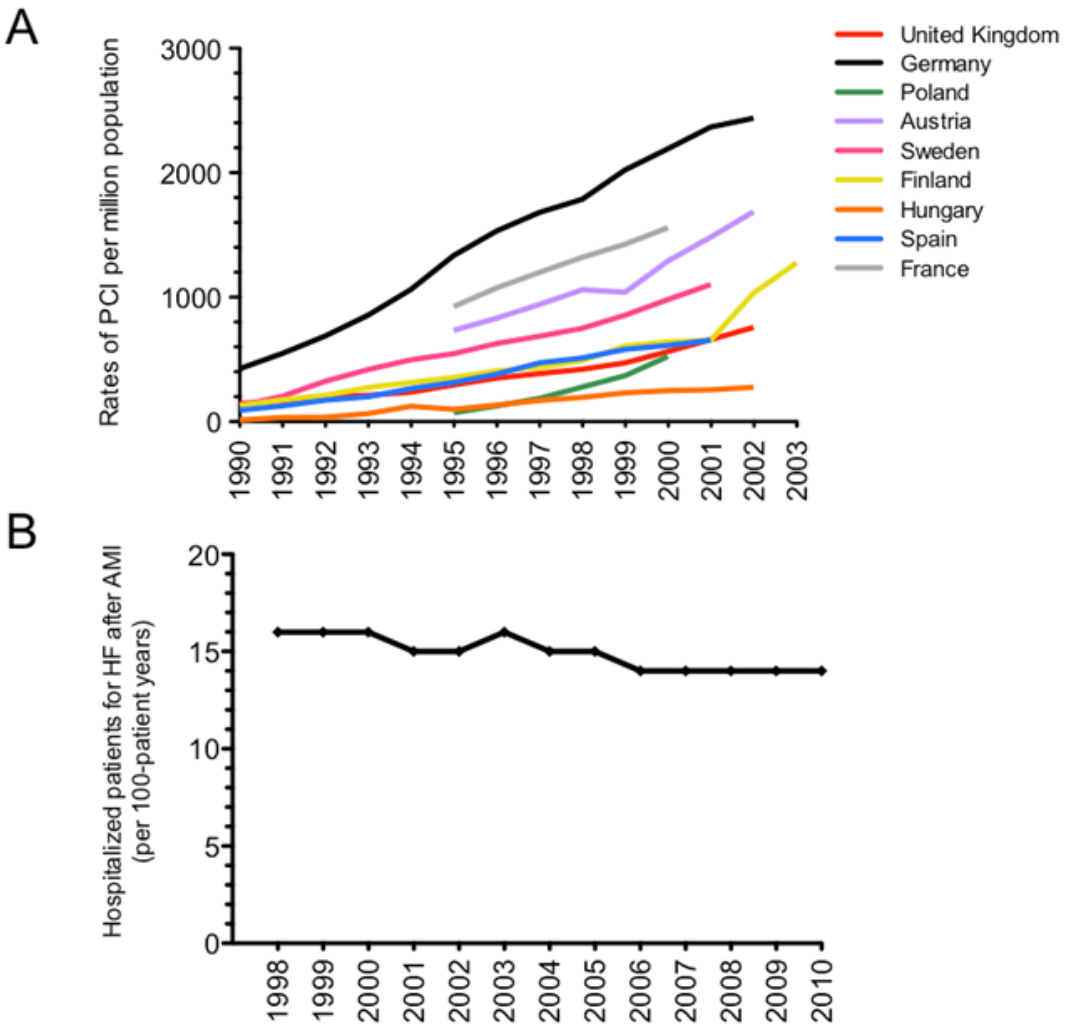


Figure 1.2 Heart failure continues to increase. A) An increase in percutaneous coronary interventions has been reported from 1990 to 2003. **B)** Hospitalised patients for heart failure (Chen et al. 2013). Taken from Chen et al. 2013.

1.2 Pathobiology of heart failure

Heart failure arises from an array of genetic and environmental causes, complicated by other factors such as age and/or systemic conditions including obesity, renal disease, and hypertension. Heart failure is a clinical syndrome caused by structural and functional defects

in the myocardium defined as the heart's inability to function to meet the metabolic needs of the organism, characterised by severe ventricular dysfunction resulting in impairment of ventricular filling or ejection of blood (Boudoulas & Hatzopoulos 2009). At the clinical level this manifests as fatigue, dyspnoea, fluid retention and reduced tissue perfusion, death from arrhythmias or insufficient pump function, increased hemodynamic overload, ischaemia, ventricular remodelling and excessive neuro-humoral stimulation (Hunt et al. 2005; Houser et al. 2012; Dassanayaka & Jones 2015). At the single cell level, cardiomyocyte contractile function is compromised (Boudoulas & Hatzopoulos 2009) due to altered cardiomyocyte geometry, organisation and calcium cycling. Cardiomyocyte loss is not met by cell replacement and extrinsic effects such as interstitial fibrosis due to cell death and inflammation further adversely affect function (Dimmeler et al. 2005; Dassanayaka & Jones 2015). Since the balance between cell survival and apoptosis is compromised during the transition towards ventricular dysfunction, both supressing apoptosis as well as promoting cell survival constitute potential therapeutic approaches for heart failure.

In the adult heart, remodelling occurs as a response to counteract injury and stress due to increased metabolic and contractile demands and can lead to cell death and pump dysfunction if chronic; if combined with mutations or structural defects, its effect is further intensified (Schirone et al. 2017; Francis & Tang 2003; van Berlo et al. 2013). The main types of cardiomyopathies that lead to heart failure are dilated cardiomyopathy (DCM) and hypertrophic cardiomyopathy (HCM); restrictive cardiomyopathies and arrhythmogenic right ventricular cardiomyopathy do not occur as frequently (Houser et al. 2012). These are caused by damage from injury (viral or drug induced), systemic conditions or genetic mutations that compromise the cytoskeleton, sarcomere or myocardial metabolism. The main cause for heart failure is reduced left ventricular function but dysfunction of pericardium, myocardium, endocardium and heart valves or great vessels alone or combined can also cause heart failure (Dassanayaka & Jones 2015), and heart failure with preserved left ventricular function is now also recognised as part of this disease spectrum (Borlaug &

Paulus 2011). MI is the most common type of cardiovascular disease that leads to heart failure, involving both hypertrophy and dilation responses.

Dilated cardiomyopathy is defined by ventricular dilation in conjunction with normal or thinned ventricular walls. Dilation comes about due to the increased wall stress and cell death which does not allow for the muscle to increase in thickness. Hypertrophy is an adaptive response to injury or cardiomyocyte loss, defined as the addition of new sarcomeres which result in chamber wall thickening and generally in an elongated phenotype. In conjunction with these global morphological changes, progressive cell death occurs, which results in diffuse fibrosis further contributing to dysfunction (van Berlo et al. 2013; Francis & Tang 2003). Excessive afterload due to hypertension, left ventricular outflow obstruction or increased wall stress after infarction are normally counteracted by hypertrophic growth without dilation. This results in concentric hypertrophy since cardiomyocytes increase DNA and protein content in an effort to increase force output and thus normalise wall stress, leading to an increase of the cross sectional thickness of cardiomyocytes (Francis & Tang 2003; van Berlo et al. 2013). In turn, chronic hypertrophy can lead to compromised diastolic relaxation and result in dilatation, decompensation and heart failure, if supported by insufficient angiogenesis for the hypertrophic growth (Sano et al. 2007). Common mutations involved in HCM are those of contractile and structural proteins such as myosin heavy chains and myosin binding proteins, which are chiefly involved in mechanotransduction and mechanosensation (Olson et al. 1998; Seidman & Seidman 2001; Morita et al. 2005). These often contain missense residues or small deletions, which incorporated into cytoskeletal and sarcomeric proteins impair normal function (Morita et al. 2005). Mutations in dystrophin, cardiac actin, desmin and titin (missense mutations, deletions and splice defects) are common in DCM (Seidman & Seidman 2001) and cause increased ventricular size, thinning of ventricular walls and cardiac conduction impairment (Chien 2000; Dalloz et al. 2001; Li et al. 1999; Olson 2004). Further, congenital heart disease with cardiac malformations commonly arises from

mutations in cardiac transcription factors (Nkx2.4, GATA4, Tbx5) or in genes regulated by these (Olson 2004). Although some inherited and acquired conditions activate cardiac hypertrophy that progress to left ventricular dilatation and later heart failure, others cause dilatation and heart failure without hypertrophy (Olson 2004). During this process, the balance between cell survival and apoptosis plays a major role in the transition from hypertrophy to ventricular dilation and as such, the suppression of apoptosis and promotion of cell survival are potential therapeutic strategies for heart failure, DCM and remodelling after MI (Olson 2004).

Current therapies include the use of angiotensin-converting enzyme (ACE) inhibitors, angiotensin-II receptor antagonists, β-adrenergic receptor antagonists, and calcium channel blockers to provide relief from myocardial workload and protection from remodelling through dilatation (Braunwald & Bonow 2012). After MI, thrombolytic drugs are used to prevent clotting and further attacks, however, more recently percutaneous coronary intervention is favoured as it reduces the risk of haemorrhagic stroke associated with thrombolytic drugs (Braunwald & Bonow 2012). Aspirin and statins are used to prevent atherosclerosis and lower cholesterol levels (Braunwald & Bonow 2012). These drugs, however, cannot regenerate myocardium and thus clinicians have turned to strategies for tissue repair, namely, autologous adult progenitor cells from mammalian myocardium or exogenous bone marrow progenitor cells reported to differentiate into cardiomyocytes and/or endothelial cells (Boudoulas & Hatzopoulos 2009; Segers & Lee 2008). Other potential strategies would include activation of controlled proliferation of cardiomyocytes (Mercola et al. 2011) and inhibition of cardiomyocyte death thereby enhancing survival and reducing the need for regeneration (Chiong et al. 2011) **(Fig. 1.3)**.

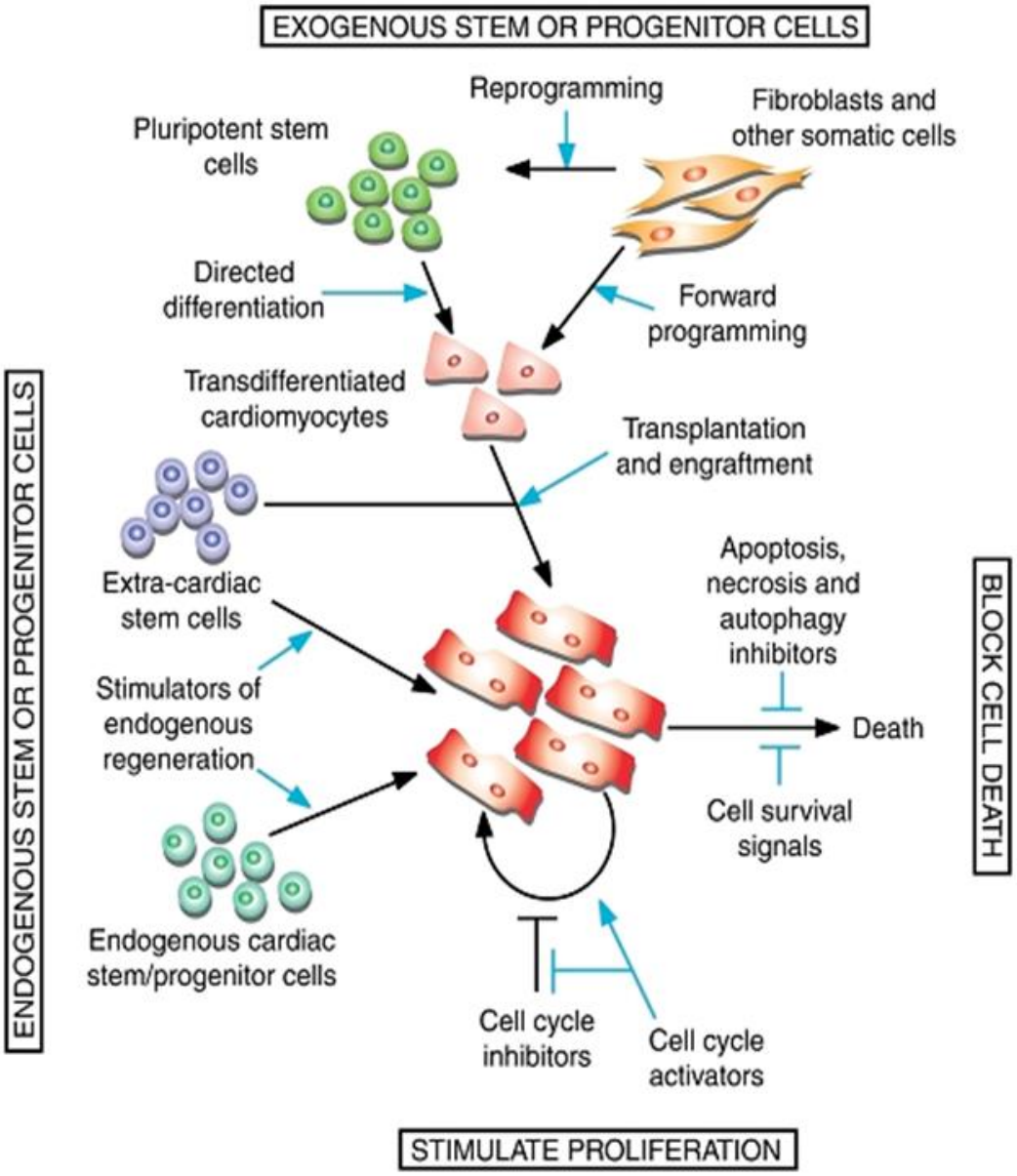


Figure 1.3 Potential approaches to increase cardiomyocyte number as a therapy. Cell death inhibition or survival increase and/or reactivation of cell division of existing cardiomyocytes could potentially increase cell number and constitute a therapeutic target. New cardiomyocytes could be generated from multipotent stem or progenitors in the heart, stem cells able to access the myocardium or ex-vivo cells through transplantation (Mercola et al. 2011). Taken from Mercola et al. 2011)

1.3 Cell death signalling pathways

Cell death is classically divided in three main types, namely apoptosis, necrosis and autophagy. However, cell death has become harder to compartmentalise in recent years since other forms of programmed cell death including necroptosis (Linkermann & Green 2014; Adameova et al. 2016), ferroptosis (Cao & Dixon 2016; Xie et al. 2016), pyroptosis (Fink & Cookson 2005; Taabazuing et al. 2017) and anoikis (Gilmore 2005) have been recognised and their potential involvement in cardiac dysfunction described (Adameova et al. 2017; Szobi et al. 2017; Adameova et al. 2016; Dhingra et al. 2017; Lee et al. 2015; Michel 2003). Apoptosis and necrosis present morphological differences but convergent signalling pathways. Autophagy is the least well characterised of all in terms of its contribution to cell death and heart failure, and describes the intracellular recycling process triggered by cellular stress, nutrient limitation, damaged organelles or accumulation of protein aggregates that contribute to cardiac cell death (Pattingre et al. 2005; Rothermel & Hill 2008). Regardless of the mechanism or classification, however, cell death is a main contributor in heart failure pathophysiology and the dissection of the pathways involved will aid the development of future therapies (Scarabelli & Gottlieb 2004; Whelan et al. 2010). A generic overview of cell death pathways is presented below, followed by a focused discussion in section 1.4 of their specific involvement in cardiac cell death.

1.3.1 Apoptosis

Apoptosis is an evolutionary conserved mechanism of cell death, triggered classically by the extrinsic pathway through cell-surface receptors and by the intrinsic pathway which involves mitochondria and the endoplasmic reticulum (ER), as shown in **Fig. 1.4** (Whelan et al. 2010).

The extrinsic (caspase-8-/10-dependent) pathway involves cell surface receptors binding to their death ligands (FasL, tumour necrosis factor-α [TNF-α]), inducing recruitment of adaptor proteins such as Fas-associated via death domain (FADD), which interacts with procaspase-8 to form the death-inducing signalling complex (DISC). Dimerisation of procaspase-8 in the complex activates caspase-8, which in turn cleaves procaspase-3 and activates caspase-3 (Bao & Shi 2007; Boatright et al. 2003).

The intrinsic pathway is activated by several biochemical and physical stimuli (loss of survival factors, toxins, DNA damage, hypoxia, radiation and oxidative stress) and involves mitochondrial and ER signals relayed by proapoptotic Bcl-2 family proteins, which cause the release of mitochondrial apoptogens (such as cytochrome c [cyt c]) resulting in formation of the apoptosome and caspase-9 activation (Youle & Strasser 2008; Antignani & Youle 2006; Nechushtan et al. 1999; Li et al. 1997; Acehan et al. 2002). However, there is overlap between the extrinsic and intrinsic pathways whereby crosstalk between these pathways can occur. The extrinsic pathway, triggered by cell surface receptors (i.e. Fas) are able to signal to the intrinsic pathway through caspase-8 mediated cleavage of Bid, a BH3-only Bcl-2 family member (Li et al. 1998). This results in the translocation of truncated tBid to the mitochondria which triggers cyt c release, activating mitochondrial-mediated pathways (Li et al. 1998; Luo et al. 1998).

The Bcl-2 family of proapoptotic proteins (Bax, Bak and BH3-domain only: Bid, Bam, Bim, Bmf, Noxa, Puma, Bnip3 and Bnip3L) and antiapoptotic (Bcl-2, Bcl-xl) proteins join both the extrinsic and intrinsic pathways. BH3-interacting domain death agonist (Bid) unites signals as it is cleaved by caspase-8/10, and its C-terminal section (tBid) leads to Bax translocation into the outer mitochondrial membrane and the formation of mitochondrial pores comprising both Bax and Bak (Wei et al. 2000). Bax, together with Bak is needed to activate the intrinsic pathway, also inserts into the outer mitochondrial membrane where it forms a conductance channel to release apoptogens such as cyt c, Smac/DIABLO and Htr2A/Omi (Crow et al. 2004; Suzuki et al. 2000). Cyt c binds to the apoptosis activating factor-1 (Apaf-1) and Adenosine Triphosphate (ATP) and attaches procaspase 9 into the apoptosome that in turn

activates procaspase-3 (Yu et al. 2005; Acehan et al. 2002). Cyt c release is thought to depend on interactions amongst Bim, Bad and Bax which results in the opening of the mitochondrial permeability transition pore (mPTP) (Belzacq et al. 2003; Cheng et al. 2003; Marzo et al. 1998; Tsujimoto et al. 1999). Caspase-3 is situated at the bottom of both the intrinsic (through caspase-9 activation) and extrinsic (through caspase-8 activation) cascade, which subsequently target proteins and enzymes for apoptosis.

There are a number of endogenous inhibitors that block either the intrinsic or extrinsic pathway (Whelan et al. 2010). The antiapoptotic Bcl proteins Bcl-2 and Bcl-xl and inhibitor of apoptosis proteins (IAP) are death antagonists which act, in the case of Bcl-2 and Bcl-xl through interactions with Bax and Bak or by preventing BH3-only proteins from binding Bax and Bak (Crow et al. 2004; Kim et al. 2006; Whelan et al. 2010); and in the case of Bcl-2, by also binding to proapoptic factors and proteins such as voltage dependent anion channels (VDAC) to block the formation of mPTP (Imahashi et al. 2004; Tsujimoto et al. 1999).

IAPs are another group of proteins that regulate apoptosis, keeping it in check under resting conditions through inhibition of caspases (Whelan et al. 2010). IAPs target Caspase-3/7 for proteosomal degradation by deploying their E3 ubiquitin/ligase activity upon binding, which prevents unregulated cyt c leakage (Suzuki et al. 2001; Yang et al. 2000). This therefore can block both the extrinsic and intrinsic pathways of cell death. These pathways are also more directly targeted by IAPs. IAPs can bind to procaspase 9, inhibiting apoptosome formation directly, and regulate pathways mediated by death receptor activation through ubiquitination of RIP1 kinase and TNF receptor-associated factor 2 (TRAF2), both of which comprise complex I formed by binding TNF to TNFR1. Their polyubiquitinated versions then recruit and activate TGF-β-activated kinase 1 (TAK1) through TAK-1 binding protein (TAB2/3) which results in the activation of survival genes (Whelan et al. 2010) although TAK1 can also trigger death (Zhang et al. 2000). cFLIP (FLICE-inhibitory protein) is another regulator of extrinsic pathways, blocking apoptosis by binding procaspase-8 to prevent DISC assembly

in a bifunctional manner (Peter 2004). In the absence of c-FLIP or when it is expressed at low levels, procaspases 8 and 10 are recruited to DISC though binding to the adaptor molecule FADD and this causes activation of caspases through homodimerization which triggers apoptosis, however in the presence of high levels of c-FLIP expression, Caspases 8 and 10 are still activated but are not released from the DISC and this may be important to processes such as proliferation (Peter 2004).

Another key regulator that is muscle specific, Apoptosis repressor protein with a CARD domain (ARC) is also able to inhibit both pathways. It attaches domains of Fas and FADD to inhibit their binding to each other and thus inhibit DISC assembly. In the context of the intrinsic pathway, it forms a complex with Bax, hindering its activation and translocation (Nam et al. 2004).

Intrinsic apoptosis signalling cascades are heterogeneous and can also proceed in a caspase independent manner (Susin et al. 1999). This typically occurs when the intrinsic pathway is activated through Bax and/or Bak in the absence of downstream caspase activation and through caspase independent effectors such as apoptosis-inducing factor (AIF) (Susin et al. 2000; Joza et al. 2001), endonuclease G (endo G) (Li et al. 2001) and HtrA2 (Suzuki et al. 2001) as well as via proteases such as cathepsins (Johnson 2000). AIF is a mitochondrial protein that is released to the cytosol and induces large-scale DNA fragmentation, resulting in chromatin condensation (Daugas et al. 2000; Susin et al. 2000) whose translocation from the mitochondria to the cytosol can be inhibited by Bcl-2 overexpression (Daugas et al. 2000). Endonuclease G is a DNase able to process internucleosomal DNA and like AIF, it is released from the mitochondria and translocates to the nucleus (Li et al. 2001). HtrA2 is a serine protease which is released from the mitochondria and can activate caspase-independent cell death through its enzymatic activity (Suzuki et al. 2001). Cathepsin B and D are lysosomal proteins also suggested to translocate to the cytoplasm (Johnson 2000); cathepsin B is able to become a dominant

execution protease (Foghsgaard et al. 2001) and cathepsin D has been implicated in Bid cleavage (Stoka et al. 2001).

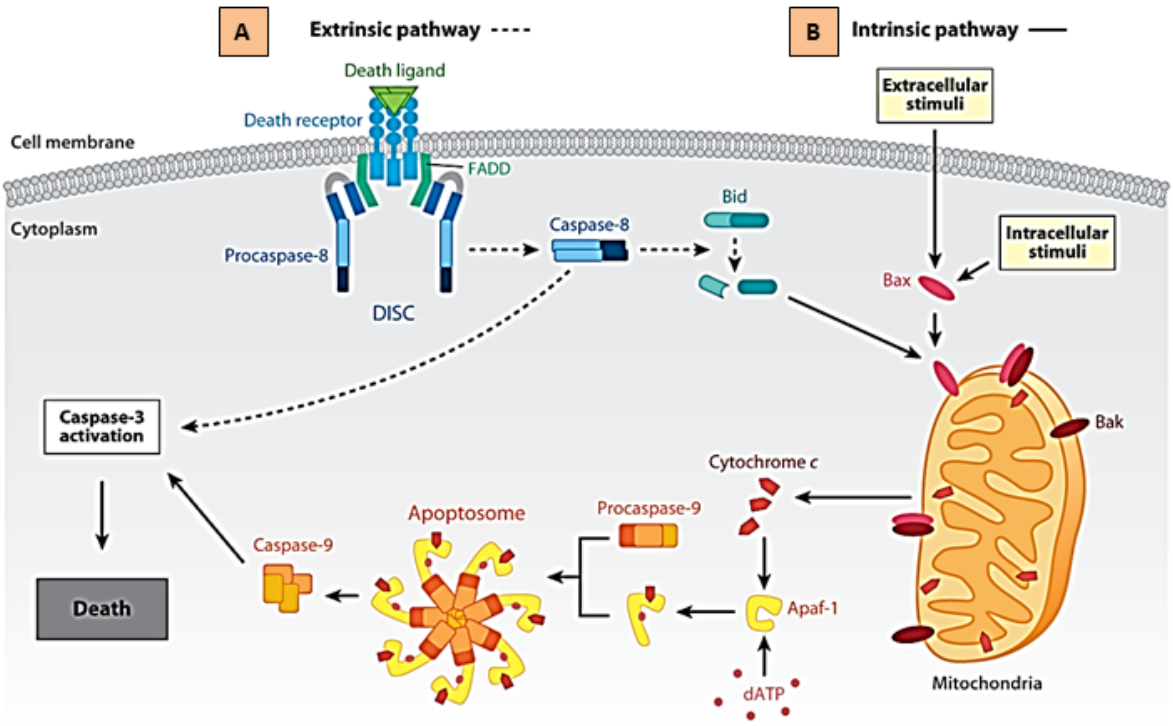


Figure 1.4 Image depicting the intrinsic and extrinsic signalling pathways in apoptosis. A) The extrinsic pathway involves ligand binding which induces the recruitment of adaptor proteins which leads to activation of procaspase-8. **B)** In the intrinsic pathway, mitochondria releases signal proteins via Bid/Bax/Bak in response to stimuli. Cyt C apoptogen release activates procaspase 9 by binding Apaf-1, which in turn, aids apoptosome formation (in conjunction with ATP). Both pathways involve activation of procaspase-3 which signals to cytoskeletal proteins and other enzymes. AIF induces DNA fragmentation after translocating into the nucleus. IAPs are caspase inhibitors (e.i.XIAP) whose effect is lifted by the release of apoptogens (i.e. Omi/HtrA2, Smac/DIABLO). Apoptosis repressor with a CARD (ARC) domain inhibits both pathways by dinging Bax and FADD on death receptors. Stimuli signal the release of calcium from ER to cytoplasm and in turn the opening of mPTP, resulting in apoptogen release (Whelan et al. 2010). Modified from Whelan et al. 2010.

1.3.2 Necrosis

Necrosis has traditionally been thought to be unregulated cell death; however, more recently evidence has shown that death in a proportion of necrotic cells can be regulated, and that

this plays an important role in MI, heart failure (HF) and stroke. Regulated necrosis initiated by death receptor activation along with simultaneous caspase inhibition has been named 'necroptosis' (Degterev et al. 2005). The term necrosis therefore, encompasses both regulated and unregulated forms.

Necrosis is characterised by loss of plasma membrane integrity and depletion of cellular ATP, although the relationship between these events is not well understood (Holler et al. 2000). This results in cells becoming swollen accompanied with organelle swelling, as opposed to the shrunken appearance of apoptotic cells with organelles that remain intact until later in the process (Whelan et al. 2010; Holler et al. 2000). This results in the break-down of the intracellular homeostasis process, which is followed by the release of cellular contents into extracellular space which triggers inflammation.

Regulated necrosis also presents two pathways (**Fig. 1.5**); the mitochondrial pathway, involving the opening of the mPTP, and the death-receptor dependent pathway, involving TNF-α signalling via binding to tumour necrosis factor-α receptor 1 (TNFR1). In the former case, during increased oxygen uptake during reperfusion ROS production increases (Whelan et al., 2010). A decrease in pH gradient as a result of a reduction in the ATP/ADP ratio also induces mPTP opening (Kokoszka et al. 2004).

The mPTP, a VDAC for molecules up to 1.5kDa, is regulated by adenine nucleotide (ADP/ATP) translocators (ANTs) (members of the Bcl-2 protein family and cyclophilin) (Kokoszka et al. 2004) and it is thought to be the main link between necrosis and prolonged myocardial ischaemia (Whelan et al. 2010). During I/R injury, high oxygen concentrations increase oxygen uptake by the respiratory chain, resulting in increased levels of reactive oxygen species (ROS). In conjunction with a drop in pH gradient as a result of decreased ATP/ADP ratios, this leads to proton gradient breakdown which results in dissipation of mitochondrial membrane potential and action potential, which in turn, results in the opening

of the mPTP (Whelan et al. 2010). ANTs are not thought to be necessary for mPTP function however, as mitochondria isolated from the hearts of VDAC1 and VDAC3-null mice showed increased calcium triggered swelling when compared with wild-type littermates that was still inhibited by employing cyclosporine A, a Cyclophilin D (CypD) inhibitor (CypD is involved in protein folding and mPTP regulation) (Baines et al. 2007). In contrast, CypD-deficient mice possess mitochondria which are more resistant to mPTP opening due to calcium stimuli and oxidative stress and have also been shown to have increased resistance to I/R injury compared to wild-type mice despite their sensitivity to standard apoptotic triggers (i.e. TNF-α and staurosporine) (Baines 2007; Baines et al. 2005; Nakagawa et al. 2005).

The second necrotic pathway involves TNF-α signalling. Death receptor-dependent necrosis involves binding TNF-α to TNFR1 to trigger formation of either of two complexes in conjunction with the attachment of adaptor proteins and RIP (a serine/threonine kinase) (Whelan et al. 2010). Binding of TNF-α to TNFR1 can promote survival or cell death, mediated via formation of either complex I or complex II respectively. In complex I, TNFR1-TRADD-RIP1 proteins are connected via death domains, RIP1 and TRAF2 are K63 polyubiquitinated by cIAP1/2 and TRAF2, which recruit transforming growth factor (TGF)-β-activated kinase 1 (TAK1), that activates nuclear factor kappa B (NF- κB)(Ea et al. 2006) and survival gene transcription (Whelan et al. 2010; Ea et al. 2006). In accordance with a pro-survival role for TAK1, TAK1 deficient cells undergo RIP1- mediated death after being exposed to TNF-α stimulation (Çöl Arslan & Scheidereit 2011). In contrast however, TAK1 has been shown to activate cardiomyocyte cell death (Zhang et al. 2000).

Complex II mediates cell death by forming after endocytosis of complex I, complex dissociation from TNFR and RIP1 de-ubiquitination by CYLD (a K63-specific deubiquitinase), which triggers assembly of the FADD-procaspase-8 complex. TRADD interacts with FADD, and the latter recruits procaspase-8 via DED-DED interactions (Wang et al. 2008; Chan et al. 2003). Procaspase-8 activation induces apoptosis via downstream caspases that cleave

and inactivate RIP1. Necrosis is induced when procaspase-8 is inhibited and RIP1 is not cleaved, RIP3 is recruited, and both are phosphorylated (He et al. 2009; Lin et al. 1999). Further, RIP3-caspase-8 and RIP1-FADD double knockout mice showed that loss of RIP3 or RIP1 rescued embryonic lethality cause by caspase-8 and FADD deficiency. Both RIP1 and RIP3 are crucial for the necrotic process to take place, however, downstream mechanisms are not well understood, although RIP1 and RIP3 are phosphorylated through their interaction and mixed lineage kinase domain like (MLKL) is thought to function downstream through interaction with RIP3 (He et al. 2009; Holler et al. 2000; Zhao et al. 2012; Moriwaki & Chan 2013; Sun et al. 2012; Chen et al. 2013).

Necrosis and apoptosis can crosstalk through several common mediators. P53 has an important role in responding to cellular stress due to DNA damage, oxidative stress and ischemia as it controls apoptosis through inducing transcription of death receptors and mitochondrial pathway components (i.e. CD95, PUMA, NOXA, BAX) (Riley et al. 2008; Brady et al. 2011; Chipuk et al. 2004). P53 is also able to modulate necrosis through accumulating in the mitochondrial matrix where it triggers mPTP opening and necrosis through Cyclophilin D (Cyp D), a critical mPTP regulator (Vaseva et al. 2012). Further, ATP levels play an important role in the interplay between apoptosis and necrosis; depletion of intracellular ATP levels switches the apoptotic cell to necrosis since high ATP levels signal for cells to undergo apoptosis and low ATP levels typically favour necrosis (Los et al. 2002; Eguchi et al. 1997).

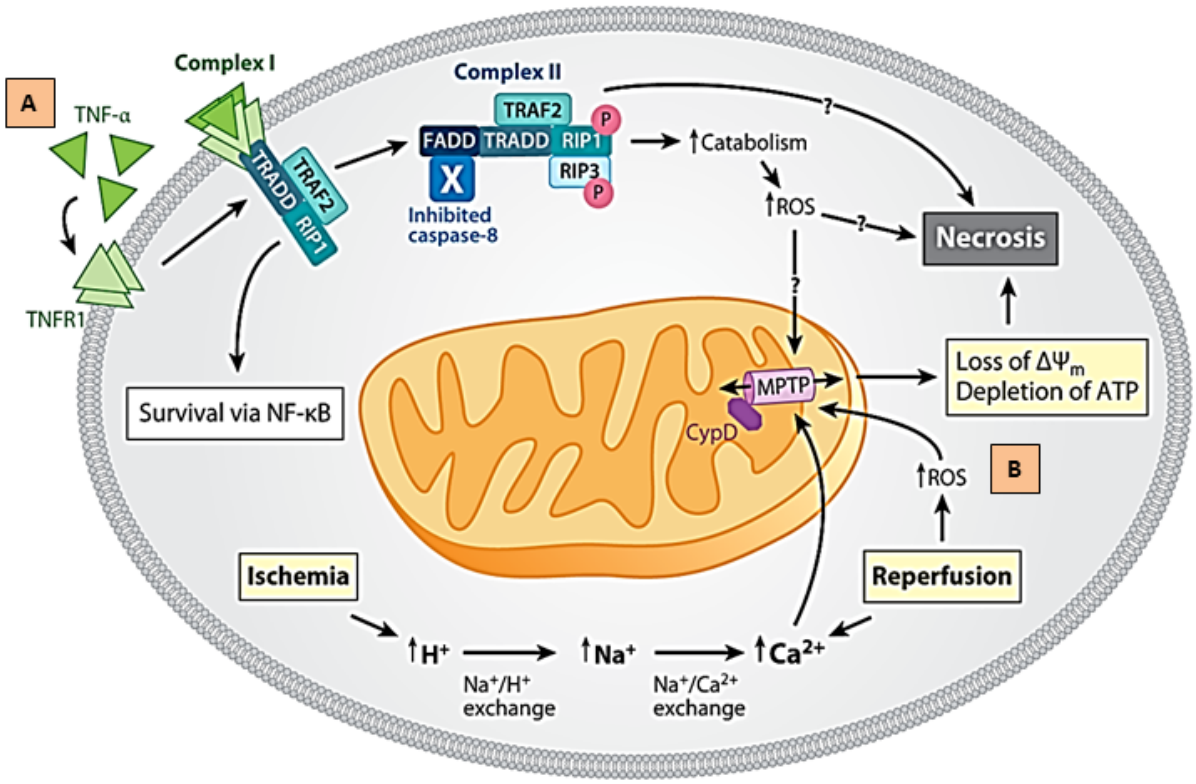


Figure 1.5 Image depicting the molecular pathways leading to necrosis after cardiac I/R injury. **A)** Death receptor-dependent necrosis. TNFR1-complex I promotes cell survival and complex II signals for cell death. Complex I is formed by TNFR1, TRADD, RIP1, TRAF2 and cIAP1/2. One model suggests that TNFR1-TRADD-RIP1 are attached via their death domains (DDs). cIAP1/2 polyubiquinates at K63 residue of RIP1 and TRAF2 and recruit TAK1 through TAB2/3 binding proteins, which activate survival genes via NFkB activation or IKK inhibition. Complex II is dissociated from TNFR1 by endocytosis. RIP1 is de-ubiquitinated by CYLD and recruits FADD-procaspase-8 through DD interactions. Upon procaspase-8 activation, caspase-8 cleaves RIP1 and inactivates necrosis or survival signals. If procaspase-8 is inhibited, RIP1 recruits RIP3 and a series of phosphorylation events occur possibly through activation of catabolic pathways and ROS increases. **B)** mPTP-dependent necrosis. Upon I/R, ATP depletion signals for mPTP opening during reperfusion when mitochondria respire and thus produce action potential. Reperfusion results in mitochondria being filled with calcium and Reactive Oxygen Species (ROS), leading to dissipation of mitochondrial membrane potential ($\Delta\Psi_m$), swelling, membrane disruption and apoptogens' release. Cyclophilin D (Cyp D) performs a crucial role regarding protein folding and in the regulation of mPTP (Whelan et al. 2010). Modified from Whelan et al. 2010.

1.3.3 Autophagy

Autophagy plays an important physiological role in energy homeostasis and functions to maintain nutrient and energy production under stress conditions (starvation, hypoxia, oxidative stress). It was initially believed a non-selective process but more recently selective types such as mitochondria-specific autophagy have been described (Nishida et al. 2015). Macroautophagy (hereafter referred to as autophagy) is the major autophagic pathway maintaining cellular quality control, homeostasis and nutrient and energy production under stress. Dysregulated and/or excessive autophagy can result in cell death and has thus been linked to a number of diseases, including cardiomyopathies and heart failure as well as cancer and neurodegeneration (Mizushima et al. 2008).

Autophagy is triggered by a lack of nutrients, cellular stress, protein aggregation or damaged organelles (Gottlieb & Mentzer 2010). The mammalian target of rapamycin (mTOR) functions as a sensor of nutrient availability, which stimulates protein synthesis and inhibits degradation through autophagy-related proteins (Atg) phosphorylation (Whelan et al. 2010). Autophagy is also regulated by AMP-activated protein kinase (AMPK), which is able to overcome mTOR suppression, and promote a gene regulatory cascade of Atg proteins, resulting in phagophore formation. The phagophore encloses protein aggregates and/or damaged organelles and forms a double-membrane autophagosome (Gottlieb & Mentzer 2010). BH3-only protein Beclin-1 and vacuolar protein sorting gene34 (VPS34) activate ubiquitin-like conjugation systems that comprise a number of Atg proteins, upon AMPK activation. LC3 (also known as Atg8) must be cleaved by Atg4 for phagophore formation (Gottlieb & Mentzer 2010), generating cytosolic LC3-I (also known as LC3a) and lipidated LC3-II (LC3b). The latter originates from the reaction between phosphatidylethanolamine and Atg7 E2-like enzyme. It attaches to the phagophore membrane, giving rise to the autophagosome that fuses with a lysosome or endosome and undergoes degradation by

lysosomal proteases. The degradation of the autophagosome's inner membrane releases its contents, macromolecules and amino acids, to be pumped back into the cytosol by permeases (Klionsky 2005; Massey et al. 2006).

The role of autophagy as a form of cell death remains controversial however, apoptosis and autophagy pathways have been found to crosstalk, and are often mutually inhibitory (Mariño et al. 2014). Generally, autophagy suppresses apoptosis inferring cytoprotection. This interplay converges at signalling points modulated by the Bcl-2 family and caspases (Delgado et al. 2014). Caspases degrade crucial Atg autophagy proteins that become pro-apoptotic (Nishida et al. 2008; Mariño et al. 2014). Overexpression of Bcl-2 protects against Atg5-mediated mitochondrial dysfunction and overexpression of Atg5 mutant K130R was unable to activate autophagy but induced cell death (Mariño et al. 2014). Further, Atg12 mediates mitochondrial-dependent apoptosis by inactivating Bcl-2 family members (Rubinsztein et al. 2012). Beclin-1 is crucial for the localisation of autophagic proteins in the pre-autophagosome (Kang et al. 2011). Autophagy is stimulated upon disruption of Beclin1-Bcl-2 complex although Beclin1 cannot interfere with the anti-apoptotic function of Bcl-2 (Maiuri et al. 2007; Pattingre et al. 2005). Further, pro-apoptotic BNIP3, Bad, PUMA and Noxa induce autophagy and may inhibit Beclin-1-Bcl-2/Bcl-xL interactions competitively (Sinha & Levine 2008).

1.4 Cell death in myocardial infarction and heart failure

MI is the commonest type of ischaemic heart disease and treatment comprises immediate mechanical reperfusion (i.e. stents, balloon angioplasty) in the case of ST-Elevation Myocardial Infarction (STEMI); however, most cases are non-STEMI, which overall is less severe and more appropriately treated with reperfusion at a later, stable stage. The myocardium is deprived of oxygen and nutrients during the ischemic phase, resulting in the accumulation of waste products (Gustafsson & Gottlieb 2007; Whelan et al. 2010). During

reperfusion, which involves the re-introduction of oxygenated blood into the myocardium, oxidative stress (ROS accumulation) and increased levels of systolic and mitochondrial calcium cause mPTP opening, caspase activation and caspase inhibitor inactivation as previously described, leading to cell death, inflammation and ultimately heart failure (Gustafsson & Gottlieb 2007; Whelan et al. 2010). Common models of MI involve coronary occlusion and coronary occlusion followed by I/R; both cause increased cell death (apoptotic, necrotic and autophagic) in the ischemic area (Whelan et al. 2010). Maximal cardiomyocyte apoptosis occurs 4.5 hrs after permanent coronary occlusion and necrotic damage after 24 hrs (Scarabelli & Gottlieb 2004). In MI, reperfusion accelerates death as this is complete within 24 hrs whereas during HF only partial and chronic levels of death are observed after 24 hrs (Wencker et al. 2003; Whelan et al. 2010).

As previously mentioned, cardiomyocyte cell death is a significant feature of the pathophysiology of heart disease (Li et al. 2000; Sivasubramanian et al. 2001; Engel et al. 2004). Surviving cardiomyocytes are subjected to increased mechanical strain prolonged by cell replacement not matching cardiomyocyte loss in this setting (Dimmeler et al. 2005). These modifications result in fibrosis due to cell death and inflammation that leads to functional deterioration, arrhythmias and ventricular dilation (Boudoulas & Hatzopoulos 2009; Dimmeler et al. 2005). Cardiomyocyte cell death can directly result in heart failure; chronic low levels lead to heart failure in transgenic mice that express a conditionally active caspase exclusively in the myocardium, and cell death inhibition by a polycaspase inhibitor has been found to be protective (Wencker et al. 2003). Furthermore, the degree of cell death in ischaemia is one of the determining factors of survival (Miller et al. 1995; Simoons et al. 1986; Brener et al. 2013).

Numerous gain or loss of function mutations and pharmacological interventions in mouse models directly point towards cell death signalling pathways as potential therapeutic targets to diminish the progression of heart failure (Hausenloy & Yellon 2013) and kinases are

crucial to signalling pathways likely to be at centre stage in cardiomyocyte death (Marber et al. 2011; Rose et al. 2010). Pharmacological and genetic inhibition of cell death, whether caspase dependent (apoptosis) or necrotic (mitochondria mediated) or tumour necrosis factor alpha (TNF-α) mediated has been shown to reduce infarct size and improve cardiac function in heart disease. In I/R, mice lacking Fas show infarct reductions (Lee et al. 2003), cardio-specific Bcl-2 overexpression decreases infarct size, cardiomyocyte apoptosis and cardiac dysfunction (Brocheriou et al. 2000; Chen et al. 2001) and pan caspase inhibitors diminish infarct size by 21-52% (Yaoita et al. 1998; Huang et al. 2000; Yang et al. 2003). Therefore, the inhibition of cell death or the potentiation of cardiomyocyte survival, are potential routes for future therapeutic strategies for heart failure. Beyond these vivid illustrative examples, a finer-grained description of the relevant evidence is present below.

1.4.1 Apoptosis in myocardial infarction and heart failure

During embryonic heart development, caspases are involved in apoptosis and in causing lethal dilated cardiomyopathy (Whelan et al. 2010; Wencker et al. 2003). It has been shown that caspase-null mice present abnormal cell death (Kuida et al. 1998). Genetic caspase-8 deficiency caused defective heart muscle development (Varfolomeev et al. 1998), caspase-3 and 9 deficiency caused developmental defects in the central nervous system in conjunction with decreased apoptosis in mice (Wang & Lenardo 2000). Fibroblasts isolated from caspase-8 null mice failed to induce apoptosis through TNF receptors, Fas/Apo1 and DR3 (Varfolomeev et al. 1998). *In vivo* caspase-8 activation in mice, achieved through a cardiospecific procaspase-8 transgene joined to a module that conferred dimerization-dependent catalytic activity, caused extensive apoptotic cell death following administration of a synthetic dimer designed to act as physical bridging mechanism (Wencker et al. 2003). This effect was shown to be reversed by pan-caspase inhibitors (Wencker et al. 2003).

Caspase-1 deletion reduced HF as shown by echocardiogram (Whelan et al. 2010), whereas overexpression of caspase 1 caused apoptotic cell death in neonatal and adult rat cardiomyocytes via Caspase 3 and 9 activation (Merkle et al. 2007). This effect was able to be inhibited by a pan-caspase (zVAD-fmk) or caspase-1-specific (RU 36384) antagonist (Merkle et al. 2007). However, caspase-8 was unaffected by transgenic caspase-1, and inhibition solely of caspase-8 (zIETD-fmk) did not prevent apoptosis. Together these results suggest that caspase-1 is involved principally or exclusively in the activation of the intrinsic apoptotic pathway. Rodents treated with poly-caspases inhibitors showed reduced infarct size following I/R (21-52% reduction) concomitant with decrease in cardiac apoptosis and a reduction in cardiac dysfunction (Whelan et al. 2010). Fas deficient mice also present reduced infarct size after MI and have been shown to secrete death ligands suggesting an extra trigger post MI (Jeremias et al. 2000). Moreover, in neonatal rat cardiomyocytes and intact adult rat hearts, overexpression of FasL caused apoptosis (Lee et al. 2003). Mice lacking both TNF receptors were found to have increased infarct and apoptosis but not necrosis as compared to wild-type littermates as well as to TNFR1 or TNFR2 deficient mice (Kurrelmeyer et al. 2000), suggesting that both TNF receptors are involved in cytoprotective mechanisms and a single gene deletion may not be sufficient to signal survival (Kurrelmeyer et al. 2000). However, the distinct proposed roles of both TNF receptors (TNFR1 as proapoptotic and TNFR2 as pro-survival) may be an alternative explanation for these findings (Hamid et al. 2009).

The intrinsic pathway has also been implicated in MI. Transgenic mice presenting deletion of Bax showed reduced infarct size and improved function post I/R in perfused hearts and mice with permanent coronary occlusion (Hochhauser et al. 2003). Cardiospecific Bcl-2 overexpression driven by MCK promoter decreased infarct size, increase cardiac function and reduced cardiac apoptosis as assessed by TUNEL staining post I/R (Brocheriou et al. 2000). The improved cardiospecific Bcl-2 expression model, which is driven by the α-MHC [Myh6] promoter, also showed improved functional recovery in perfused hearts, decreased

cell death as measured by lactate dehydrogenase (LDH) release and TUNEL staining, reduced infarct sizes and decreased AIF release from mitochondrial fractions (Imahashi et al. 2004) and I/R (Chen et al. 2001).

Both myocytes and non-myocytes present in the ischemic zone undergo cell death during permanent coronary occlusion and I/R, and as shown by both a primate model and HF human patients, non-myocytes are heavily affected by apoptosis (Potts et al. 2005). The interaction between myocytes and non-myocytes are affected by non-myocytes undergoing apoptosis; disruptions to these interactions are involved in the cause of HF especially as non-myocytes present low levels of Apaf-1 which makes them more susceptible to apoptosis (Potts et al. 2005). Low levels of Apaf-1 in neonatal cardiomyocytes correlated with lack of cyt-c release and sensitisation by both XIAP inhibition or restoration of Apaf-1 levels. Low levels of Apaf-1 were also shown to be responsible for caspase 9 activation by endogenous XIAP, but the direct effect on caspase-3 was not assessed (Potts et al. 2005). The use of a small molecule inhibitor of serine protease activity against pro-apoptotic Omi/HtrA2 (UCF-101) in two rodent models, however, was shown to reduce infarct size post I/R and increase cardiac functional recovery concomitant with reduction of IAP loss (Bhuiyan & Fukunaga 2007; Liu et al. 2005).

Caspase activation is involved in the development of heart failure. Cardiospecific transgenic mice expressing low levels of caspase-8 due to a modification in an allele of conditionally active caspase showed low levels of apoptosis and developed lethal dilated cardiomyopathy at 8-9 weeks, suggesting that low sustained levels of cardiac apoptosis is involved in the development of HF (Wencker et al. 2003). This effect was reversed by the use of a pan-caspase inhibitor. In addition, cardiospecific expression of caspase-1 in mice showed cardiomyocyte hypertrophy after 4 months and caspase-1 deficient mice showed reduced cardiac hypertrophy when compare to wild-type littermates (Merkle et al. 2007).

Gαq is a subunit of the heterotrimeric Gq protein which is dissociated after interaction with a receptor bound to an agonist, such as type 1 angiotensin, α1-adrenergic and endothelin receptor, and it's function is to activate protein kinase C (PKC) downstream (Sánchez-Fernández et al. 2014). Cardiospecific overexpression of Gαq, driven by αMHC promoter, was shown to cause cardiac hypertrophy related to the stimulation of the fetal gene program and heart failure. Nix/Bnip3L is a BH3-like protein which, when overexpressed, results in apoptosis and death and that was found to be to be transcriptionally activated in the cardiospecific Gαq overexpressing mice (D'Angelo et al. 1997). In Gαq transgenic females, it was found that a splice variant of Nix/Bnip3L (sNix) was protective against apoptotic peripartum cardiomyopathy as defined by reduced apoptosis, improved cardiac function and decreased early death (Yussman et al. 2002). Ablating Bnip3 (a BH3-like protein) in mice, was shown to reduce apoptosis post I/R and prevented ventricular remodelling. Bnip3 forced expression increased cardiac apoptosis deriving in LV dilatation in mice not subjected to myocardial stress, and conditional overexpression also increased apoptosis and infarct size pre- coronary ligation (Diwan et al. 2007). This suggests that myocardial injury can be salvaged by inhibition of apoptosis and that Bnip3 is an important mediator of apoptosis and remodelling under unstressed conditions and in the infarcted heart.

1.4.2 Necrosis in myocardial infarction and heart failure

Evidence suggests that cardiomyocytes that have undergone I/R in conjunction with hypoxia following ischaemia, anaerobic metabolism and intracellular acidosis; since all these events contribute to mPTP opening. However, no direct link between necrosis pathways (RIP1-RIP3 axis) and I/R has been identified. CypD null mice have been shown to present reduce infarct size after I/R and CypD null cardiomyocytes to be resistant to oxidative stress and calcium-induced cell death compared to wild-type; though still respond to apoptotic stimuli (Baines et al. 2005). Transgenic mice overexpressing CypD present enlarged mitochondria as defined

by electron microscopy assessment and increased cell death induced by hydrogen peroxide compared to wild-type (assessed by PI staining) (Baines et al. 2005). Necrostatin-1, an inhibitor of RIP1 kinase activity, was shown to reduce infarct size post I/R and this was not dependent on CypD nor mPTP opening (Smith et al. 2007; Lim et al. 2007). In rodents, Necrostatin-1 administration reduced infarct size, inhibited RIPK1/RIPK3 phosphorylation and cell death (Oerlemans et al. 2012). In a porcine I/R model, intravenous administration of Necrostatin-1 prior to reperfusion reduced infarct size and preserved ventricular function (Koudstaal et al. 2015).

Cardiac necrosis has been suggested to be even more prevalent than apoptosis and that both contribute towards the evolution of cardiac failure (Guerra et al. 1999). This study assessed the cleavage pattern of DNA of patients with idiopathic and ischemic heart failure using molecular probes (Guerra et al. 1999). Doxycycline driven cardiospecific transgenic inducible mice that overexpressed the β2a subunit of the L-type calcium channel (LTCC), the primary source of calcium influx in cardiomyocytes which is linked to HF which enhances open channel probability, showed that necrosis is associated with HF due to calcium overload (Nakayama et al. 2007). Mice overexpressing low and high levels of LTCC displayed hypertrophy by 4 months with fibrosis and exacerbated cell death associated with calcium overload. This was reduced with verapamil, an LTCC inhibitor. Further, these mice showed no caspase-3 activation, no increased TUNEL staining and cardiospecific expression of Bcl-2 did not prevent HF (Z. Chen et al. 2001). In conclusion, it is likely that the development of heart failure and DCM are as a result of a combination of exacerbated apoptosis and necrosis (Xie et al. 2013; Adameova et al. 2016; Strzyz 2017).

1.4.3 Autophagy in myocardial infarction and heart failure

Autophagy is a conserved process comprising bulk degradation and recycling of cytoplasmic components such as organelles and proteins. In the heart, autophagy plays a crucial role in the turnover of organelles at basal levels under normal conditions and it is upregulated in response to stress (Nishida & Otsu 2008). Exacerbated levels of wall stress lead to the accumulation of damaged mitochondria and harmful protein aggregates in the failing heart; damaged mitochondria generate ROS and decrease ATP production, which activates the energy sensor AMPK. In turn, autophagy is upregulated by both ROS accumulation and AMPK activation (Nishida 2016).

Autophagy has been shown to be induced during coronary occlusion, I/R, in failing human hearts and cardiomyopathies (Knaapen et al. 2001; Sawa Kostin et al. 2003; Matsui et al. 2007; Tannous et al. 2008). It was also induced in mice by ischaemia and exacerbated by reperfusion with two different mechanisms for autophagy present for each stage. Ischaemia activated autophagy through AMPK activation as is the case in coronary occlusion, and is inhibited by cardiospecific overexpression of dominant-negative AMPK (Matsui et al. 2007). During reperfusion, the LC3II/LC3I ratio was increased in murine hearts but was independent of AMPK activation and involved Beclin-1 upregulation, which was decreased in Blc-2 dominant-negative mice. I/R in Blc-2 dominant-negative mice showed a decrease in infarct size compared to wild-type littermates concomitant with reductions to TUNEL-positive cells in the ischemic area (Matsui et al. 2007). Mice treated with an activator of AMPK (A-769662) pre I/R displayed increased LV contractile function, diminished necrosis and reduced infarcts post injury (Kim et al. 2011). However, genetically modified mice expressing inactivated AMPK did not observe this cardioprotective effect, pointing towards the specificity of the inhibitor (Kim et al. 2011). Therefore, autophagy is broadly involved during myocardial injury.

Human failing hearts displayed exacerbated number of autophagosomes, but whilst this suggests that autophagy is present, its role i.e. whether this is cardioprotective or detrimental in this context, is currently under investigation (Hein et al. 2003; S. Kostin et al. 2003; Delbridge et al. 2017; Sciarretta et al. 2011). Cardiospecific deletion of Atg5 in adult mice (*MerCreMer*) driven by *Cre* recombinase though MLC2v promoter in a tamoxifen-inducible manner after transverse aortic constriction (TAC) displayed increase number of TUNEL positive cardiomyocytes (Nakai et al. 2007). These mice also showed increased levels of caspase-12 (involved in endoplasmic reticulum stress-induced apoptosis), increase proteosomal activity, protein synthesis and proteasome linked degradation, increased LV enlargement and cardiac dysfunction (Nakai et al. 2007). However, no activation of caspase-3 and -9 was observed (Nakai et al. 2007). Another study showed that Atg5 embryonic deletion did not cause any abnormalities at birth, however, when subjected to hemodynamic stress mice developed cardiac enlargement and failure (Whelan et al. 2010). Beclin-1 dominant-negative mice (driven by cardiospecific promoter α-MHC) subjected to pressure overload showed a decrease in cardiac autophagy, as assessed by expression of a cardiospecific LC3-GFP reporter and lysosomal markers (such as cathepsin D) (Zhu et al. 2007). Beclin-1 dominant-negative mice also presented reduced remodelling, as compared to increased autophagy in the LVs in wild-type (Zhu et al. 2007). Therefore, Beclin-1 overexpression increases autophagy and pathological remodelling (Zhu et al. 2007).

However, Beclin-1 silencing by siRNA inhibited autophagy on cultured rat neonatal cardiomyocytes whilst protecting from doxorubicin induced cell death (Pizarro et al. 2016). Similarly, Rho-Kinase inhibitor fasudil was shown to reduce apoptosis in high glucose-induced H9c2 cell (a model of diabetic cardiomyopathy) through activations of autophagy, as assessed by increased LC3-II/LC3-I ratio, Beclin-1 expression and the number of autophagosomes (Gao et al. 2016).

Despite the clear involvement of Beclin1, the mechanism by which its inhibition decreases autophagy in conjunction with reduction of pathological remodelling and reduces infarct size in I/R has not been fully elucidated (Ma et al. 2015; Sciarretta et al. 2012). It is suggested that I/R injury may impair autophagosome clearance after left coronary artery ligation as defined by the assessment of the expression of the LC3-GFP reporter (Ma et al. 2012). Further, I/R caused Beclin1 increases and decreases in LAMP1 and LAMP2 (lysosomal proteins). This, in turn, provoked ROS levels to increase and were prevented using a ROS scavenger. ROS accumulation caused cardiomyocyte death as measured by the potentiometric mitochondrial dye TMRE. This effect was attenuated by cyclosporine A treatment, a CypD inhibitor (Ma et al. 2012). ROS induce autophagy via Beclin-1 dependent pathway associated with autophagy-related cell death (De Meyer & Martinet 2009; Scherz-Shouval et al. 2007). Therefore, Beclin-1 dominant-negative mice may be able to clear autophagosomes more efficiently through enhanced lysosome fusion and not a reduction in autophagosome formation (Ma et al. 2012).

Bcl-2 is also involved in cardiomyocyte homeostasis by supporting cell survival through metabolic pathways. This is illustrated by the effects of Bcl-2 cardiospecific overexpression, which reduced ischemic reperfusion (I/R) injury as a result of reduced acidification and rate of ATP consumption (Imahashi et al. 2004). Further, it is also involved in autophagy whereby it interacts with Beclin1, which is of central importance in regulating autophagosome formation (He et al. 2012; Pattingre et al. 2005), as shown by the fact that suppression of Bcl-2-sensitive cell death induced autophagy and necrosis (Maloyan et al. 2010). This highlights the close interplay, at the molecular level, of the three notionally separate death pathways and an essential role of the mitochondrion in each.

All these forms of cell death are present in heart failure, and share overlapping signalling pathways. The role of autophagy in heart failure is yet to be resolved. However, pharmacological and genetic inhibition of apoptosis and necrosis reduces infarct size and

improves cardiac function in heart disease. This is exemplified by mice which lack Fas show infarct size reductions post I/R (Lee et al. 2003). Further, cardiospecific overexpression of antiapoptotic Bcl-2 decreases infarct size, cardiomyocyte apoptosis and cardiac dysfunction (Brocheriou et al.; Z. Chen et al. 2001). In addition, polycaspase inhibitors reduce infarct size by 21-52% (Yaoita et al. 1998; Huang et al. 2000; Yang et al. 2003). Inhibiting cell death and increasing cardiomyocyte survival are therefore plausible routes for future therapeutic strategies to prevent, delay, or lessen heart failure.

1.5 Metabolism

The heart is the most metabolically active organ and as such, mitochondria comprise 25 to 30% of cell volume across mammalian species and are the second most densely packed structure after myofilaments in cardiomyocytes (Barth et al. 1992; Schaper et al. 1985). This is needed to meet the active process of contraction and relaxation, that requires huge amounts of energy, using about 90% of cellular ATP (Brown et al. 2016). Actin is released from myosin through an ATP-dependent process necessitated for contraction (myosin heads cycle through cross-bridges with actin) and relaxation. Calcium is sequestered back into the sarcoplasmic reticulum during diastole; a process that is also ATP-dependent. Cardiac function is sustained by metabolic supply and demand pairing, primarily with calcium acting as a feedback signal (Balaban 2009a; Balaban 2009b). High efficiency is required for mitochondria to respond to the contractile needs; this demand is not only ever-changing but it also relies on the ability of blood to carry oxygen (Brown et al. 2016).

Bioenergetic homeostasis is achieved through a mitochondrial network that comprises the supply of mitochondrial ATP, which transfers energy along the cell through intracellular buffering systems (**Fig. 1.6**). Carbon sources from food substrates are employed by

mitochondria, catabolised and passed through the Krebs cycle to be finally channelled through a number of redox reaction along the inner mitochondrial membrane. These substrates are oxidised, creating a proton electrochemical gradient, known as the mitochondrial membrane potential ($\Delta\Psi_m$) (Mitchell 1961). Protons which re-join the mitochondrial matrix via complex V (mitochondrial ATP synthase) release energy which phosphorylates ADP, and in turn regenerates ATP. This is exported out of the mitochondria and energy is distributed throughout the cell through reversible phosphate exchange networks (mainly catalysed by reactions involving creatine kinase and adenylate kinase) (Balaban 2002; Carrasco et al. 2001).

In HF, components of cardiac bioenergetics such as oxygen availability, substrate oxidation, mitochondrial ATP production and ATP transfer to the contractile apparatus are altered (Rosca & Hoppel 2013). Abnormalities in mitochondria are present in HF, not only as a result of reduced ability to generate ATP (although capacity is reduced under resting condition in HF compared to control) but also attributed to cardiomyocyte injury and death, which in turn leads to disease progression (Brown et al. 2016). Anomalous mitochondria are sources of ROS production (which are capable of inducing cellular damage) and they can promote programmed cell death (through the release of cytochrome c and caspase activation). As such, mitochondria play a role in directly influencing ongoing cell injury and death (Brown et al. 2016) and anomalies have been implicated in cardiovascular disease and HF through abnormal calcium homeostasis, vascular smooth muscle disease, disrupted myofibrillar networks and altered cell differentiation (Brown et al. 2016).

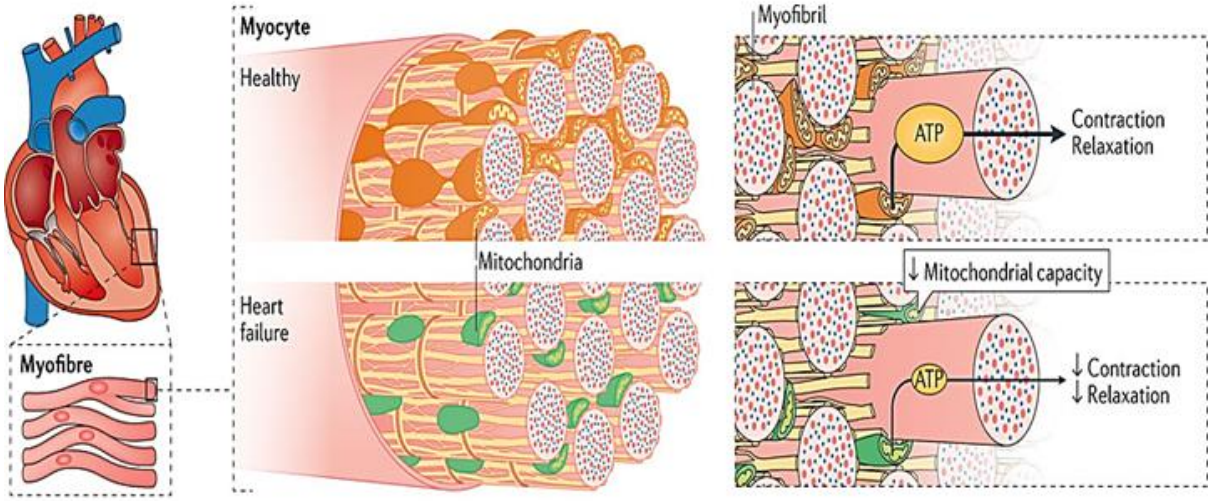


Figure 1.6 Schematic representation of impaired mitochondrial capacity and function in heart failure. Mitochondria are highly abundant in the myofibrils within cardiomyocytes. They generate the high levels of ATP required to maintain contractile and relaxation functions of the heart. Reduced mitochondrial capacity to produce and transfer energy in the context of heart failure leads to energy deficits within cardiomyocytes. This in turn affects all processes requiring energy – particularly the mechanical functions (Brown et al. 2016). Taken from Brown et al. 2016.

1.6 Metabolism in myocardial infarction and heart failure

In the cardiomyocyte, mitochondria are located within the subsarcolemmal, perinuclear and intrafibrillar areas and whilst they work in unison with other structures they are in many ways independent units. Mitochondrial dynamics (fission, fusion and autophagy) are greatly regulated processes that are crucial for energy production and maintenance of organelle structural integrity (Suliman & Piantadosi 2015; Thomas & Gustafsson 2013). Abnormal biogenesis, fragmentation and hyperplasia in mitochondria have been reported in HF in humans (Sebastiani et al. 2007), guinea pigs (Goh et al. 2016) and dogs (Sabbah et al. 1992), possibly caused by abnormal expression of proteins involved in the regulation of mitochondrial dynamics (Lehman & Kelly 2002). Since a number of these factors act as mitochondrial metabolism regulators, it is possible that these changes are linked to the

decreased capacity for fatty acid oxidation which features in HF (Lai et al. 2014; Lemieux et al. 2011).

Mitochondria possess their own DNA (mtDNA) and genetic code (distinct from the host-cell nuclear DNA), however, over 99% of mitochondrial proteins come from nuclear-encoded DNA. Many inherited familial cardiomyopathies implicate mtDNA mutations (Bates et al. 2012) both in children and adults. Mitochondria are maternally inherited in humans (Margulis 1975) as a result of high mitochondrial density in the egg combined with mitochondrial degradation in sperm during fertilization (Sato & Sato 2013). mtDNA is particularly susceptible to oxidative stress and mutation, possibly due to its proximity to sites for mitochondrial ROS generation combined with poor repair mechanisms and a lack of protective histones (Brown et al. 2016). Thus mtDNA likely contributes to impaired function of mitochondria that can potentiate heart failure.

Indeed, mitochondrial mutations in proteins that are involved in energy homeostasis have been shown to contribute to cardiomyopathies. Mitochondrial 'heteroplasmy' refers to the presence of mutated mtDNA alongside nonmutated copies. Many recent approaches aim to reduce the extent of heteroplasmy using selective reduction of heteroplasmy, which may prevent transmission resulting in genetic mitochondrial disease (Bacman et al. 2013; Paull et al. 2012; Yamada et al. 2016). This may not only benefit HF related diseases as mitochondrial dysfunction such as elevated ROS production, abnormal energetics and mitochondrial ion homeostasis dysfunction are also present in a number of other disease (Brown et al. 2016).

ROS production takes place when ROS formation outperforms compensatory signals and endogenous scavenging systems are unable to meet the demands posed by the environment (Aon et al. 2010; Murphy & Steenbergen 2008b). ROS are generated at various sites inside and outside of the mitochondria (Murphy & Steenbergen 2008a; Nabeebaccus et

al. 2011); at sites in the inner mitochondrial membrane but also by components of the ETC and the Krebs cycle in the mitochondrial matrix (Orr et al. 2013) (**Fig. 1.7**). Under physiological conditions, ROS production is low and is safeguarded by intracellular and intramitochondrial scavenging systems (Murphy 2009). However, when ROS production overcomes scavenging capacity, pathological ROS levels occur in the heart; this can damage protein and lipids, trigger cell death and cause cellular energy systems to collapse (Zorov et al. 2006; Aon et al. 2006). Both increased ROS production and ROS-dependent damage has been observed in HF patients as well as in models of disease (Goh et al. 2016; Ide et al. 1999).

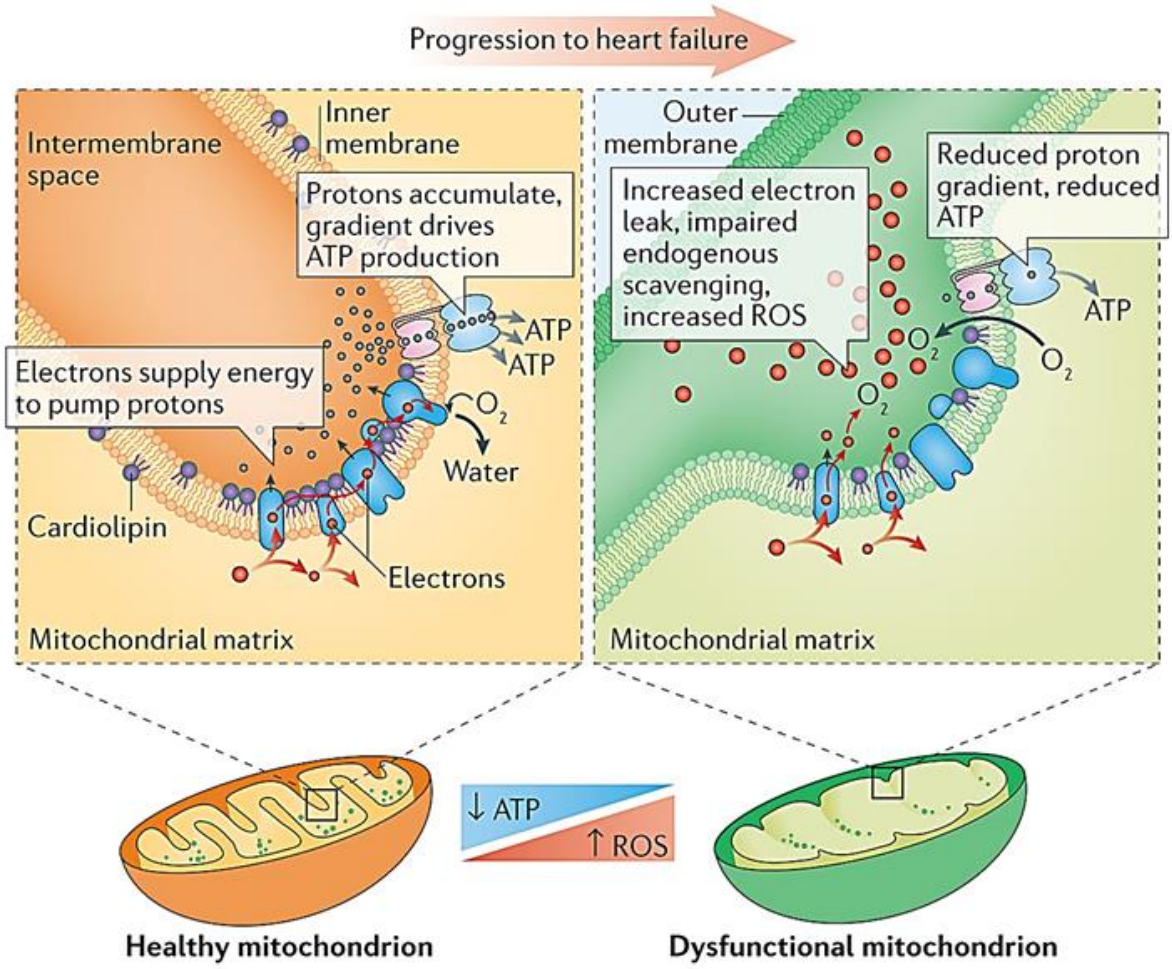


Figure 1.7 Abnormal mitochondrial energy production along the inner membrane. Enzyme complexes in change of energy production are located in the mitochondrial inner membrane, helped by phospholipids (I.e. cardiolipin). Failing mitochondria display altered morphology, reduced ATP-generating capacity, increased production of ROS, altered cardiolipin levels and dysfunctional supercomplexes (Brown et al. 2016). Taken from Brown et al. 2016.

1.7 The protein kinase complement of the human genome

Protein kinases are a key class of enzymes whose role in universal signalling cascades is to couple extra- and intracellular signals to effector pathways for survival, differentiation, apoptosis, cell growth and chromosome integrity (Grueneberg et al. 2008). Nearly 70 years ago, the discovery that kinases were regulated by reversible phosphorylation sparked great interest in protein regulation and function by this mechanism. In 2002, the kinome (also known as the protein kinase human complement) was classified as having 518 putative protein kinase genes and 106 protein kinase pseudogenes. Of these, 244 kinases were attributed to disease loci and cancer amplicons (Manning et al. 2002) as defined by the assessment of the genomic sequence and chromosomal mapping. Here the involvement of kinases in cardiac disease will be introduced.

1.7.1 Classification and mode of action

Kinases are grouped according to sequence similarity of their kinase domain (**Fig. 1.8**) (Manning et al. 2002). There are seven major families, namely, AGC (comprising protein kinases A, G and C), Ca^{2+}/calmodulin-dependent protein kinase (CAMK), Casein kinase 1 (CK1), CMGC (including cyclin-dependent kinase [CDK], mitogen-activated protein kinase [MAPK], glycogen synthase kinase [GSK3] and CDC-like kinase [CLK]), tyrosine kinases (TKs), tyrosine kinase-like (TKL) kinases, and STE20-related kinases, including MAP4K4, which activate 'downstream' MAPK family members (Manning et al. 2002). A second type of classification is based on the residues that kinases phosphorylate. There are two salient classes, namely TKs and serine/threonine kinases.

Kinases are regulated by secondary messengers (cyclic AMP, Ca^{2+}, hormones, cGMP and certain phospholipids) under stress conditions and also in response to growth factors. Secondary messengers are intracellular and triggered by a primary messenger, such as neurotransmitters, hormones, growth factors, chemokines and cytokines. Kinases act in conjunction with cell surface transmembrane receptors which become activated by ligand binding (Receptor TKs), extracellular stimuli or intracellular signal mediators. This initiates a chain of kinase activation which results in altered gene transcription and cellular functional changes (Kyriakis & Avruch 2012). Receptor TK activation is linked to event which culminates in the activation of phospholipase C (PLC), protein kinase C (PKC), mitogen-activated protein kinase (MAPK) and phosphatidylinositol 3-kinase (PI3K). MAPKs interact with domains of other kinases, scaffold proteins and transcription factors to prevent crosstalk between related upstream elements and ensure specificity (Sharrocks et al. 2000).

Specificity is regulated by factors such as interacting kinases, scaffold proteins or transcription factors (Sharrocks et al. 2000). Phosphorylation of residues that bridge the phosphor-acceptor site is another mechanism by which specificity is conferred, although some proteins such as JunB have docking sites but no phosphor-acceptor residues. JunB recruits kinases such as JNK for transphosphorylation of other proteins (e.g. JunD). Therefore, docking domains can aid the assembly of signalling complexes or bind transcriptional regulatory proteins (Sharrocks et al. 2000). Further, an auto inhibitory domain enables regulation and safeguards the activity of the kinase domain in the off-state by interfering with its function (ligand binding, subcellular localisation or enzymatic activity). Binding of a second molecule on the auto-inhibitory domain reverses inhibition (Kyriakis & Avruch 2012; Pufall & Graves 2002).

In addition, selectivity has been linked to the folded conformation for the P-loop (also known as the glycine-rich loop) due to its conformational variability for particular kinases. The P-loop, normally exists in an extended conformation and is a stretch of approximately nine

aminoacids. In the P-loop folded conformation, the binding site assumes a tunnel-like shape which provides a hydrophobic enclosure to inhibitors. Inhibitors that induce this folded conformation at the P-loop are often more selective, particularly if they interact favourably with conserved Tyr or Phe residues from the P-loop (Guimarães et al. 2011).

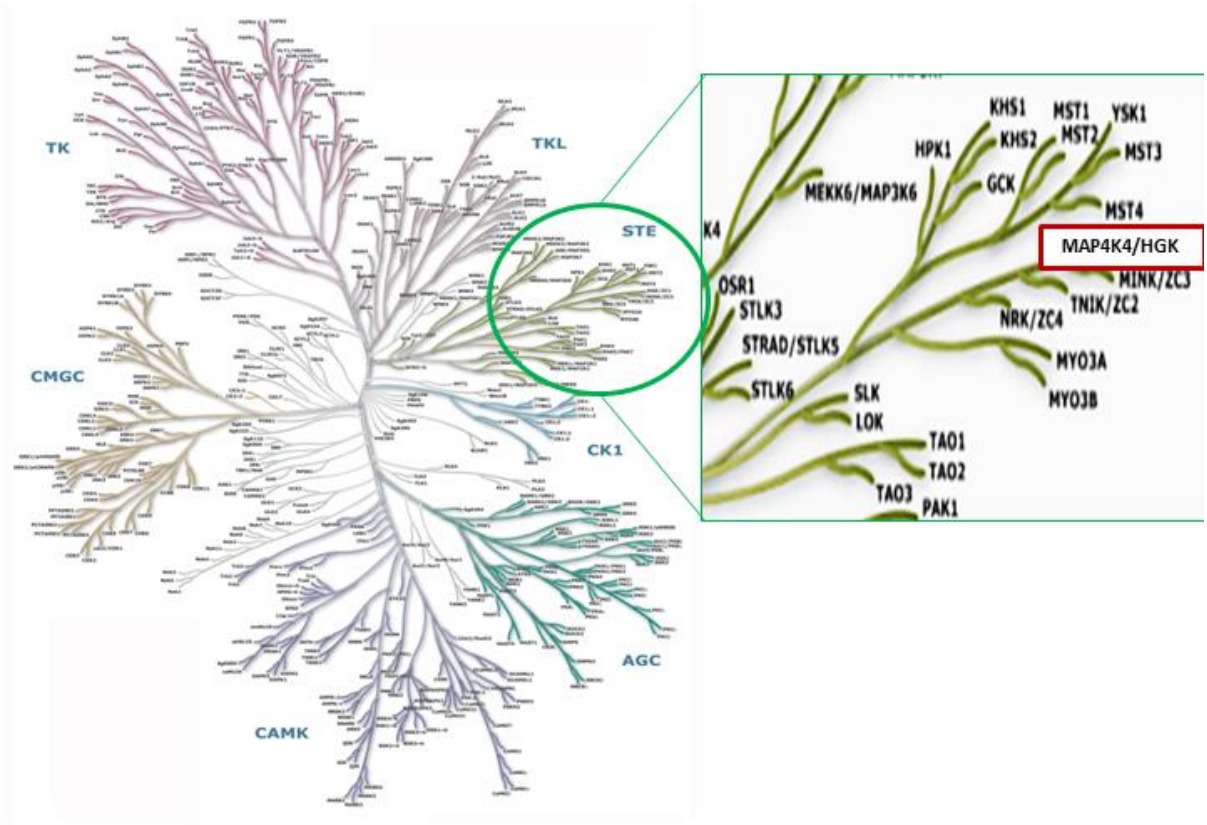


Figure 1.8 Dendogram showing the protein kinase families as per protein sequence homology. There are seven major families, namely, AGC, CAMK family, Casein kinase 1 (CK1) family, CMGC family (including CDK, MAPK, GSK3 and CLKs), STE family (activates MAPK family), tyrosine kinases (TKs) and tyrosine kinase-like (TKL) kinases (Manning et al. 2002). Modified from Manning et al. 2002

1.7.2 Structure

Kinases display a well conserved structure within the ATP-binding pocket, despite structural differences outside of this region between families (Engh & Bossemeyer 2002). The ATP-binding site presents five distinct areas; the sugar and adenine regions, the hydrophobic pocket, hydrophobic channel and phosphate binding region (Engh & Bossemeyer 2002; Shchemelinin et al. 2006). ATP comprises two halves and each needs a different environment for binding; the kinases' triphosphate-binding surface is formed by a cluster of conserved residues, most of which directly take part in catalysis (e.g. Lys72, Asp184, Asn171 and Lys168) (Engh & Bossemeyer 2002). In the active complex, ATP phosphates interact with the backbone through hydrogens of the Glycine flap (Glycine-rich loop that binds the ATP molecule at the binding site), though these interactions are only conserved within the family and not the wider kinome. The adenosine-binding groups, however, are less well conserved. The adenosine region is hydrophobic and at least two hydrogen bonds are formed by the N-1 and N-6 amino groups of the adenine ring with the NH and carbonyl groups of the adenine hinge region (Engh & Bossemeyer 2002). The kinases' ATP-binding site offers a surface area that immerses the nucleotide and adjacent sites allow for larger molecules including drugs to bind. This is also known as the hydrophobic pocket and channel and ranges within the kinase family as well as playing a role regarding inhibitor selectivity (Engh & Bossemeyer 2002).

The ATP-binding site is targeted by kinase inhibitors as, historically, the principal method for kinase inactivation. This site plays a crucial role in inhibitor binding and selectivity, since the many 'type I' inhibitors compete with ATP at the binding site (Shchemelinin et al. 2006) . As such this site is targeted for drug development, through screening of compound libraries complying in size, polarity and other parameters that would allow them to fit into the ATP binding site. Methodologies for detection of kinase inhibition in compound screening employ fluorescently or radioactively labelled phosphates or peptides. The similarity of the ATP

binding pockets across closely and even distantly related protein kinases is a principal challenge to successful drug development, but one that can be addressed through approaches like large scale kinase panel screenings, screening initiatives and crystallographic studies to define and impart appropriate compound selectivity (Anderson et al. 2006).

By contrast, allosteric binding sites are recognised by so-called 'type II' inhibitors and render the catalytic domain inactive by changing its conformation, and these can also be located at surfaces away from the ATP-binding pocket (Engh & Bossemeyer 2002). Drugs in principle can also bind to substrate interaction sites, providing an alternative route for selectivity, but inhibition of high-avidity protein interactions has proven challenging (Engh & Bossemeyer 2002). Further, inhibitors that bind both the ATP site and the substrate pocket can confer increased specificity (Anderson et al. 2006) as well as disruption of interactions with secondary messenger such as calcium for CaMKII. The idea of interrupting only a subset of the kinase's functionality by interrupting specific localisation (such as membrane targeting rather than cytosolic localisation) represents another possible methodology for kinase targeting (Churchill et al. 2005; Dorn & Mochly-Rosen 2002). This could potentially be used for targeting mutant versions of kinases which cause genetic cardiomyopathies, in the way that BCR-ABL is stabilised (and inhibited) in its inactive state by Imatinib binding to the altered ATP binding site in the mutant form only (Kerkelä et al. 2006).

1.7.3 Mitogen-activated protein kinases (MAPKs)

MAPKs' signal transduction pathways are ubiquitous and highly evolutionarily conserved mechanisms that play a major role in eukaryotic cell regulation. They enable cells to integrate responses to diverse stimuli such as hormones, growth factors, cytokines, agents acting through G protein-coupled receptors, transforming growth factor (TGF)-β-related

agents which act via Ser/Thr kinase receptors, pathogens-associated molecular patterns (PAMPs) and danger-associated molecular patterns (DAMPs) that recruit pattern recognition receptors (PRRs), and environmental stresses (these are known as stress-activated protein kinases – SAPKs) (Chang & Karin 2001; Keshet & Seger 2010; Rincón & Davis 2009; Rose et al. 2010). MAPK pathways are therefore involved in a wide range of cellular functions such as cell division, apoptosis, protein biosynthesis, differentiation, gene expression and metabolism. Their dysregulation ultimately leads to functionally relevant signalling abnormalities in a number of pathologies including cancer, diabetes, inflammatory and cardiovascular disease.

MAPKs are activated by dual phosphorylation of their conserved Thr/Tyr residues and target Ser/Thr residues of downstream kinases, scaffold proteins, and other substrates (Kyriakis & Avruch 2012; Chang & Karin 2001; Keshet & Seger 2010). MAPK signalling is often described in terms of three-tiered kinase cascades. The cascade begins with a MAP kinase kinase kinase (MAPKKKs or MAP3Ks) such as MEKK1, TAK1 and ASK-1, which function most proximally to the initiating signal. MAP kinase kinases (MAPKKs or MAP2Ks) such as MKK4, MKK7, MKK3 and MKK6 operate downstream from MAP3Ks. The cascade concludes with terminal MAPKs and SAPKs such as ERK, JNK and p38, which are the final effectors. In general, a MAP3K phosphorylates a MAPK2, leading to the phosphorylation (and activation) of a MAPK, which in turns acts upon (through phosphorylation) non-kinase substrates including transcription factors and MAP kinase-activating protein kinases (MAPKAPKs). However, in addition to this familiar scheme, MAPKKK kinases (MAPKKKKs or MAP4Ks) activate MAP3Ks, which are able to attach to the plasma membrane in response to activation (Qi & Elion 2005), as shown in **Fig. 1.9.** MAP3Ks possess bulky regulatory domains activated by interaction with small GTPases (Rho and Ras regulators) and are involved in ubiquitination, autoinhibition and oligomerisation (Kyriakis & Avruch 2012; Chang & Karin 2001; Keshet & Seger 2010; Rincón & Davis 2009). Rap2-GTP interacts with MAP4Ks via its C-terminal citron homology domain (CHD) and this enhances

MAP4K4 related JNK activation (Machida et al. 2004). MAPKs are also able to associate with scaffolding proteins and influence their activity and localisation, resulting in gene transcription, inflammatory, apoptotic, growth and differentiation signals (Morrison & Davis 2003; Qi & Elion 2005).

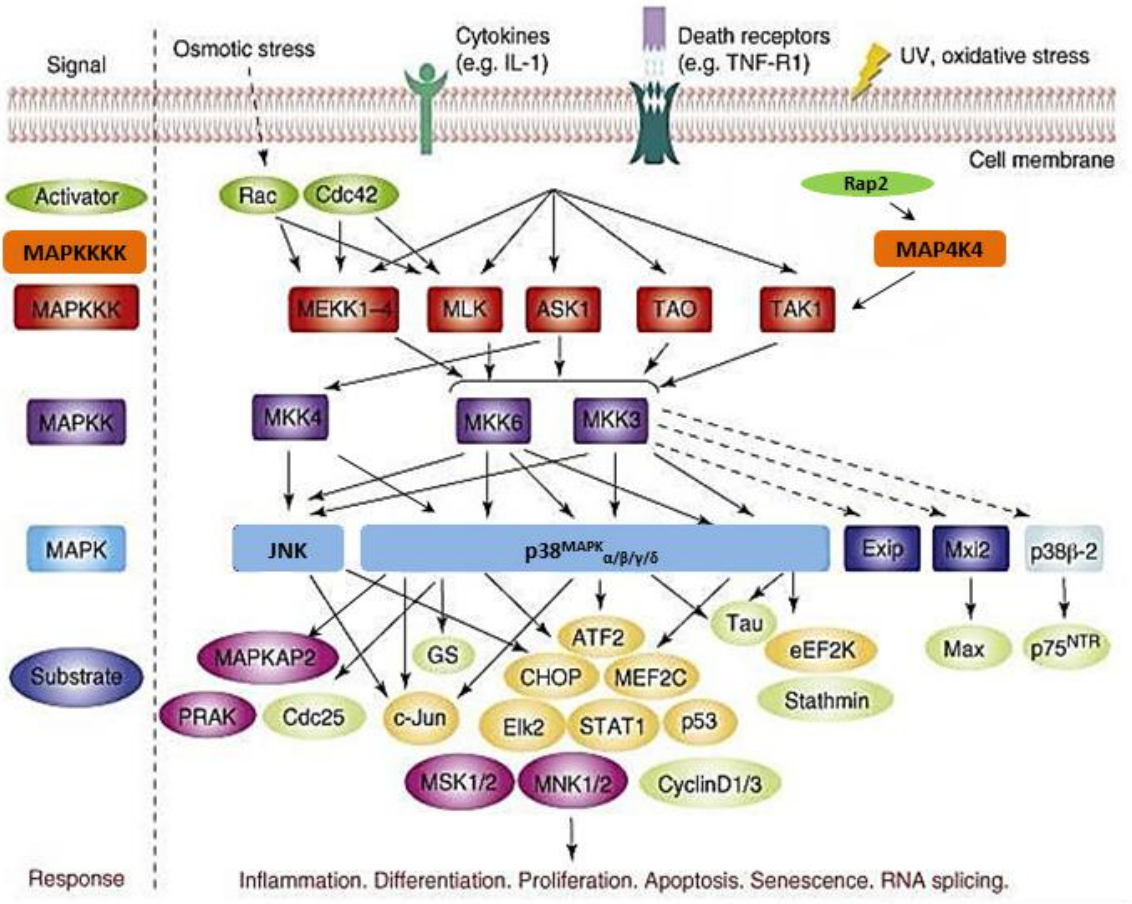


Figure 1.9 Scheme showing signal transduction pathways activated by various kinases (Coulthard et al. 2009). Cell type and stimuli (intra or extracellular) define the transduction which is activated; with the three MAPK signalling pathways culminating in the activation of SAPKs (ERK1/2, JNK1/2/3, p38α/β/Y/δ or ERK5). This results in proliferation, differentiation, cell motility, apoptosis, osmoregulation and metabolism. Rap2-GTP interacts with MAP4K4 via its C-terminal citron homology domain (CHD) and this has been shown to enhance MAP4K4 related JNK activation (Machida et al. 2004). Further, MAP4K4 couples TAK1 and JNK1/2 and regulates cell death (Xie et al. 2007a). Adapted from Coulthard et al. 2009.

1.8 MAPKs in heart failure

Kinases have been shown to perform functions in cardiac development (Rose et al., 2010) as well as during cardiac disease progression, including DCM, hypertrophy and I/R injury (Wang 2007; Marber et al. 2011; Rose et al. 2010; Marber et al. 2010). As previously mentioned, MAPKs signalling involves autophosphorylation, phosphorylation and dephosphorylation events in a kinase cascade encompassing four stages: MAP4Ks→MAP3Ks→MAP2Ks→MAPKs. The terminal MAPKs JNK, ERK1/2 and p38 phosphorylate non-kinase substrates (i.e. transcription factors), scaffolding proteins and other kinases (Rose et al. 2010; Wang 2007; Kyriakis & Avruch 2012).

MAPK signalling is an important feature in human heart failure; whereby cardiomyocyte cell death is not matched by cell replacement following compensatory mechanisms (macrophage infiltration, cardiac remodelling) (Bing 1994). This is illustrated by the presence sporadic cell death in failing dilated human hearts (Narula et al. 1996; Olivetti et al. 1997) with increased prevalence in deceased heart failure patients over those who died due to acute MI (Kytö et al. 2004). The idea that protein kinases are able to regulate cell death in the cardiac setting is central to this thesis. These are thought to fulfil important roles in the cause of HF post DCM, HCM and MI: as key examples, PKC isozymes (PKCα, β, ε, λ and ζ), AMPK and protein kinase D (PKD) have defined roles in hypertrophy and HF, others (CaMKII, ROCK1 and TAK1) variably trigger cell death and survival, and another subset (MAP4K4, PKCδ and PKCθ) act more uniformly as death agonists (Hallows et al. 2010; Sin & Baillie 2012; Zhang et al. 2000; Fiedler et al. 2014a; Fiedler et al. 2014b; Fiedler et al. 2014c; Potts et al. 2005; Palaniyandi et al. 2008). Here we will focus on the MAP kinases and their involvement in HF.

1.8.1 MAP kinases in heart failure

ERK1/2 are the first described MAPK; they are activated by tyrosine kinase receptors and GPCRs, are known to protect against cell death and trigger cardiac hypertrophy (although it is not necessary for hypertrophy development) (Rose et al. 2010; Wang 2007). ERK1/2 inhibition or deletion was shown to sensitise the heart to failure after exposure to long term pressure overload concomitant with increased TUNEL staining (Purcell et al. 2007). MEK1 transgenic mice showed increased ERK1/2 phosphorylation levels and I/R related cell death was reduced (Bueno et al., 2000). However, Erk2 heterozygous mice presented enhanced infarction areas and TUNEL staining, suggesting that ERK2 is involved in apoptosis prevention (Lips et al. 2004). ERK1/2 play a role in cGMP-dependent protein kinase (PKG)-mediated cardioprotection in adult cardiomyocytes, as shown by the decreased levels of infarct size and cell death after PKG pharmacological inhibition or genetic silencing, concomitant with increased phosphorylated ERK1/2 levels (Das et al. 2008). GATA4 phosphorylation has also been proposed as the cardioprotective mechanism for ERK1/2 in NRVCs (Aries et al. 2004; Liang et al. 2001), although in adult cardiomyocytes GATA4 acts as a survival factor (Huang et al. 2008). In cardiomyocytes, NFkB activation was observed as IL-10 inhibited TNFα related apoptosis through ERk1/2 upregulation (Dhingra et al. 2009). Pharmacological inhibition of ERK1/2 (PD98059) reduced the protective effect of IL-10 against TNFα-induced activation of NFkB as well as cardiomyocyte apoptosis (Dhingra et al. 2009). Further, protection independent of ERK1/2 activity was observed after deletion of Ask1 on c-raf-1 knockout murine model, which presented reduced apoptosis, dilation and lethality with no changes to ERK1/2 activity observed (Yamaguchi et al. 2004).

JNK is activated by many diverse MAP3Ks (MEKK1, MEKK2, MEKK3, Mixed Lineage Kinase-2 and -3 [MLK2/MEKK10, MLK3/MEKK11]), working through the MAP2Ks MKK4 and MKK7 (Kyriakis & Avruch 2012). JNK activation can take place due to a number of different stimuli (including inflammatory cytokines, hyperosmolarity, I/R, UV, heat shock, oxidative stress, DNA damage and growth factors), it is activated by mechanical overload in the myocardium and I/R, and is implicated in heart remodelling, hypertrophy and cardiac cell

death (Bogoyevitch et al. 1996; Ramirez et al. 1997; Wang et al. 1998). The use of JNK inhibitors in I/R resulted in reduced apoptosis and infarct size, indicating a role for JNK in promoting cell death under ischemic stress (Ferrandi et al. 2004; Milano et al. 2007). In support of this, continuous JNK activation triggered procaspase-9 and -3 activation, Bax-Bad interaction (Baines et al. 2002) and AIF translocation to the nucleus (Song et al. 2008; Juan Zhang et al. 2009). However, JNK inhibitors have been reported to inhibit multiple other kinases *in vitro*, including ERK, with similar potency to JNK (Wei et al. 2011). As such, the JNK cardioprotective pathway is controversial, as its activation and inhibition have both been associated with cardiomyocyte survival (Kaiser et al. 2005). Dominant-negative mouse models showed decreased cell death after I/R injury, yet pharmacological inhibition in vitro increased apoptosis (Shao et al. 2005). Combined JNK/p38 inhibition increased I/R injury and p38 inhibition rescued it, suggesting JNK mainly signals for survival (Kaiser et al. 2005). JNK knockout mice showed increased cell death and reduced fractional shortening after TAC, supporting the notion of JNK mainly promoting survival (Tachibana et al. 2006). It has been shown that JNK1 is able to protect mouse heart from short-term ischemia (5 min) but not long-term (20 min) (Wei et al. 2011), suggesting a time-dependent switch in function. This suggests that JNK1 has extensive influence in reperfusion injury; illustrated by the fact that 5 min of ischemia caused more damage than 20 min when the inhibitor (SP600125) was present in both conditions (Wei et al. 2011).

p38 exists as four isoforms of which p38α and p38β are ubiquitously expressed and relevant in the heart. p38 functions in at least wo pathways: the established one which is analogous to the JNK and ERK1/2 pathways involving MAP3Ks and MEKK1-4 upstream, TAK1 and ASK1 to activate the MAP2K level (MKK3, MKK6 and perhaps MKK4) and the non-conventional activation pathway through the TAK1-binding protein TAB1 and the necrosis-mediated death-receptor pathway (De Nicola et al. 2013). P38 has been shown to regulate cardiac gene programs for development of cardiac remodelling, cardiomyocyte hypertrophy, metabolism, contractility, proliferation and cell death (Wang 2007). However, the mechanism

leading to cardiac pathological phenotypes is controversial (Wang 2007). P38 activation has been reported to be involved with pathological hypertrophy concomitant with high levels of p38 activity in injured heart muscle contributing to maladaptive remodelling as defined by contractility and ECM deposition (Asrih et al. 2013). During ischaemia, inhibition of p38 has been shown to have a cardioprotective role in both pharmacological and genetic models. As such, a p38α/β inhibitor was tested in clinical trials for cardiovascular and respiratory diseases (Denise Martin et al. 2012). However, outcome of the trial was neutral compared to placebo for cardiovascular endpoints even though it was well tolerated (Newby et al. 2014; O'Donoghue et al. 2016; Kompa 2016). Cardiospecific p38 knockout mice developed to adulthood, were fertile and exhibited normal cardiac structure and function (Nishida et al. 2004). When subjected to pressure overload, these mice developed significant levels of cardiac hypertrophy, dysfunction, heart dilatation, cardiac fibrosis and apoptosis. This suggests that p38 plays a critical role in cardiomyocyte survival (Nishida et al. 2004).

Heart failure hereditary cardiomyopathies have been shown to cause abnormal activation of MAPKs. Mutations to Lmna (which encodes L-type nuclear lamins) cause laminopathy, which is a cardiomyopathy with or without different types of skeletal dystrophy that leads to deathly arrhythmias and heart failure (Lu et al. 2011); cardiac dysfunction caused by Lmna was improved by pharmacological inhibitors which target the terminal MAPKs (ERK1/2, JNK and p38) as well as deletion of ERK1 (Chatzifrangkeskou et al. 2016; Wu et al. 2011; Laurini et al. 2018).

ERK5 is the least studied MAPK and its activation is induced by MEK5 (MAP2K) after MAP3Ks activation (MEKK2 and MEKK3) (Rose et al. 2010). Its activation can be induced by various growth factors (such as EGF, NGF, VEGF and FGF-2), oxidative and hyperosmotic stress, serum and UV. It has antiapoptotic and antihypertrophic roles in the myocardium (Rose et al. 2010).

1.8.2 MAP3 kinases in heart failure

Apoptosis signal-regulating kinase 1 (ASK1/MEKK5) is activated by stress stimuli (TNF-a, ROS, Fas) and phosphorylates MKK4/7, MKK3/6, which in turn activates JNK and p38 (Ichijo et al. 1997). It is concerned with growth and death signals in cardiomyocytes in response to pathological stimuli (Choi et al. 2011). Recently, ASK1 has been shown to contribute to acute ischemia/reperfusion injury: using an ASK1 inhibitor, infarct size reduction was observed in an isolated perfused heart model of cardiac injury (Lanier et al. 2017). Tumour necrosis factor receptor-associated factors (TRAFs) are crucial to ASK1 regulation, since TRAF2, 5 and 6 increase ASK1 activity (Nishitoh et al. 1998). Deletion of TRAF2 and 6 in mice showed a reduction in JNK and p38 activity post ASK1 activation by hydrogen peroxide, suggesting that this pathways is important in ROS induced mechanisms involving ASK1 (Noguchi et al. 2005).

Cardiospecific and inducible ASK1 overexpression showed no induction of hypertrophy or pathology at 3 and 12 months of age and when stimulated with isoproterenol treatment or pressure overload the response was identical to controls. However, ASK1 overexpression promoted cardiomyopathy and increased TUNEL upon pressure overload stimulation and MI. Furthermore, MKK4/4 and JNK1/2 (but not p38 or ERKs) and Bax were heavily activated post pressure overload stimulation. Calcineurin Aβ deletion reduced ASK1-associated cardiomyopathy following 8 weeks of pressure overload, suggesting that the mechanism at play is calcineurin-dependent (Liu et al. 2009). These studies suggest that ASK1 plays a critical in cell death rather than growth responses.

In addition, ASK1 knockout mouse hearts showed no morphological or histological defects, along with normal structure and function (Yamaguchi et al. 2003). Knockout mice subjected

to coronary artery ligation or TAC showed significantly smaller increases in left ventricular end-diastolic and end-systolic ventricular dimensions and smaller decreases in fractional shortening in both models compared to wild-type (Yamaguchi et al. 2003). TUNEL-positive cardiomyocytes were decreased in ASK1 knockout mice after MI or TAC compared to wild-type (Yamaguchi et al. 2003). Furthermore, overexpression of a constitutively active mutant of ASK1 induced apoptosis in rat neonatal cardiomyocytes (Yamaguchi et al. 2003). ASK1 kinase activity was shown to increase in wild-type mouse hearts after MI or TAC (Yamaguchi et al. 2003). Therefore, ASK1 plays a crucial role in the regulation of left ventricular remodelling via promotion of apoptosis (Yamaguchi et al. 2003).

RAF-1 and ASK1 interact in vitro and in vivo and inhibit apoptosis through mechanisms independent of MEK-ERK1/2 (Chen et al. 2001; Yamaguchi et al. 2004). RAF-1 inhibits ASK1 by binding the N-terminal regulatory fragment in HeLa cells and hence antagonises ASK1-induced apoptosis (Chen et al. 2001). *Raf-1* knockout mice present left ventricular systolic dysfunction, heart dilation, increased apoptosis and increased ASK1 activation without lethality. These mice were subjected to ASK1 deletion and displayed improved heart function, reduced dilation and fibrosis, possibly as a result of the decrease in TUNEL positive cells (Yamaguchi et al. 2004).

Ras provides the molecular interaction between receptors and kinases to activate the Ras-Raf-MEK-ERK1/2 pathway (Kyriakis & Avruch 2012). Ras is a small GTP-binding protein that activates Raf (a MAP3K), which activates MEK1 (MAP2K1) and ERK1/2 in the cytosol. This pathway is activated by stimuli that trigger mitosis such as growth factors (EGF and PDGF), insulin or cytokines such as interleukin-1β (IL-1β) (Wan et al. 2006; Yu et al. 2008) and TGF-β (Ieda et al. 2009; Matsumoto-Ida et al. 2006).

MAPK/ERK kinase kinase-1 (MEKK1) is thought to mediate cardiac hypertrophy activated by Gαq in mice as its overexpression showed cardiac enlargement and mechanical dysfunction;

and this is thought to act through JNK since MEKK1 homozygous disruption in embryonic stem cells impaired JNK activity selectively induced by oxidative stress (Minamino et al. 2002). This hypothesis proposing a protective role against hypertrophy is further strengthened by the findings showing that *Mekk1*$^{-/-}$ mice displayed reduced JNK activity levels, cytokine induction, apoptosis and dysfunction (Sadoshima et al. 2002). Previously discussed evidence on JNK/p38 dual inhibition (Kaiser et al. 2005) and *Jnk1*-null mice showing increased I/R injury and cell death (Tachibana et al. 2006) support the notion that the phenotypic effects of MEKK1 ablation are attributable to the experimentally observed lack of JNK activation due to oxidative stress in embryonic stem cells.

TAK1 (MAP3K7) is the best described activating target of MAP4K4 which is necessary for the activation of JNK, as suggested by the TAK1 kinase-negative mutant (Yao et al. 1999). TAK1 is involved in many signalling pathways which may contribute to its role in inducing hypertrophy, fibrosis, myocardial dysfunction, cell death and heart failure (concomitant with p38 activation), as shown by the induction of these pathological phenotypes in adult mouse hearts as a result of an activating TAK1 mutation in vivo a week after TAC (Zhang et al. 2000). TAK1 is a constituent of many membrane receptor complexes involved in cell death (i.e. TNFR1 and TLRs) and TGF-β is upregulated in rodents and humans when cardiac hypertrophy is present as well as by TAK1 activity in cardiomyoctes (Hein et al. 2003; Zhang et al. 2000; Teekakirikul et al. 2010). Further, TAK1 is activated in cultured cardiomyocytes induced by C2-ceramide and hydrogen peroxide, causing cell death via JNK activation concomitant with TAK1 activation via MAP4K4 (Fiedler et. al., under revision). In addition, JNK activation in the adult heart using a tamoxifen-inducible model was shown to cause lethal cardiomyopathy concomitant with ECM remodelling and loss of connexin 43 which led to gap junction signalling dysfunction (Petrich et al. 2004; Petrich et al. 2003; Ursitti et al. 2007). Further, TAK1 was found to be activated in NRVC due to oxidative stress (Chen et al. 2000).

1.8.3 MAP4K kinases in heart failure

The S. cerevisiae Sterile 20 (STE20) family of serine-threonine protein kinases can be divided into two subgroups based on the positioning of their catalytic domains: the p21-activated kinases (PAKs, C-terminals) and the germinal center-like kinases (GCKs, N-terminals) (Delpire 2009).

P21-activated protein kinases have been implicated in heart failure; cardiospecific Pak1 deletion in mice led to increased hypertrophy induced by angiotensin II or pressure overload (Liu et al. 2011). The absence of Pak1 increased apoptosis in response to aortic constriction, with impaired systolic function, ventricular dilation and fibrosis (Liu et al. 2011). This suggests a cardioprotective role for Pak1.

MAP4K4 (Mitogen-activated protein kinase kinase-4 (MAP4K4), also known as hematopoietic progenitor kinase-/germinal center kinase-like kinase (HGK) or Nck interacting kinase (NIK)) is a member of the STE20 family of serine-threonine protein kinases that mediate varied responses such as motility, fate, cell cycle and stress (Puri et al. 2008). TNIK (Traf and Nck-interacting kinase) and MINK (Misshapen/NIK-related kinase) are the most similarly related, and are members of the germinal center kinase (GCK) group.

Most Ste20 family kinases are activated through phosphorylation of a primary site in the activation segment of the kinase (Delpire 2009), as this stabilises the activation segment in a conformation that is appropriate for substrate binding (Delpire 2009). Numerous Ste20 kinases may need further phosphorylation at secondary sites by upstream kinases (Ras-GTP, Rap2-GTP, Cdc42-GTP, Rap1-GTP and Rac1-GTP) or from autophosphorylation to achieve full activity (Delpire 2009). In mouse, MAP4K4 is activated at aspartate (D) 152 as replacing it with aspargine (N) abolished kinase activity (Su et al. 1997). In human, many

amino acid residues in the N-terminal kinase domain have been implicated in MAP4K4 regulation such as lysine 54 (K54), aspartate 153 (D153), threonine 181 (T181), threonine 187 (T187) and threonine 191 (T191) (Wright et al. 2003; Vitorino et al. 2015; Yue et al. 2014). Mutation of T187 to E increased catalytic activity as shown by in-vitro kinase assays using purified MAP4K4 mutant protein as an enzyme and myelin basic protein (MBP) as the substrate (Wright et al. 2003), suggesting it as a phosphorylation site. T191 mutation to glutamate (E) or K54 to arginine (R) was found to abolish kinase activity completely, indicating these residues are required for activity.

The C-terminal domain of MAP4K4 possesses a citron-homology domain (CNH) which determines its association with other proteins (Wright et al. 2003). MAP4K4 interaction with Rap2 requires the presence of the whole CNH domain (Machida et al. 2004), which also binds human guanylate-binding protein (hGBP) (Luan et al. 2002). The C-terminal domain is involved in regulation of activity through acting upon protein-protein interaction; full JNK activation by MAP4K4 necessitates both MAP4K4 kinase activity and the C-terminal domain which mediates MAP4K4 association with MEKK1 (Su et al. 1997). Whilst protein-protein interaction seems to determine MAP4K4 kinase activity, conversely, MAP4K4 interaction with other proteins does not need its kinase activity; wild-type MAP4K4 and kinase-inactive MAP4K4 showed similar binding affinity to transcription factor STAT3 in human embryonic kidney (HEK) cells, as assessed by co-immunoprecipitation (Wright et al. 2003), suggesting that kinase-dead Map4K4 prevents STAT3 phosphorylation although MAP4K4 is not a STAT3 kinase. In agreement with this, MAP4K4 interacts with PYK2 (proline-rich tyrosine kinase 2) through the C-terminal portion and association does not necessitate catalytic activity (Loftus et al. 2013).

Many STE20 protein kinases in mammalian tissues may overlap in their substrates and exhibit functional redundancies. Although originally studies demonstrated a role for MAP4K4 upstream of JNK signalling cascade (Liu et al. 1999; Collins et al. 2006; Su et al. 1997; Yao

et al. 1999), these conclusions were based on co-transfection, dominant-interfering mutations, and high expression of exogenous MAP4K4. In several later loss-of-function studies, MAP4K4 was not required for MAPK activation, as expected (Danai et al. 2013; Aouadi et al. 2009; Wang et al. 2013), though short- and long-term adaptations must be considered as a basis for these negative results.

Further, neither siRNA mediated depletion nor adenoviral overexpression had an effect on JNK in HEK cells (Danai et al. 2013), Further, loss of MAP4K4 did not inhibit JNK phosphorylation by TNFα in adipocytes or skeletal muscle (Tang et al. 2006; Wang et al. 2013), suggesting that the activation of JNK is independent of MAP4K4 in some cell types. However, MAP4K4 knockdown in macrophages was protective and reduced mortality in murine inflammatory response in vivo and in vitro through activation of TNFα expression independent of the JNK1/2, p38 and NFkB pathways (Aouadi et al. 2009). JNK siRNA knockdown decreased triglyceride deposition in adipocytes whilst MAP4K4 knockdown increases their accumulation (Danai et al. 2015) and TNFα activation by JNK is unaffected by MAP4K4 conditional knockdown in endothelial cells (Flach et al. 2015). Compensatory mechanisms might be responsible for these conflicting results. Recently, studies have indicated a high level of overlap and redundancy in MAP4K4 function in the Hippo pathway (Zheng et al. 2015). The most closely related kinases to MAP4K4, TNIK (Traf and Nck-interacting kinase) and MINK (Misshapen/NIK-related kinase) might play a role in this context in some settings. In a model of neurodegeneration in mice, MAP4K4, MINK1 and TNIK act redundantly to regulate DLK/JNK signalling and targeting all three but not any individually is required to protect neurons (Larhammar et al. 2017). This circuit has importance for the present study, as all ATP-competitive inhibitors of MAP4K4 also inhibit TNIK and MINK, given their identical amino acid sequence in the ATP-binding domain.

Alternative signalling components to JNK are employed by MAP4K4 to mediate its effects. The NFkB pathway has been found to be employed by MAP4K4 to increase expression of

adhesion molecules ICAM-1 and VCAM-1 in response to TNFα, independent of JNK signalling (Flach et al. 2015). Small molecule inhibitors of MAP4K4 activity dampens TNFα upregulation in a lipopolysaccharide challenge model (Ammirati et al. 2015), in agreement with findings using siRNA mediated MAP4K4 knockdown (Aouadi et al. 2009). However, T-cell specific MAP4K4 knockout (CD4-Cre) promotes Th17 differentiation and accumulation in adipose tissue which results in insulin resistance in vivo (Chuang et al. 2014). On the other hand, another study recently reported that the same cell specific KO led to inhibition of CD4 T-cell proliferation and enhanced T-cell differentiation in vitro (Huang et al. 2014). The dichotomous results in T cells could be explained by the fact that on study was performed in vivo, using animals that were 2-26 week old (Chuang et al. 2014) and the second study was performed in vitro utilising cells isolated from 8-12 week old mice (Huang et al. 2014). More recently, MAP4K4 deletion in CD4(+) T cells was found to increase macrophages, lymphocytes and neutrophils and to affect CD4(+) T cell differentiation in a model of lung inflammation in mice (Jin et al. 2016).

In metabolism, MAP4K4 was initially shown to increase glucose transport and triglyceride synthesis upon knockdown (Tang et al. 2006). It was also reported to negatively regulate mTOR in relation to mediating translation of key adipogenic regulators (Guntur et al. 2010). MAP4K4 was found to regulate SREBP-1 and lipogenesis in an mTOR-dependent fashion (Danai et al. 2013) and to be necessary for full activation of AMPK in response to nutrient stress signals. However, adipose-specific MAP4K4 KO obese mice show no metabolic phenotype indicating that in vivo these effects are confounded by complex regulation or redundancy in the context of adipose tissue (Danai et al. 2015).

Various studies have implicated MAP4K4 as an upstream regulator of proteins involved in cytoskeletal dynamics or adhesion such as Arp2 (LeClaire et al. 2015), Farp1 (Schwaid et al. 2015), moesin (Vitorino et al. 2015), IQSEC (Yue et al. 2014) and Pyk2 (Loftus et al. 2013). MAP4K4 deletion in endothelial cells caused reduced migration and disrupted angiogenesis

(Vitorino et al. 2015). MAP4K4 has also been shown to modify endothelial barrier function and permeability through Rap GTPases (Pannekoek et al. 2013). Other substrates of MAP4K4 that have been reported are ERM (Baumgartner et al. 2006) and the Na^+-H^+ exchanger NHE1 (Yan et al. 2001).

The MAP4K4-TAK1-JNK pathway is believed to be involved in heart failure. MAP4K4 is highly enriched in the heart and was first described as implicated in this pathway in signalling to TNFα and other inflammatory cytokines for the activation on JNK but not p38 (Yao et al. 1999). MAP4K4 is implicated in human cancer as it is able to switch off Smad proteins and control TGF-β-BMP signals (Kaneko et al. 2011), involved in causing larger tumours and poor prognosis (Liu et al. 2011; Liu et al. 2011). As previously mentioned, increased MAP4K4 activity is linked to obesity and diabetes (Elbein et al. 2009; Isakson et al. 2009; Sartorius et al. 2012), it is involved in the immune response (Mack et al. 2005; Chuang et al. 2014) and its knockdown protects against LPS-induced lethality in macrophages (Aouadi et al. 2009). In cancer cells, p53 upregulates MAP4K4 and activates JNK to induce apoptosis (Miled et al. 2005). *SOX2* gene silencing induces apoptosis via MAP4K4 activation (Chen et al. 2014). In beta pancreatic cells, MAP4K4 knockdown brings about survival (Bouzakri et al. 2011). Further, MAP4K4 is an upstream regulator of DLK/JNK signalling in neurons (Larhammar et al. 2017).

MAP4K4 is activated in failing human and murine hearts (driven by I/R, mechanical load, myh6 (cardiomyocyte specific)-TNF-α or $G_q$overexpression) and in rat neonatal cardiomyocytes (RVNM) undergoing cell death. *In vitro*, this is mediated by TAK1-JNK and TNF-α is the most potent activator of this pathway (Fiedler et al. in revision). Furthermore, cardiospecific overexpression of MAP4K4 (Myh6-MAP4K4) increases cell death and cardiac dysfunction in combination with either pressure overload (Fiedler et. al, in revision) or genetic stimuli. The latter, was induced by G_q overexpression driven by the Myh6 promoter, which results in mild dilated cardiomyopathy (Sano et al. 2004; Hayakawa et al. 2003).

Cardiospecific MAP4K4 overexpression subjected to Myh6-G_q overexpression induced early mortality within 3 months (heart failure concomitant with apoptosis) (Fiedler et. al., in revision). Further, mice overexpressing MAP4K4 and Myh6-G_q displayed increased Rho effector-associated coil coil protein kinase 1 (ROCK) cleavage (cleaved by caspase-3 in human heart failure) as well as increased caspase-3 activity (Chang et al. 2006). Similarly, MAP4K4 overexpression in RNVM also induced apoptosis (Fiedler et. al., in revision) and MAP4K4 suppression by RNA interference, dominant-negative mutation and pharmacological inhibition was protective against cell death stimuli. In human induced pluripotent stem cell-derived cardiomyocytes (iPSC-CMs) shRNAmir-based knockdown was also protective against oxidative stress (Fiedler et. al., in revision). Taken together, these data suggest an important role for MAP4K4 in potentiating diverse pro-cell death stimuli that leads to heart failure.

The evidence regarding the role of MAP4K4 in the heart specifically to date is incomplete. On the other hand, it has been suggested that MAP4K4 plays a pathobiological role, as illustrated by its interaction with TAK1 and downstream activation of JNK (Yao et al. 1999) and p38 (Zohn et al. 2006). Particularly, because both of these kinases have been described to have pro-death functions in cardiac muscle cell (Fiedler et. al., in revision; Rose et al. 2010; Zhang et al. 2000). This, in turn, proposes MAP4K4 as a sensible starting point for the development of novel small-molecule inhibitors (Fiedler et. al., in revision).

1.9 Induced pluripotent stem cells (iPSCs) as a tool for drug discovery

The main limitations of animal models (cost, expertise and time required to maintain animal colonies and perform surgical procedures, physiological fidelity to human) have stirred scientists in the direction of human tissue modelling using induced pluripotent stem cells (iPSCs) (Cibelli et al. 2013; Ebert et al. 2012). Particularly, in terms of safety evaluation, further complexity is added by the fact that agents are designed to act on a human target,

and therefore this complicates the translation of results from non-human animal models to human toxicity (Ebert et al. 2012). Although advances in iPSC technologies are not able to replace animal models fully when it comes to the study of disease mechanisms and drug pre-clinical evaluation, they present advantages over classical *in vitro* models, particularly by utilising integrated high-performance approaches (Ebert et al. 2012). Mouse somatic cells (such as skin fibroblasts) were shown to be reprogrammed into a pluripotent state by using a cocktail of four reprogramming factors present in embryonic stem cells (OCT4, SOX2, KLF4 and c-MYC), thus generating cells with similar gene expression profile and developmental potential to embryonic stem cells (ESCs) and were called iPSCs (Takahashi & Yamanaka 2006). Only a year later two research teams had been able to generate this cell type from human fibroblasts (Takahashi et al. 2007; Yu et al. 2007).

Human iPSC technology evolved rapidly since and groups around the world have managed to turn many cell types to iPSCs and then differentiate them into many human cell types (neurons, cardiomyocytes, and hepatocytes) and patient-specific adult cells for drug discovery and disease modelling. These technologies have advantages such as their human origin, easy accessibility, expandability, avoidance of ethical concern linked to human ESCs and the potential for the development of personalised medicine using patient-specific iPSCs (Shi et al. 2016).

In terms of the advances reported in the field, reprogramming technology has been able to bypass problems such as genomic integration (Robinton & Daley 2012; Yu et al. 2011) and reprogramming efficiency of iPSC lines (Dick et al. 2011; Rais et al. 2013). In addition, much work has been carried out in the area of characterisation of iPSCs, their suitability and safety for cell therapy as well as the characterisation of specific disease models (Robinton & Daley 2012). Further, the idea of correcting single-gene mutations responsible for diseases like cystic fibrosis and thalassemia for cell transfusion therapies using gene editing strategies have been explored (Chang & Bouhassira 2012; Hanna et al. 2007; Somers et al. 2010;

Wang et al. 2012). In particular, CRISPR-Cas9 technology permits the fast generation of genetically defined human iPSC-based disease models (Shi et al. 2016). Also, these cells are a crucial constituent of the more physiologically representative platforms used in tissue engineering which incorporate 3D structures and multiple cell types.

1.9.1 Characterisation of iPSC-derived cardiomyocytes

Initially embryonic body (EB) formation has been used for the differentiation of embryonic stem cells through forced aggregation and suspension techniques (Kurosawa 2007). Then monolayer protocols were able to produce purer populations of cardiomyocytes, in some cases through the use of lineage-specific antibiotic selection were favoured (Lian et al. 2012), and protocols shifted away from animal derived feeder cells and the use of products of animal origin (Ludwig et al. 2006) toward molecularly defined growth factor conditions (Brons et al. 2007; Yang et al. 2008; Yao et al. 2006), for readier use in in vivo regenerative therapies, and in accordance with the 3R's of animal and animal product usage.

In differentiating EB formations, beating areas can be seen four days post- seeding (Mummery et al. 2012). In terms of differentiation efficiency, initially all strategies from pluripotent ESCs or iPSCs produced a mixture of nodal, atrial and ventricular cells, which are similar to the fetal cardiac phenotype, as assessed by expression or cardiac RNA and proteins markers by qRT-PCR and immunostaining (typically against the troponins) (Willems et al. 2009). However, 80-90% purity in cardiomyocytes has been achieved more recently (Kolanowski et al. 2017; Lian et al. 2012). This was accomplished through the use of defined growth factors or pharmacological inhibitors (Kolanowski et al. 2017) with serum free strategies to yield around 1 million cardiomyocytes/cm^2 without selection or sorting (Lian et al. 2012).

The extensive characterisation of pluripotent stem cell-derived cardiomyocytes arrived at the

conclusion that they resemble immature human fetal cardiomyocytes (Willems et al. 2009), as assessed by gene expression, the expression of contractile proteins, myofibrillar structure, electrophysiology, metabolic profile, calcium handling and force generation (Lundy et al. 2013; Binah et al. 2007; J. Zhang et al. 2009; Dolnikov et al. 2006; Kita-Matsuo et al. 2009; Kolanowski et al. 2017). As such, maturation of iPSC-CMs is of paramount importance in the field. Prolonged culture for ESC and hiPSC-CMs has been reported to increase maturation as defined by RNA expression and contractile properties (Babiarz et al. 2012; Lundy et al. 2013). Moreover, the use of T3 hormone (Burridge et al. 2015; Lee et al. 2010) or calsequestrin (CSQ; a calcium handling protein) overexpression (Dolnikov et al. 2006) have also been identified as strategies which improve maturation, as well as electrical stimulation, stretching and biochemical stimulation (redox signalling, VEGF, β-adrenergic) (Kolanowski et al. 2017). In addition, cardiac tissue engineering techniques encompass another approach for improved maturation since this increases force development and structural features (Mannhardt et al. 2016; Mannhardt et al. 2017), discussed in more detail below.

1.9.2 Engineered heart tissue (EHT) as a platform for drug evaluation

As previously mentioned, engineered heart tissue strategies have been able to more closely mimic the environment of the intact human heart as well as to provide more mature cardiomyocytes in terms of contractile and structural properties; since this technology has made possible full assessment of contractile properties which is restricted in 2D (Mannhardt et al. 2016; Uzun et al. 2016; Ogle et al. 2016). EHTs are three-dimensional, force-generating heart muscle constructs from isolated single cells (Zimmermann et al. 2002; Zimmermann et al. 2000; Eschenhagen et al. 1997). Constructs are generated on a fibrin-based matrix using flexible silicone posts which provide auxotonic stretching conditions (Breckwoldt et al. 2017; Hansen et al. 2010). This is based on the principle of hydrogel

formation with dissociated cells in casting moulds with a defined preload (Eschenhagen et al. 2012; Hirt et al. 2014), in which cardiomyocytes remodel the hydrogel, align and spontaneously and coherently beat. This allows the assessment of crucial heart function parameters such as force, contraction and relaxation kinetics under stable conditions that mimic physiological settings.

Important features for maturity include cardiomyocyte alignment, orientation, sarcomeric organisation, modulation of cardiac repolarisation and contractile force. EHT presents high degree of cardiomyocyte alignment and orientation, and cross-striated cardiomyocytes, close in morphology to the classical rod shape of adult ventricular cardiomyocytes (Hirt et al. 2014). This is an improvement as compared to human embryonic stem cells and iPSC-CMs cultured in monolayers since these cells are polymorphic, small, uniformly oriented and present disarrayed sarcomeres along with an immature ultrastructure (Yang et al. 2014). Long-term culture improves structural and functional properties of hiPSC-CMs in monolayers (Lundy et al. 2013). After one year, cardiomyocyte size increases and sarcomeres and better organised, presenting higher levels of cardiac marker proteins, longer action potentials and signs of metabolic switch that can be simulated by microRNA let-7 overexpression (Kuppusamy et al. 2015). EHTs are only in culture for 2 weeks before initial measurements. However, the impact of load is likely to account for their increased cardiomyocyte development since inclusion of metal braces caused hypertrophy in neonatal rat EHT (Hirt et al. 2012). In cardiomyocytes, contractile force results from the interaction between electrical activation, calcium handling and myofilament. Ionotropic agents have been found to cause smaller positive ionotropic effects than in human non-failing human hearts, perhaps due to the less developed ultrastructure (Mannhardt et al. 2016). EHTs beat spontaneously, regulation of contractile function is less pronounced than in native tissue and no force-frequency relationship has been observed. This is possibly due to the immaturity of t tubules and SR organisation as, in native cardiomyocytes t tubules are 12-15nm, and small differences are known to cause dysfunction of the calcium induce calcium release

mechanism (Gómez et al. 1997). Further, native human heart tissue has primarily been studied under isometric conditions and EHT under physiological auxotonic conditions; whilst the impact has not been well described, auxotonic conditions have shown 50% lower forces than under isometric conditions in adult rat ventricular cardiomyocytes (Nishimura et al. 2004).

Initial work with EHTs from human embryonic stem cells and hiPSC-CMs were able to generate constructs and characterise them (Schaaf et al. 2011; Tulloch et al. 2011; Kensah et al. 2013; Nunes et al. 2013; Thavandiran et al. 2013; Zhang et al. 2013). More recently however, EHTs have been used to study contractile force as a platform for drug testing in hiPSC-CMs (Stoehr et al. 2014; Mannhardt et al. 2017), rat cardiomyocytes (Eder et al. 2014; Hirt et al. 2014; Stoehr et al. 2014) and murine cells (Kensah et al. 2013). This has been of particular interest to the field of cytotoxic screening and drug discovery as many drugs fail in clinical trials due to either cardiotoxicity or inducing arrhythmia (Eder et al. 2015).

It has been found that human EHT stimulated at 2Hz for the first week and at 1.5Hz thereafter developed 1.5x higher forces than non-stimulated hEHT at day 14 (Hirt et al. 2014). These constructs also showed improved longitudinally oriented cardiomyocytes and higher cytoplasm-to- nucleus ratio, illustrating that sustained electrical field stimulation further improves EHT properties and thus, maturation.

Further, proof of principle studies have shown that a variety of drug effects can be replicated in hiPSC-EHTs (Mannhardt et al. 2016), including effects on inotropy, lusitropy, clinotropy and chronotrophy. hiPSC-CMs were found to have well-developed sarcomeric organisation and alignment as well as high mitochondrial density as shown by transmission electron microscopy, confocal immunofluorescence and western blot analysis. They were found to express calcium handling proteins and caveolin and juntophilin, suggesting emerging t tubules. However, these structures are still less developed than in native heart tissue as they

were irregular and smaller in size. Post rest potentiation is directly related to the capacity of the SR to store and release calcium; it was found to be small in EHTs suggesting that the SR is not fully developed but it is functional. EHTs replicated canonical responses to physiological and pharmacological regulators of inotropy, membrane mediators of pacemaking, SR-based calcium related mediators of pacemaking, modulators of ion-channel currents and proarrhythmic compounds with unparalled precision (Mannhardt et al. 2016). This suggests great similarity between hiPSC-CMs in EHT and in human heart, thus proposing EHT as a useful drug testing and disease modelling tool.

2. The aim

To date, the evidence regarding the role of MAP4K4 in the heart is limited. However, the pathobiological role suggested by its interaction with MAPKs TAK1 and the subsequent activation of JNK (Yao et al. 1999) and p38 (Zohn et al. 2006) poses a strong case since all these MAPKs have demonstrated pro-death functions in cardiac muscle cell (Fiedler et al., in revision; Rose et al. 2010; Zhang et al. 2000). MAP4K4 involvement in human cardiomyocyte death has been suggested by biochemical studies, mouse models, human and rodent cardiomyocytes (Fiedler et al., manuscript in revision). This, in turn, proposes MAP4K4 as a sound provisional starting point for the development of novel small-molecule inhibitors (Fiedler et. al., manuscript in revision). Consequently, the need to test the effects on pharmacological inhibition of MAP4K4 for adverse effects in a humanised platform for improved target validation and compound development is paramount. This is of key importance as lack of pre-clinical human validation is known to have played a part in hampering therapeutic progress (Ebert et al. 2012). Further, the potential involvement of MAP4K4 in mitochondrial and contractile function in the heart has not been previously explored.

Three ATP competitive inhibitors of MAP4K4 were used; firstly, the inhibitor prototype (IC4-001) identified in-house, developed through 3D field-point modelling and screening *in silico* and found to interfere only with 5 kinases out of a panel of 140; MINK (one of the most closely related kinases to MAP4K4), MLK1, MLK3, NUAK1 and GCK (Imperial Innovations Limited, UP Patent Office Application GB1716867.5, MAP4K4 inhibitors, 13 October 2017, Fiedler et. al, in revision). Secondly, GNE-495, which is a recently published MAP4K4 inhibitor (Ndubaku et al. 2015) shown to be active *in vivo*, with 7 off-target effects against a panel of 61 kinases (Crawford et al. 2014), including the most closely related to MAP4K4, MINK (Vitorino et al. 2015). Thirdly, a new generation in-house MAP4K4 inhibitor based on IC4-001, DMX-5804, was tested. This compound has an improved potency for MAP4K4 inhibition as compared to IC4-001 (10-fold increase, IC50 3 vs 34 nM) whilst retaining selectivity, and displaying reduced clearance; 80-fold improvement; the free plasma concentration was 334 and 8 nM, 1 and 10 hr after 50 mg kg^{-1} respectively reduced clearance (Fiedler et. al., in revision) (See Section 2.2 for more information on the properties of the inhibitors). DMX-5804 was shown to protect against H_2O_{2-} and menadione-induced oxidative stress in hiPSC-CM CorV.4U 2D culture, as measured by the number of viable cells using CellTitre-Glo (Promega) and cardiac troponin release (Imperial Innovations Limited, UP Patent Office Application GB1716867.5, MAP4K4 inhibitors, 13 October 2017, Fiedler et. al, in revision).

To this end, the aim of this project is to deploy pharmacological approaches in hiPSC-CMs as a platform for target validation, and more specifically assess their effect under more complex and faithful conditions provided by human engineered heart tissue. In this study, this is explored in human cardiomyocytes derived from pluripotent stem cells both in 2D and 3D models; to test the hypothesis that pharmacological inhibition of MAP4K4 will result in protection against oxidative stress induced cell death, mitochondrial dysfunction and contractile dysfunction both in cultured human cardiomyocytes and cardiac tissue. Therefore, we aimed to:

- Determine whether pharmacological inhibition of MAP4K4 has **adverse** effects on human cardiomyocyte metabolism and calcium cycling that might confound its use in cardioprotection
- Determine whether pharmacological inhibition of MAP4K4, under conditions of sublethal stress, has **beneficial** effects on human cardiomyocyte metabolism and calcium cycling
- Determine whether cardioprotection by pharmacological inhibition of MAP4K4 can be conferred in **3D human engineered heart tissue**, and whether contractile function is preserved

2. Methods

2.1 hiPSC-CM culture

Purified iCell cardiomyocytes from Cellular Dynamics International (CDI CMC-100-110-001) were purchased, plated and maintained as per the manufacturer's instructions. In brief, thawed cells were transferred to Plating Medium (M1004), counted using the Vi-Cell cell viability analyser (Beckman Coulter 731050) and 10,000 cells/well were seeded in 96-well plates (Greiner 675090) for death assays and 20,000 cells/well for Seahorse analysis of mitochondrial respiration. Plates were coated with 0.1% gelatin in PBS (Life technologies 14190-144) for 30 min at 37°C, aspirated prior to cell plating. Cells were cultured in Plating Medium for 2 days, followed by Maintenance Medium (M1003) thereafter. Medium was changed every day subsequently.

Purified ventricularly enriched CorV.4U cardiomyocytes from Axiogenesis (Ax-B-HC03-1M) were purchased, plated and maintained as per the manufacturer's instructions. In brief, thawed cells were transferred to Cor.4U Medium, counted using the Vi-Cell cell viability analyser. 20,000 cells/well were seeded in 96-well plates (Greiner 675090) for death assays, 60000 cells/well for Seahorse analysis of mitochondrial respiration and calcium transient analysis in CellOPTIQ. Plates were coated with fibronectin coating solution made out of fibronectin stock solution (1 mg/ml, Sigma, F1141) in PBS with Ca2+ and Mg2+ to a final concentration of 10 µg/ml fibronectin (Dilution 1:100). Dishes were kept for 3h at 37°C and aspirated prior to cell plating. In brief, 3 ml Cor.4U Medium were transferred into a 50 ml tube (tube A) and warmed to 37°C. 1 ml of pre-warmed Cor.4U Medium was transferred into another 50 ml tube (tube B). The cells were transferred from liquid nitrogen on dry ice directly to a 37°C water bath and the vial thawed until the frozen cell suspension detached from the bottom of the vial and only a small ice clump can be seen (approx. 2 min). The cell suspension was then pipetted directly into tube A. The cryovial was then rinsed with 1 ml Cor.4U Culture Medium from tube B and added to the cell suspension in tube A, to make up a total final volume of 5 ml. The number of viable cells were counted using ViCell, and 60,000/well were seeded in Mattek 96 multiwell plates (P96G-1.5-5-F) or Seahorse plates

(XF24 FluxPak, 100850-001). Medium was changed 24 h after seeding, and every day subsequently.

2.2 MAP4K4 pharmacological inhibition

MAP4K4 inhibitors were added to cells 45 min before or at the same time as treatment with stressors, as specified. Inhibitors were added at 10, 3 or 1 μM, in Maintenance Media, Cor.4U Media or EHT media, as appropriate to the recipient cell model. Inhibitors remained present for the duration of cell culture unless specified. Three inhibitors were used: the top in-house compound from pharmacophore modelling IC4-001, its derivative DMX-5804 (DMX-5804), and a published inhibitor of MAP4K4, GNE-495 (Ndubaku et al. 2015; Vitorino et al. 2015). The in-house compounds were tested for activity against MAP4K4 and selected other human protein kinases using the HTRF Transcreener ADP assay (Fiedler et. al., in revision) (Table **2.1**). The kinases tested in depth for IC50 determination were chosen based on off-target activity shown in selectivity screenings which tested the inhibitors at 1μM (Fiedler et al., in revision). The potency of GNE-495 was similarly assessed; the *in vitro* biochemical activities of GNE-495 against a selected subset of kinases were measured as the IC_{50} (Table **2.2**). The selected kinases had shown that their activities were inhibited by 1μM GNE-495 (Vitorino et al. 2015). For pharmacokinetic properties of the in-house compounds see Table **2.3** and for GNE-495 see Table **2.4**.

Target	IC4-001 pIC50 (fold selectivity)	DMX-5804 pIC50 (fold selectivity)
MAP4K4	7.46	8.55
MINK1/MAP4K6	7.42	8.18
TNIK/MAP4K7	7.03	7.96
GCK/MAP4K2	5.91 (35)	6.50 (112)
GLK/MAP4K3	4.52 (871)	4.95 (3981)
KHS/MAP4K5	5.22 (174)	6.36 (153)
ABL1	4.52 (865)	5.80 (560)
Aurora B	4.88 (380)	5.49 (560)
FLT3	5.66 (63)	5.31 (1148)
GSK3	4.57 (776)	4.66 (7762)
MLK1/MAP3K9	6.28 (15)	7.19 (23)
MLK3/MAP3K11	6.09 (23)	6.99 (36)
NUAK	6.16 (20)	6.88 (47)
VEGFR	5.72 (55)	5.72 (675)

Table 2.1 Comparison of IC4-001 and DMX-5804 potency (IC_{50}) against human MAP4K4, other MAP4Ks, and selected other protein kinases. Modified from Fiedler et. al, in revision.

Kinase	pIC50(μM)
MAP4K4	8.66
MLK1	6.48
MINK (MAP4K6)	8.28
GCK	6.36
Mer	5.94
Rsk3	6.27
Rsk4	6.25
PAK4	5.93

Table 2.2 In vitro pIC_{50} values for GNE-495. Modified from Vitorino et al. 2015

Compound	IV PK (1 mg kg^{-1})				Oral PK (50 mg kg^{-1})			
	Cl (L hr^{-1} kg^{-1})	$t_{1/2}$ (h)	C_{max} (nM)	V_d (L kg^{-1})	AUC_{inf}	C_{max} (nM)	T_{max} (h)	$t_{1/2}$ (h)
IC4-001	5.33	0.1	3262	1.05	2162	295	1.00	3.7
DMX-5804	2.50	0.6	1590	1.22	63733	13847	1.00	1.8

Table 2.3. Pharmacokinetic (PK) properties of the in-house MAP4K4 inhibitors. Plasma concentrations were determined after intravenous or oral administration of compounds at the doses shown. AUC_{inf}, area under the plasma concentration-time curve from time 0 to infinite; Cl, clearance; C_{max}, peak concentration; $t_{1/2}$, plasma half-life; T_{max}, time of peak concentration; V_d, volume of distribution (Fiedler et. al., in revision). Modified from Fiedler et al., in revision.

IV PK (1 mg kg^{-1})					Oral PK (5 mg kg^{-1})				
Species	Cl (L hr^{-1} kg^{-1})	$T_{1/2}$(h)	C_{max}(nM)	V (L/kg)	AUC_{inf} (h·µM)	C_{max} (nM)	T_{max}(h)	F%	$C_{u,brain}$(µM)
Mouse	1.14	1.5	2700	1.6	5.3	1400	1.0	47	0.008
Rat	0.45	3.4	4000	1.2	12.0	1500	4.0	40	N.D.
Dog	0.54	1.8	3900	1.1	21.0	1200	1.7	37	N.D.

Table 2.4. Pharmacokinetic properties of GNE-495 in three preclinical species: mouse, rat, and dog. GNE-495 was administered by intravenous (IV) and oral routes at 1 and 5 mg/kg, respectively, in each species (three animals per group) (Ndubaku et al., 2015). GNE-495 showed good in vivo profile in all species tested, with low clearances, moderate terminal half-lives, and reasonable oral exposure levels (*F* = 37–47%) (Ndubaku et al., 2015). Very minimal brain exposure was observed in mice (measured unbound brain concentration at 1 h time point = 0.008 μM). Adapted from Ndubaku et al., 2015.

2.3 Cell death induction

hiPSC-CMs were treated with H_2O_2 (Sigma, H1009), doxorubicin (Calbiochem, CAS 23214-92-8) and menadione (Sigma, M5625-25G). The reagents were dissolved in distilled H_2O for H_2O_2 and DMSO for doxorubicin and menadione. Cells were treated with the indicated concentrations and durations of exposure.

2.4 Cell death assays

DRAQ7 staining: DRAQ7 is a live cell-impermeant fluorescent DNA dye, which is taken up by permeabilised cells as it binds dsDNA (a measure of membrane integrity) (Wlodkowic et al. 2013), with peak absorbance at 697nm. The cells were co-stained with Hoescht 33342, a membrane-permeant blue nuclear dye (460-490nm). Cells were stained with 3μM Draq7 (Biostatus, 1533453-55-2) and 5μg/mL Hoescht 33342 (Molecular Probes, 23491-52-3) at 37°C for 15 min. Image acquisition was performed using the Cellomics ArrayScan VTI High Content Screening platform (X-Cite series 120 Q; Thermo Scientific) and its automated Zeiss Observer Z1 epifluorescence microscope. The percentage of DRAQ7 positive cells was calculated using the ArrayScan image acquisition and analysis software (Thermo Fisher).

Adenylate Kinase Activity assay (ToxiLight, Lonza, LT07-217): This assay of intracellular enzyme release was performed as per manufacturer's instructions. In brief, reagents were

brought to room temperature before use. AK detection reagent (AKDR) was reconstituted in assay buffer and left for 15 min at room temperature to ensure complete rehydration. The culture plate was brought to room temperature. 20 µl of cell supernatant was transferred to a luminescence-compatible 96 well plate. 100 µl of AKDR was added to each well and left for 5 min at room temperature before reading in luminometer.

2.5 Immunocytostaining (2D)

Cells were fixed with 3.7% formalin in PBS for 10-15 min, washed 3 times in PBS, and washed between each subsequent step. Non-specific binding sites were blocked and cells permeabilised with 4% BSA 0.2% Triton-X in PBS for 30 min at RT. Primary and secondary antibodies (Table **2.5**) were each incubated in 4% BSA 0.2% Triton-X in PBS for 1 hr at RT. Nuclei were counter-stained with DAPI (2ug/ml, Life Technologies) in PBS for 10 min at RT. Fluorescence was recorded using the Cellomics ArrayScan VTI High Content Screening platform or stored at 4°C to await availability of the platform. Image acquisition was performed using the Cellomics ArrayScan VTI High Content Screening platform (X-Cite series 120 Q; Thermo Scientific) and its automated Zeiss Observer Z1 epifluorescence microscope.

Target	Species raised	Product code	Company	Dilution	Class
Cleaved caspase-3	Rabbit	9664S	Cell Signalling	1:100	monoclonal/ IgG
Phospho-p38 MAPK(Thr180/Tyr182)	Rabbit	9211S	Cell Signalling	1:100	polyclonal/ IgG
Phospho-JNK(Thr183/Tyr185)	Rabbit	9251S	Cell Signalling	1:100	polyclonal/ IgG
Phospho-ERK1/2(Thr202/Tyr204)	Rabbit	4370S	Cell Signalling	1:100	monoclonal/ IgG
Cleaved BID	Goat	PA19016	Thermo Scientific	1:50	polyclonal/ IgG
Rabbit Isotype	Rabbit	Ab27472	Abcam	1:100	polyclonal/ IgG
Goat Isotype	Goat	Sc-2028	Santa Cruz	2µg/ml	polyclonal
Rabbit IgG	Goat	4412S	Cell Signalling	1:200	polyclonal, F(ab')2 fragment, Alexa 488-conjugated
Goat IgG	Donkey	A-11058	Thermo Scientific	1:400	polyclonal, cross-adsorbed, Alexa 594-conjugated

Table 2.5 Antibodies

2.6 Mitochondrial respiration analysis

The Seahorse extracellular flux analyser XF24 (Agilent) was used to assess cellular metabolism in hiPSC-CMs. 20,000 cells/well were plated onto 0.1% gelatin coated XF24 plate for CDi and 60,000 cells/well for Axiogenesis, as previously described, and treated 12 and 5 days after plating, respectively. One hr before and for the duration of the assay, media was replaced by bicarbonate-free Seahorse assay medium containing DMEM Base (8.3g/L of medium, Sigma) supplemented with 10mM glucose, 2mM Glutamax-1 100x (Gibco), 1mM sodium pyruvate (Gibco) in distilled H_2O, pH adjusted to 7.4 (See Table **2.6**). Plates were incubated at 37°C in a non-CO_2 incubator (INCU-Line, IL10 Digital incubators, VWR) for one hr before the assay. Each assay cycle involved 4 min mixing, 2 min waiting and 2 min measuring, as suggested by the manufacturer. Three cycles were performed for the determination of the basal oxygen consumption rate (OCR) and extracellular acidification rate (ECAR), and readings were recorded every 15 seconds for the 2 measuring min in each cycle. Mitochondrial membrane modulators 1μM oligomycin A (Abcam), followed by 0.5μM FCCP (Abcam) and 1μM antimycin A/rotenone (Sigma and Abcam) were injected and measured for 3 cycles each. Basal respiration, ATP production, maximal respiration, spare respiratory capacity and proton leak were defined by the differences between average measurements 3-12, 3-6, 7-12, 7-3, 6-12, respectively, and non-mitochondrial respiration is determined by average measurement 12.

Reagent/Instrumentation	Company	Product code
INCU-Line, IL10 Digital incubators	VWR	390-0385
Base DMEM	Sigma	D5030-10X1L
Glucose	Gibco	A2494001
Sodium pyruvate	Gibco	11360070
Glutamax	Gibco	35050061
Oligomycin	Abcam	ab141829
FCCP	Abcam	ab120081
Antimycin A	Sigma	A8674-25MG
Rotenone	Abcam	ab143145
XF24 FluxPak	Seahorse Bioscience	100850-001
Seahorse XFe24 Analyzer	Agilent	N/A

Table 2.6 Seahorse assay reagents and instrumentation

2.7 Protein quantification

40µL 1x RIPA buffer (Sigma) per well was used to lyse cells and total protein quantification was performed using the Pierce BCA Protein Assay Kit (Thermo Scientific) as per the manufacturer's instructions. Absorbance was measured at 562nm using a Paradigm plate reader (Molecular Devices).

2.8 hiPSC-CMs thawing for human engineered heart tissue (hEHTs) generation

iCell cardiomyocytes were thawed as previously described. Cells were counted using a haemocytometer.

CorV.4U cardiomyocytes were thawed as previously described. Cells were counted using a haemocytometer.

2.9 EHT generation

Fibrin-based hEHTs were generated between flexible silicone posts as previously described (Breckwoldt et al. 2017; Schaaf et al. 2011; Hansen et al. 2010), with minor modifications. 1.8mL per well of 2% agarose in PBS were pipetted into a 24-well plate and Teflon spacers placed inside each well to produce a casting mould and the agarose left to set for 15 min. The spacers were removed from each well and a pair of silicone posts was inserted from above.

A master mix was prepared for EHTs in blocks of 4 and therefore $4x10^6$ iPSC-CM were re-suspended in: 340µl fibroblast medium, 60µl 2x DMEM and 10µl bovine fibrinogen (see Section **2.10** and Table **2.7** for media components). Fibrinogen must be added last and mixed 15 times prior to pipetting into moulds. 3µl bovine thrombin was not put into the master mix but pipetted into individual PCR tubes. Master mix and bovine thrombin were then mixed and pipetted quickly into agarose moulds with silicone posts, as the hydrogel would solidify within the pipette tip if a delay occurred at this point.

After 90 min standard incubation (37°C, CO_2 7%, O_2 40%, humidity 100%), 300µL EHT media per well was added to hydrate the gels (see below for media components), and the EHTs were incubated for a further 50 min. EHTs were placed in a fresh 24-well plate with 1.5mL EHT media per well. EHTs were fed with 1.5ml EHT medium Mondays, Wednesdays, and Fridays for maintenance. Teflon spacers and silicone racks were washed in de-mineralised water and autoclaved for re-use. Force measurements were performed by utilising optical tracking of EHTs, as detailed below.

2.10 EHT solutions

Fibroblast medium: Heat-inactivated fetal calf serum 10%, glutamine (200mM) 1%, penicillin/streptomycin (P/S) 1%, made in DMEM.

10x DMEM: 670mg DMEM powder in 5ml cell culture-grade water, filter-sterilise and store at 4^{o}C.

2x DMEM: 10x DMEM solution 2 ml, horse serum 2 ml, 0.2 ml P/S, cell culture-grade water 5.8 ml, sterile filtered and stored at 4^{o}C.

EHT media: Horse serum 10%, insulin 0.1%, aprotinin 0.1% (33µg/ml), 1% P/S, made in DMEM.

Aprotinin: 33 mg/ml in cell culture-grade water, filter-sterilise, aliquot, and store at 20^{o}C.

Fibrinogen: 200 mg/ml in pre-warmed 0.9% NaCl in sterilised cell culture-water. Add 72.1 µL aprotinin (33 mg/ml stock) to 25ml fibrinogen solution, mix, aliquot, and store at -20^{o}C.

Thrombin: 100 U/ml in 60% sterile PBS and 40% in sterilised cell culture-grade water. Aliquot and store at -20^{o}C (see Table **2.7** for details).

Reagents/Instrumentation	Company	Product code
Fibrinogen	Sigma	F8630-5g
Aprotinin	Sigma	A1153-100mg
Thrombin	Biopur	BP11-10-1104
Agarose	Invitrogen	15510-027
10xDMEM	Gibco	52100-021
Penicillin/Streptomycin (P/S)	Gibco	15140
DMEM	Biochrom	F0415
Insulin	Sigma	I9278
Glutamine (Life 25030-081	Thermo Fisher Scientific	25030-081
Horse serum	Gibco	26050
White box EHT Technologies	EHT Technologies GmbH	A0001
Teflon spacers	EHT Technologies GmbH	N/A
Silicon racks	EHT Technologies GmbH	N/A

Table 2.7 EHT reagents and instrumentation

2.11 Force calculation in EHTs and contractile assessment

The optical tracking technology was developed to automatically recognise the EHT construct and calculate frequency, fractional shortening, contraction and relaxation time parameters as well as the minimum, mean, maximum and standard deviation for these parameters (Hansen et al. 2010) (Fig **2.1**). This involved the use of video optical recording coupled to a program that recognises the EHT constructs and calculates contraction parameters in real-time (Hansen et al. 2010), on the basis of post deflection distance (d), post length (L) and radius

(R), and the elastic modulus (E), using the formula $F = 3pER^4d4L^{-3}$ (Schaaf et al., 2011). Contraction parameters are calculated by using edge detection software to recognise the extremities of the EHT (where the EHT is formed around the posts), which tracks the movements of the EHT's edges over time. The silicone posts around which the EHTs are formed were made to geometry YM (Young's Modulus) 1.7mPa, length 10mm, radius 0.5mm. Thus, force can be calculated by directly relating this to fractional shortening (Vandenburgh et al. 2008). Shortening and subsequent peak recognition is then used to calculate contraction and relaxation by addition of the time domain. The temperature of the device is set to 37°C and composition of the ambient air can be set to the same concentrations as a cell culture incubator.

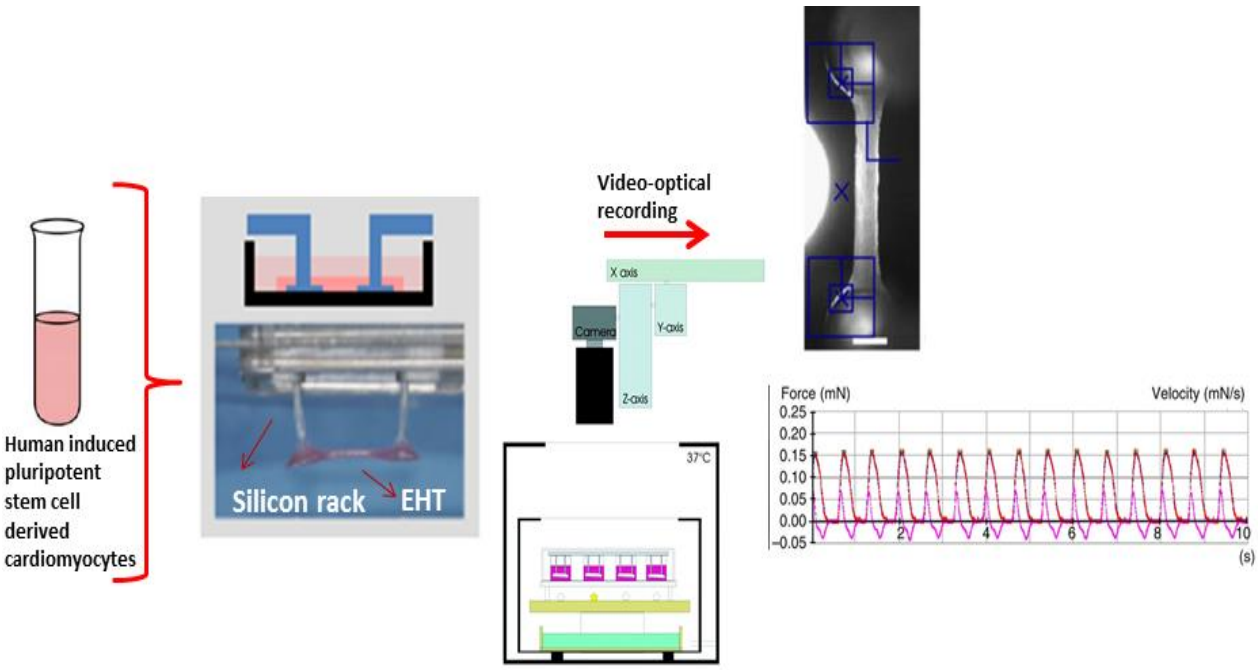


Figure 2.1 Schematic illustration of the EHT generation process and contractile assessment. Left, hiPSC-CMs were allowed to set in hydrogel to form a strip of tissue which deflects silicone posts around which it forms as it contracts spontaneously. Center, the optical tracking technology automatically recognises the EHT construct and calculates frequency, fractional shortening, contraction and relaxation times. Upper right, the blue

crosses define the top and bottom reference positions for each EHT. Lower right, in the representative recording, the red line indicates force and the magenta line velocity. Scale bar 1mm. Modified from Breckwoldt et al. 2017 and Hansen et al. 2010.

2.12 Immunocytochemistry

EHTs were washed twice for 5 min with PBS on a rocker while still attached to the posts, were fixed with Histofix (Carl Roth GmbH, P087) overnight at 4 ºC, and washed twice for 5 min with PBS. EHTs were then removed from the silicone posts with scissors; at this point, the fixed EHTs can be stored in PBS at 4 ºC. EHTs were permeabilised/blocked for 24 hr with blocking solution (Tris-buffered saline 0.05 M, pH 7.4, 10% FCS, 1% BSA, 0.5% Triton X-100) at 4 ºC on a rocker in a 2ml tube. EHTs were stained overnight at 4 ºC with primary antibodies (Table **2.8**) in blocking solution minus FCS, on a rocker in a 2ml tube. EHTs were washed three times for 5 min with PBS at RT. Secondary antibodies were also incubated overnight at 4 ºC in blocking solution minus FCS on a rocker in a 2ml tube in the dark. Isotypes were not used due to the high cost per EHT – positive controls (death agonist showing over 80% signal) and negative controls (DMSO control showing 0% signal) were used. EHTs were washed three times for 5 min with PBS in the dark at RT. 0.8 µM Hoechst 33342 was used for 10 min at room temperature on a rocker in a 2ml tube in the dark. EHTs were washed once for 5 min in the dark at RT. Constructs were mounted in Vectashield mounting media with DAPI (H-1200) between a cover slip and an indented glass slide (Academy, single cavity, N/A141). EHTs were visualised using a Zeiss Confocal Microscope.

Target	Species raised	Product code	Company	Dilution	Class
Cleaved caspase-3	Rabbit	9664S	Cell Signalling	1:100	monoclonal/ IgG
Rabbit IgG	Goat	4413S	Cell Signalling	1:200	polyclonal, F(ab')2 fragment, Alexa 555-conjugated
F-Actin	N/A	A12379	Invitrogen	1:100	488 Alexa Phalloidin

Table 2.8 Antibodies and probes used for EHT immunocytochemistry

2.13 Calcium dynamics assessment

CellOPTIQ technology was used to analyse calcium transients in 2D culture, as described (Fattah et al. 2016). CorV4U iPSC-CMs were seeded at a density of 60,000/well on Mattek 96 multiwell plates (Mattek, P96G-1.5-5-F). 4 µM Fura-4F-AM (Molecular Probes, F-14175) was loaded into hiPSC-CMs in serum-free phenol-free DMEM (Thermo Fisher Scientific, A14430-01). Cells were then incubated for 30 min at 37°C. This was followed by a media change before placing the plate on the instrument stage for 20-30 min, allowing the indicator to de-esterify and the cells to acclimatise. After configuring the run, locating the samples, and focussing on the cells, the dye was excited intermittently with two LEDs at 360 and 380nm, and the emitted fluorescence at wavelengths <580nm is registered by one photomultiplier at a sampling rate of 2.5 KHz. Ratiometric calcium transients were analysed off-line using CellOPTIQ software.

2.14 Statistical Analysis

Experimental data were plotted in GraphPad Prism5 (Graphpad Software) and error bars indicate standard error of the mean. Comparisons of multiple samples with one variable were analysed by one-way ANOVA. Comparisons of multiple samples with two variables were analysed by two-way ANOVA with Bonferroni's correction. Comparisons of time series were done pairwise by repeated measures ANOVA. Student's t-test was performed for significance in two groups with one variable being assessed. A p value < 0.05 was considered significant and statistical significance is denoted by $*p < 0.05$, $**p < 0.01$, $***p < 0.001$ compared to the corresponding control.

3. Results

Chapter 3: Effects of MAP4K4 inhibition on cell death in 2-dimensional human iPSC-CM culture.

Kinases play an important role in cardiomyocyte death (Marber et al. 2011; Rose et al. 2010; Zhang et al. 2000; Yao et al. 1999; Zohn et al. 2006), which in turn is an important feature in heart disease that contributes to heart failure. MAP4K4 is a relatively unexplored mitogen activated protein kinase whose involvement in cardiomyocyte death has been shown by a) activation in failing human hearts concurrent with caspase-3 activation, b) activation in genetic and pathobiological mouse models of heart disease, c) gain-of-function mutations driving failure in mouse heart, and d) dominant-negative mutations and RNA interference in cultured rat cardiomyocytes being cardioprotective against pro-cell death insults (Fiedler et. al., in revision). In the human setting, shRNAmir-mediated knockdown of MAP4K4 in hiPSC-CMs showed a reduction in cell death after being subjected to oxidative stress, measured by loss of membrane integrity, suggesting that MAP4K4 also plays a pro-death role in human cardiac muscle cells (Fiedler et. al, manuscript in revision).

However, the role of MAP4K4 in cell death has not yet been fully studied in human iPSC-CMs. In particular, whether MAP4K4 plays a role in human cardiomyocyte metabolism or contractile function is not known. Many drugs fail in clinical trials due to either cardiotoxicity or inducing arrhythmia, with the drug discovery pipeline rarely including testing in a human cardiac context (Eder et al. 2015). Since MAP4K4 inhibition is a promising approach in treating heart failure, we used human cardiac myocytes produced from pluripotent stem cells — hiPSC-CMs — to evaluate pharmacological inhibition of MAP4K4 in the context of human cardiac myocyte survival. Such a system can be used to provide a more relevant testbed for therapeutic studies, thereby providing greater confidence in successful clinical translation.

As a first step, we used a novel and specific inhibitor of MAP4K4 to elucidate its role in cell death in hiPSC-CM. The inhibitor prototype (IC4-001) (Imperial Innovations Limited, UP Patent Office Application GB1716867.5, MAP4K4 inhibitors, 13 October 2017, Fiedler et. al,

in revision) was used, oxidative stress was conferred with hydrogen peroxide (H_2O_2), and the effect on cell death in hiPSC-CMs was assessed.

3.1 Optimisation of conditions for human cardiac muscle cell death induced by H_2O_2

To optimise induction of oxidative stress-mediated cell death in hiPSC-CMs (iCell), serial dilutions of H_2O_2 were tested. Cell death was measured by immunofluorescent staining to visualise cleaved caspase-3 after 24 hr treatment. Loss of membrane integrity was monitored by measuring DRAQ7 uptake. There was a dose-dependent increase in cleaved caspase-3 positive cells (Fig.**3.1A**) and DRAQ7 positive cells (Fig.**3.1B**), evident at all concentrations ≥ 500μM. Since maximal loss of membrane integrity (DRAQ7 uptake) was reached from 500μM at 24 hr but not evident at the next lowest concentration, 200 μM, we tested intermediate concentrations and earlier time-points to achieve a more suitable range for testing MAP4K4 inhibition in cell death, to avoid potential benefits being confounded by a saturating or maximal death signal. To accomplish this, it is important to establish conditions in which any increase or decrease induced by additional treatments can be detected. 350μM was sufficient to induce loss of membrane integrity at 4 hr (Fig.**3.1C**), and 200 μM at 8 hr (Fig.**3.1C**), with neither reaching maximal induction of cell death. H_2O_2 treatment at 350μM induced a 62 % loss of membrane integrity at 4 hr and a 64 % loss by 200 μM at 8 hr. Subsequent experiments therefore encompassed all time points up to 24h and concentrations up to 500μM.

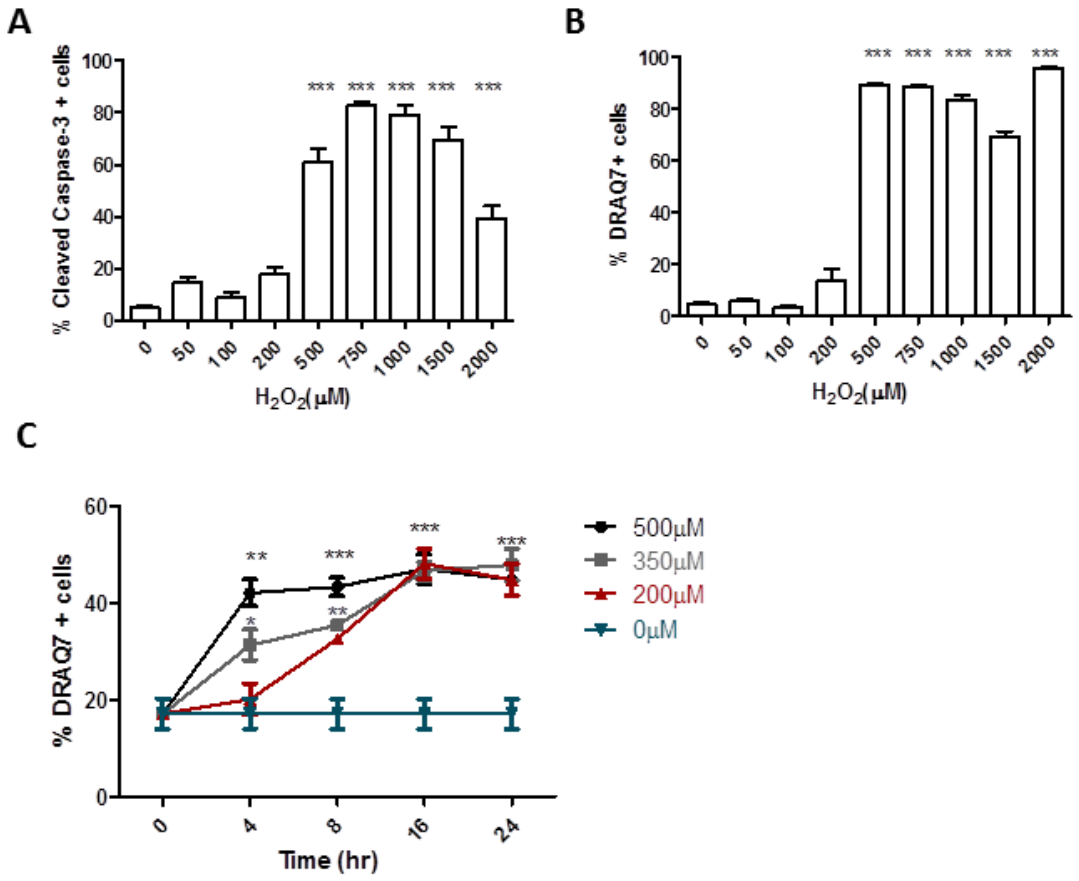


Figure 3.1 Induction of cell death by H_2O_2 measured after 4-24 hrs treatment at indicated concentrations. Whole wells were imaged using Cellomics ArrayScan VTI high content screening instrument and the % of cleaved caspase-3 or DRAQ7 positive cells calculated using ArrayScan image acquisition and analysis software. **A)** Cleaved caspase-3 positive cardiomyocytes. **B)** DRAQ7 positive cardiomyocytes. **C)** Induction of cell death (DRAQ7 uptake) by H_2O_2 at the indicated concentrations, over the 24 hour timecourse. Data shown are the mean of 4 independent biological replicates (4 technical replicates per experiment). Two-way ANOVA, N=4, *P < 0.05 , **P < 0.01, ***P < 0.001 compared to vehicle control.

3.2 Effect of the MAP4K4 inhibitor IC4-001 on plasma membrane disruption induced by H_2O_2

To determine whether MAP4K4 inhibition was protective against the loss of membrane integrity induced by oxidative stress, cell death was monitored by measuring DRAQ7 uptake after H_2O_2 treatment, building on the conditions established in Fig **3.1**. To recapitulate, DRAQ7-positive iCell cardiomyocytes were detected after treatment with 500 μM H_2O_2 for up to 24 hr, and were first detected from 4 hr onwards (Fig. **3.1B**, **C**). Since loss of membrane integrity was maximal using 500 μM for 24 h, we tested lower concentrations and earlier time-points systematically here, to achieve a range more suitable for testing the effects of MAP4K4 inhibition on this complementary assay of cell death. At the concentration tested, 10 μM, IC4-001 protected against 500μM H_2O_2-induced loss of cell membrane integrity at 4 hr, but not the later time-points tested (Fig. **3.2A, B**). Therefore, under the conditions tested, the compound delayed, but did not prevent, the loss of cell membrane integrity. Because a fall-off is expected from cell-free activity against a recombinant target versus in-cell activity, due in part to drug permeation and stability, re-examining this question with more evolved compounds could be informative.

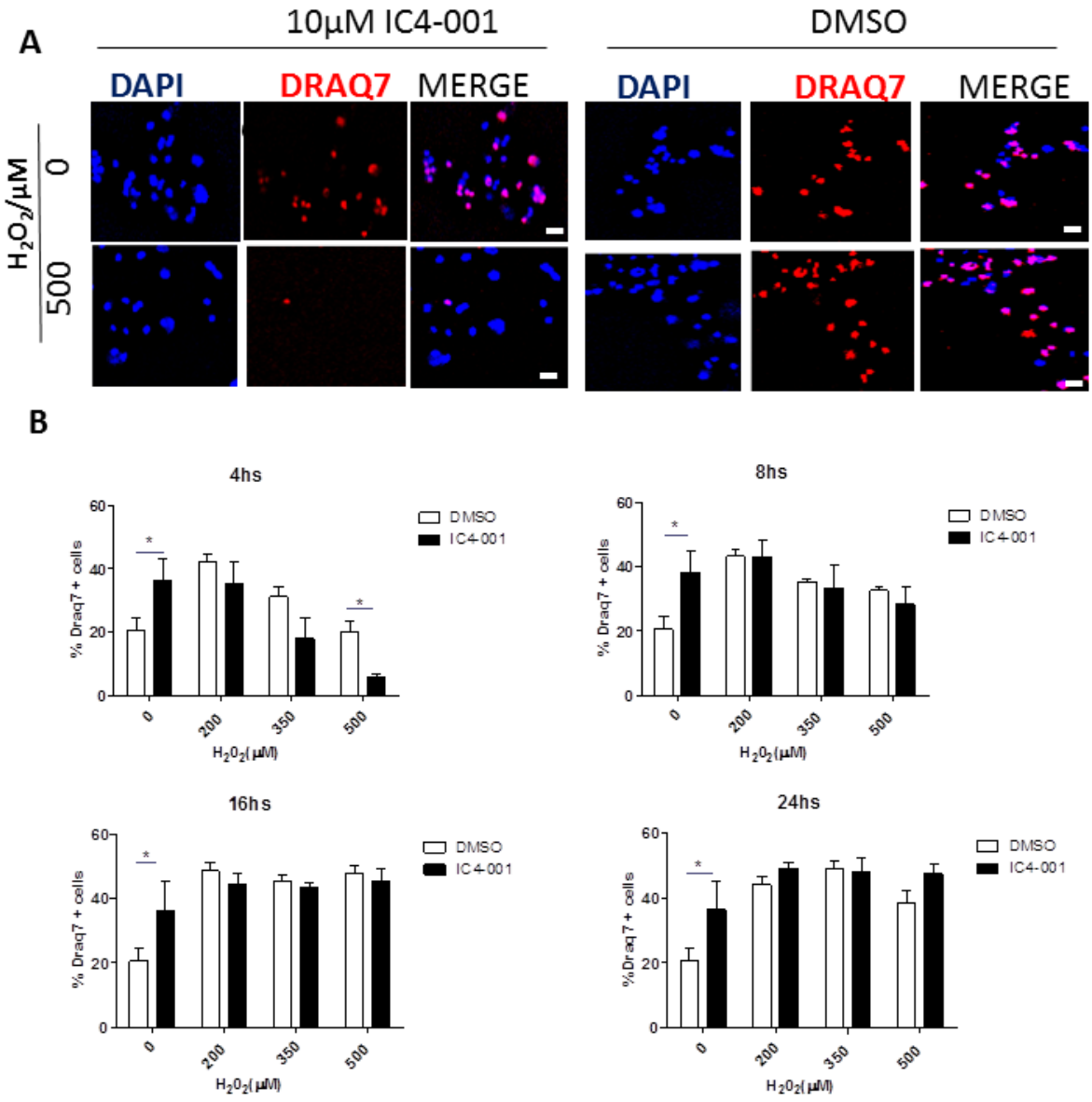


Figure 3.2 Loss of plasma membrane integrity in the presence of MAP4K4 inhibitor in response to H_2O_2 in hiPSC-CMs. A) MAP4K4 pharmacological inhibition protects from 500 µM H_2O_2 induced loss of membrane integrity (DRAQ7 uptake) **B)** Representative images acquired using the Cellomics for treated and untreated groups at 4 hs. Data shown are mean of 4 independent biological replicates (4 technical replicates per experiment). Two-way ANOVA, *P < 0.05, **P < 0.01, ***P < 0.001 compared to vehicle control. Scale bars represent 10µm.

3.3 Effect of the MAP4K4inhibitor IC4-001 on caspase-3 activation induced by H_2O_2

As an alternative to the loss of cell membrane integrity, we next studied caspase activation as an instrumental biochemical event in apoptosis. hiPSC-CMs were treated with 50 µM to 2000 µM H_2O_2 for 24 hr. Caspase-3 activation was evident at all concentrations tested (assessed by levels of cleaved caspase-3), with substantial activation induced from 500 µM H_2O_2. Pharmacological inhibition of MAP4K4 by 10 µM IC4-001 conferred protection against the cleavage of caspase-3 induced by 500 to 750 µM H_2O_2 (comparing DMSO + IC4-001 to H_2O_2 + IC4-001 treated cells) (Fig. **3.3A-C**). Protection was also seen at a statistically significant level at the lowest concentration tested, 50 µM (Fig. **3.3A, B**). Thus, in this exploratory study, the most consistent results were obtained at 500-750 µM, with significant protection also found at 50 µM H_2O_2. To re-examine the intermediate concentrations more closely, a timecourse was performed. This revealed that MAP4K4 inhibition was protective at 500µM and below at 4 and 8 hr treatment (Fig. **3.3C**). No benefit was seen at 16 hr, at which time caspase-3 cleavage in the cells had returned to basal levels. Overall, these data show that pharmacological inhibition of MAP4K4 is protective against H_2O_2-induced activation of caspase-3.

In summary, pharmacological inhibition of MAP4K4 by IC4-001 protected against loss of cell membrane integrity at 4 hr, but not at later time points (Fig. **3.2A, B**). Though inhibition of caspase-3 was achieved even at 8 hr (Fig. **3.3A, B**), preservation of membrane integrity was not (Fig. **3.2A, B**). Therefore, pharmacological inhibition of MAP4K4 is protective against H_2O_2-induced caspase-3 cleavage but not against loss of cell membrane integrity. First, MAP4K4 drives activation of caspase-3 by H_2O_2, but additional MAP4K4-independent pathways may be activated that result in loss of membrane integrity. Second, caspase-3 activation can be rescued at extended time periods but loss of membrane integrity cannot;

these data indicate that H_2O_2-induced loss of plasma membrane integrity in these cells is not dependent on caspase-3 activity. Third, it is also plausible that incomplete inhibition of caspase-3 cleavage is not sufficient to rescue cell viability overall.

In the absence of any pro-death stimuli however (indicated by 0 H_2O_2, Fig. **3.2**), IC4-001 by itself results in loss of plasma membrane integrity, though not activation of caspase-3. This indicates that the compound itself may be toxic (off-target effect on one or more protein kinases, off-target effect unrelated to protein kinases); however, this would seem unlikely since inhibitor treatment in the presence of H_2O_2 was protective. Conversely, it could suggest that MAP4K4 activity is required for baseline cell survival, as suggested for the MAP4K4 target TAK1 (Li et al. 2014); in other words, MAP4K4 may function as a positive or negative regulator of cell death depending on the external environment and corresponding stimuli. Another possibility is that, the differences could be related to a confounding effect of the drug on detachment of DRAQ7+ cells.

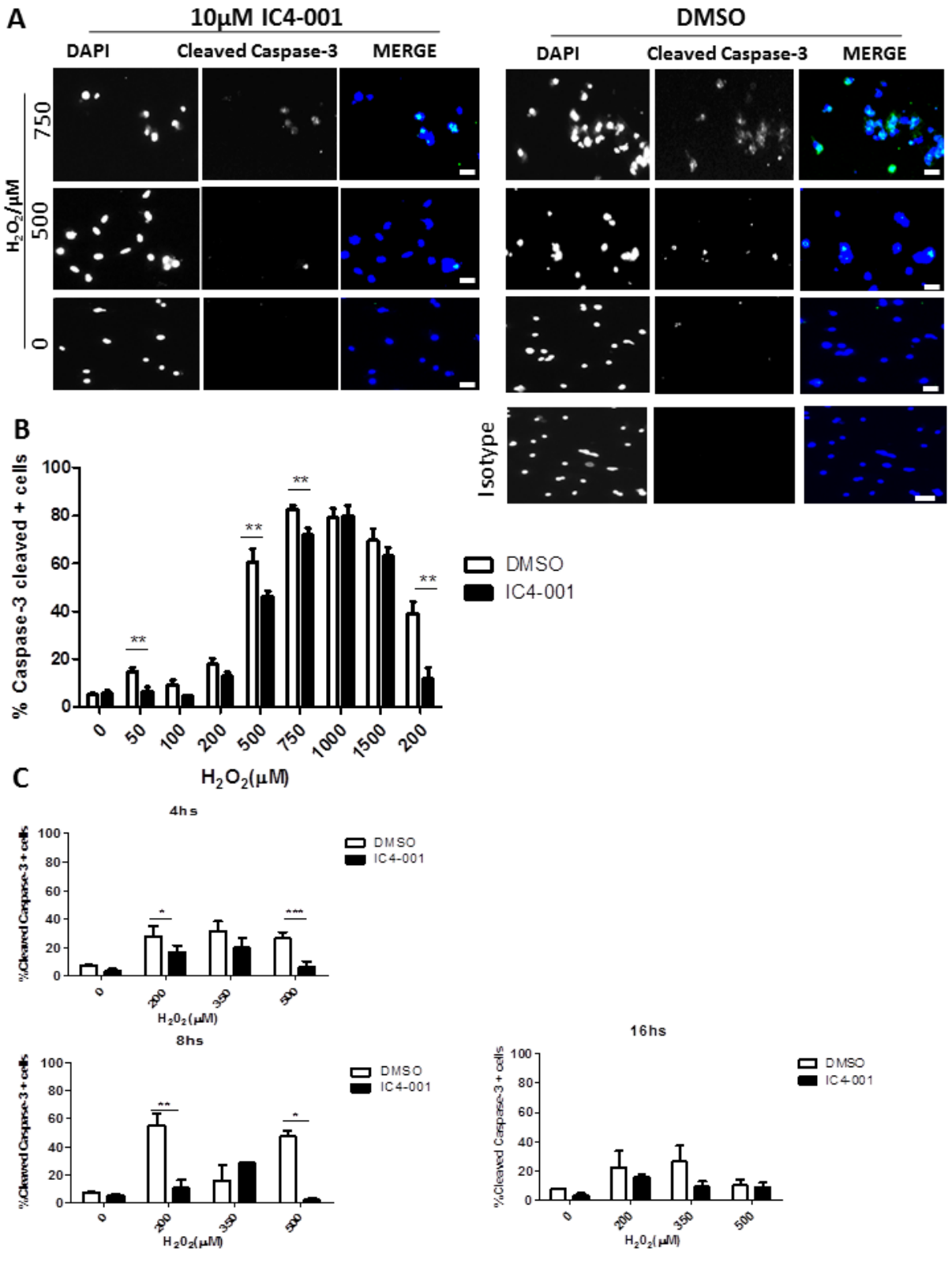

A
10μM IC4-001
DMSO
DAPI
Cleaved Caspase-3
MERGE
H2O2/μM
750
500
0
Isotype
B
% Caspase-3 cleaved + cells
H2O2(μM)
DMSO
IC4-001
C
4hs
8hs
16hs
%Cleaved Caspase-3+ cells

Figure 3.3 Cleaved caspase-3 in the presence of MAP4K4 inhibitor in response to H_2O_2 in hiPSC-CMs. A) Cells were treated with H_2O_2 in the presence of IC4-001 or DMSO vehicle control from 0 to 2000 µM, for 24 hours and caspase-3 visualised by immunostaining. Quantification is shown. **B)** Representative images acquired for quantification shown in part A are shown. **C)** At earlier time points, MAP4K4 pharmacological inhibition protects from 500µM H_2O_2 induced caspase-3 cleavage (4 and 8 hours). Data shown are mean of 4 independent biological replicates per experiment. Two-way ANOVA, *P < 0.05, **P < 0.01, ***P < 0.001 compared to vehicle control.

3.4 Effect of the MAP4K4 inhibitor IC4-001 on BID cleavage induced by H_2O_2

The BH3-only protein BID is activated in the mitochondrial apoptosis pathway and acts as a switch between extrinsic and intrinsic cell death pathways (Joglekar et al. 2016). To test whether MAP4K4 plays a role in induction of mitochondrial-dependent cell death by H_2O_2-induced oxidative stress, hiPSC-CMs were treated with 200 µM, 350 µM and 500 µM H_2O_2 for 4 to 24 hr and BID cleavage was assessed. In this way, based on experience with related end-points, intermediate concentrations of H_2O_2 and early time-points were evaluated from the onset.

All concentrations tested successfully induced BID cleavage by 16 hr treatment compared to vehicle control (DMSO) at corresponding timepoints, however, activation was not consistent at 8 hr (Fig. **3.4A, B**). Pharmacological inhibition of MAP4K4 did not prevent BID cleavage under any conditions tested (Fig. **3.4A, B, C**). Cell detachment of cells may have confounded results due to fixation and wash steps during immunostaining or have led to an underestimation of DRAQ7+ cells in the DMSO groups. In addition, scan-length may have affected these results since long scan times can affect fluorescence intensity.

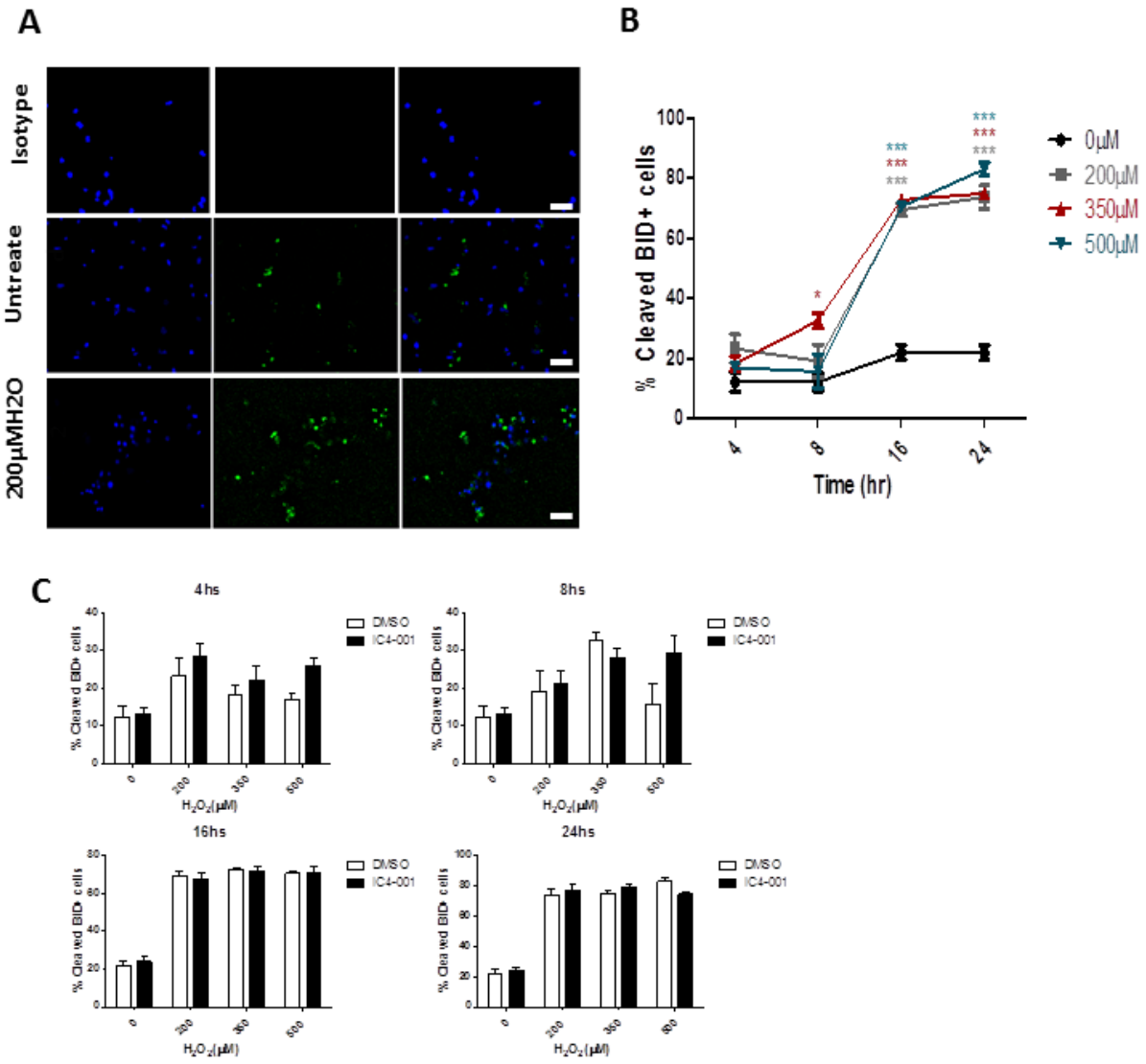


Figure 3.4 BID cleavage in the presence of MAP4K4 inhibitor in response to H_2O_2 in hiPSC-CMs. A) Representative images for treated and untreated groups. **B)** H_2O_2 titration and time course: H_2O_2 activates BID cleavage in hiPSC-CMs. **C)** MAP4K4 pharmacological inhibition does not supress H_2O_2 induced BID cleavage. Data shown are mean of 2 independent biological replicates (4 technical replicates per experiment). Two-way ANOVA, *P < 0.05, **P < 0.01, ***P < 0.001 compared to vehicle control. Bar, 10 µm.

3.5 Effect of H_2O_2 and IC4-001 on downstream MAPK activation

To both evaluate the activity of MAP kinases downstream of MAP4K4 and identify potential effectors as biomarkers for animal and clinical studies, hiPSC-CMs were treated with H_2O_2 and immunofluorescently stained to visualise phosphorylated MAPKs, p38 and ERK. In addition, activation of MAPKs by MAP4K4 in human cardiomyocytes has not yet been tested.

Neither MAP4K4 inhibition nor H_2O_2 treatment by itself induced any activation of p38 measured by Thr180/Tyr182 phosphorylation levels (Fig. **3.5A, B**). However, a number of cells were lost during on treatment by H_2O_2 while cells were retained under control conditions (Fig.**3.5C**). This may reflect that pro-death stimuli likely cause cells to adopt a more rounded, less adherent phenotype. These cells would be more easily dislodged under the conditions of the assay, namely immunostaining, which involves a number of repeated wash steps in addition to others (fixation, antibody incubation). Further, baseline levels of phosphorylated p38 were already high; 80 % of cells were positive for phospho-p38 even in the absence of any treatment, where more than 1000 cells were still attached (see DMSO treatment, H_2O_2 0 µM, Fig. **5C**). Thus any further increase in activity might be obscured. In contrast, ERK activity (Thr202/Tyr204), was lower at baseline (12 % of cells were positive for phospho-ERK) and was not affected in a statistically significant manner by H_2O_2 treatment or by MAP4K4 inhibition (Fig. **3.6**). These data suggest that neither ERK nor p38 mediate H_2O_2-induced cell death in this cell type, even under similar conditions in which MAP4K4 inhibition was protective (measured by activation of caspase-3).

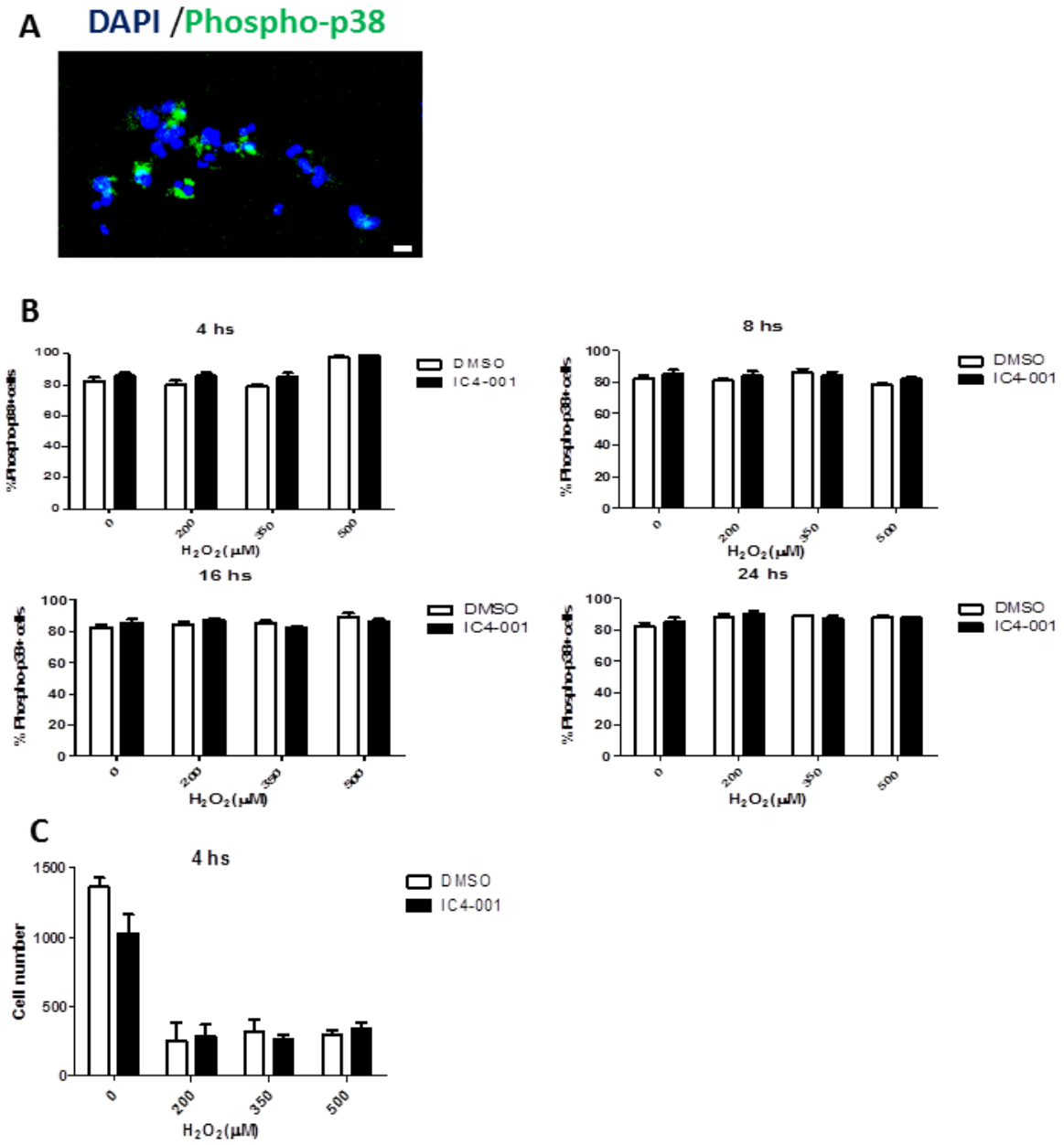


Figure 3.5 Assessment of p-38 phosphorylation in the presence of MAP4K4 inhibitor in response to H_2O_2 in hiPSC-CMs. A) Representative image at baseline conditions (in the presence of IC4-001) **B)** Assessment of p-38 phosphorylation (a potential effector of MAP4K4) in MAP4K4 pharmacologically inhibited hiPSC-CMs in response to H_2O_2 by immunocytochemistry. **C)** Cell number at 4 hours after treatment. Data shown are mean of 2 independent biological replicates (4 technical replicates per experiment). Two-way ANOVA, *P < 0.05, **P < 0.01, ***P < 0.001 compared to vehicle control. Bar, 10μm.

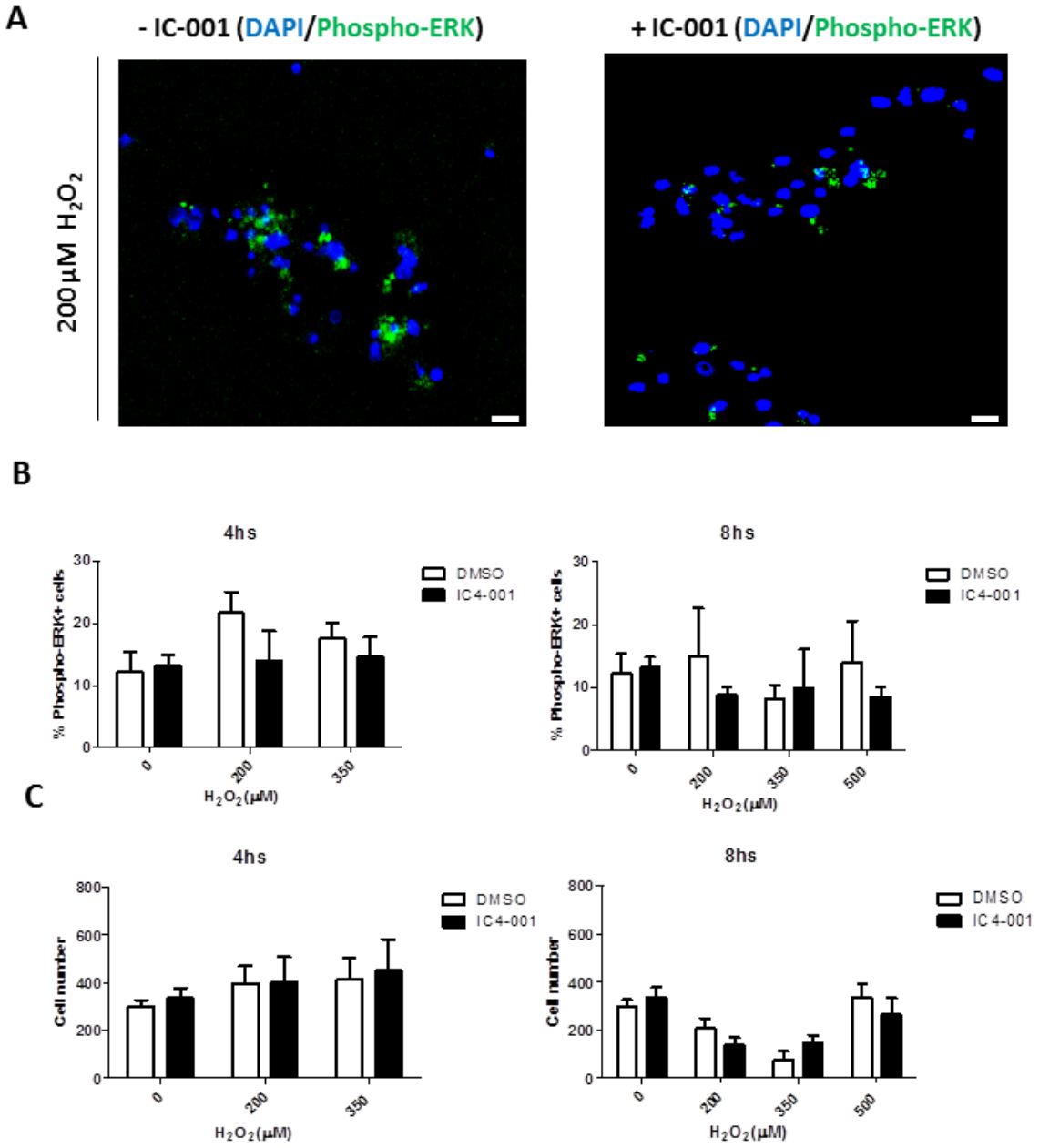


Figure 3.6 Assessment of ERK phosphorylation in the presence of MAP4K4 inhibitor in response to H_2O_2 in hiPSC-CMs. A) Representative images acquired using the Cellomics. **B)** Assessment of ERK phosphorylation (a potential effector of MAP4K4) in MAP4K4 pharmacologically inhibited hiPSC-CMs in response to H_2O_2 by immunocytochemistry. **C)** Cell number at 4 and 8 hours after treatment. Data shown are mean of 2 independent biological replicates (4 technical replicates per experiment). Two-way ANOVA, *P < 0.05, **P < 0.01, ***P < 0.001 compared to vehicle control. Bar, 10µm.

3.6 Synopsis of main findings

These exploratory results collectively point towards a pro-apoptotic role for MAP4K4 in human cardiomyocytes subjected to oxidative stress. We show here that pharmacological inhibition of MAP4K4 can protect against H_2O_2-induced caspase-3 cleavage up to 24 hr and against loss of plasma membrane integrity, although the latter effect was lost at extended timepoints (past 4 hr). Under conditions where caspase-3 activity was suppressed by pharmacological inhibition of MAP4K4, loss of membrane integrity was still observed. One plausible explanation is that loss of plasma membrane integrity may be driven, at least in part, on effectors other than caspase-3, whose suppression is insufficient for cell rescue.

In contrast to caspase-3, activation of BID by oxidative stress (a marker of mitochondrial mediated cell death), was not abrogated by pharmacological inhibition of MAP4K4. This indicates that MAP4K4 is not involved in activation of BID in human cardiomyocytes. It also raises the possibility that BID-dependent signalling pathways might mediate loss of plasma membrane integrity.

When potential signalling pathways downstream of MAP4K4 were explored, it was found that activation of the MAPKs p38 and ERK were unaffected by H_2O_2 or by MAP4K4 inhibition alone, indicating that H_2O_2 mediated cell death in human cardiomyocytes is not dependent on signalling through these MAPKs. Further, reducing baseline activity of MAP4K4 does not affect MAPK activities. However, it should be noted that baseline levels of p38 activity, as measured by phosphorylation levels, were already high, so any further increase might be obscured.

However, recurring technical issues affect this portfolio of microscopy-based results and observations must be tested using additional approaches. DRAQ7- and immunofluorescence-mediated visualisation of caspase-3 cleavage, BID cleavage and MAPK phosphorylation in these 2D studies often gave unreliable results, for reasons likely

including cell detachment and scan length. As such, sublethal concentrations and alternative assays distinct from microscopy were favoured in subsequent studies.

3.7 Discussion

To elucidate the role of MAP4K4 in cardiac cell death, MAP4K4 was inhibited using an in-house pharmacological agent and cell death induced by H_2O_2 treatment, as a model of ROS (oxidative stress). This is a relevant agent, since H_2O_2 levels *in vivo* increase by 250% 30 min after ischemia and in the early reperfusion phase by 600 % (Slezak et al. 1995). Further, MAP4K4 mediated signalling is implicated in ischemic human hearts, since its activity is increased in patients with ischemic cardiomyopathies (Fiedler et. al., in revision) as well as in response to H_2O_2 in isolated neonatal rat cardiomyocytes (NRVM).

It was found that pharmacological inhibition of MAP4K4 was protective against H_2O_2-induced caspase-3 activation. This result is in agreement with previous studies in which MAP4K4 activation was associated with increased caspase-3 activity (Fiedler et al., manuscript in revision). In contrast however, caspase-3 activity was not induced in this cell line in response to H_2O_2, measured by a fluorescent readout of caspase-3 activity in the whole well using Apo-ONE Homogeneous caspase3/7 Assay (Evie Maifoshie, PhD Thesis 2014, Imperial College London). This may reflect differences in whole well-based testing and high-content (individual cell-based) imaging coupled to inferring activation by alternative means; from caspase-3 cleavage (required for its activity) or activation of caspase-3 substrates. In addition, relative sensitivities of these assays might differ, since the former represents the average of the whole well, and effects may be diluted in the event of a non-uniform response. Confirmation can be sought by utilising the NucView caspase-3 substrate in the Cellomics platform and/or a caspase-3-YFP sensor under a cardiospecific promoter (Fujita et al. 2008).

These data could also indicate that H_2O_2-induced cell death is not wholly dependent on caspase-3 activity; that MAP4K4 inhibition prevents caspase-3 activation but cannot sustain cell membrane integrity would suggest alternative pathways. Measurement of plasma membrane integrity is a general readout of cell death that does not discriminate between cell death modes (Wlodkowic et al. 2013), and caspase-independent cell death has been observed. In I/R and heart failure an increase in caspase-3 activation (as measured by protein levels of cleaved caspase-3) is observed (Narula et al. 1999; Scheubel et al. 2002), however, DNA fragmentation might be achieved through Apoptosis Inducing Factor (AIF) released from apoptotic mitochondria (Bröker et al. 2005) as part of a caspase-independent apoptotic mechanism. Alternatively, over longer periods of time, low, prolonged levels of caspase-3 remaining might be sufficient to cause cell death. This notion is supported by a study in which low, prolonged levels of active caspase-8 in the heart eventually resulted in failure due to ongoing, low levels of cell death (Wencker et al. 2003).

Pharmacological inhibition of MAP4K4 protected against H_2O_2 induced loss of cell membrane integrity initially, but progressively (i.e. at later timepoints) could not. Previously, MAP4K4 shRNAmir mediated knockdown in hiPSC-CMs reduced H_2O_2-induced cell death measured by DRAQ7 uptake, further supporting a pro-apoptotic role for MAP4K4 in human cardiac muscle cells (Fiedler et. al., in revision). In the present study however, MAP4K4 did not confer protection from BID cleavage, as a measure of mitochondria mediated cell death, in agreement with the lack of protection from loss of plasma membrane integrity observed. Knockdown versus direct inhibition of kinase activity might account for different results, where in the first, scaffolding activities are additionally affected. Another difference here, is that knockdown is a more long-term approach while pharmacological inhibition is transient, and dependent on the stability of the compound. IC4-001 has a relatively short half-life of ~18 min, as shown by microsomal stability studies and limited aqueous solubility. This cannot be directly extrapolated from liver microsome clearance to culture conditions; two very different environments, however it cannot be excluded that inhibitor activity might have

been lost at later time-points. During the course of establishing these assays, a further compound with an improved half-life and efficacy was developed that was additionally utilised in subsequent experiments. Toxicity due to kinase related or non-kinase related off target effects could be a reason for the DRAQ7 findings although unlikely since protection was observed for caspase-3 cleavage. A more likely possibility, however, is that incomplete inhibition of caspase-3 activity was not sufficient to rescue cell viability.

H_2O_2 treatment induced cell loss, presumably due to cell death and greater propensity for loss during fixation and immunostaining. Further, the longer duration of the scan for cleaved caspase-3 immunostaining may compromise sensitivity of the dye due to loss of signal. In subsequent studies, a detection kit for adenylate kinase (AK) is used in order to bypass these limitations. Adenylate kinase activity is an indicator of loss of plasma membrane integrity. Levels would be expected to increase in most types of cell death and thus can be used to measure cell viability.

The activity of MAP kinases described as being downstream of MAP4K in other systems was explored in order to identify potential effectors in human cardiomyocytes. p38 is activated by upstream MAP3Ks including MEKK1-4, TAK1 and ASK, as well as TAB1 via TAK1 (De Nicola et al. 2013) and targets transcription factors and cytoplasmic proteins. In the heart, it regulates hypertrophy, inflammation, metabolism, contractility, proliferation and cell death (Wang 2007). Of the four isoforms, p38α has the most cardiovascular relevance (Denise Martin et al. 2012). It is activated in I/R in rat hearts, overexpression enhances cell death and dominant-negative mutations and inactivation reduce apoptosis (Kaiser et al. 2004). In addition, a p38 inhibitor reduced ischemia, fibrosis, superoxide levels and improved function (Sy et al. 2008; Denise Martin et al. 2012). The most likely downstream effector of MAP4K4, JNK, is activated in I/R (Fryer et al. 2001) and selective inhibitors reduce infarct size and apoptosis (Milano et al. 2007). Further, in NRVM MAP4K4 lies upstream of JNK but not p38 or ERK (Fiedler et. al., in revision). In contrast to p38 and ERK activity, JNK is associated more with cell survival and would not be expected to be activated by pro-death

signals. JNK was not successfully tested due to technical issues regarding antibody performance.

ERK1/2 phosphorylates substrates such as transcription factors (Kyriakis & Avruch 2012) in addition to kinases and cytoskeletal proteins in the cytoplasm (Ramos 2008). It regulates proliferation, cytokinases, cell death, differentiation, gap junction formation, actin and microtubule formation, hypertrophy, cytokinesis and senescence (Ramos 2008). ERK1/2 are necessary for heart development (Ramos 2008) and cardiac inhibition increases susceptibility to failure (Purcell et al. 2007).

Neither MAP4K4 inhibition nor H_2O_2 treatment induced p38 activation in contrast with the literature. However, the antibody is not isoform specific and during ischemia the β isoform specifically is cardioprotective (Liu et al. 2011). Also, p38 inhibition might be protective in other studies due to effects on contractility or ECM remodeling rather than direct inhibition of cell death. Alternatively, in this particular cell type, H_2O_2-induced cell death might simply not be dependent on p38. This could have been confirmed by utilising commercially available inhibitors to p38, to test whether its activity is required for H_2O_2 -mediated cell death in human cardiomyocytes. ERK1/2 activity was also unchanged by either H_2O_2 treatment or MAP4K4 inhibition.

Oxidative stress is a salient feature during I/R injury as the increased formation of ROS by mitochondria damages and kills cardiomyocytes. H_2O_2 yielded some variability in responses and proved difficult to titrate reliably in previous experiments in our hands, previous members of the lab and collaborators, hence other oxidative stress mediators will be explored in subsequent studies. This variability might reflect the instability of H_2O_2 in culture conditions (Kaczara et al. 2010).

iCell cardiomyocytes were found to yield inconsistent results using a number of different assays and techniques, both in our hands and other members of the MAP4K4 team. Batch to batch variation and varying cell quality in this cell line, meant that migration to a more

reliable cell line was imperative, both for this study and related ones carried out by the project team.

A limitation of approaches used here (DRAQ7 and immunostaining) however, is that, they induced cell detachment, presumably due to cell death by high concentrations of H_2O_2 and greater propensity for loss during fixation and immunostaining. Indeed, many members of the MAP4K4 team frequently encountered inconsistencies in results. Cell loss may therefore have confounded these results to some extent, although at least 200 cells remained in each case, and results were confirmed in two independent experiments. Therefore, sublethal concentrations of the cell death signal were favoured in subsequent experiments. Though preliminary therefore, this data suggests that oxidative stress-induced cell death in human cardiomyocytes can occur independently of MAPK activation. To further explore this more reliably, alternative approaches could be applied to reduce or obviate cell loss from washout, using culture supernatants (cardiac troponin release), live cell imaging of reporter lines, or 3D constructs embedding the cells in biomaterials. In addition, the role of these kinases in human cardiomyocytes could also be explored using virus-mediated knockdown, overexpression or more evolved pharmacological inhibitors. Additional hiPSC-CM cell lines could also be utilised to confirm these results.

Overall, these findings strengthen the usefulness of human stem cell-derived cardiomyocytes, both as part of patient-specific models of inherited disorder or, in this case, as a tool for target discovery and drug development. Despite their limitations, such as functional immaturity and lack of key cell-cell interactions, even in 2D human stem cell-derived cardiomyocytes have a proven track record when it comes to predictive power (Burridge et al. 2014; Devalla et al. 2015; Gintant et al. 2016; Passier et al. 2016). From these initial pilot studies we took forward a number of improvements: 1) using human engineered heart tissue (hEHT) as a model to address the problem of cell loss during processing in 2D cultures, as well as to better mimic the biochemical, functional and contractile properties of the intact human heart (Eder et al. 2015); 2) adding an additional

hiPSC-CM cell line ,since results could be variable from batch to batch in CDI cells used here and additional cell sources would provide greater confidence in testing the role of MAP4K4 in human systems; 3) comparing other MAP4K4 inhibitors with improved stability and different off-target profiles. Where similar results are obtained independent of line, 2D vs 3D, and inhibitor, this will give greater confidence both in the strategy from a clinical perspective, and in furthering our understanding of the role of MAP4K4 mediated signalling in human heart disease in a robust manner.

4. Results

Chapter 4: Assessment of the effects of MAP4K4 inhibitors on cardiac mitochondrial function

Adenosine triphosphate (ATP) is critical for providing energy to the heart to maintain function. Respiration, the process by which ATP is generated, occurs mainly in the mitochondria. Metabolism of glucose (glycolysis) or fatty acids (beta oxidation) in the cytosol generates Acetyl CoA that drives the Krebs (or citric acid, or tricarboxylic acid; TCA) cycle in the mitochondria. Products from the Krebs cycle (NADH and FADH2) in turn drive the electron transport chain. Both glycolysis and the citric acid cycle themselves produce ATP, but it is the electron transport chain which is the final and most productive stage of ATP generation. Thus mitochondria are the main generators and suppliers of ATP through enzymatically controlled oxidation and reduction reactions in the electron transport chain (Nicholls et al. 2010). During cellular injury, decreased mitochondrial oxygen consumption and impaired glycolytic flux are present, impairing the ability of the mitochondria to meet the energetic demands of the heart (Hill et al. 2009). As such, mitochondria play a crucial role in mediating the response to oxidants formed during acute and chronic cardiac dysfunction.

As previously discussed, oxidative stress is a salient feature during I/R injury as the increased formation of reactive oxygen species (ROS) by mitochondria damages and kills cardiomyocytes through pathways classically involved cellular hypoxia (Muntean et al. 2016). H_2O_2 levels *in vivo* increase after ischemia and during early reperfusion (Slezak et al. 1995). MAP4K4 activity increases in ischemic human hearts and in response to H_2O_2 in isolated rat cardiomyocytes (NRVM) (Fiedler et. al., in revision). Menadione, an endogenous ROS generator through redox cycling (Criddle et al. 2006; Loor et al. 2010), has been shown to cause cell death in pancreatic cells (Criddle et al. 2006), embryonic chick cardiomyocytes (Loor et al. 2010), and hiPSC-CMs (Burridge et al. 2016). Here, oxidative

stress was conferred using H_2O_2 and menadione in hiPSC-CMs, and the effect of pharmacological inhibition of MAP4K4 on metabolic function was assessed.

The study of bioenergetics in intact cells may provide a more physiologically representative view of mitochondrial function than methods using isolated mitochondria or by measuring of the activity of complexes separately (Readnower et al. 2012). Here, we used a system that analyses extracellular flux (XF24 Seahorse Bioscience) to measure responses of the two main energy-producing pathways, mitochondrial respiration and glycolysis. The oxygen consumption rate (OCR) represents mitochondrial respiration, whereas the extracellular acidification rate (ECAR) of the media (lactate, a by-product of glycolysis and main contributor of protons) represents glycolytic flux. The platform relies on fluorophores that generate a fluorescent signal to photodetectors that measure particular analytes (O_2 or H^+) in the media and the continuous real-time pH and oxygen concentration measurements are used to determined OCR and ECAR.

Two sources of commercially available human cardiomyocytes were used to generate hEHT. iCell hiPSC-CMs were used in initial studies. However, issues were sometimes encountered with iCell cardiomyocytes in terms of batch to batch variation and cell quality, so an alternative source was sought. The more ventricularly enriched CorV.4U hiPSC-CMs were subsequently used. These were selected on the basis of higher pathophysiological relevance since mechanical dysfunction, fibrosis, and cardiomyocyte loss most commonly involve the left ventricle as the site of heart failure (Harvey & Leinwand 2011; White & Chew 2008; Dimmeler et al. 2005), most particularly as the result of acute myocardial infarction.

Three inhibitors of MAP4K4 were used; firstly, the inhibitor prototype (IC4-001) identified in-house and used in Chapter 3 (Imperial Innovations Limited, UP Patent Office Application GB1716867.5, MAP4K4 inhibitors, 13 October 2017, Fiedler et. al, in revision). Secondly, GNE-495, which is a recently published MAP4K4 inhibitor (Ndubaku et al. 2015; Crawford et

al. 2014; Vitorino et al. 2015). Thirdly, the next-generation in-house MAP4K4 inhibitor, DMX-5804, was tested, a member of the same chemical series, chosen on the basis of proven protection against cell death in both human cardiomyocyte lines and the successful reduction of infarct size in mice (Imperial Innovations Limited, UP Patent Office Application GB1716867.5, MAP4K4 inhibitors, 13 October 2017, Fiedler et. al, in revision). Here we use these novel, complementary, and highly selective inhibitors of MAP4K4 to elucidate its role in metabolic function in human cardiomyocytes.

Human cardiomyocytes were exposed to H_2O_2 and menadione stimuli and the effect of pharmacological inhibition of MAP4K4 on metabolic function was assessed both under unstimulated and stimulated conditions.

4.1 The effects of H_2O_2 on mitochondrial function in iCell cardiomyocytes.

To study whether the stress-activated enzyme MAP4K4 plays a role in metabolic processes in the stressed human heart, and to test compound safety, we simulated oxidative stress by adding H_2O_2 to hiPSC-CMs, pharmacologically inhibited MAP4K4 and assessed mitochondrial respiration using the Seahorse XF24 Extracellular Flux Analyzer.

Using the relevant agents, respiratory processes can be probed to measure specific features in a given system. Here, we used a workflow that encompassed the use of Oligomycin, FCCP, Rotenone and Antimycin A. Oligomycin inhibits mitochondrial ATP synthase and hence can be used to measure ATP synthesis if administrated at the optimal concentration (Agilent Seahorse XF Cell Mito Stress Test Kit, User Guide 103015-100). 1 μM oligomycin was used as previously optimised in-house for the iCell cardiomyocytes (Carolina Pinto Ricardo, PhD Thesis 2017, Imperial College London, submitted). The uncoupling agent FCCP creates pores in the mitochondrial membrane, consequently decreasing the proton gradient that drives the electron transport chain. Maximal mitochondrial respiration can be measured upon FCCP administration at the optimal concentration (Agilent Seahorse XF Cell Mito Stress Test Kit, User Guide 103015-100). The optimal concentration for this cell line had previously been identified to be 0.5 μM (Carolina Pinto Ricardo, PhD Thesis 2017, Imperial College London). Rotanone and Antimycin A are complex I and III inhibitor respectively and here, they are used to measure non-mitochondrial respiration; these were employed at 1 μM, the concentration recommended by Seahorse Bioscience (Agilent Seahorse XF Cell Mito Stress Test Kit, User Guide 103015-100) and validated by Cellular Dynamics International (Application Protocol, Version 1.0, 2016; AP-CM2XF96161209). These mitochondrial modulators were injected in a specific order (firstly oligomycin, followed by FCCP and finally Rotanone and Antimycin A as a simultaneous injection) and 3 measurements were taken after each injection to determine: basal respiration, ATP

production, maximal respiration, spare respiratory capacity, proton leak and non-mitochondrial respiration. This workflow and a representative output is summarised in (Fig. **4.1**).

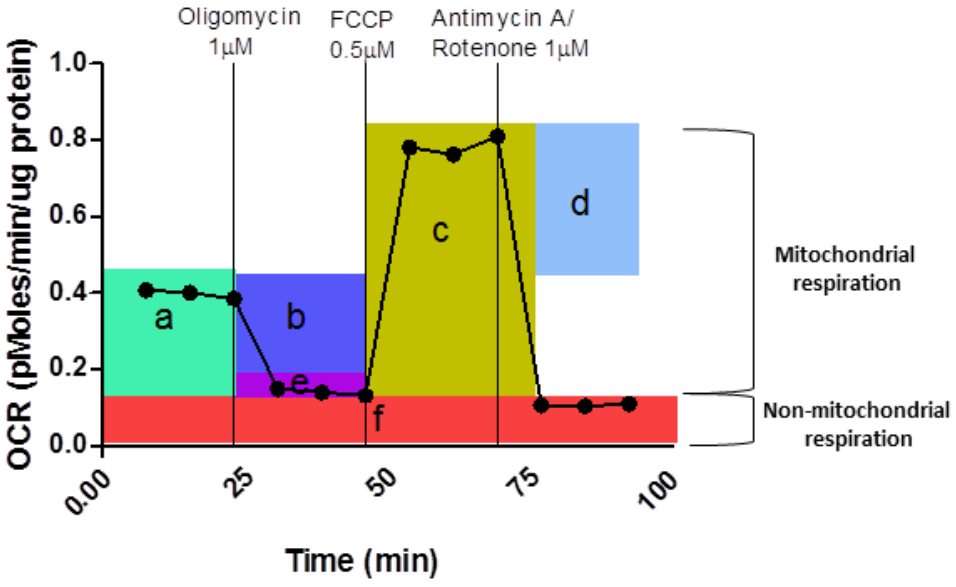


Figure 4.1 Mitochondrial respiration in iCell hiPSC-CMs after 12 days in culture as measured by oxygen consumption rate (OCR). Representative trace for the XF24 extracellular flux analyser mitochondrial stress test. The mitochondrial modulators oligomycin, FCCP, Rotanone and Antimycin A were injected as shown to determine: basal respiration (a), ATP production (b), maximal respiration (c), spare respiratory capacity (d), proton leak (e) and non-mitochondrial respiration (f).

Suitable conditions for H_2O_2 treatment in hiPSC-CMs were first optimised, with the aim of impairing but not completely abolishing OCR. H_2O_2 completely abrogated OCR at 50µM from 30 min treatment (Fig. **4.2A, B**). At a lower concentration however, 25µM, oxygen consumption was reduced but still detected at 30 min treatment and was lost by 60 min exposure (Fig. **4.2C**). Therefore, H_2O_2 was subsequently used at 25 µM for 30 min.

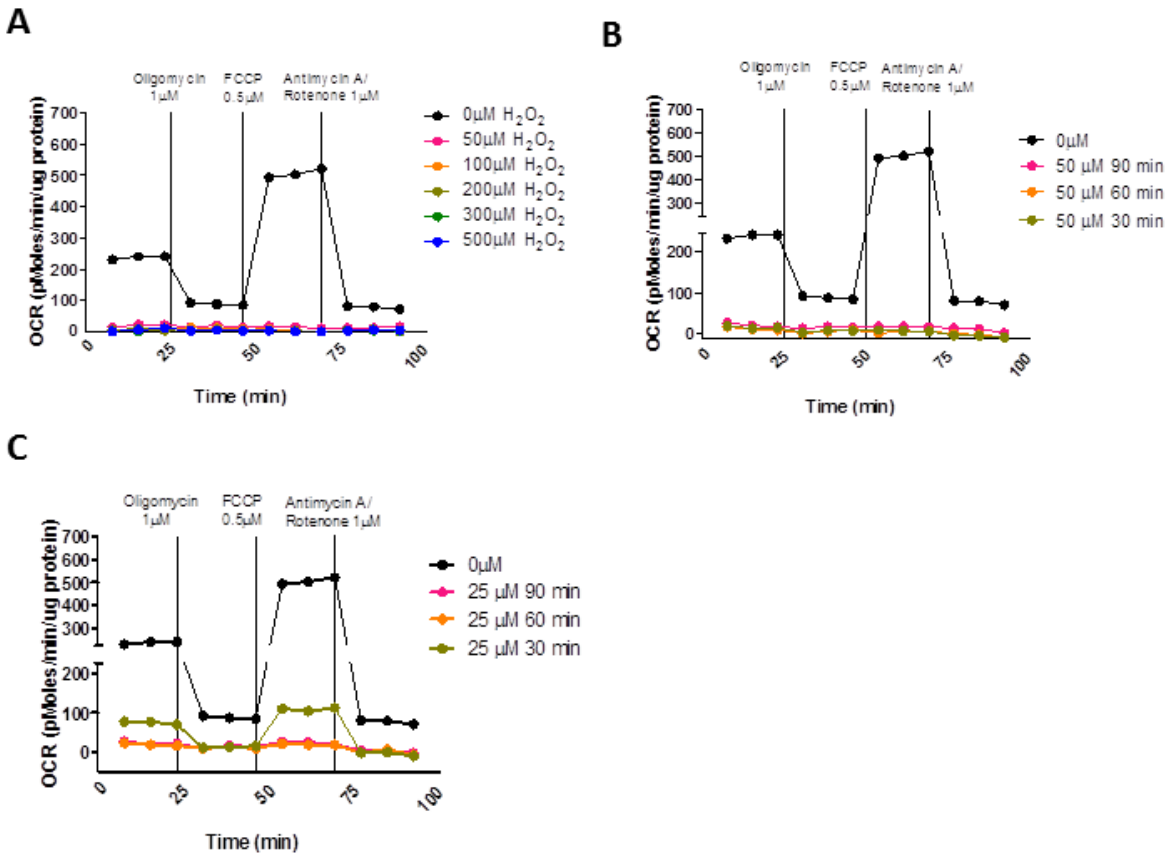


Figure 4.2 The effect of H_2O_2 on mitochondrial respiration in iCell hiPSC-CMs. OCR was assessed using a XF24 extracellular flux analyser. **A)** 50 µM to 500 µM H_2O_2 for 24 hrs. **B)** 50 µM H_2O_2 for 30 to 90 min **C)** 25 µM H_2O_2 for 30 to 90 min. Values were normalised to total protein content per well. N = 2 experiments (4 replicates per experiment).

4.2 Effect of the MAP4K4 inhibitor IC4-001 on mitochondrial function in iCell cardiomyocytes.

To test whether MAP4K4 inhibition affected mitochondrial function impairment induced by oxidative stress, iCell hiPSC-CMs were treated with 10µM IC4-001 for 45 min followed by exposure to 25µM H_2O_2 for 30 min. Pharmacological MAP4K4 inhibition alone (10µM) evoked no change in the mitochondrial respiration profile compared to vehicle control (DMSO) (Fig. **4.3A, B**) and, did not protect against H_2O_2-induced OCR reduction (Fig. **4.3A, B**).

When the separate phases of respiration were analysed, it was found that H_2O_2 alone yielded a decrease in basal mitochondrial respiration, maximal respiration and non-mitochondrial respiration (Fig. **4.4A, C, F**). MAP4K4 inhibition protected basal mitochondrial respiration from H_2O_2-induced OCR reduction as shown by the 2-fold increase in OCR (Fig. **4.4A**), with no effects observed due to addition of IC4-001 alone. The effect of IC4-001 subjected to H_2O_2, in turn, is not significantly different from the control groups, suggesting the partial restoration of normal levels of basal mitochondrial respiration. There was an increase in proton leak after MAP4K4 inhibition compared to the H_2O_2 treated group (Fig. **4.4E**), suggesting a possible protective mechanism. To further examine these findings, a reduced concentration, 12.5μM H_2O_2, was used, as a 50% reduction in these parameters on H_2O_2 treatment would permit the optimal detection of the effect of the inhibitor, whether positive or negative. The results were consistent in terms of the general trend (Fib. **4.3B**), however no significant differences with IC4-001 were observed for the individual phases of mitochondrial respiration at this H_2O_2 concentration (Fig. **4.5A-F**).

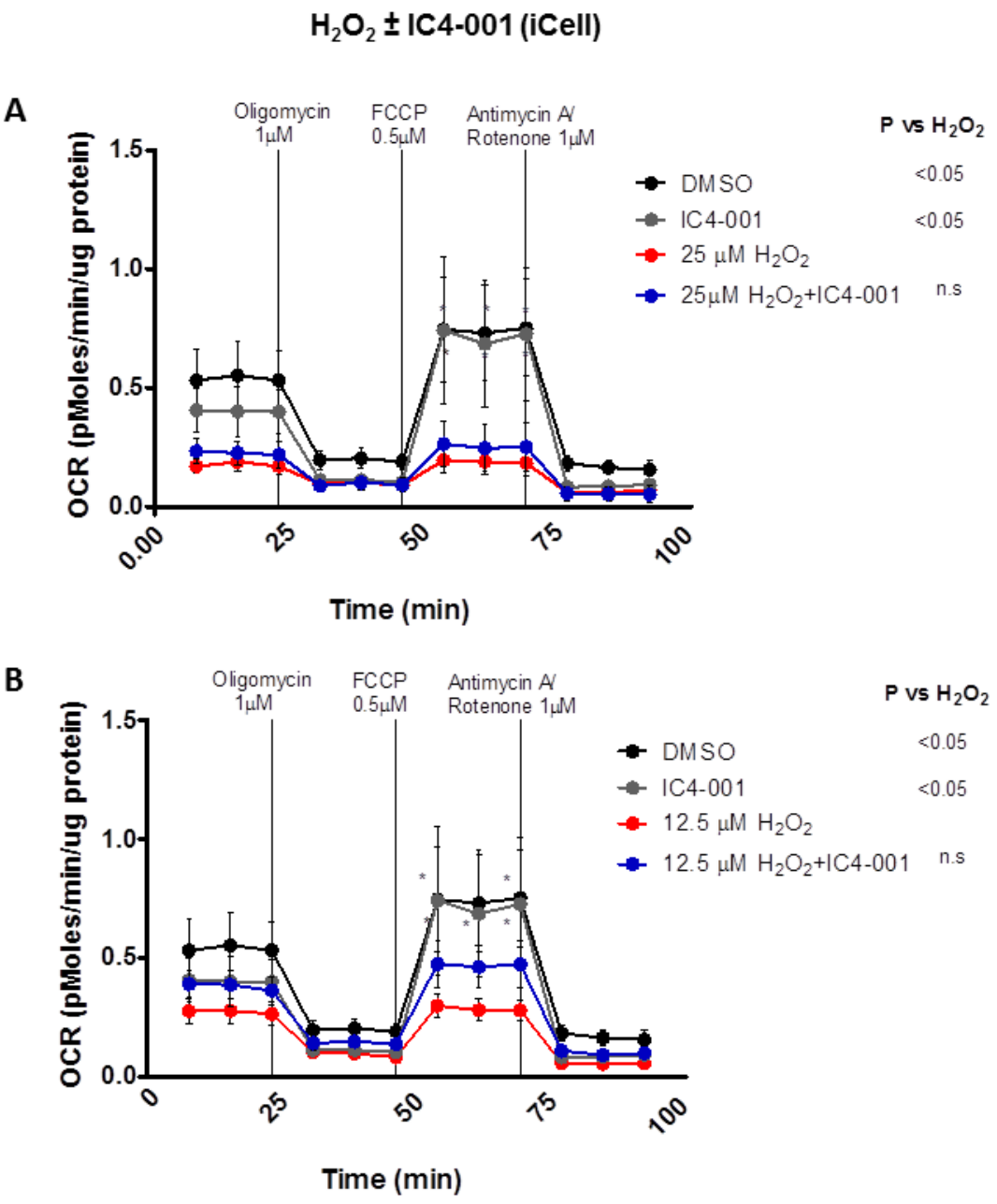


Figure 4.3 The effect of 10µM MAP4K4 inhibitor IC4-001 following H_2O_2 treatment on mitochondrial respiration in hiPSC-CMs. iCell hiPSC-CMs were kept in culture for 12 days and treated with H_2O_2 and OCR was assessed. **A)** The effect of IC4-001 after 25 µM H_2O_2. **B)** The effect of IC4-001 after 12.5 µM H_2O_2. Values were normalised to total protein content per well (µg). Two-way ANOVA, *P < 0.05, **P < 0.01, ***P < 0.001. N= 4 experiments (3 replicates per experiment).

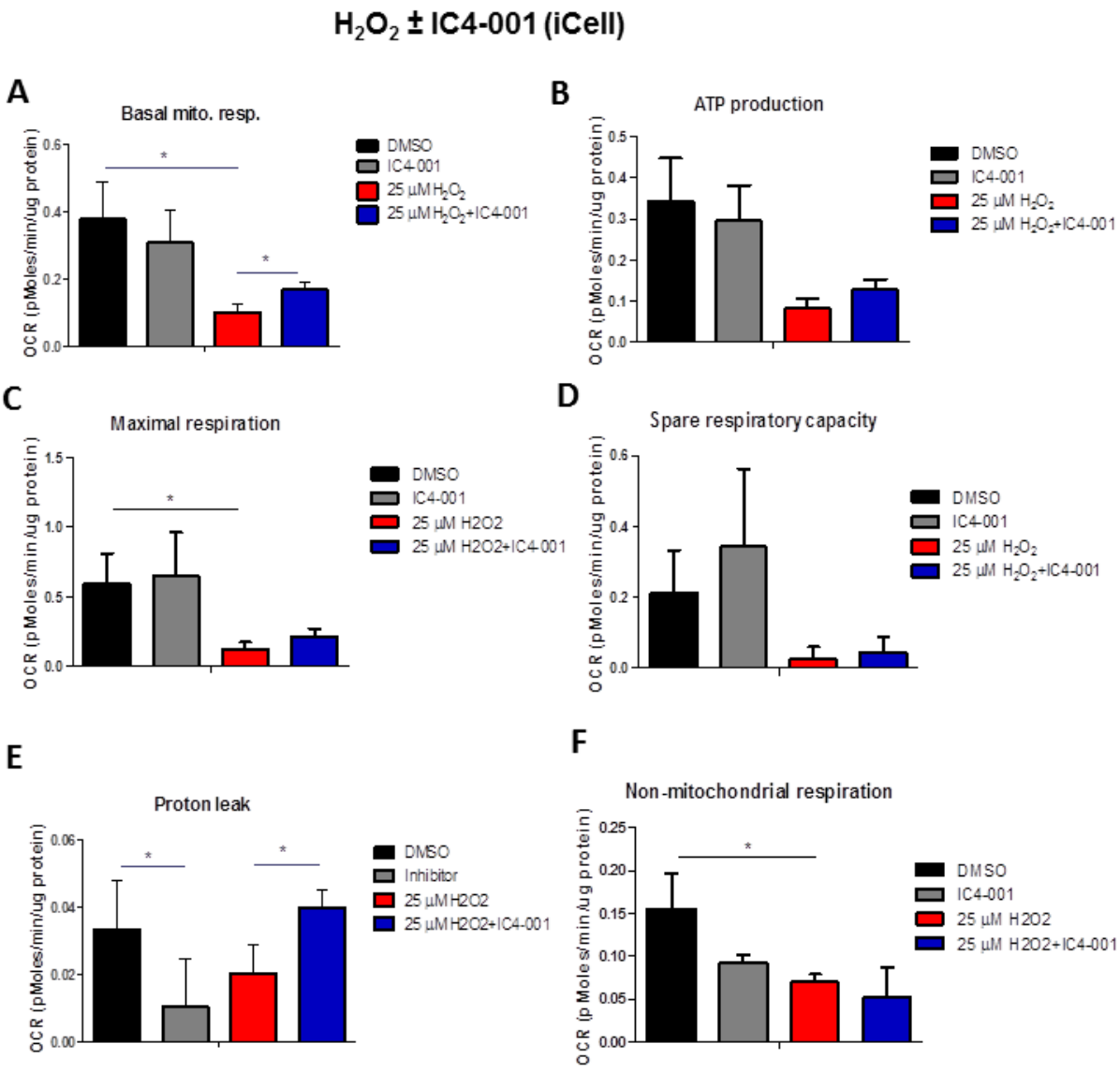


Figure 4.4 Individual components of mitochondrial respiration on MAP4K4 inhibitor IC4-001 following 25 µM H_2O_2 treatment in iCell hiPSC-CMs, calculated as shown in Figure 4.1. A) Basal mitochondrial respiration. **B)** ATP production. **C)** Maximal respiration **D)** Spare respiratory capacity. **E)** Proton leak. **F)** Non-mitochondrial respiration. Values were normalised to total protein content per well (µg). One-way ANOVA, N=4, *P < 0.05, **P < 0.01, ***P < 0.001

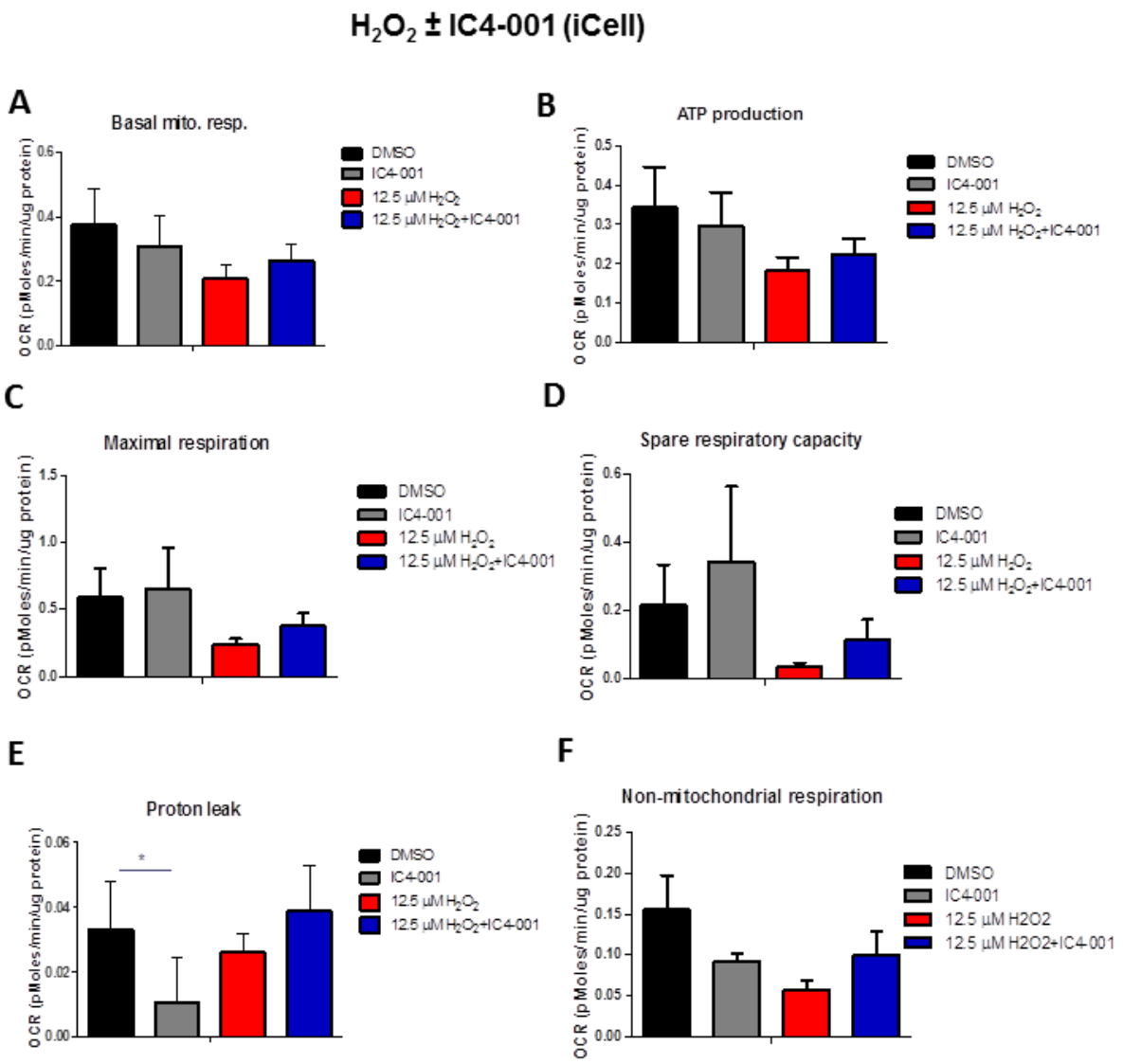


Figure 4.5 Individual components of mitochondrial respiration on MAP4K4 inhibitor IC4-001 following 12.5 µM H_2O_2 treatment in iCell hiPSC-CMs, calculated as shown in Figure 4.1. A) Basal mitochondrial respiration. **B)** ATP production. **C)** Maximal respiration **D)** Spare respiratory capacity. **E)** Proton leak. **F)** Non-mitochondrial respiration. Values were normalised to total protein content per well (µg). One-way ANOVA, error bars: ±S.E.M, N=4, *P<0.05, **P<0.01, ***P<0.001

Basal glycolysis (Fig **4.6**), evaluated by the extracellular acidification rate (ECAR, a measure of proton release) resembled basal mitochondrial respiration results (Fig **4.4A**) as basal ECAR showed protection. MAP4K4 inhibition (10 μM), rescued the 0.25-fold decrease in ECAR induced by 25 μM H_2O_2 at 30 min during the complete timecourse, restoring it to similar levels as for IC4-001 treatment alone (Fig. **4.6A**). Under similar conditions, MAP4K4 inhibition was able to rescue the decrease in basal glycolysis induced by H_2O_2. Levels were restored to 80 % of inhibitor treatment alone (Fig. **4.6B**). In either case, IC4-001 did not affect ECAR (**4.6 A, B**). It was also determined that reduction in OCR and ECAR by H_2O_2 was not confounded by loss of cells, since total protein content remained stable (Fig. **4.6C**). Thus, despite little effect on OCR, MAP4K4 inhibition protected against H_2O_2-induced defects in anaerobic glycolysis, the mode of metabolism that is reactivated in pathologically stressed cardiomyocytes.

Taken together, these results suggest MAP4K4 inhibition protects against H_2O_2-induced mitochondrial dysfunction in hiPSC-CMs. As follow-up experiments, corroboration was sought using complementary cell lines, stressors, and MAP4K4 inhibitors.

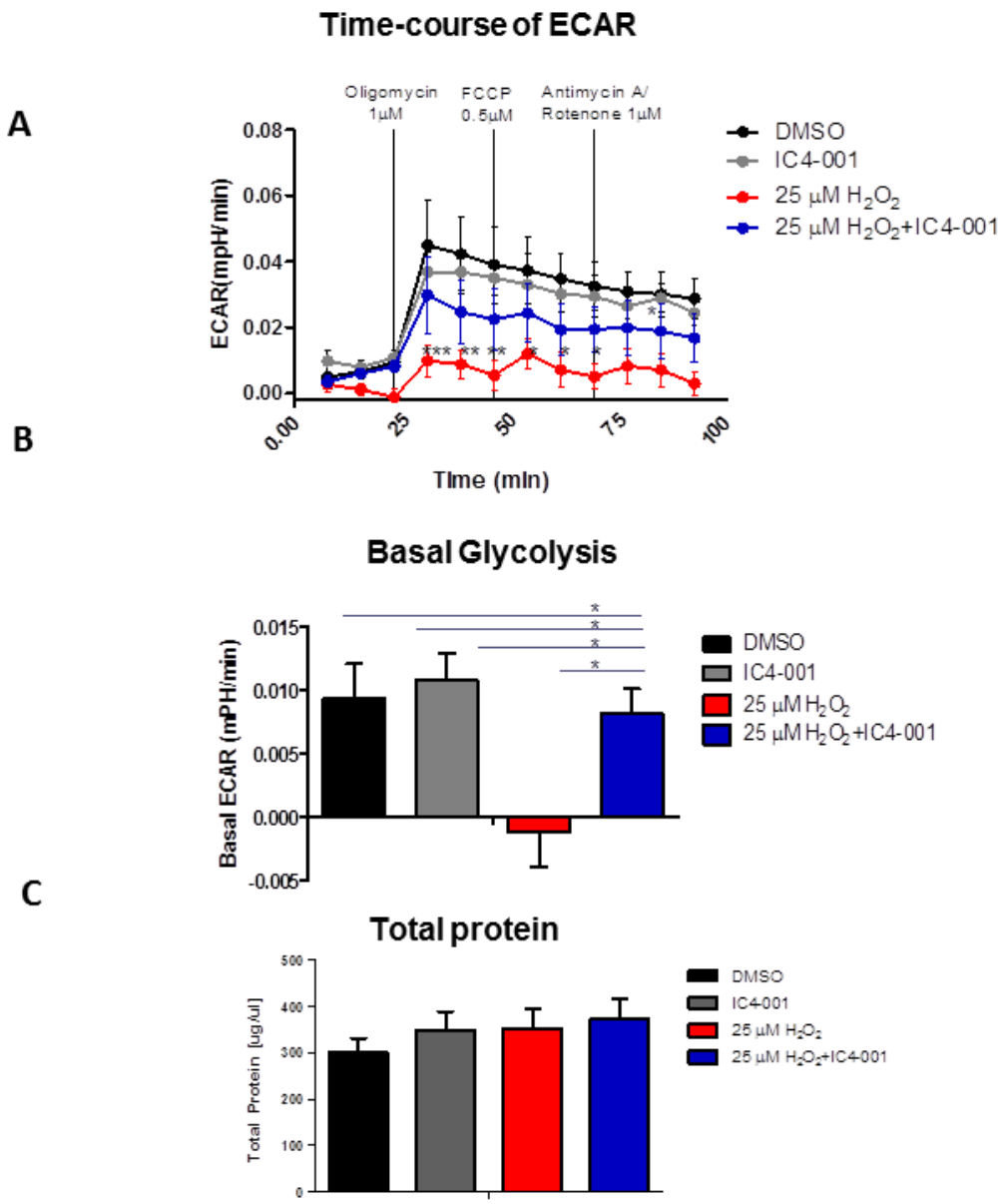


Figure 4.6 The effect of MAP4K4 inhibitor IC4-001 following H_2O_2–induced mitochondrial dysfunction on glycolysis and total protein in iCell hiPSC-CMs. A) The effect of 10µM MAP4K4 inhibitor following H_2O_2 treatment measured by ECAR time-course. **B)** The effect of 10µM MAP4K4 inhibitor following H_2O_2 treatment on basal glycolysis as measured by ECAR. **C)** Total protein assessment was performed by BCA assay. Values were normalised to total protein content per well (µg). Two-way ANOVA (A) and One-way ANOVA (B, C). *P < 0.05, **P < 0.01, ***P < 0.001. Data are the mean of 4 independent experiments (3 replicates per experiment).

4.3 The effects of menadione on mitochondrial function in iCell cardiomyocytes.

To test whether impaired mitochondrial function induced by endogenous ROS can be rescued by MAP4K4 inhibition in a similar manner to exogenous ROS, menadione was used, which generates ROS endogenously through redox cycling (Criddle et al. 2006). To identify a menadione concentration capable of impairing OCR whilst not completely abolishing it, a number of concentrations were tested. At 1 hr, at concentrations from 3 μM, menadione completely abolished respiration (Fig. **4.7A, B**). Lower concentrations partially reduced respiration rate however this did not reach statistical significance (Fig. **4.7C**). When duration of treatment was increased to 2 hr, 3 μM and 4 μM menadione impaired OCR in a statistically significant manner (Fig. **4.7D, E**), and 4 μM menadione was chosen as the concentration to be used in subsequent studies.

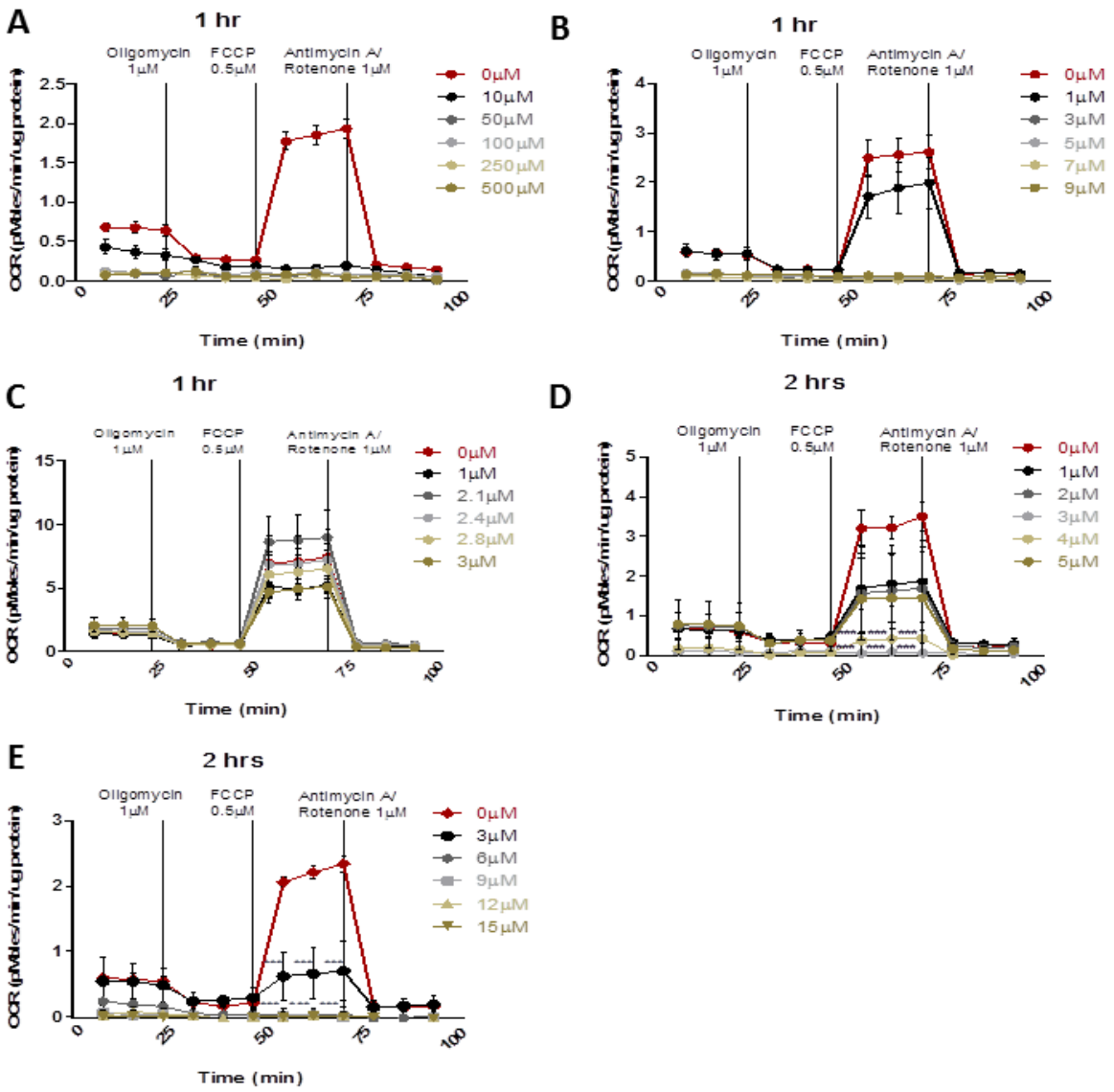
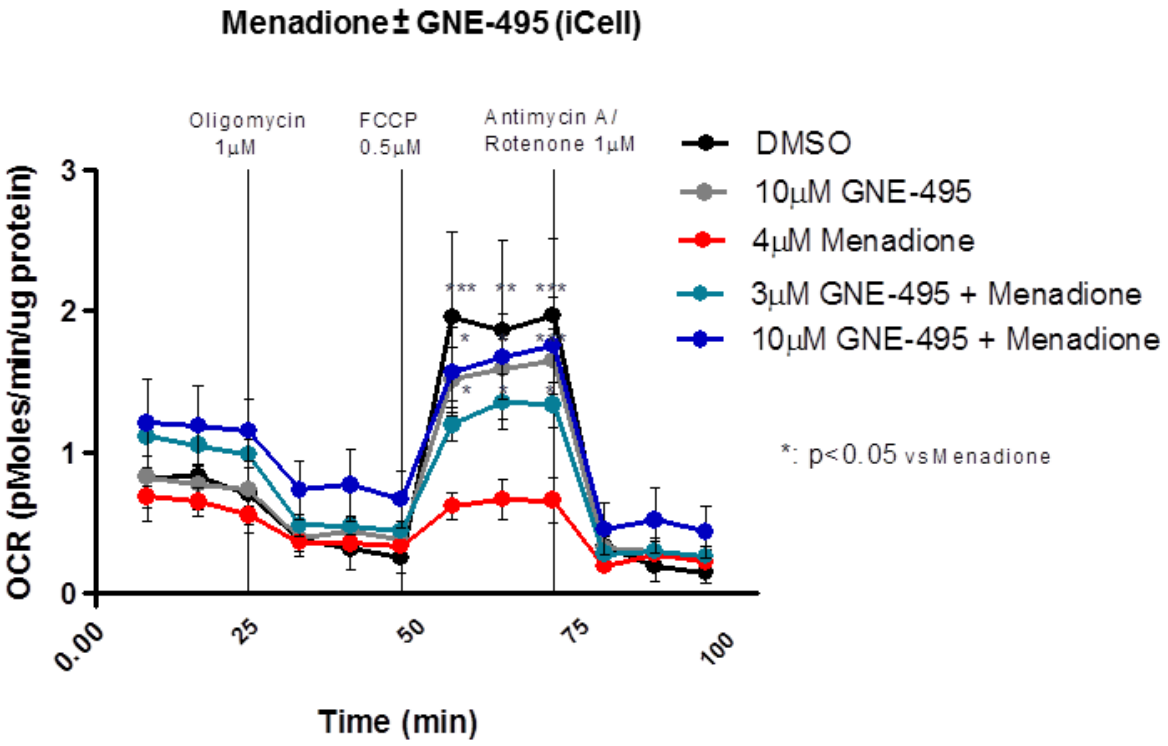


Figure 4.7 The effect of menadione on mitochondrial respiration in iCell hiPSC-CMs. hiPSC-CM were treated with menadione and OCR measured. **A)** 10µM to 500µM menadione treatment for 1 hr **B)** 1µM to 9µM menadione treatment for 1 hr **C)** 1µM to 3µM menadione treatment for 1 hr **D)** 1µM to 5µM menadione treatment for 2 hrs **E)** 1µM to 5µM menadione treatment for 2 hrs . Values were normalised to total protein content per well (µg). N=2 for A, B, C, N=3 for D and E. Two-way ANOVA, *P < 0.05, **P < 0.01, ***P < 0.001

4.4 Effect of MAP4K4 inhibitor GNE-495 on mitochondrial function in iCell cardiomyocytes.

To ascertain whether MAP4K4 mediates impaired mitochondrial respiration induced by endogenous ROS production, an alternative MAP4K4 inhibitor was used, GNE-495. (Ndubaku et al. 2015).

Under optimised conditions (4 μM for 2 hr), menadione reduced mitochondrial respiration levels as measured by OCR, and MAP4K4 inhibition (GNE-495) alone showed no change in mitochondrial respiration profile (Fig. **4.8**). MAP4K4 inhibition by GNE-495 protected against menadione-induced OCR reduction at 10 μM GNE-495 (Fig. **4.8**). When individual components were analysed, menadione significantly reduced maximal respiration and proton leak with no effect to other parameters (Fig. **4.8**). 3 and 10 μM GNE-495 were able to restore maximal respiration levels to that of control (DMSO) at least partially, confirming protection from mitochondrial dysfunction induced by endogenous ROS production (Fig. **4.9**). These concentrations of the inhibitor used were towards the high end of the spectrum, and ideally 1μM should have been used. Indeed this concentration was included in subsequent experiments. The concentrations used here (3 and 10 μM) were initially favoured in order to maintain consistency across the MAP4K4 team. Further, the high cost of the cells coupled with only having 20 wells available per run were important factors which precluded us from testing numerous concentrations alongside each other. MAP4K4 inhibition also rescued the decrease in ECAR, restoring it to normal levels although this was only significant for 10μM GNE-495 (Fig. **4.10A**), with no effects observed due to addition of GNE-495 alone. Basal glycolysis, evaluated by ECAR, did not reach significance (Fig. **4.10B**). Taken together, these results suggest that MAP4K4 inhibitor GNE-495 rescued menadione-induced mitochondrial dysfunction in hiPSC-CMs, in this setting; and thus, that MAP4K4 is involved in mitochondrial dysfunction induced by endogenous ROS in human cardiomyocytes.



	P vs Menadione
DMSO	<0.001
10µM GNE-495	<0.001
3µM GNE-495 + Men	n.s
10µM GNE-495 + Men	<0.05

Figure 4.8 The effect of 10µM MAP4K4 inhibitor GNE-495 following menadione treatment on mitochondrial respiration in iCell hiPSC-CMs. hiPSC-CM were kept in culture for 12 days before treatment. GNE-495 protects from menadione-induced mitochondrial dysfunction as measured by OCR. Values were normalised to total protein content per well (µg). Two-way ANOVA, *P < 0.05. Data are the mean of 4 independent experiments (4 replicates per experiment).

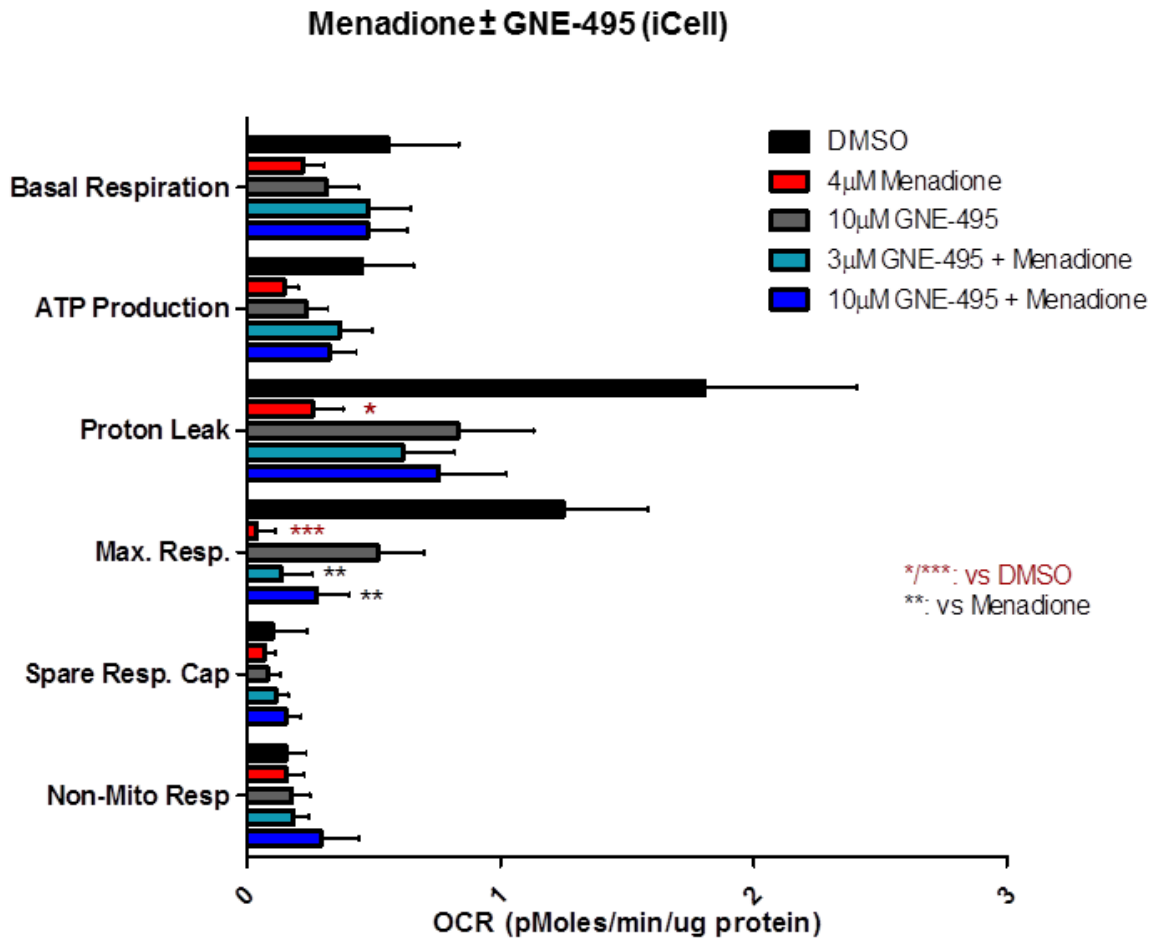


Figure 4.9 Individual components of mitochondrial respiration in response to MAP4K4 inhibitor GNE-495 following menadione treatment. iCell hiPSC-CM were kept in culture for 12 days before treatment. OCR was assessed for Basal mitochondrial respiration, ATP production, Maximal respiration, Spare respiratory capacity, Proton leak and Non-mitochondrial respiration. Values were normalised to total protein content per well (µg). One-way ANOVA, *P < 0.05, **P < 0.01, ***P < 0.001 compared to vehicle control (DMSO). Data are the mean of 4 independent experiments (3 replicates per experiment).

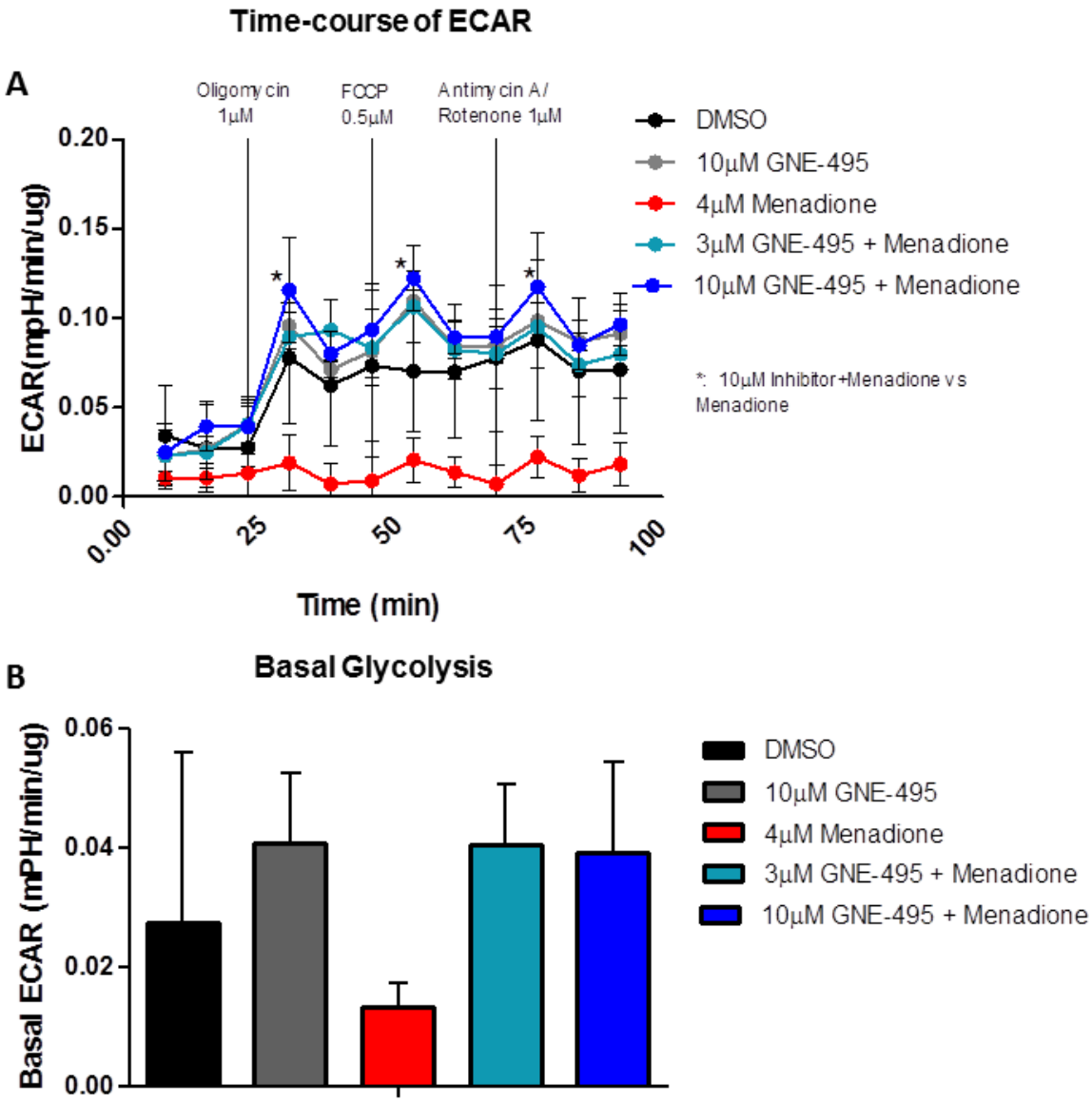


Figure 4.10 The effect of MAP4K4 inhibitor GNE-495 on menadione-induced mitochondrial dysfunction as measured by ECAR. iCell hiPSC-CM were kept in culture for 12 days before treatment. MAP4K4 Inhibition effects on **A)** ECAR time-course and **B)** basal glycolysis levels, with and without menadione treatment. Values were normalised to total protein content per well (µg). Two-way ANOVA (A) and One-way ANOVA (B). Data are the mean of 4 independent experiments (3 replicates per experiment).

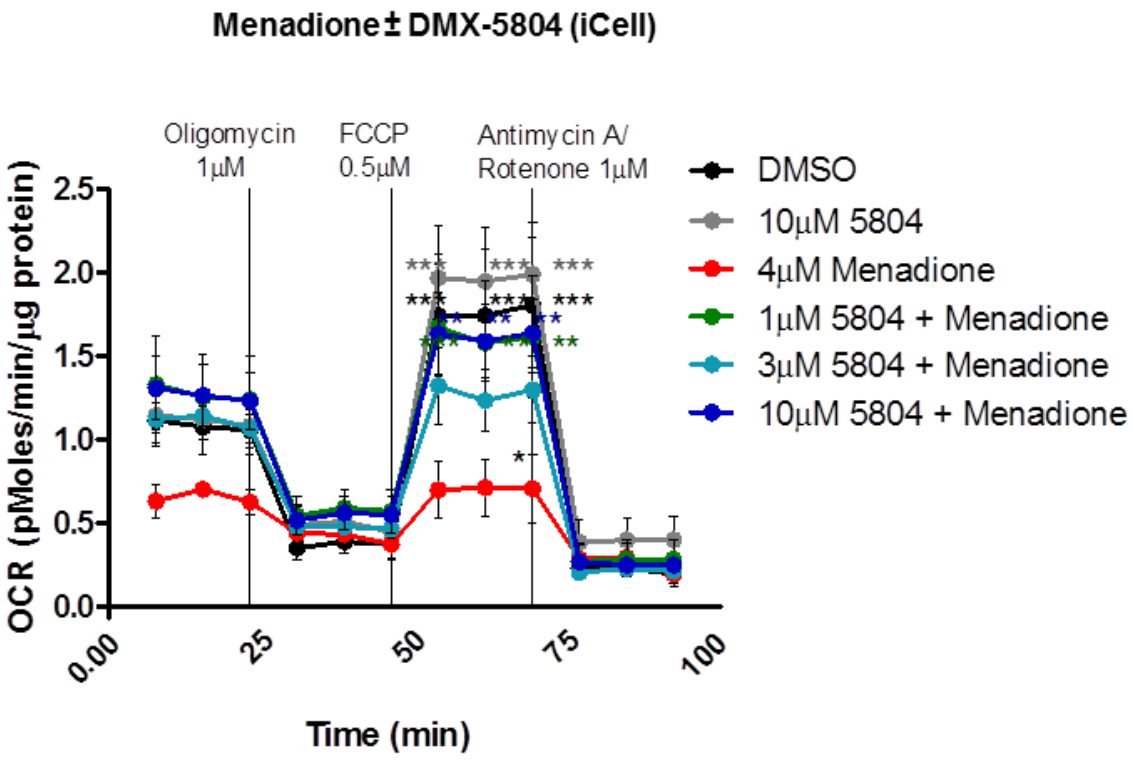
4.5 Effect of MAP4K4 inhibitor DMX-5804 on mitochondrial function in iCell cardiomyocytes.

To further investigate the role of MAP4K4 in cardiac metabolism, the new generation in-house MAP4K4 inhibitor, DMX-5804, was tested, which has improved potency and stability.

MAP4K4 inhibition (DMX-5804) alone showed no change in mitochondrial respiration profile (Fig. **4.11**). Similarly to both prior inhibitors tested, MAP4K4 inhibition by DMX-5804 protected against menadione-induced OCR reduction (Fig. **4.11**). However in contrast, the individual components of mitochondrial respiration did not show protection (Fig. **4.12**).

To evaluate whether these observations were the result of MAP4K4 inhibition rescuing cell number rather than mitochondrial function per cell, cell death was assessed under the conditions tailored for these metabolic studies. Adenylate kinase (AK) activity was measured after menadione treatment to assess loss of plasma membrane integrity; however, no differences were observed (Fig. **4.13**), suggesting that the effects observed indicate mitochondrial function per se.

Taken together, these results suggest that all three pharmacological inhibitors of MAP4K4 (IC4-001, GNE-495, and DMX-5804) partially restore menadione-induced mitochondrial dysfunction in iCell hiPSC-CMs, though with some difference in the phase or phases protected. Because the Imperial and Genentech compounds have largely complementary off-target effects, the data support the inference that MAP4K4 or an indistinguishable kinase mediates mitochondrial dysfunction induced by endogenous ROS in human cardiomyocytes. Further, inhibition alone does not adversely affect mitochondrial function, suggesting the safety of MAP4K4 as a druggable target.



	P vs Menadione
DMSO (***)	<0.001
10µM 5804 (***)	<0.001
1µM 5804 + Men (**)	<0.01
3µM 5804 + Men	n.s
10µM 5804 + Men (**)	<0.01

Figure 4.11 The effect of 10µM MAP4K4 inhibitor DMX-5804 following menadione treatment on mitochondrial respiration in iCell hiPSC-CMs. A) DMX-5804 (5804) protects from menadione-induced mitochondrial dysfunction as measured by OCR. Values were normalised to total protein content per well (µg). Two-way ANOVA, *P < 0.05, **P < 0.01, ***P < 0.001. Data are the mean of 4 independent experiments (4 replicates per experiment).

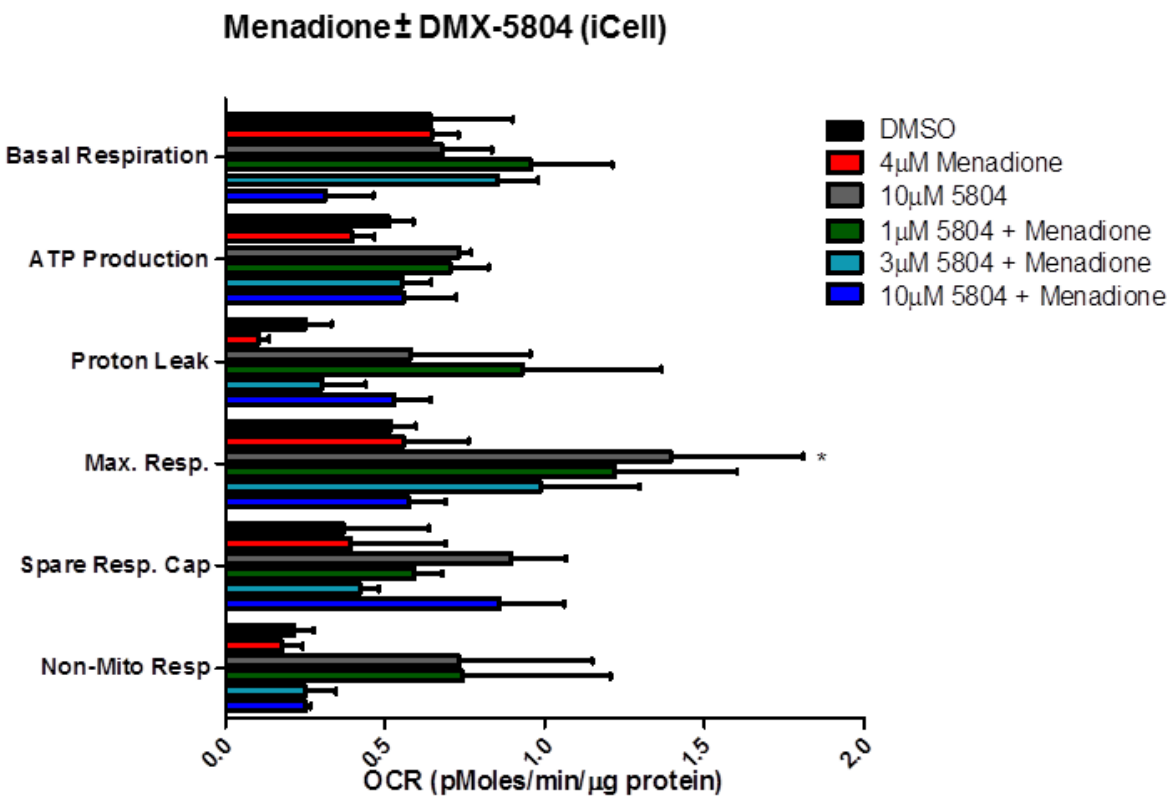


Figure 4.12 Individual components of mitochondrial respiration in response to MAP4K4 inhibitor DMX-5804 (5804) following menadione treatment in iCell hiPSC-CMs. OCR was assessed for Basal mitochondrial respiration, ATP production, Maximal respiration, Spare respiratory capacity, Proton leak and Non-mitochondrial respiration. Values were normalised to total protein content per well (µg). One-way ANOVA, NSD compared to vehicle control (DMSO). Data are the mean of 4 independent experiments (3 replicates per experiment).

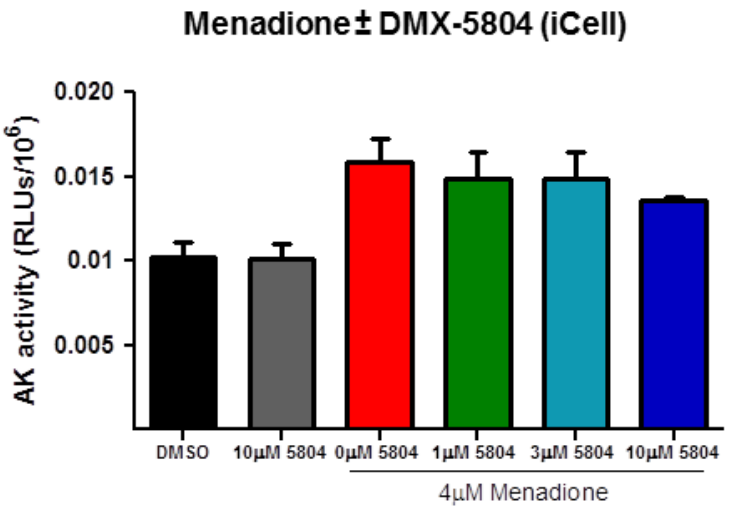


Figure 4.13 Assessment of plasma membrane integrity in DMX-5804-treated iCell hiPSC-CMs in response to menadione. The effect of MAP4K4 inhibition by DMX-5804 (5804) and 4µM menadione on cell death as measured by loss of cell membrane integrity (AK activity). One-way ANOVA; *P < 0.05, **P < 0.01, ***P < 0.001. Data are the mean of 2 independent experiments (4 replicates per experiment).

4.6 Optimisation of seeding density, oligomycin and FCCP concentration for assessment of mitochondrial respiration in CorV.4U cardiomyocytes.

For additional validation, the mitochondrial rescue experiments were repeated in CorV.4U human ventricular muscle cells. To optimise experimental conditions, the effect of cell density on mitochondrial function was explored and 60,000 cells per well was chosen for subsequent experiments (Fig. **4.14**).

Agents used for probing mitochondrial function were first optimised for use in this cell line. Following injection of 0.5,1 and 1.5 µM oligomycin, the biggest drop in OCR (by 0.36 fold compared to basal OCR) was observed at 1 µM and thus, this concentration was used for subsequent assays (Fig. **4.15A**). Using 1µM as the set oligomycin concentration, FCCP was

then injected at up to 2 µM. 0.5 µM FCCP resulted in the biggest increase in OCR (by 5.9 fold), and thus was used in future experiments (Fig. **4.15B**).

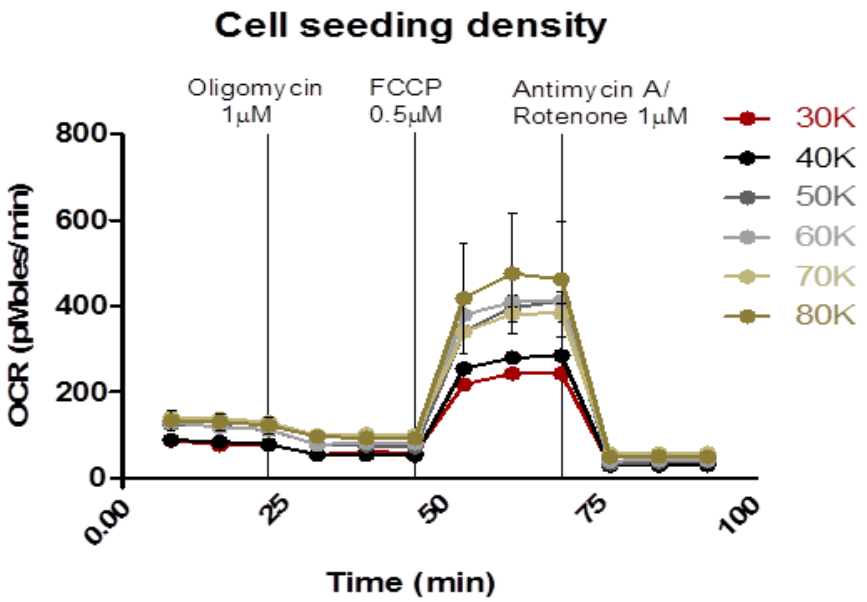
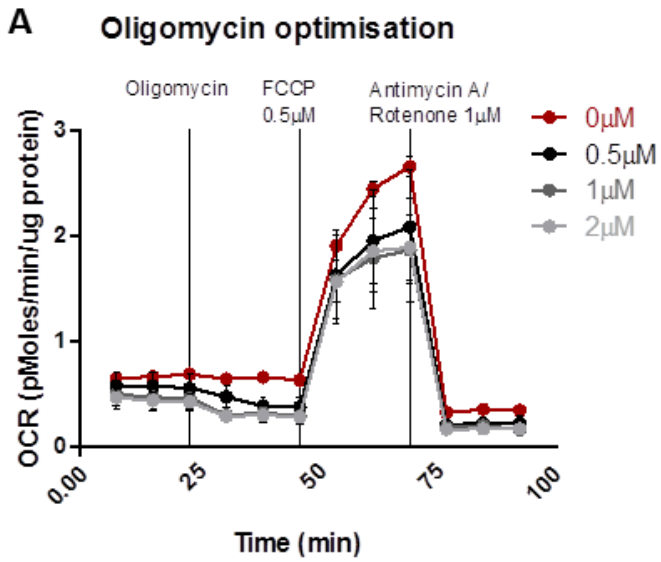
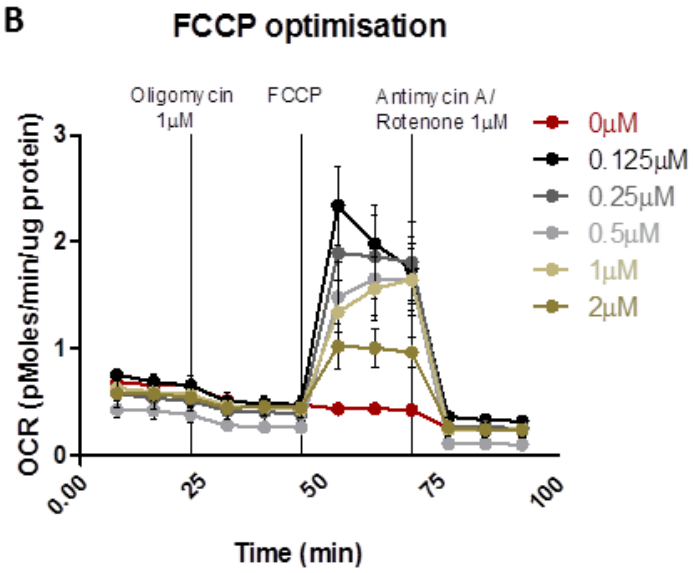


Figure 4.14 Cell seeding number optimisation for CorV.4U hiPSC-CMs. A) CorV.4U hiPSC-CMs were seeded from 30,000 to 80,000 cells per well and OCR measurements were performed as per mito stress test. 60,000 cell per well was chosen as the seeding density for later studies. Data are the mean of 2 independent experiments (3 replicates per experiment).



Oligomycin concentration /µM	Average fold decrease in OCR
0.5	0.13
1	0.36
2	0.32



FFCP concentration/ µM	Average fold increase in OCR
0.125	4.60
0.25	5.7
0.5	5.9
1	2.29
2	1.79

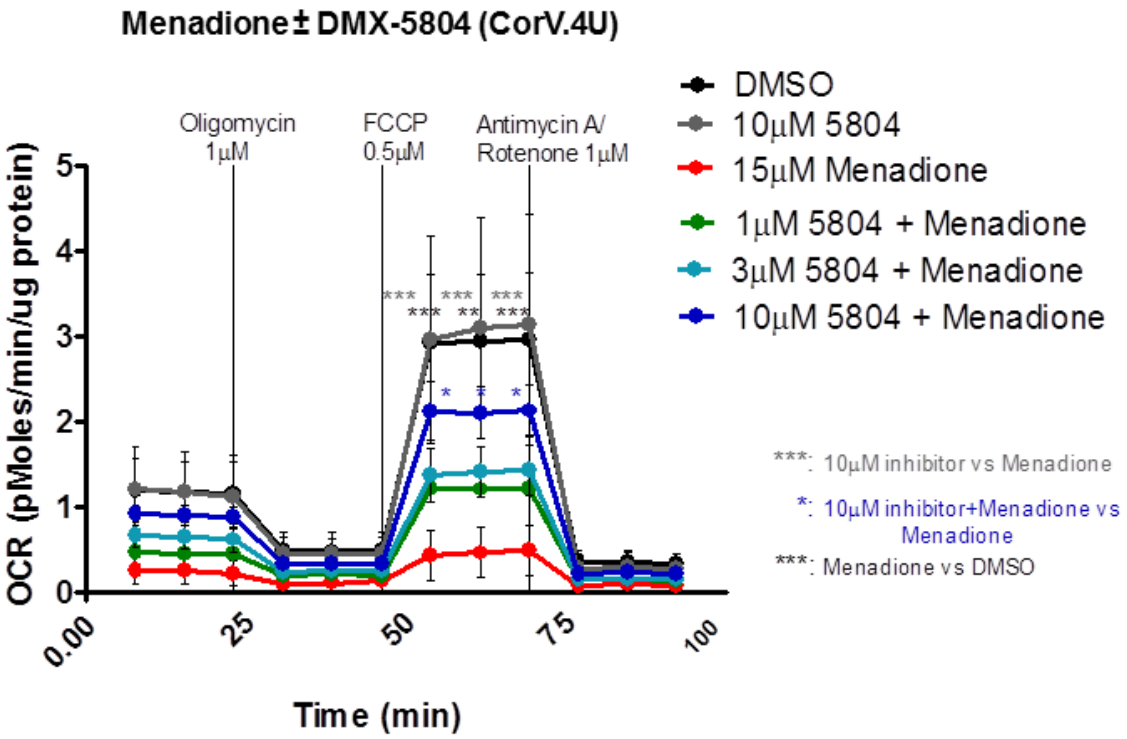
Figure 4.15 Oligomycin and FCCP concentration optimisation in CorV.4U hiPSC-CMs. A) Oligomycin concentration was optimised by injecting 0.5, 1 and 2µM oligomycin following basal OCR measurement. The biggest decline in OCR was observed at 1µM oligomycin. **B)** Following oligomycin optimisation, FCCP was injected at 0.125, 0.25, 0.5, 1 and 2 µM, with the biggest increase in OCR observed at 0.5 µM. Data are the mean of 1 experiment (4 replicates per experiment).

4.7 Effect of MAP4K4 inhibitor DMX-5804 on mitochondrial function in CorV.4U cardiomyocytes.

The in-house next-generation MAP4K4 inhibitor, DMX-5804, was tested in CorV.4U human ventricular myocytes. Menadione reduced mitochondrial respiration levels as measured by OCR, using 15 μM for 2 hr. DMX-5804 protected against menadione-induced OCR reduction at 10 μM, though not at lesser concentrations, and by itself provoked no change in mitochondrial respiration (Fig. **4.16**). Of the separate components of mitochondrial respiration, maximal respiration also showed protection at 10 μM DMX-5804 (Fig. **4.17**). DMX-5804 did not, however, rescue the decrease in ECAR (Fig. **4.18A**). Basal glycolysis, evaluated by ECAR, did not reach significance (Fig. **4.18B**).

To evaluate whether cell death accounted for the effect seen in OCR, loss of plasma membrane integrity was assessed under identical conditions. AK activity was measured to appraise loss of membrane integrity, however no differences were observed (Fig. **4.19**), confirming that the effect observed is due to changes to mitochondrial function per cell, not differences in cell loss.

Taken together, these results suggest that pharmacological inhibition of MAP4K4 (DMX-5804) restores menadione-induced mitochondrial dysfunction in hiPSC-CMs, in the setting of acute oxidative stress. As such, these results point towards a role for MAP4K4 in mitochondrial dysfunction induced by endogenous ROS in human cardiomyocytes. Furthermore, of relevance to future safety considerations, no adverse effects were seen for DMX-5804, on any of the respiration parameters, suggesting that MAP4K4 activity is not required for the maintenance of baseline metabolic function.



	P vs Menadione
DMSO (***)	<0.001
10µM 5804 (***)	<0.001
1µM 5804 + Men	n.s
3µM 5804 + Men	n.s
10µM 5804 + Men (*)	<0.05

Figure 4.16 The effect of 10µM MAP4K4 inhibitor DMX-5804 following menadione treatment on mitochondrial respiration in CorV.4U hiPSC-CMs. hiPSC-CM were kept in culture for 6 days before treatment. **A)** DMX-5804 (5804) protects from menadione-induced mitochondrial dysfunction as measured by OCR. Values were normalised to total protein content per well (µg). Two-way ANOVA,*P < 0.05, **P < 0.01, ***P < 0.001. Data are the mean of 4 independent experiments (4 replicates per experiment).

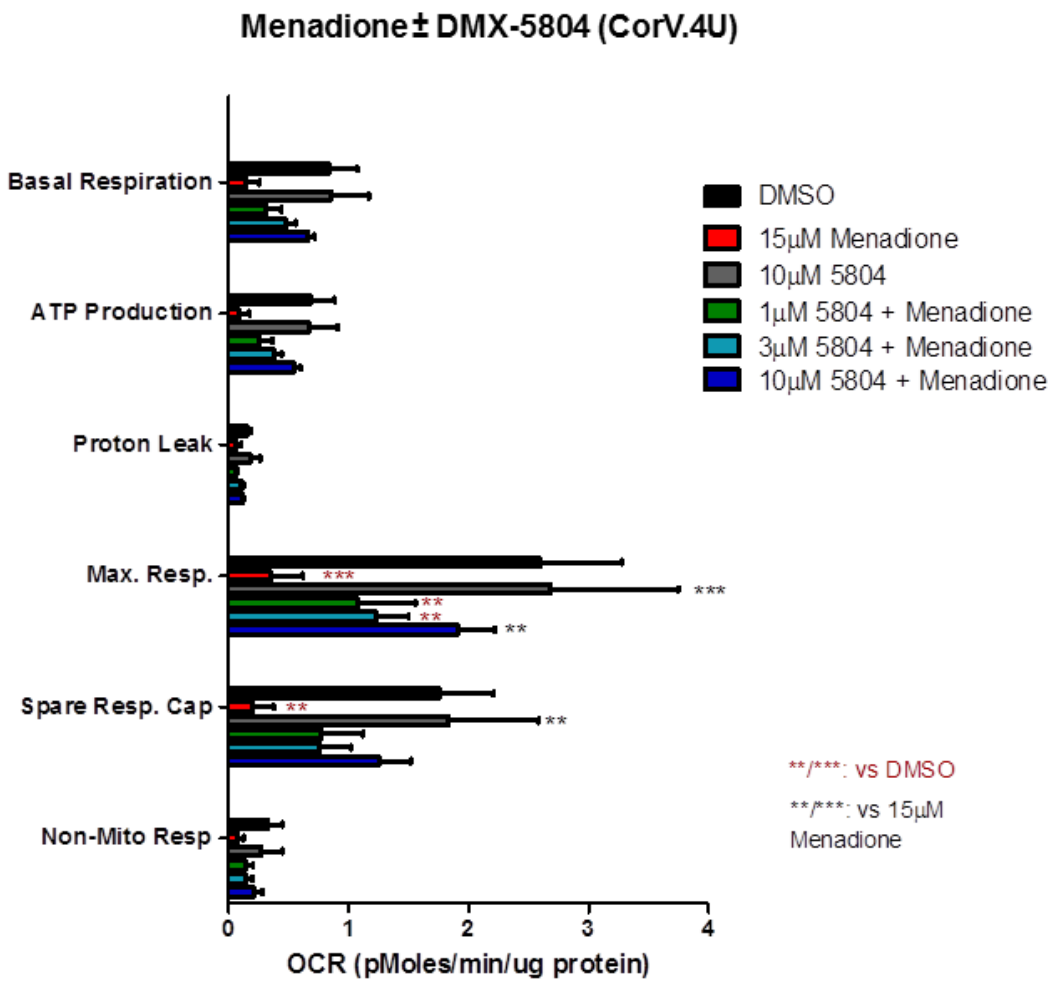


Figure 4.17 Individual components of mitochondrial respiration in response to MAP4K4 inhibitor DMX-5804 (5804) following menadione treatment in CorV.4U hiPSC-CMs. OCR was assessed for Basal mitochondrial respiration, ATP production, Maximal respiration, Spare respiratory capacity, Proton leak and Non-mitochondrial respiration. Values were normalised to total protein content per well (µg). One-way ANOVA, *P < 0.05, **P < 0.01, ***P < 0.001 compared to vehicle control (DMSO). Data are the mean of 4 independent experiments (3 replicates per experiment).

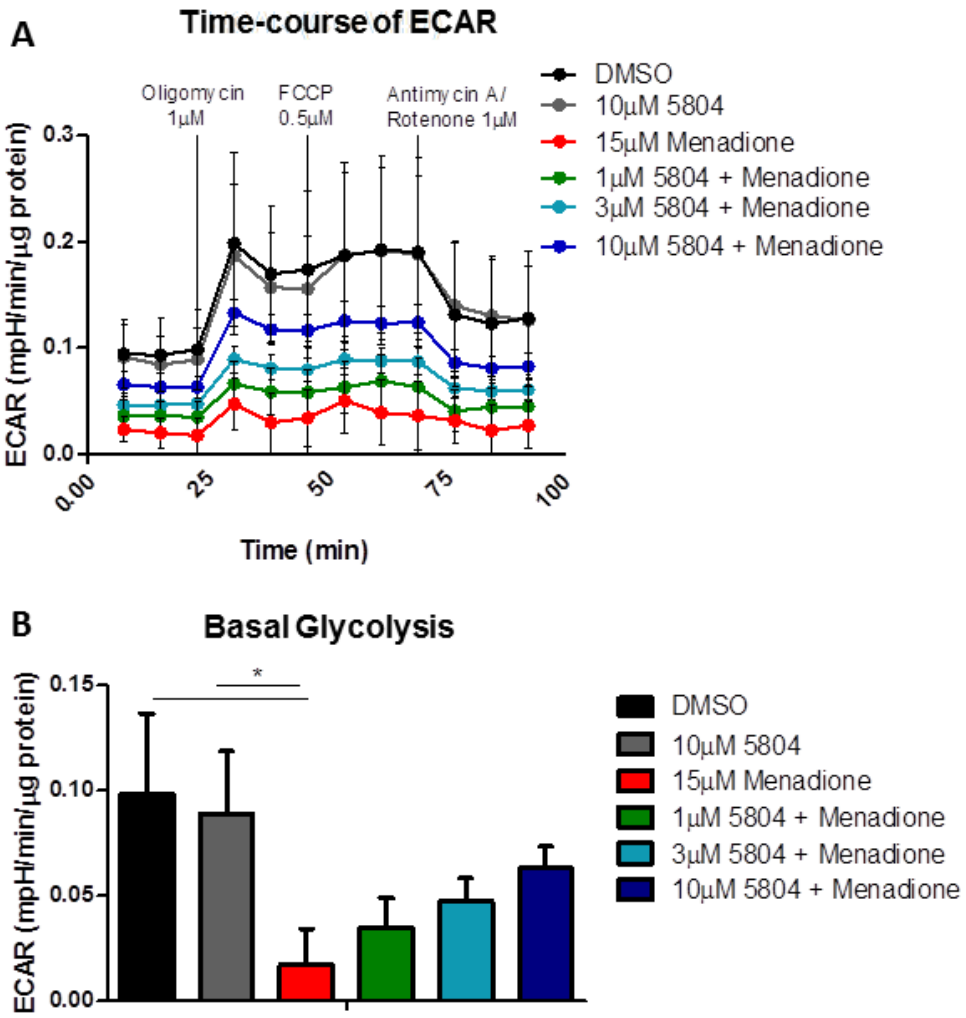


Figure 4.18 The effect of MAP4K4 inhibitor DMX-5804 on menadione-induced mitochondrial dysfunction as measured by ECAR in CorV.4U hiPSC-CMs. DMX-5804 (5804) effects on **A)** ECAR time-course and **B)** basal glycolysis levels, with and without menadione treatment. Values were normalised to total protein content per well (µg). Two-way ANOVA (A) and One-way ANOVA (B), *P < 0.05. Data are the mean of 4 independent experiments (3 replicates per experiment).

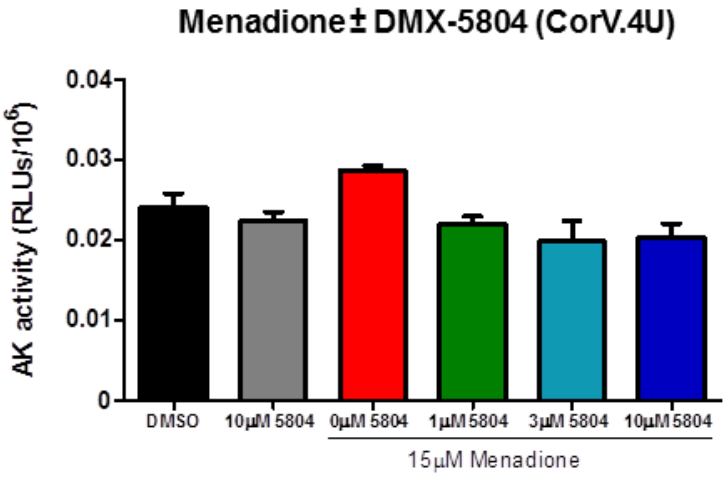


Figure 4.19 Assessment of plasma membrane integrity in DMX-5804-treated CorV.4U hiPSC-CMs in response to menadione. The effect of DMX-5804 (5804) and 15µM Menadione on cell death as measured by loss of cell membrane integrity (AK activity). One-way ANOVA; *P < 0.05, **P < 0.01, ***P < 0.001. Data is the mean of 2 independent experiments (4 replicates per experiment).

4. 8 Synopsis of main findings

Here we show that both exogenous (H_2O_2) and endogenous ROS (menadione) reduce mitochondrial respiration levels in human cardiomyocytes as measured by the oxygen consumption rate (OCR).

Pharmacological inhibition of MAP4K4 using 3 different inhibitors in two human cardiac muscle cell lines was at least partially protective against decreased mitochondrial function induced by exogenous or endogenous ROS, and did not by itself affect basal respiration or glycolysis.

The two cell lines employed, though overall indicative of a role for MAP4K4 in mitochondrial dysfunction, displayed varying results. In iCell hiPSC-CMs, IC4-001 protected basal respiration and basal ECAR from H_2O_2-induced dysfunction; GNE-495 protected against menadione-induced OCR reduction, preserving maximal respiration and the decrease in ECAR. In this cell line, MAP4K4 inhibition by DMX-5804 also protected against menadione-induced OCR reduction, however, the individual components of mitochondrial respiration did not show protection. It was confirmed that cell death was not a confounding factor since AK activity was unchanged. Thus, the effects observed were a result of direct involvement of MAP4K4 in mitochondrial dysfunction.

In CorV.4U hiPSC-CMs, DMX-5804, protected against menadione-induced OCR reduction and maximal oxidative capacity. However, DMX-5804 was not able to rescue the decrease in ECAR. Similarly, cell death was not a confounding factor, since AK activity was unaffected.

Taken together, these results with complementary interventions and human cell lines strongly suggest that pharmacological inhibition of MAP4K4 can protect against mitochondrial dysfunction induced by acute oxidative stress in human cardiomyocytes.

4.9 Discussion

Ischemia reperfusion exposes mitochondria to oxidative stress, causing damage and altering respiration rates, which directly impacts on cardiac contractility and survival. To test whether MAP4K4-dependent signalling is involved in mitochondrial impairment induced by oxidative stress, exogenous and endogenous stressors were used, and MAP4K4 inhibition achieved using three different compounds. Importantly, MAP4K4 did not impair baseline mitochondrial function of either iCell or CorV.4U human iPSC-derived cardiomyoyctes.

In the ventricularly enriched cell line CorV.4U which was employed since the left ventricle is highly affected in heart failure (Harvey & Leinwand 2011; White & Chew 2008) and due to better cell quality. DMX-5804 protected against menadione-induced OCR and did not affect baseline mitochondrial function. Among the separate components of mitochondrial respiration, maximal oxidative capacity also showed protection by DMX-5804. DMX-5804 however, did not rescue the decrease in ECAR, a measure of proton release and thus, glycolytic function. These observations were similar to findings on iCell hiPSC-CMs.

Maximal respiratory capacity refers to the maximum activity of electron transport and substrate oxidation achievable by cells under specific assay conditions. MAP4K4 inhibition protected from menadione-induced decreases in maximum respiratory capacity. A decrease in maximum respiratory capacity is a strong indicator of mitochondrial dysfunction (Brand & Nicholls 2011), although uncoupling through use of agents such as FCCP could have significant consequences. In this study, FCCP uncoupled rates were carefully titrated to avoid this, since also media composition could affect the response to FCCP (Nicholls et al. 2010).

Mitochondria have ‘reserve capacity’ in the physiological range, which is depleted under conditions of stress such as pressure overload (Kingsley-Hickman et al. 1990) or ischemia (Gong et al. 2003). During volume and pressure overload (Strauer 1987) and ischemia (Smith et al. 1996; Sako et al. 1988), myocytes develop an increased ability to consume oxygen, suggesting a mechanism for depletion of this reserve capacity in an environment in which oxygen availability is limited. Therefore, the availability of this reserve capacity is crucial to contest oxidative stress and when it is exceeded protein damage and cell death occurs (Hill et al. 2009), accompanied by decreased OCR. Spare respiratory capacity was exhibited normal levels in the presence of the inhibitor alone in CorV.4U hiPSC-CMs although this was not the case in iCell hiPSC-CMs. This suggests that these cell lines present different mechanisms but also points to a change in respiratory capacity as a possible mechanism for MAP4K4-mediated protection.

DMX-5804 protected against menadione-induced OCR reduction in iCell hiPSC-CMs. However, the individual components of mitochondrial respiration did not show protection, possibly due to alternative off-target effects compared to the other two inhibitors. It was also notable that while the overall effect of 4 μM menadione was significant, the individual components were not. This could represent a lack of power due to high variability, or to the overall effect resulting from a combination of factors.

These results suggest that pharmacological inhibition of MAP4K4, studied most extensively with DMX-5804, can partially restore menadione-induced mitochondrial dysfunction in human stem cell-derived cardiomyocytes. Some individual aspects, however, might be affected by menadione through MAP4K4-independent mechanisms in this cell background. These results are in agreement with the findings observed for IC4-001 in iCell cardiomyocytes, whereas the final refinement (change in cell line to CorV.4U) enabled us to resolve protection at the level of the individual components of mitochondrial respiration.

Our results, collectively, indicate that mitochondrial dysfunction induced by endogenous ROS is dependent on MAP4K4 activity, however some differences were observed with the different inhibitors. This may reflect differences in off-target effects, which may be positive or negative in this setting, or exogenous ROS-induced mitochondrial dysfunction being less dependent on MAP4K4 signalling pathways than endogenous ROS. As no ATP-competitive inhibitor distinguishes MAP4K4 from TNIK and MINK, we do not exclude the possibility that these related STE kinases function in the pathway, redundantly.

It was not possible, in our hands, to directly compare inhibitors for chiefly two reasons. Firstly, the availability of the cells was a limiting factor since these lines are very costly. Secondly, the automated platform used is only able to read one plate at a time, it takes a few hours for the assay to run and our facilities have only one Seahorse XF Analyzer. In future, the use of more than one platform at any given time would increase the number of inhibitors and cell lines we are able to directly compare and would confirm our findings.

H_2O_2 is one of the most broadly used agents to induce oxidative stress in vitro (Gille & Joenje 1992). H_2O_2 is a small, non-charged molecule that easily crosses membranes and localises in many sub-cellular compartments (Bienert et al. 2006). Pharmacological inhibition of MAP4K4 by IC4-001 partially protected against H_2O_2-induced mitochondrial dysfunction in iCell CMs. H_2O_2 is a generator of extracellular ROS and as such, the partial rescue observed by MAP4K4 inhibition might have been as a result of MAP4K4-independent effects or mitochondria-independent effects. Although H_2O_2 addition to cell culture is a widely used model, H_2O_2 does not resemble I/R conditions as closely as an endogenous generator of ROS might (Kaczara et al. 2010; Kinnula et al. 1992). Further, H_2O_2 concentration and time exposure are difficult to control because availability of H_2O_2 changes over time as the agent is depleted from the medium as well as due to the dynamic mechanisms affecting its availability (Kaczara et al. 2010). As a result, menadione, an endogenous generator of ROS was also tested. Menadione is a polycyclic aromatic ketone that generates intracellular ROS

at multiple sites through redox cycling and has been shown to activate apoptosis (Kinnula et al. 1992; Criddle et al. 2006; Loor et al. 2010). In our hands, menadione yielded more consistent results.

In iCell cardiomyocytes H_2O_2 disrupted mitochondrial respiration as expected, decreasing OCR (Garrity et al. 2015). H_2O_2-exposure for very short time periods showed that all mitochondrial function is abolished well before H_2O_2 levels are sufficient to increase caspase-3 cleavage or membrane permeability. However, MAP4K4 inhibition (IC4-001) was not protective against loss of OCR. H_2O_2 may signal through both MAP4K4 dependent and independent pathways. Basal ECAR however, was rescued by MAP4K4 inhibition (IC4-001) and normal levels restored. This suggests that impairment of glycolysis may be MAP4K4-dependent in this cell line. In terms of the individual respiration phases, MAP4K4 inhibition protected against loss of basal mitochondrial respiration, maximal respiration and non-mitochondrial respiration from H_2O_2-induced OCR reduction. Oxygen consumption dedicated to preserving the proton gradient as a result of proton leak was assessed, amongst other respiratory parameters, and it was found that MAP4K4 inhibition by the initial compound prototype (IC4-001) protected proton leak levels from H_2O_2-induced reduction by restoring them to normal levels. This may indicate proton leak to be acting as an alternative adaptive mechanism by modulating the production of ROS in the mitochondria or a decrease in mitochondrial efficiency since increased proton leak through the inner mitochondrial membrane may be facilitated by uncoupling proteins or leakage through damaged respiratory complexes (Hill et al. 2009).

Our results indicate that MAP4K4 may be involved in regulating metabolism in the heart and in particular, in driving dysfunction in the setting of acute oxidative stress. This is in agreement with recent findings reporting the involvement of MAP4K4 in metabolism (Virbasius & Czech 2016) where MAP4K4 deletion suppressed insulin sensitivity and suppressed lipid synthesis (Danai et al. 2015). Further, MAP4K4 siRNA knockdown can

improve substrate uptake, conferring increased glucose sensitivity in skeletal muscle cells (Bouzakri & Zierath 2007). In future, different substrates (or no substrate) should be tested to provide an indication as to the mechanism for metabolic activity and further clarify the role of MAP4K4 signalling in this cell type.

Therefore, MAP4K4 inhibition preserves mitochondrial function in human cardiomyocytes in the setting of acute oxidative stress. Conversely, MAP4K4 is not required for baseline mitochondrial function in human cardiomyocytes. In terms of future safety considerations, we have successfully shown that MAP4K4 inhibitors evoked no adverse effect on any of the functional parameters involved in mitochondrial respiration assessed here.

5. Results

Chapter 5: The effects of MAP4K4 inhibitor DMX-5804 on calcium handling

Calcium cycling, a hallmark of the cardiac failure phenotype, is susceptible to redox- and phosphorylation-dependent abnormalities (Gorski et al. 2015; Fearnley et al. 2011). Calcium handling is the main determinant of cardiomyocyte contractility, in particular calcium release from the sarcoplasmic reticulum (SR). Calcium signalling is highly regulated in myocytes and is directly related to the force of cardiac muscle contraction (Marks 2013). Calcium cycling refers to the release and reuptake of intracellular calcium, which is able to drive muscle contraction and relaxation; this is hugely altered in failing hearts and results in impaired contractility and arrhythmias (Bers 2008). Numerous potential therapies have been reported as unsuccessful due to their involvement in causing either arrhythmia or cytotoxicity (Eder et al. 2015). As such, it is important to evaluate calcium cycling as part of the compound's safety profile.

Here, the effects of oxidative stress on calcium dynamics in hiPSC-CMs were assessed, in the absence or presence of the MAP4K4 inhibitor DMX-5804. Calcium dynamics studies were performed using the optical platform CellOPTIQ (Fattah et al. 2016). CorV.4U hiPSC-CMs were used as they present reduced cell type heterogeneity and were selected based on their higher physiological relevance (Harvey & Leinwand 2011; White & Chew 2008; Dimmeler et al. 2005). Menadione is, as previously mentioned, an endogenous ROS generator (Criddle et al. 2006; Loor et al. 2010) which has been shown to cause cell death in pancreatic cells (Criddle et al. 2006), hiPSC-CMs (Burridge et al. 2016) and embryonic chick cardiomyocytes (Loor et al. 2010). The work presented attempts to shed light into the mechanistic implications of MAP4K4 inhibition following oxidative stress, and whether this may be benefit the contractile machinery or simply impact cell survival.

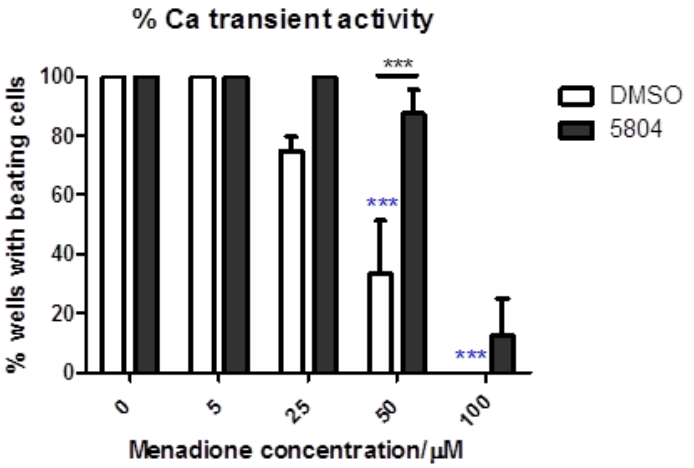
5.1 Effects of the MAP4K4 inhibitor DMX-5804 on menadione-induced calcium handling impairment in CorV.4U hiPSC-CMs

As an attempt to gain insight into whether MAP4K4 inhibitor DMX-5804 exerts an effect on calcium homeostasis following oxidative stress, calcium cycling was assessed using the CellOPTIQ platform. Calcium transients were measured by using Fura-4-AM (Stosiek et al. 2003), a ratiometric dye, and by analysing the ratio between the two wavelengths to give measurements that are unaffected by movement or variation in cell layer thickness. Following optimisation of dye concentration and cell seeding density, 4μM Fura-4 and 60,000 cells/well were chosen for our studies (data not shown).

CorV.4U cells in 2D cultures were treated with 0-100μM menadione for 24 hr. A concentration-dependent decrease in calcium transient activity was observed in the presence of menadione, with the percentage of calcium cycling wells significantly decreasing with 50 μM and 100 μM from 100% to 33% and 0% respectively (Fig. **5.1 A**). Calcium transient amplitude (Fig. **5.2 A**), a measure of calcium release, was also decreased from 100% to 37% and 0% respectively, consistent with this observation (Fig. **5.1 A**).

At 50 μM menadione, MAP4K4 inhibition (10μM DMX-5804) protected against menadione-induced calcium cycling impairment, as measured by the % wells that are cycling (2-fold increase), with 21 of 24 wells presenting spontaneous calcium oscillations when MAP4K4 was inhibited compared to 8 in the absence of DMX-5804 (Fig. **5.1 A, B**) (87.5% are cycling in the presence of both DMX-5804 and menadione, versus 33% cycling only in the presence of menadione).

A



B

	Beating	Non-beating	Total number wells
50 µM Menadione	8	16	24
5804+ Menadione	21	3	24

Figure 5.1 The effect of DMX-5804 on calcium handling for menadione-treated CorV.4U hiPSC-CMs. Cells in 2D cultures were treated with 0-100µM menadione for 24 hr in the presence of 10µM DMX-5804 (5804). **A)** Calcium transient activity in menadione- and 5804-treated hiPSC-CMs as measured by the % of wells that contain beating cell areas. **B)** Table showing number of beating and non-beating wells for 50µM menadione- and 5804-treated hiPSC-CMs. Two-way ANOVA for DMSO vs 5804 (black), one-way ANOVA for DMSO only (blue); N=4, ***P < 0.001.

A number of further parameters were analysed to more thoroughly assess the dynamics of calcium cycling. MAP4K4 inhibition alone did not alter the change in transient amplitude, calcium release rate as measured by time to transient peak, reuptake rate as measured by time to 75% decay, transient duration and cycle length; showing that DMX-5804 does not adversely affect calcium cycling at baseline, an important safety feature for a potential pharmacological agent (**Fig 5.2 A-E**). However, DMX-5804 did not prevent the changes induced by 50 µM menadione to the calcium handling parameters analysed (**Fig. 5.2 A-E**).

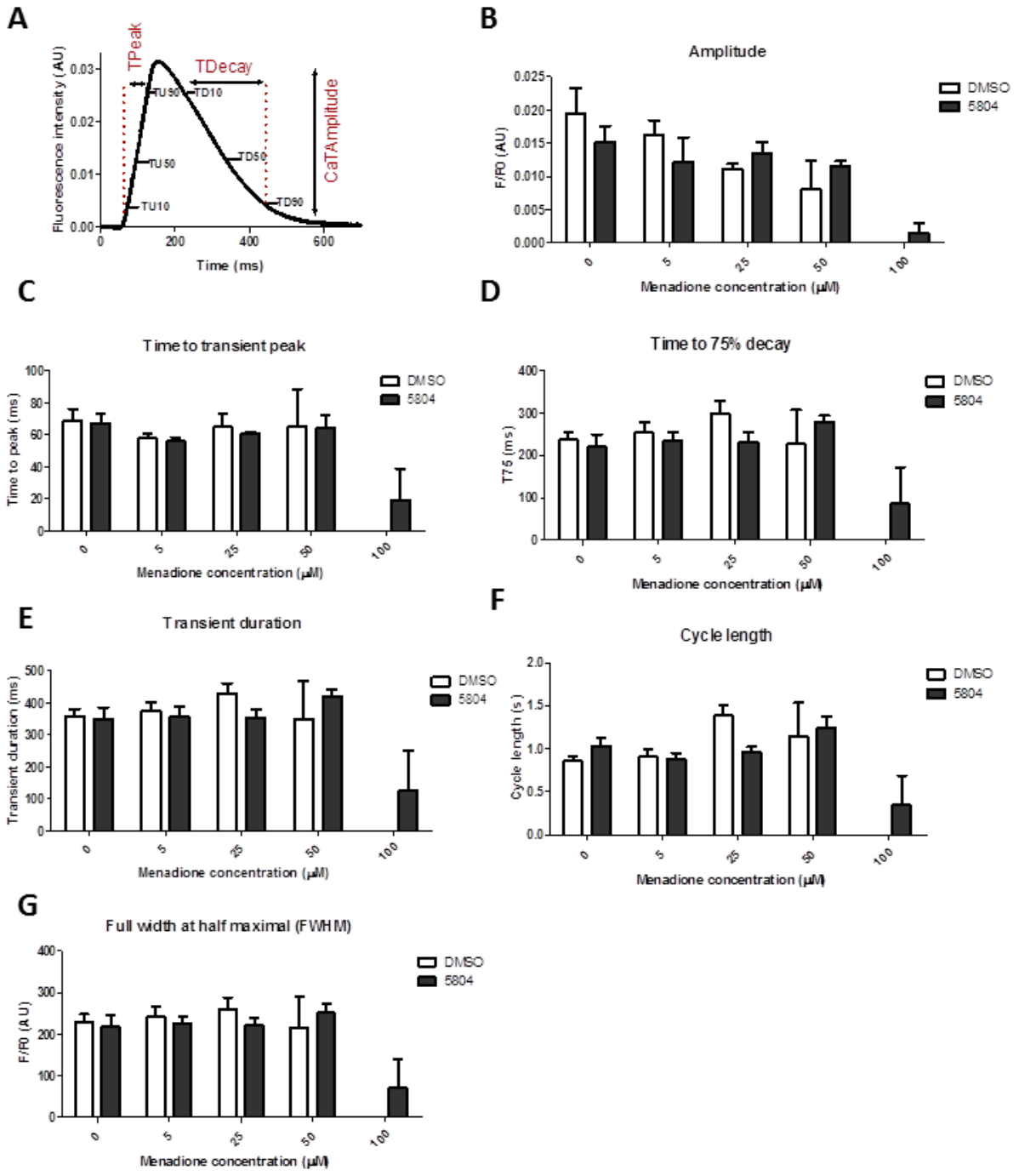


Figure 5.2 The effect of MAP4K4 inhibitor DMX-5804 on calcium dynamics in menadione-treated CorV.4U hiPSC-CMs. A) Analysed calcium transient outputs **B)** Amplitude; **C)** Time to transient peak ; **D)** Time to 75% decay ; **E)** Transient duration; **F)** Cycle length; and **G)** Full-width at half maximal (FWHM) in menadione- and DMX-5804 (5804)-treated hiPSC-CMs. Two-way ANOVA; NDS N=4

Under the conditions tested, the percentage of wells that exhibit calcium cycling and the amplitude of the calcium transient in the cycling cells were highly sensitive to oxidative stress, whereas beating rate and kinetics of the calcium transient in cycling cultures were not. Thus, MAP4K4 inhibition preserves calcium cycling in hiPSC-CMs, in the setting of acute oxidative stress.

5.2 Effects of MAP4K4 inhibitor DMX-5804 on menadione-induced cleaved caspase-3 induction, membrane integrity and mitochondrial membrane potential in CorV.4U cardiomyocytes

To elucidate the extent to which the functional effect seen in the presence of MAP4K4 inhibitor DMX-5804 is due to changes to calcium cycling, cell death was monitored under the same conditions (menadione treatment) by measuring caspase-3 cleavage and loss of membrane integrity (AK activity). It was found that menadione induced cell death at 50μM and 100 μM as measured by both caspase-3 cleavage and loss of membrane integrity (AK activity, Fig. **5.3 A, B**). Further, MAP4K4 inhibition (10 μM DMX-5804) protected from both caspase-3 cleavage and loss of membrane integrity (AK activity) at both concentrations of menadione (Fig. **4 A, B, D**). This suggests that no impairment of calcium transient activity was observed under sub-lethal oxidative stress; rather, the rescue of calcium transient activity is due to protection from cell death, which translates into the presence of a larger number of healthy, calcium-cycling cells. This conclusion is further supported by the rescue of cell number itself at 50 μM menadione by 10 μM DMX-5804 (Fig. **4 C**).

Therefore, MAP4K4 inhibition protects from menadione-induced caspase-3 cleavage and loss of membrane integrity, and the surviving cells show unimpaired calcium dynamics under the conditions tested. Together, these results suggest pharmacological inhibition of MAP4K4 as a potentially effective and safe means of cardioprotective therapy.

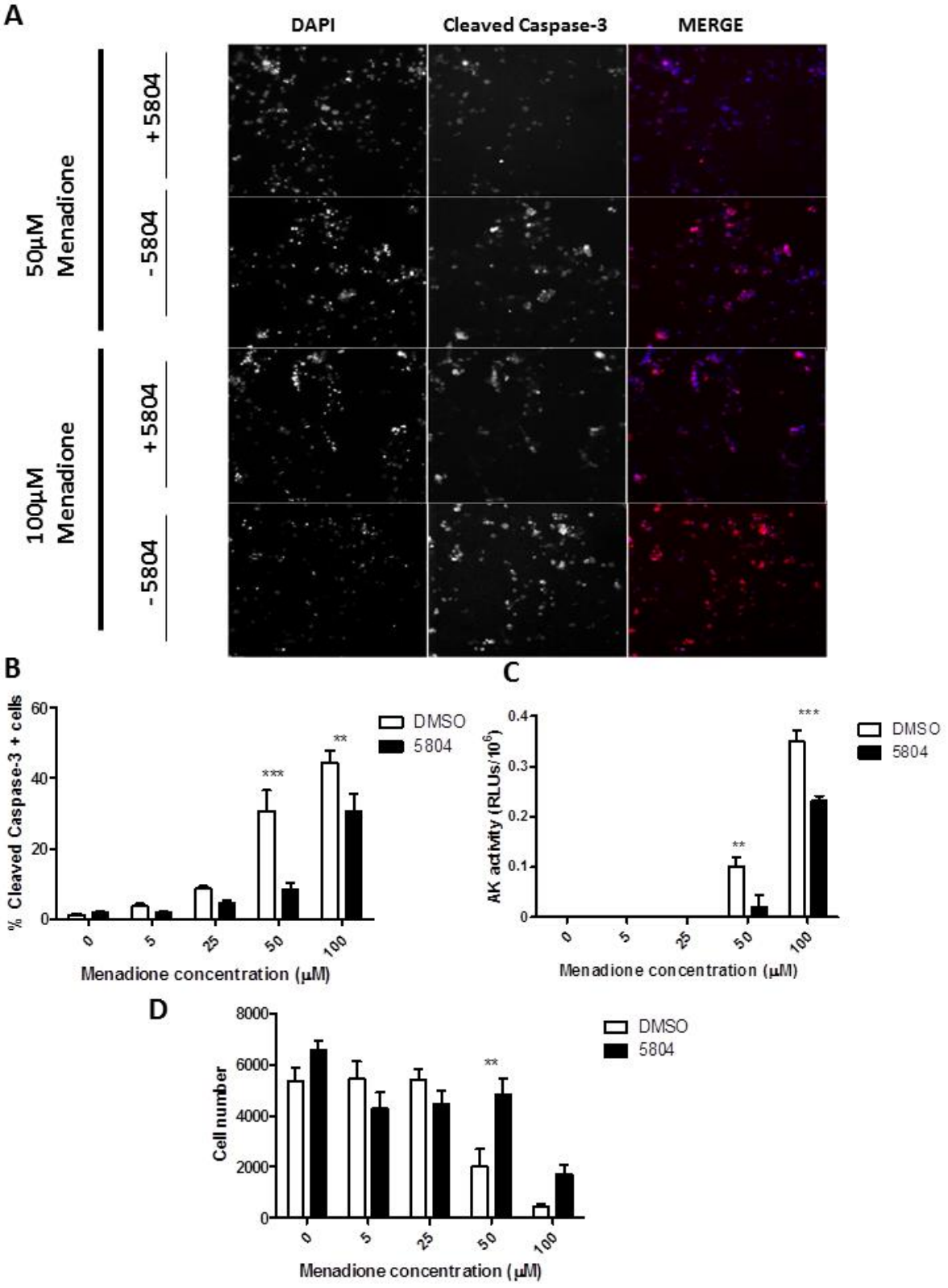

A
DAPI
Cleaved Caspase-3
MERGE
50µM Menadione
100µM Menadione
+ 5804
- 5804
B
% Cleaved Caspase-3 + cells
DMSO
5804
Menadione concentration (µM)
C
AK activity (RLUs/10^6)
DMSO
5804
Menadione concentration (µM)
D
Cell number
DMSO
5804
Menadione concentration (µM)

Figure 5.3 Cell death in MAP4K4 pharmacologically inhibited CorV.4U hiPSC-CMs in response to menadione in 2D. A) Representative images of immunohistochemistry (cleaved caspase-3) acquired using Cellomics ArrayScan VTI high content screening instrument for treated and untreated groups. **B)** The effect of DMX-5804 (5804) on % of cleaved caspase-3 positive CorV.4U cells as measured by immunohistochemistry. **C)** The effect of DMX-5804 (5804) on loss of membrane integrity as measured by loss of membrane integrity (AK activity) N=3 **D)** Cell number count. Two-way ANOVA, N=2, *P < 0.05, **P < 0.01, ***P < 0.001. 10x Magnification.

5.3 Summary

Here we tested the inhibitor of MAP4K4, DMX-5804, and its effect on calcium cycling in hiPSC-CM upon menadione-induced oxidative stress.

The prevalence and amplitude of calcium cycling were highly sensitive to oxidative stress, whereas the kinetics of the calcium transient in cycling cultures were not. DMX-5804 increased the number of wells with observable calcium transients, but did not rescue the depression of the transient amplitude in the remaining cycling cells. The decrease in numbers of wells with observable calcium transients correlates well with the observations of cell loss at 50 and 100 μM menadione under similar culture conditions, and cell loss was significantly rescued by DMX-5804: the MAP4K4 inhibitor was confirmed to protect from menadione-induced cleaved caspase-3 induction and loss of membrane integrity, in this setting.

Taken together, this strongly suggests that the effect of MAP4K4 inhibition to increase the number of cycling wells is due to increased cell survival and not to improvement of calcium cycling in individual cells.

Discussion

Calcium cycling is crucial to proper contractile function and anomalies are the hallmark of heart disease. It is also susceptible to redox- and phosphorylation-dependent abnormalities (Gorski et al. 2015). Under the conditions tested, the percentage of wells that exhibit calcium cycling was highly sensitive to oxidative stress, whereas beating rate and kinetics of the calcium transient in cycling cultures were not. Menadione-induced cell death, measured by both caspase-3 cleavage and loss of membrane integrity (AK activity), occurred at the same concentration that calcium transients were lost. DMX-5804 increased the number of wells with observable calcium transients, but did not preserve from the depression of the transient amplitude observed in the cardiomyocytes that are still actively cycling calcium.

The reduction in numbers of wells with apparent calcium transients correlates well with the observations of cell loss at 50 µM menadione under similar plating conditions, which was also rescued by DMX-5804. This strongly suggests that the effect of MAP4K4 inhibition to increase the number of cycling wells is due to increased cell survival and not to improvement of calcium cycling in individual cells. Moreover, of relevance to potential future safety considerations, no adverse effect of DMX-5804 was seen on any of the functional parameters. Conceivably, as only spontaneous calcium cycling was tested, the presence of calcium transients was likely more dependent on cell number and confluency, than if paced or chronotropically stimulated cultures had been used.

A concern regarding the use of hiPSC-CMs is their immaturity which results in phenotypes considerably different from those observed in native cardiomyocytes (Liang et al. 2013; Lan et al. 2013). In terms of calcium handling, hESC-CMs and hiPSC-CMs derived from embryoid bodies-based methods were found to sometimes lack functional SR stores and thus rely on trans-sarcolemmal calcium entry for contraction (Gutstein et al. 2001; Bers 2002; Lee et al. 2011). The usefulness of these cells depends on their calcium handling properties (Lee et al. 2011). Calcium handling parameters values (diastolic calcium, calcium

transient amplitude, time to peak and calcium decay rate, cycle length) have been reported not to be significantly different amongst independent hiPSC-CM lines in a monolayer (Hwang et al. 2015), suggesting comparability and reproducibility in hiPSC-CM in monolayer format. These hiPSC-CM lines, compared to adult rabbit and mouse CMs, were only slower in terms of time to peak and calcium transient decay rates whilst all other parameters were not different. Our values for the vehicle control group are considerably lower (cycle length 0.95 s vs 2 s, time to peak 0.065 s vs 0.4-0.6 s for hiPSC-CMs, 0.02 F_{ratio} vs 0.3-0.4 F_{ratio} for other hiPSC-CMs and adult CMs), although calcium decay rate had comparable values for our line and mouse CMs (0.25 s vs 0.2 s for mouse CMs). However, discrepancies could be due to differences in set up or the use of dyes as they are phototoxic and can cause temporal degradation of the sample and signal quality overtime and thus limit recording times (Leyton-Mange et al. 2014). In future, the introduction of genetically encoded voltage indicators could help to overcome this, as they have been successfully used to image hiPSC-CM action potential during drug screening (Chang Liao et al. 2015). It is most likely that the differences are due to the fact that the cardiomyocytes were stimulated at 0.5Hz for 20 second trains in the literature, whereas ours were not since our platform does not have the capacity to pace the cultures. Other have (Denning et al. 2016), however, reported transient durations of 260 ms for human adult myocytes and 300-700ms for hiPSC-CMs; this is in agreement with our value of 350 ms. Cycle length was reported to be 0.8-1s for human adult cardiomyocytes and 0.8-2 s for hiPSC-CM (Denning et al. 2016); also in agreement with a value of 0.95 s.

In terms of measuring electrical activity, hiPSC-CMs display heterogeneity in their signal, which means that action potential measurements are expected to be noisier than calcium measurements since calcium transients are slower. As such, this electrophysiological parameter was favoured in our studies. Further, confirmation at the single cell level and a finer dose-response at 30-45 μM menadione would be beneficial next steps. In addition, efforts to establish the time window in which to give DMX-5804 after ROS increase which would confer protection would be informative. However, these findings strongly suggest that

the effect of MAP4K4 inhibition observed in spontaneous calcium transients is due to increased cell survival.

Taken together, these findings suggest that the effect of MAP4K4 inhibition to rescue the percentage of spontaneously cycling wells is a result of increased cell survival under the conditions tested, not inherent improvements in calcium cycling. This difference from the mechanism underlying mitochondrial function in Chapter 4 plausibly results from the higher concentrations of menadione required for suppression of the endpoints here. Moreover, these findings further validate previous findings regarding the safety of MAP4K4 pharmacological inhibition.

6. Results

Chapter 6: 3-dimensional human engineered heart tissue as a testbed for assessing effects of MAP4K4 inhibitors on cardiac cell death and contractility.

To study the role of MAP4K4 in human cardiac muscle cell death, our group previously used shRNAmir-based technology to knockdown expression of MAP4K4 in iCell hiPSC-CMs. MAP4K4 was knocked down followed by the induction of cell death by 250μM H_2O_2, showing a 2-fold reduction of cardiomyocyte death measured by loss of membrane integrity (DRAQ7 uptake). This suggests that MAP4K4 plays a pro-apoptotic role in human cardiomyocytes upon oxidative stress, and that inhibiting its activity therefore, would be cardioprotective in the human heart (Imperial Innovations Limited, UP Patent Office Application GB1716867.5, MAP4K4 inhibitors, 13 October 2017, Fiedler et. al, in revision).

As previously discussed, the mechanisms by which MAP4K4 mediates cell death has not been fully studied in this or any other human cardiac system. Apart from activation of TAK1-JNK, the signalling pathways downstream of MAP4K4 and functional consequences including potential involvement in contractility have not been elucidated. Many drugs fail in clinical trials due to either cardiotoxicity or inducing arrhythmia (Eder et al. 2015). Since MAP4K4 inhibition is a promising approach in designing new therapies for treating heart failure, we used human engineered heart tissue (hEHT) to more fully evaluate pharmacological inhibition of MAP4K4 in the context of contractile function and survival prior to the clinical trial stage. Using a 3-dimensional system such as this has the advantage of more closely recapitulating the environment of the intact human heart. EHTs are three-dimensional, force-generating heart muscle constructs from single isolated cells (Zimmermann et al. 2002; Zimmermann et al. 2000; Eschenhagen et al. 1997). EHT has been used to study contractile force as a platform for drug testing in hiPSC-CMs (Stoehr et al. 2014; Mannhardt et al. 2017), rat cardiomyocytes (Eder et al. 2014; Marc N. Hirt et al. 2014) and murine cells (Kensah et al. 2013). Our laboratory has recently implemented a

technology to generate fibrin-based EHTs in 24-well format between flexible silicone posts under auxotonic stretching conditions (Hansen et al. 2010).

We therefore aimed to further expand previous findings which used knockdown approaches, along with those described in previous Chapters. While those studies were conducted in human cardiomyocytes in 2-dimensional cultures, in this Chapter contractility is explored in 3-dimensional models of intact human cardiac tissue.

Mitochondria generate energy required for both cardiac contractility and maintaining survival. Oxidative stress, which leads to ROS formation and cellular damage, was simulated by doxorubicin (Burridge et al. 2016) and menadione (Criddle et al. 2006; Loor et al. 2010). The three inhibitors of MAP4K4, described in the introductory pages to Chapter 4 were employed. Initially the prototype, IC4-001, was tested to confirm safety and model suitability by measuring contractile properties in hEHT. Subsequently, the published inhibitor GNE-495 and the next generation compound DMX-5804 were tested in more depth for cell death protection and preservation of contractile properties following oxidative stress. Here we use these novel and specific inhibitors of MAP4K4 to elucidate the effect of pharmacological MAP4K4 inhibition on cell death and contractility in human cardiac tissue.

In short, the work presented attempts to bridge the gap between animal studies and clinical trials, in target discovery and drug development, by using a human platform that even more closely resembles the environment of the native human heart.

6.1 Effect of MAP4K4 inhibitor IC4-001 on force of contraction and beating rate in iCell-derived hEHT.

To investigate the role of MAP4K4 in a 3D model of cardiac tissue, fibrin-based hEHTs were generated as previously described (Hansen et al, 2010) from human iPSC-CMs, using iCell cardiomyocytes co-cultured with fibroblasts. The potential effect of MAP4K4 inhibition on

baseline function was first tested. Contractility analysis was performed using video optical recording to measure force and other contractile parameters in real-time (Fig. **6.1A**). At baseline, spontaneous post-deflecting contractions were seen from 6 days after generation, with peak force after day 10 (Fig. **6.1 B, C**); thus, all treatments were made after day 10. Up to 10 μM IC4-001 was well tolerated, however a much higher dose (100 μM) caused contraction to cease after 1 hr, indicated by the decrease in force and beats per minute (BPM, Fig. **6.1 C, D**). This shows that, MAP4K4 inhibition does not adversely affect contractile function or beating rate in the presence of up to 10 μM IC4-001, a value 20- to 300-fold above the EC50 for cytoprotection (IC_{50} 34 nM; EC_{50} 3-30 nM for H_2O_2 and 200-500 nM for menadione; Fiedler et al, manuscript in revision). The observation that this was reversible suggests an inhibitory effect on excitation-contraction coupling, rather than a consequence of large-scale cell death.

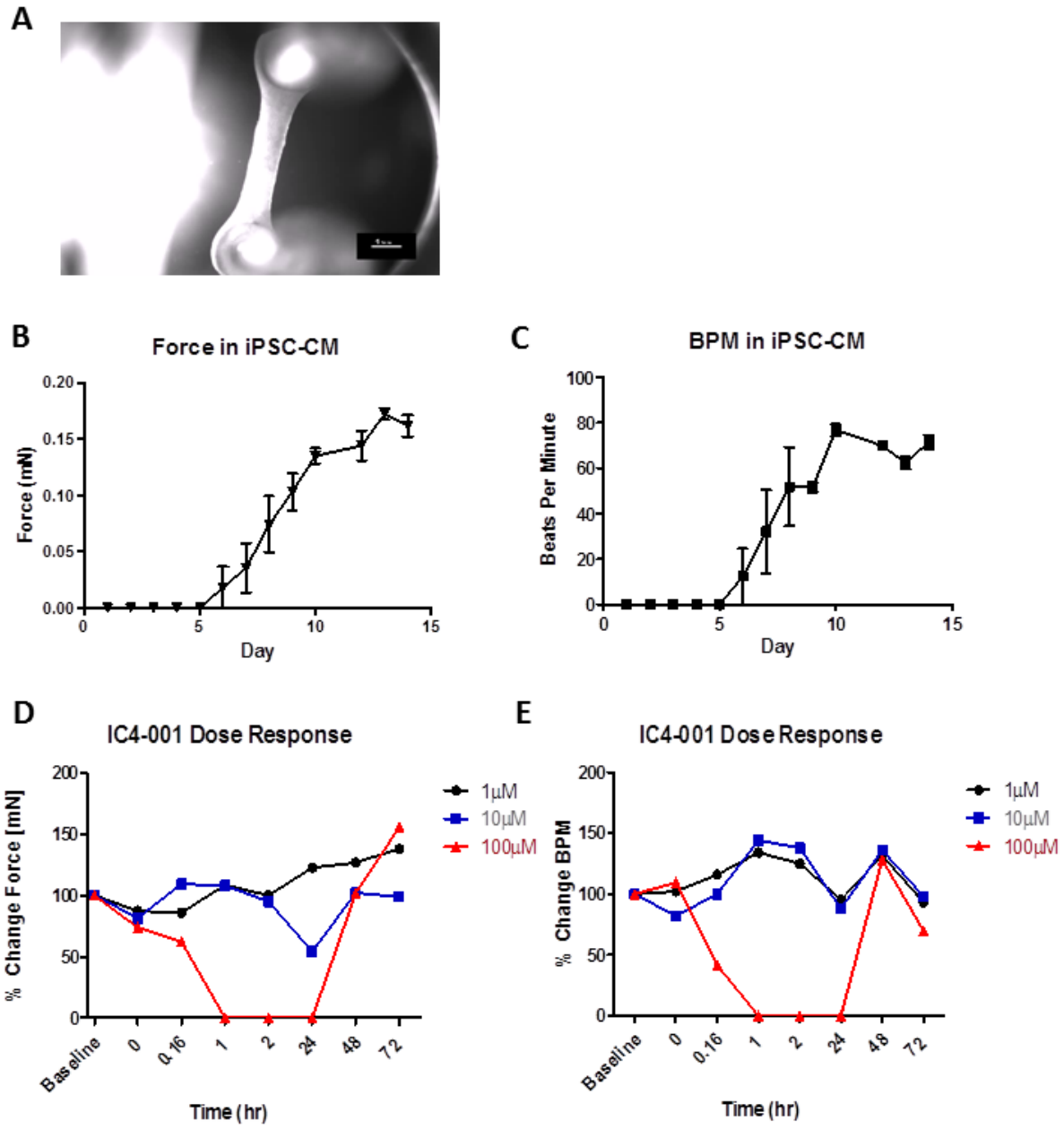


Figure 6.1 The effect of MAP4K4 inhibitor IC4-001 on contraction measurements in hEHT. A) Representative image of a fibrin-based iCell hiPSC-CM-derived EHT in culture 12 days after generation. Scale bar 1 mm. **B)** Force generation (mN) in iCell derived hEHT. N=4. **C)** Beat per minute (BPM) in iCell-derived hEHT N=4. **D)** Effect of IC4-001 with increasing concentrations on force generation in hEHT. **E)** Effect of IC4-001 showing the change in BPM in hEHT. N=2 for each dose, each on a separate EHT.

6.2 Effect of pharmacological inhibition of MAP4K4 by IC4-001 on long term contractile function in hEHT including systolic and diastolic function.

The effect of MAP4K4 inhibition on baseline function was assessed. Contractility measurements were taken for 0, 1, 10, 20, 30 and 80 min, and then daily for up to 30 days. No significant changes in force or BPM were observed with 10 μM IC4-001 after 10-80 min (Fig. **6.2A, B**). A 0.75-fold decrease in BPM was observed at 1 and 13 days after the drug was administered on day 1 (Fig. **6.2 A, B**). In terms of force, there was an increase at 3 days when MAP4K4 was inhibited (Fig. **6.2 A**). This suggests that the inhibition of MAP4K4 caused no negative effect on force generation.

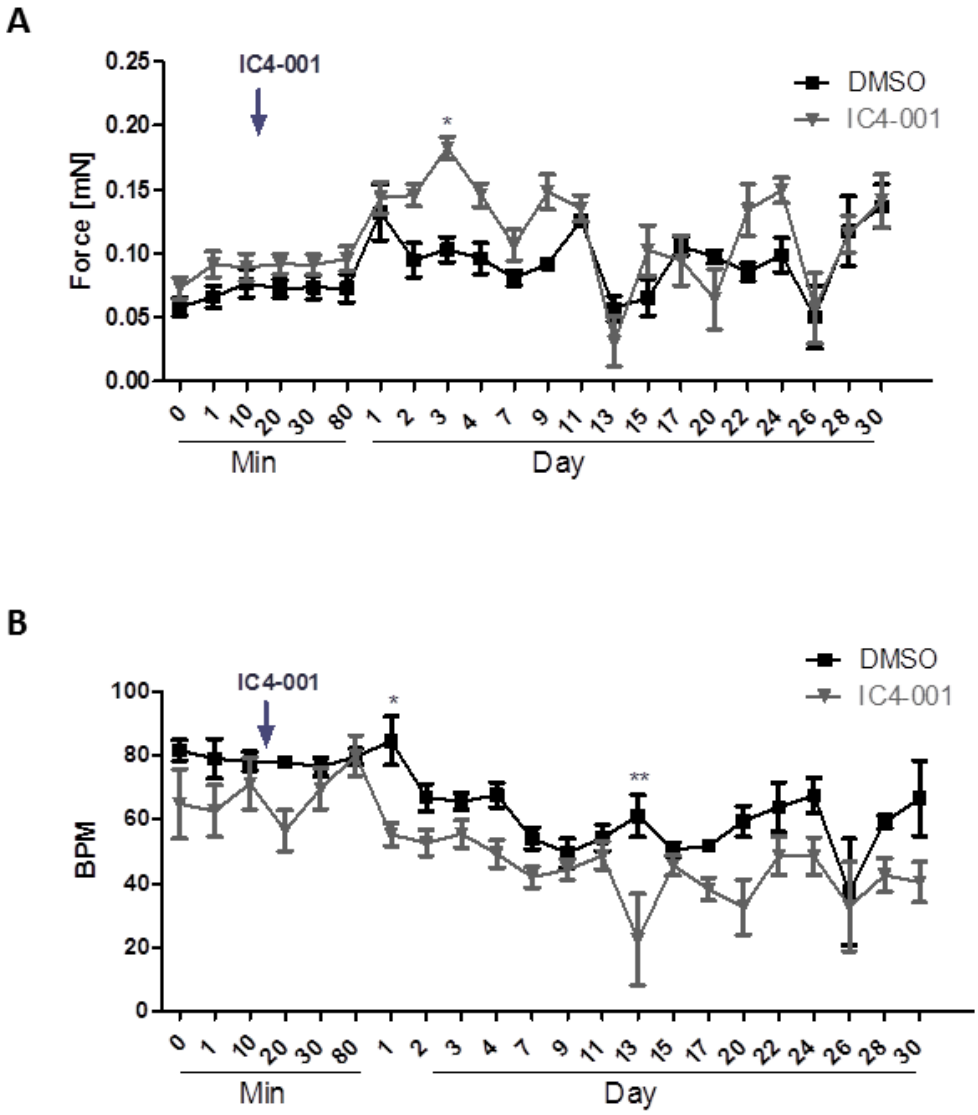


Figure 6.2 Long term effect on contraction measurements after pharmacological inhibition of MAP4K4 in hEHT. A) iCell hEHT were treated with 10 µM IC4-001 up to 30 days and measurements of force were recorded. **B**) iCell hEHT were treated with 10 µM IC4-001 up to 30 days and measurements of beats per minute (BPM) were recorded. Two-way ANOVA; N=5 Post-test *P < 0.05, **P < 0.01 vs DMSO. EHT were quiescent at occasional time points, and one inhibitor-treated EHT did not beat throughout. These are registered as zero values.

To study the effect of MAP4K4 pharmacological inhibition on systolic and diastolic function, the time from 20% contraction to peak (T_1) and time from peak to 20% relaxation (T_2) were measured. No statistically significant differences were found between MAP4K4 inhibition and

vehicle control (Fig. **6.3 A, B**), suggesting that MAP4K4 inhibition does not alter systolic and diastolic function.

In summary, pharmacological inhibition of MAP4K4 did not impair long term contractile function in hEHT since it did not alter force, BPM, systolic and diastolic function.

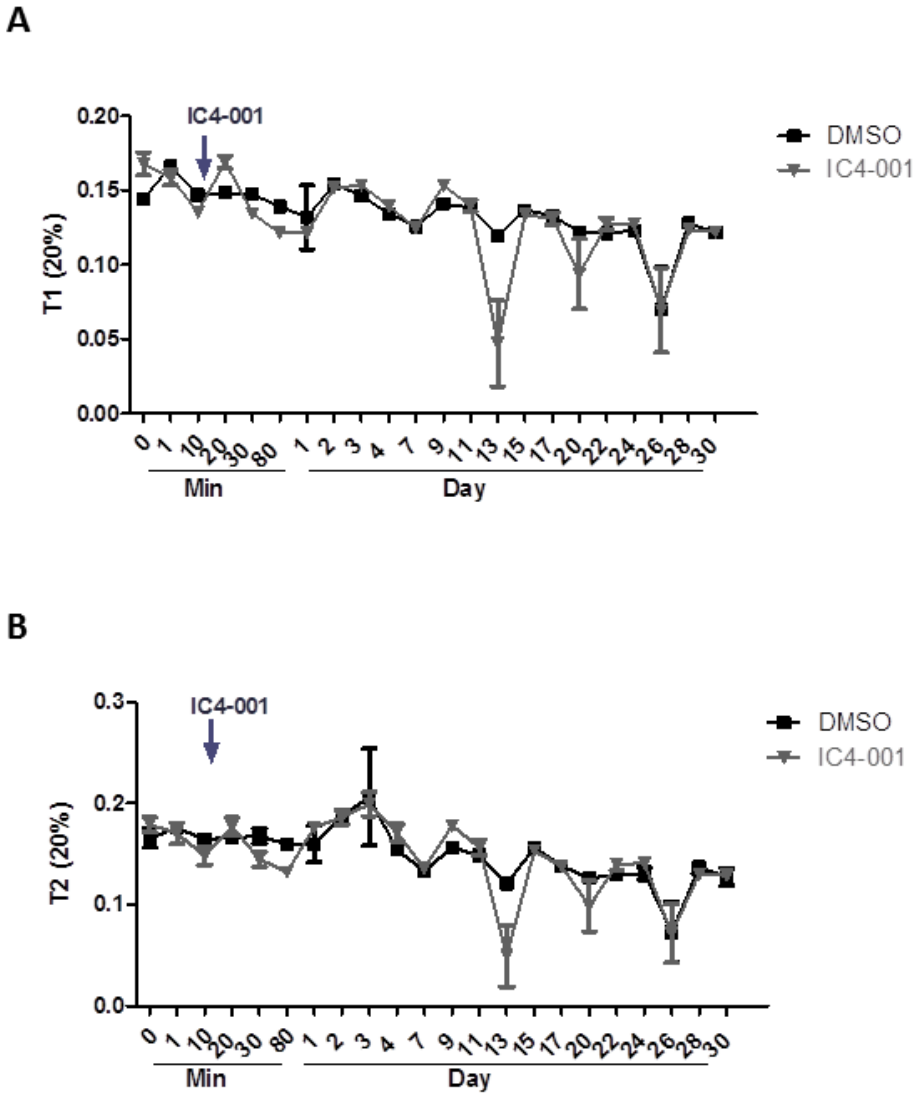


Figure 6.3 Systolic and diastolic assessment after pharmacological inhibition of MAP4K4 in hEHT. A) iCell-derived hEHT were treated with 10 µM IC4-001 up to 30 days and measurements of time from 20% contraction to peak (T_1) were recorded. **B**) iCell-derived hEHT were treated with 10 µM IC4-001 up to 30 days and measurements of time from peak to 20% relaxation (T_2) were recorded. Two-way ANOVA; N=5 NSD.

It was later found that IC4-001, the initial prototype for the in-house inhibitor of MAP4K4, has a short half-life of 18 and 19 min respectively in mouse and human liver microsomes (Fiedler et. al., in revision) and as such, it is unlikely to be active in the prolonged timecourse shown in Figure **6.2**. To circumvent this limitation, a published inhibitor of MAP4K4 that has a longer half-life was used for subsequent studies, GNE-495.

Inconsistencies in the response to isoprenaline (data not shown; responses were inconsistent wherein some experiments, isoprenaline did not cause any changes), possibly due to batch to batch variation in the iCell cell line led to the subsequent use of a ventricularly enriched CorV.4U cell line. The latter cells also provide a more physiologically relevant model when studying cell death since it is cell death in the left ventricle that is most prominent during heart failure (Harvey & Leinwand 2011; White & Chew 2008; Sabbah 2000).

6.3 Generation of hEHT using CorV.4U CMs

To investigate the role of MAP4K4 in an alternative 3D model of cardiac tissue, fibrin-based hEHTs were generated as previously described (Hansen et al, 2010) from human iPSC-CMs, using the ventricular enriched cell line CorV.4U alongside iCell hiPSC-CMs for comparison, and both were co-cultured with fibroblasts.

The contractile function of the constructs was assessed. Force was similar, and post-deflecting contractions were observed 7 days after generation for both cell lines (Figure **6.4A**). Beating rate, measured as BPM tended to increase in hEHT generated from CorV.4U hiPSC-CMs after day 8 though this was not statistically significant (Figure **6.4B**). Therefore, both cell line were shown to be suitable for future studies, however, CorV.4U was favoured in subsequent experiments due to the previous inconsistencies observed in iCell data and

the added physiological relevance, as previously mentioned (Harvey & Leinwand 2011; White & Chew 2008).

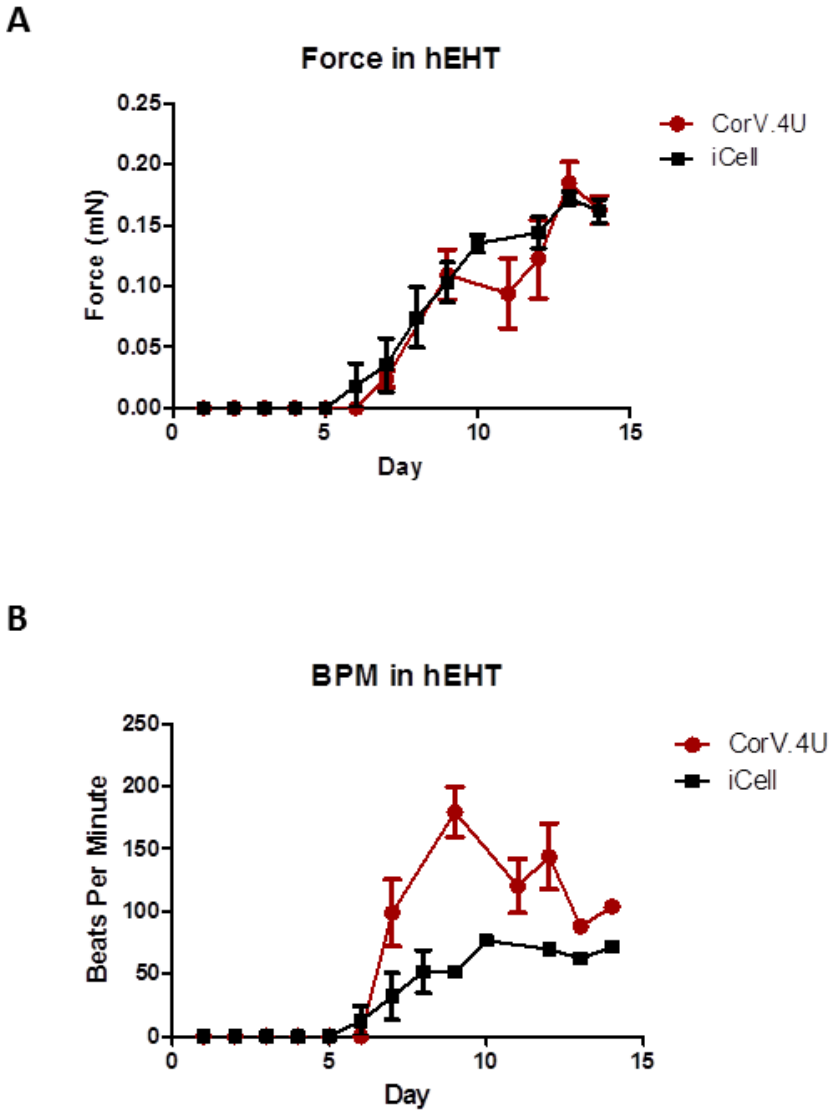


Figure 6.4 Contractile profile of human EHT generated from CorV.4U and iCell hiPSC-CMs measured by force and BPM over 14 days. Fibrin-based hEHTs were constructed with hiPSC-CMs and contractility analysis was performed. **A)** Force generation (mN) in iCell and CorV.4U derived hEHT **B)** BPM in iCell- and CorV.4U-derived hEHT. NSD N=4-8

6.4 Effect of MAP4K4 inhibitor GNE-495 on force and beating rate in CorV4U-derived hEHT treated with doxorubicin

To test the effect of MAP4K4 inhibition,GNE-495 (Ndubaku et al. 2015) was used. Doxorubicin (Dox) is one of the most potent anticancer drugs and DNA intercalating agents, but elicits ROS-mediated cardiocytotoxicity (Kim et al. 2006). Doxorubicin is widely used experimentally as it is stable in culture and more easily titrated than other potential death signals. EHTs were exposed to 24 hr Dox treatment, and AK activity was measured following media changes 24, 48 and 72 hr post-treatment, to assess loss of membrane integrity. This method for quantitatively measuring cell death as loss of plasma membrane integrity is especially well-suited to the 3D cardiac tissue constructs, compared to DRAQ7 uptake. On loss of integrity, AK is released into the media and can be detected using a luminometer.

10 μM doxorubicin induced a time-dependent increase in AK release by the CorV.4U-derived hEHT compared to untreated controls, with cell death from 24 hr, which increased progressively at 48 and 72 hr (Fig. **6.5 A**). Doxorubicin decreased force of contraction after 48 hr (Fig **6.5 B**) as expected from extrapolation from our 2D studies. However, the rate of synchronous beating did not change at any concentration tested up to 48 hr after treatment (Fig. **6.5 B, C**). Thus, although a fraction of the cardiomyocytes present have died, electrical and mechanical connectivity persists among those cardiomyocytes that are still viable.

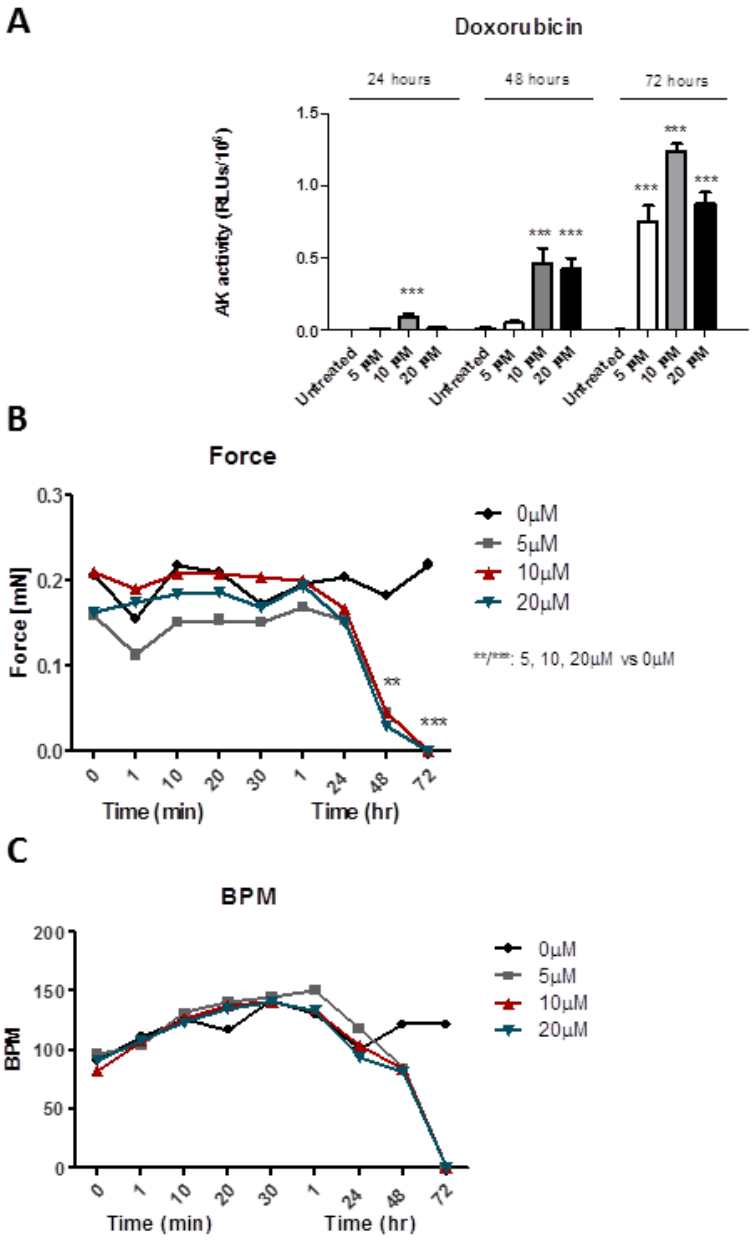


Figure 6.5 Induction of cell death by doxorubicin in CorV.4U-derived EHTs. A) After 24 hr Dox exposure, adenylate kinase (AK) activity was measured after 24, 48 and 72 hr following media changes at each timepoint. N=3 **B)** After 24 hr Dox exposure, force was measured after 24, 48 and 72 hr following media changes at each timepoint. **C)** After 24 hr Dox exposure, BPM was measured after 24, 48 and 72 hr following media changes at each timepoint. Two-way ANOVA; *P < 0.05, **P < 0.01, ***P < 0.001. N=2 for each dose, each on a separate EHT.

Under conditions chosen for induction of cell death (10μM Dox for 24 hr), GNE-495 protected against Dox-induced cell death, measured by AK release at 24 hr, and protection was maintained at both 48 and 72 hr after treatment (Fig. **6.6A**). With Dox plus 3 μM GNE-495, beating rate was preserved at 48 and 72 hr and force preserved at 24 hr though not later. More variable results were seen at 10 μM, and statistical significance was not reached (Fig. **6.6 B, C**). GNE-495 was replenished daily for the duration of the experiments. Further, adding GNE-495 alone at either concentration did not induce cell death, alter BPM, or alter force generation (Fig **6.6 A-C**). Therefore, GNE-495 protects from doxorubicin-induced cell death and, less completely, from doxorubicin-induced contractile dysfunction in CorV.4U-derived hEHT.

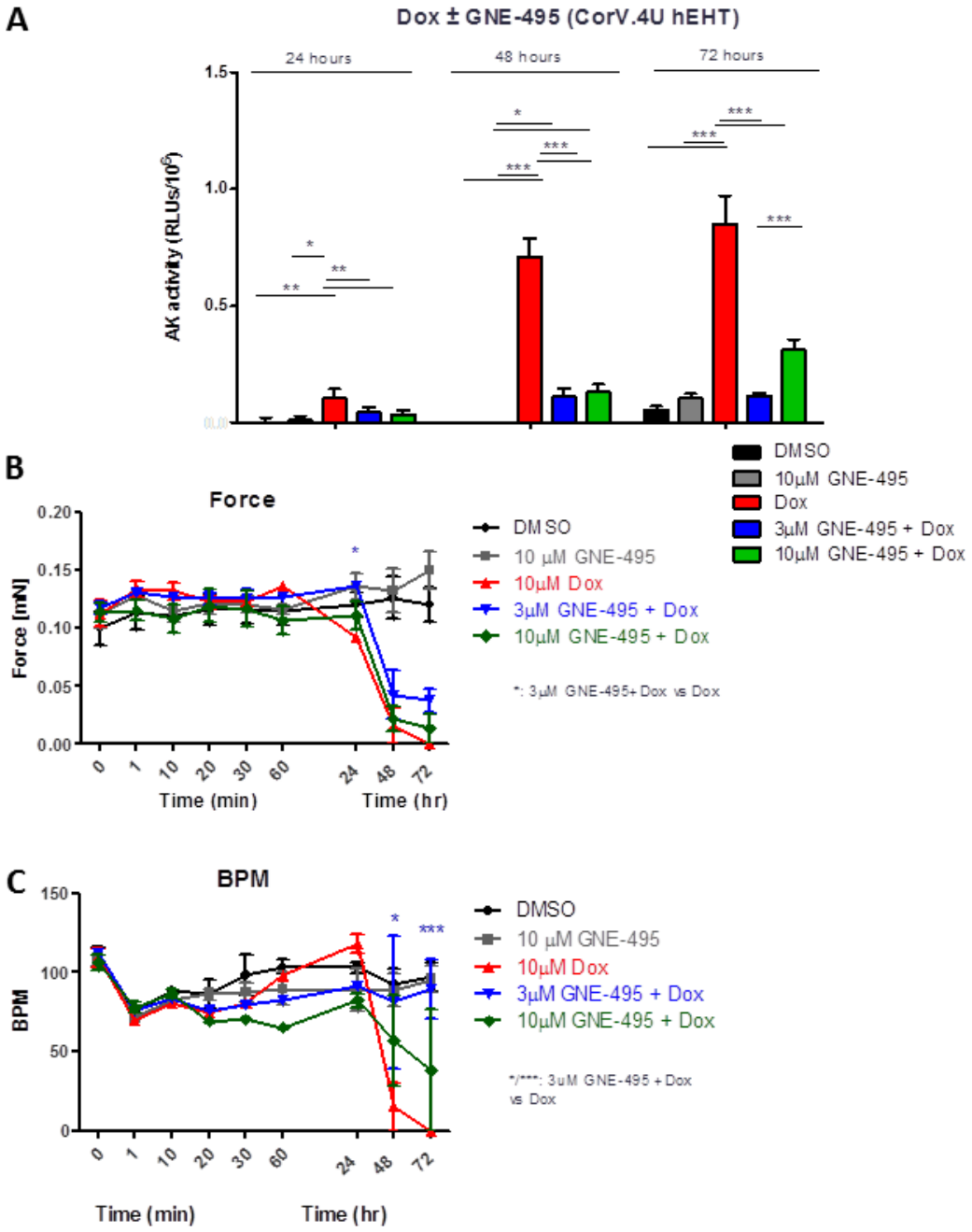


Figure 6.6 Plasma membrane integrity and contractility assessment of MAP4K4 inhibitor GNE-495-treated CorV.4U-derived hEHT subjected to doxorubicin. A) The effect of GNE-495 on cell death at 24, 48 and 72 hr as measured by loss of cell membrane integrity (AK activity) CorV.4U-derived hEHT. **B)** The effect of GNE-495 on Dox-induced decrease in force and on **C)** BPM reduction at 24 hr CorV.4U-derived hEHT. Two-way ANOVA; *P < 0.05, **P < 0.01, ***P < 0.001. N=3 for each dose, each on a separate EHT.

6.5 Cytotoxic and contractile screening of DMX-5804 in iCell-derived hEHT

To further investigate the role of MAP4K4 in a 3D model of cardiac tissue, a next-generation in-house inhibitor was tested, DMX-5804, which was the exemplar among several dozen analogues and was taken forward successfully into mice (Imperial Innovations Limited, UP Patent Office Application GB1716867.5, MAP4K4 inhibitors, 13 October 2017, Fiedler et. al, in revision).

After cell death induction (24 hr 10μM Dox exposure), adenylate kinase (AK) activity was measured after 24, 48 and 72 hr treatment to assess loss of membrane integrity in iCell-derived hEHTs. The iCell cell line was used here to keep consistency with contemporaneous data from other members of the MAP4K4 project team and allow for direct comparison. DMX-5804 was protective from Dox-induced cell death at 10 μM, 24 and 48 hr (Fig. **6.7A**); however, this effect was not sustained by 72 hr after treatment. Addition of DMX-5804 alone did not induce loss of membrane integrity, alter BPM, or impair force generation. However, unlike the beneficial effect seen with GNE-495 in iCell-derived hEHTs, neither beating rate nor force was preserved after treatment with Dox in these cells (Fig. **6.7B, C**).

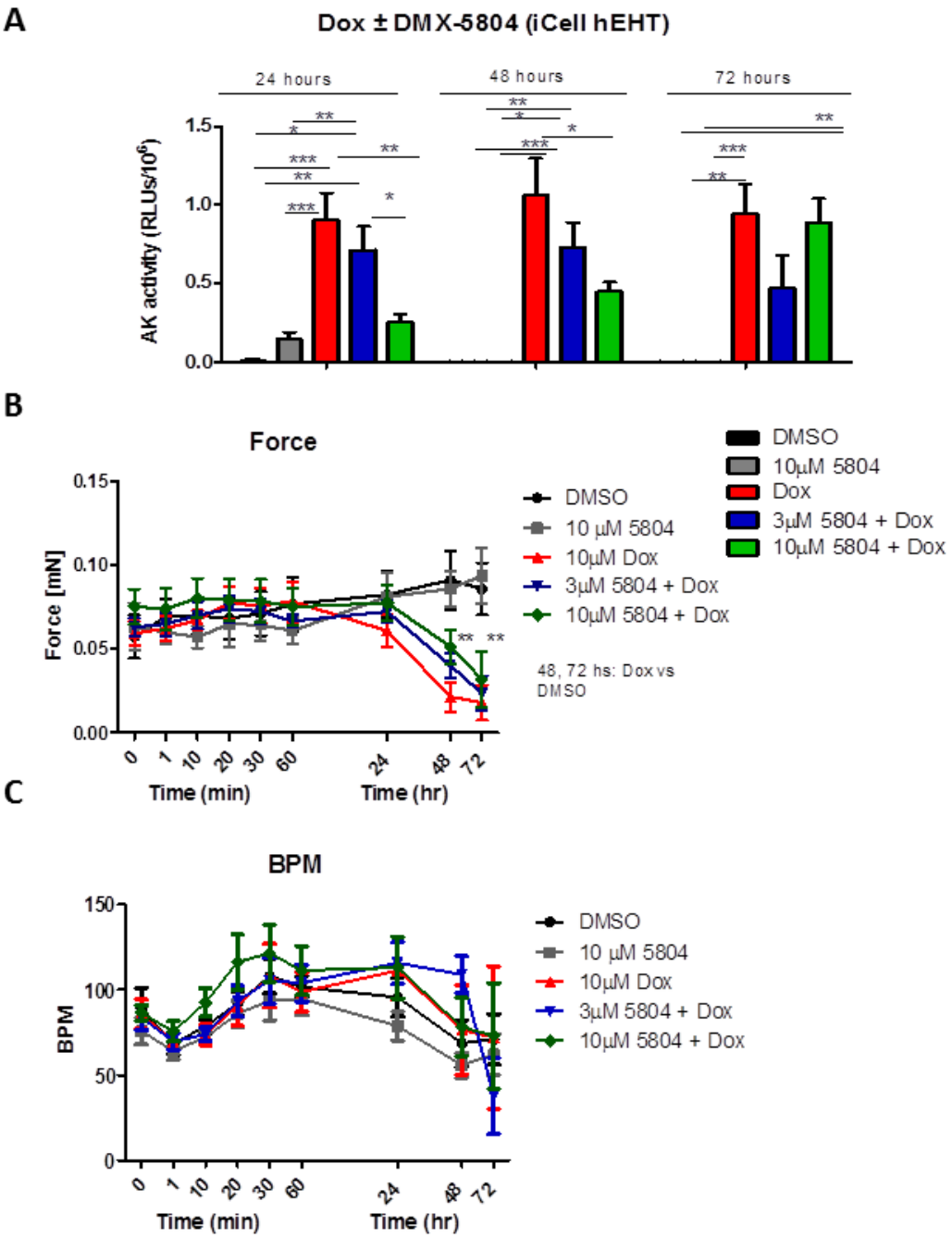
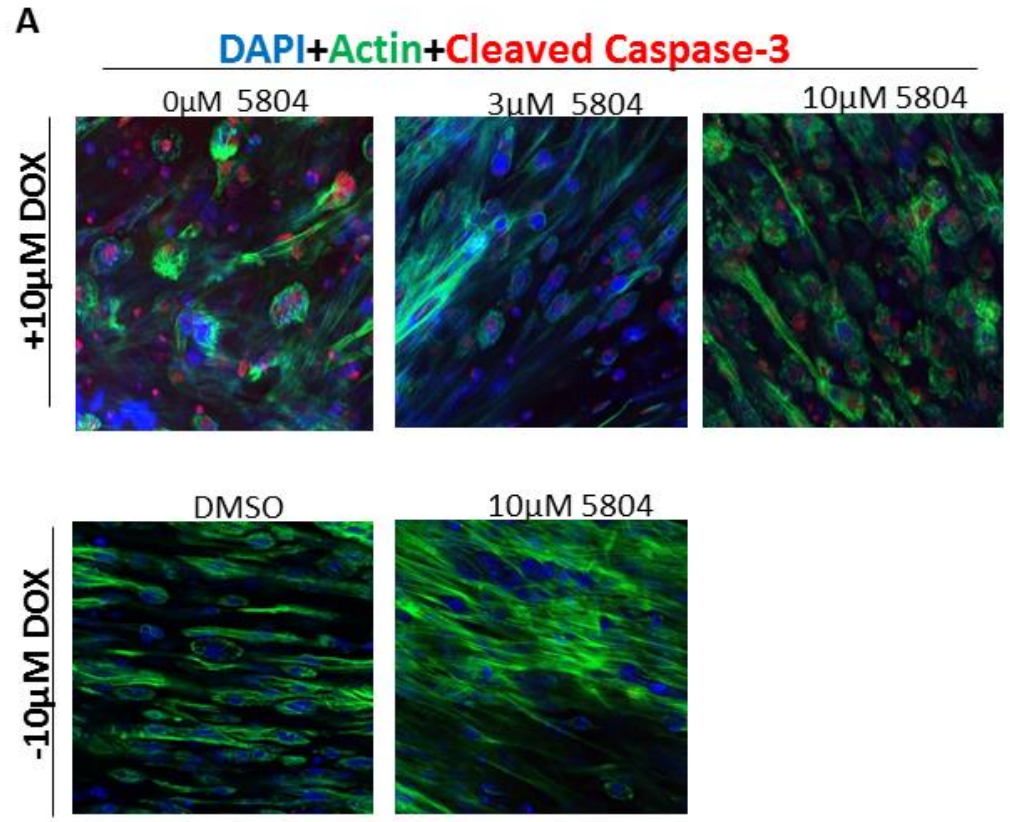


Figure 6.7 Plasma membrane integrity and contractility assessment of MAP4K4 inhibitor DMX-5804-treated iCell-derived hEHT subjected to doxorubicin. Effect of DMX-5804 (5804) on doxorubicin-induced toxicity in iCell-derived hEHT measured from **A)** increased adenylate kinase activity; **B)** decreased force of contraction and **C)** decreased beating rate (BPM) . Two-way ANOVA; N=3-5, *P < 0.05, **P < 0.01, ***P < 0.001.

To further explore the effect on cell death and dissect a possible mechanism in this system, hEHT derived from iCell hiPSC-CMs were treated with 10µM Dox in combination with DMX-5804 for 24 hr, after which the tissue was fixed and immunostained. Cell death was

measured by immunofluorescent staining to visualise cleaved caspase-3. 10μM Dox induced caspase-3 cleavage in 80% of the cells as compared to the vehicle control (DMSO), indicating extensive cell death (Fig. **6.8A**, **B**). Pharmacological inhibition of MAP4K4 showed partial protection against cleavage of caspase-3 by Dox, although this was only statistically significant at 3 μM DMX-5804 (Fig. **6.8A, B**).

Therefore, MAP4K4 inhibition by DMX-5804 protects from doxorubicin-induced loss of membrane integrity, partially protects from caspase-3 cleavage but does not rescue contractile dysfunction in hEHT. Inconsistencies in cell death results observed both in these experiments and by others in terms of batch to batch variation and cell quality (Katie Chapman, personal communication), together with a greater response in CorV.4U cells, and higher physiological relevance, led to use of CorV.4U cells for subsequent experiments.



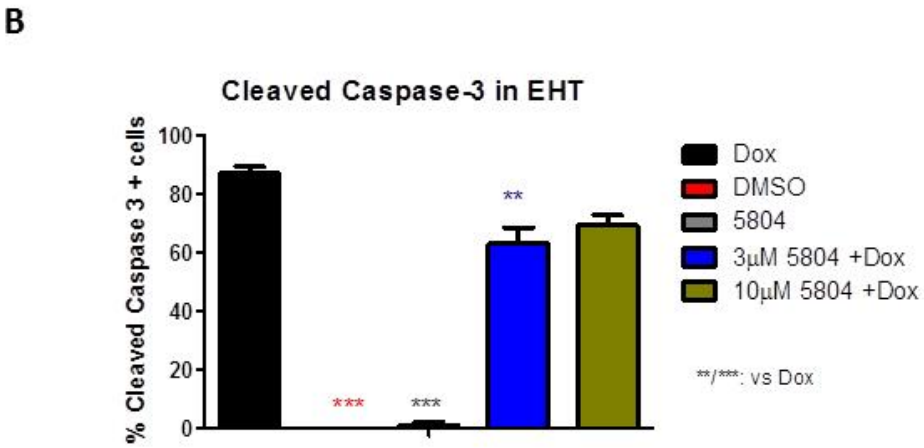


Figure 6.8 Cleaved caspase-3 levels after DMX-5804 treatment subjected to doxorubicin in iCell hEHT. A) Representative images acquired for 10µM Dox treated and untreated groups in the presence and absence of DMX-5804 (5804). **B)** MAP4K4 pharmacological inhibition in response to 10µM doxorubicin at 3 and 10 µM 5804. One-way ANOVA, N=3-4, *P < 0.05, **P < 0.01, ***P < 0.001. 20x Magnification

6.6 Optimisation of hEHT without fibroblast co-culture and the use menadione as the death signal for the cytotoxic and contractile assessment of DMX-5804 in CorV4U-derived hEHT

The best cell death assay applied to hEHT in our hands (AK activity), is one which does not separate the contribution from different cell types, i.e. fibroblasts and cardiomyocytes. The contribution fibroblasts may have had to the results observed previously, and to what extent these may be masking the effect on hiPSC-CMs was unknown.

To circumvent the limitation posed by the contribution fibroblasts may have to the results observed, fibrin-based hEHTs was generated as previously described by (Hansen et al, 2010) from human iPSC-CMs, using the ventricularly enriched CorV.4U cell line without the addition of fibroblasts. Post-deflecting contractions were observed 7 days after generation both in the presence and absence of fibroblasts (Fig. **6.9 A, B**). Force and BPM were not significantly different in hEHT using CorV.4U with or without co-cultured fibroblasts. Time from 20% contraction to peak (T_1) and time from peak to 20% relaxation (T_2) respectively were more variable in the absence of fibroblasts at early time points although this was not statistically significant nor observed at later time points (Fig. **6.9 C, D**).

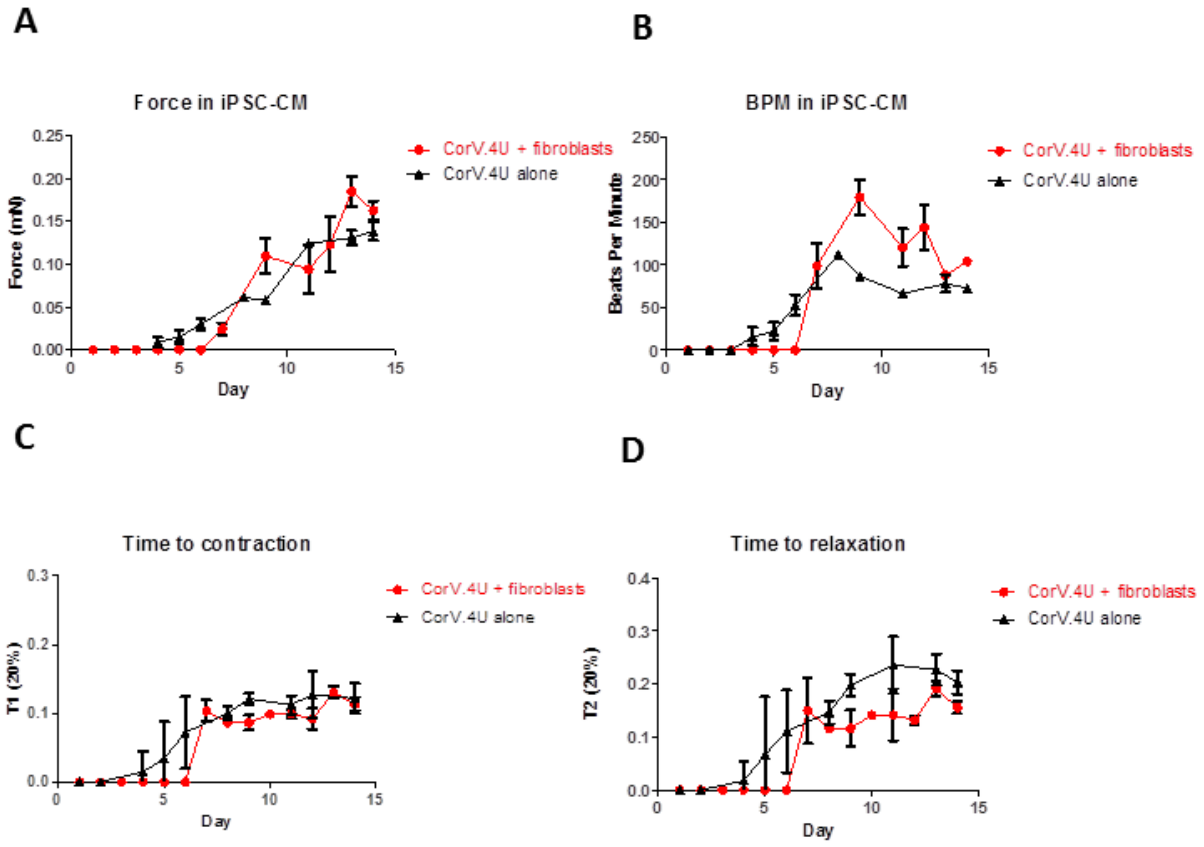


Figure 6.9 Contractile profile of CorV.4U-derived hEHT generated in the presence or absence of fibroblasts. A) Force generation (mN). **B)** BPM. **C)** Time from 20% contraction to peak (T1 (20%)). **D)** Time from peak to 20% relaxation (T2 (20%)). Unpaired t-test; NSD at day 14, N=6-10

Since doxorubicin is known to exert oxidative stress through a number of pathways (Burridge et al. 2016), a more reductionist stressor was sought. Menadione is an endogenous producer of ROS and as such it is more physiologically relevant in the setting of ischemic reperfusion, and expected to more closely mimic stress in native heart tissue.

Following menadione exposure, AK activity was measured after 24, 48 and 72 hr treatment to assess loss of membrane integrity. Menadione induced cell death after 24 hr at all concentrations tested, although by 48 hr only 5 and 10uM were effective and no significant effect was observed at 72 hr (Fig. **6.10**). Since the medium was changed between timepoints, this means that AK release has dropped at later times. This could either be due to cell death becoming complete or a reversal of the effect of menadione.

Menadione decreased force of contraction in a dose dependent manner compared to control (DMSO) after 10 min (Fig.**6.11 A**). BPM was also decreased in a dose dependent manner after 20 min at all concentrations tested (Fig. **6.11B**). Time to contraction, as measured by time from 20% contraction to peak T1 (20%) decreased in a dose dependent manner compared to control (DMSO) after 10 min whereas time to relaxation, as measured by time from peak to 20% relaxation T2 (20%) was also decreased in a dose dependent manner after 20 min at all concentrations tested (Fig. **6.11C, D**). Measurements were not made for 72 hs as all treated groups had stopped beating as recorded by earlier timepoints.

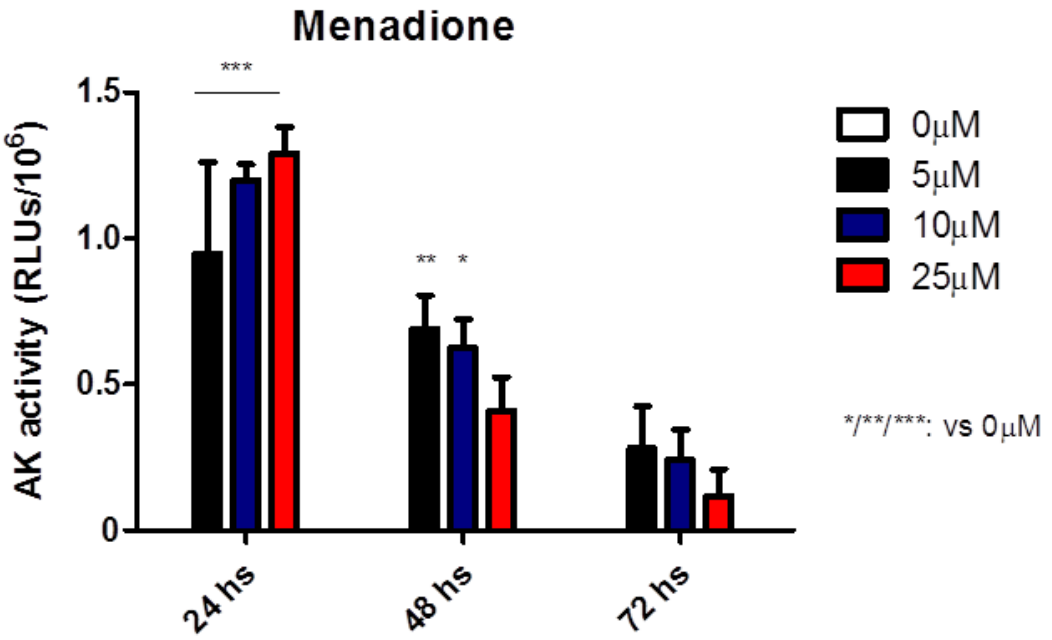


Figure 6.10 Induction of cell death by menadione in CorV.4U EHTs as measured by loss of plasma membrane integrity. A) After 24 hr menadione exposure, adenylate kinase (AK) activity was measured at 24, 48 and 72 hr following media change after each timepoint. Two-way ANOVA; N=3, *P < 0.05, **P < 0.01, ***P < 0.001.

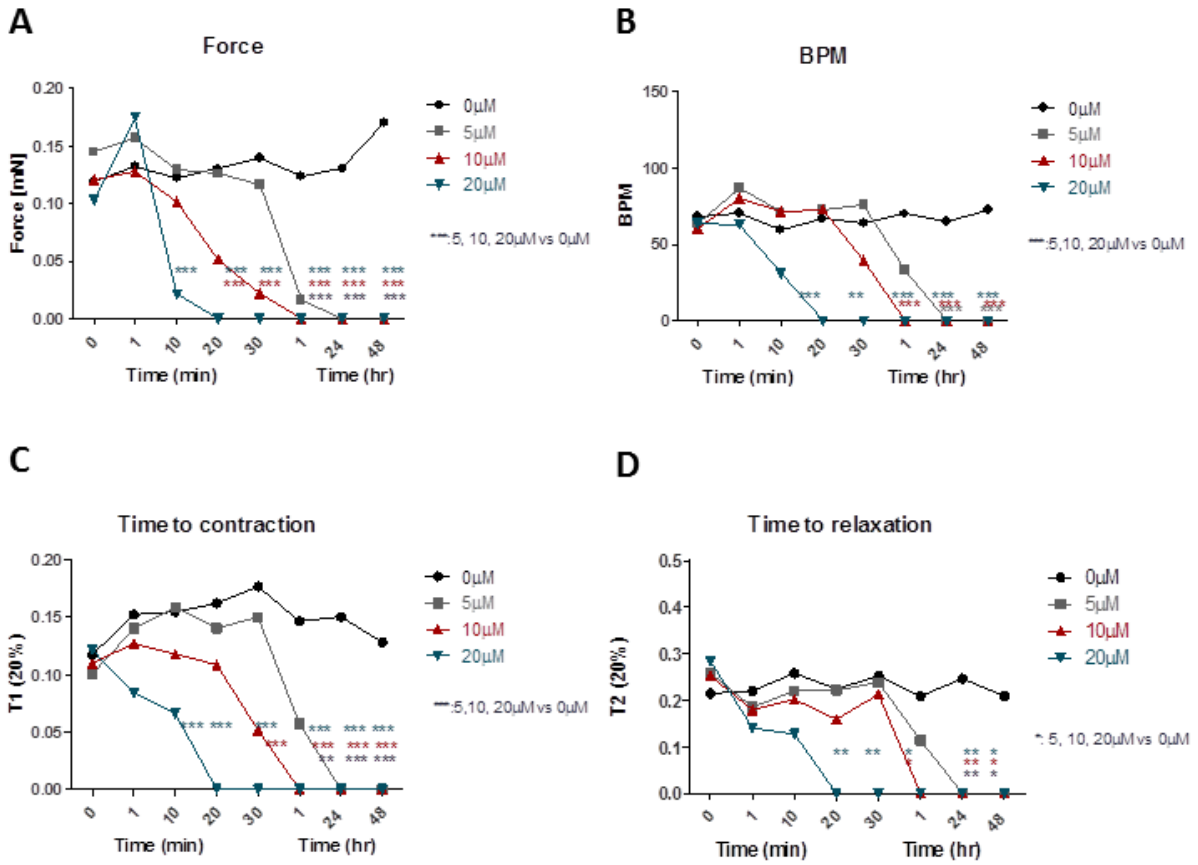


Figure 6.11 The contractile effect of menadione in CorV.4U-derived hEHT. After 24 hr menadione exposure, **(A)** force, **(B)** BPM, **(C)** T1 (20% and **(D)** T2(20%) was measured at 24, 48 and 72 hr. Two-way ANOVA, error bars: ±S.E.M, N=2, *P < 0.05, **P < 0.01, ***P < 0.001.

Thus, optimisation of hEHT (CorV.4U cells without fibroblast co-culture) and the use menadione as the oxidative stress signal were three refinements chosen in preparation for the cytotoxic and contractile assessment of DMX-5804. Absence of fibroblasts in hEHT constructs did not have an effect on their contractile properties and menadione induced loss of membrane integrity and contractile impairment.

Under optimised conditions for induction of cell death (24 hr 10μM menadione exposure), Adenylate kinase (AK) activity was measured after 24, 48 and 72 hr treatment to assess loss of membrane integrity in the context of MAP4K4 inhibition. Using DMX-5804, pharmacological inhibition of MAP4K4 was protective from cell death at 10 μM DMX-5804, 24 hr after treatment (Fig. **6.12**). Little cell death occurred on the subsequent days, and

protection was not seen, below these markedly reduced levels. MAP4K4 inhibition alone (DMX-5804) at 10 μM, did not induce AK release, suggesting that this compound is not cytotoxic.

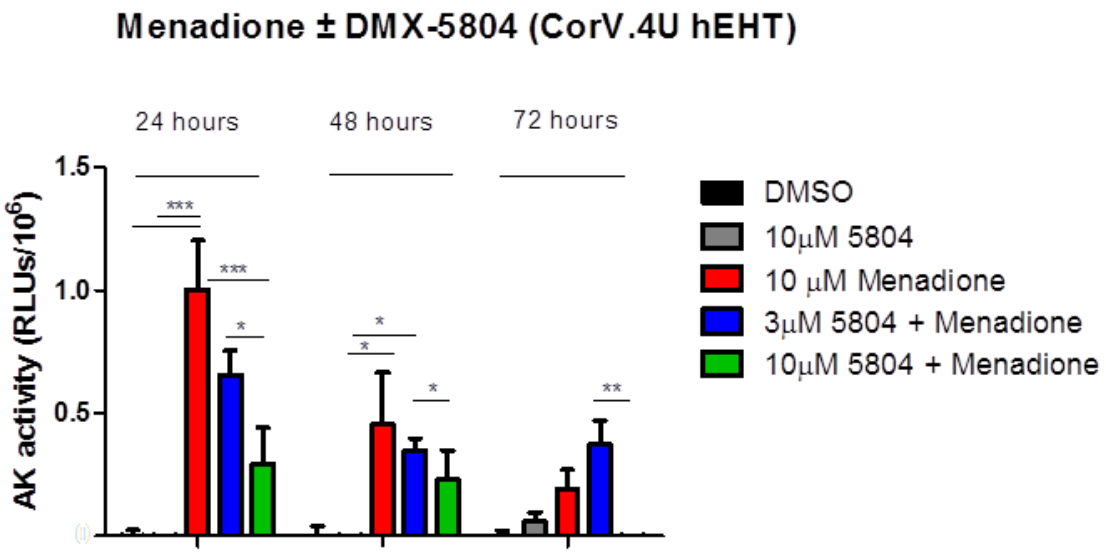


Figure 6.12 Plasma membrane integrity assessment of MAP4K4 inhibitor DMX-5804-treated CorV.4U-derived hEHT subjected to menadione. A) The effect of DMX-5804 (5804) on menadione-induced cell death at 24, 48 and 72 hr as measured by loss of cell membrane integrity (AK activity). Two-way ANOVA; N=5, *P < 0.05, **P < 0.01, ***P < 0.001.

In terms of the contractile assessment, it was found that MAP4K4 inhibition alone (DMX-5804) did not alter force, BPM nor time to contraction or relaxation (Fig **6.13 A, B, C, D**). Menadione reduced all parameters as expected; spontaneous beating and, hence, force generation were decreased within 60 min and abolished at 24 hr (Fig **6.13**). When MAP4K4 was inhibited and hEHT treated with menadione, force was preserved for 60 min and 24 hr at 3μM DMX-5804 and for 30 and 60 min at 10μM DMX-5804 (Fig **6.13A**). Beating rate was preserved for 60 min and 24 hr at both 3μM and 10μM DMX-5804 (Fig. **6.13B**). Thus, the rescue of contractile function by 3 or 10 μM DMX-5804 was virtually complete at these time

points, although no later ones. Similarly, time from contraction to peak and time from peak to relaxation were preserved for 60 min and 24 hr at both 3μM and 10μM DMX-5804 (Fig. **6.13 C, D**). At later timepoints, 10μM DMX-5804 and menadione treated EHTs regained function (1 out of 5 EHTs) and showed improved function (2 out of 5 EHTs).

Therefore, MAP4K4 inhibition protects from menadione–induced cell death at 24 hr as measured by loss of cell membrane integrity (AK activity) and preserves contractile properties in hEHT derived from ventricularly enriched cardiomyocyte cultures.

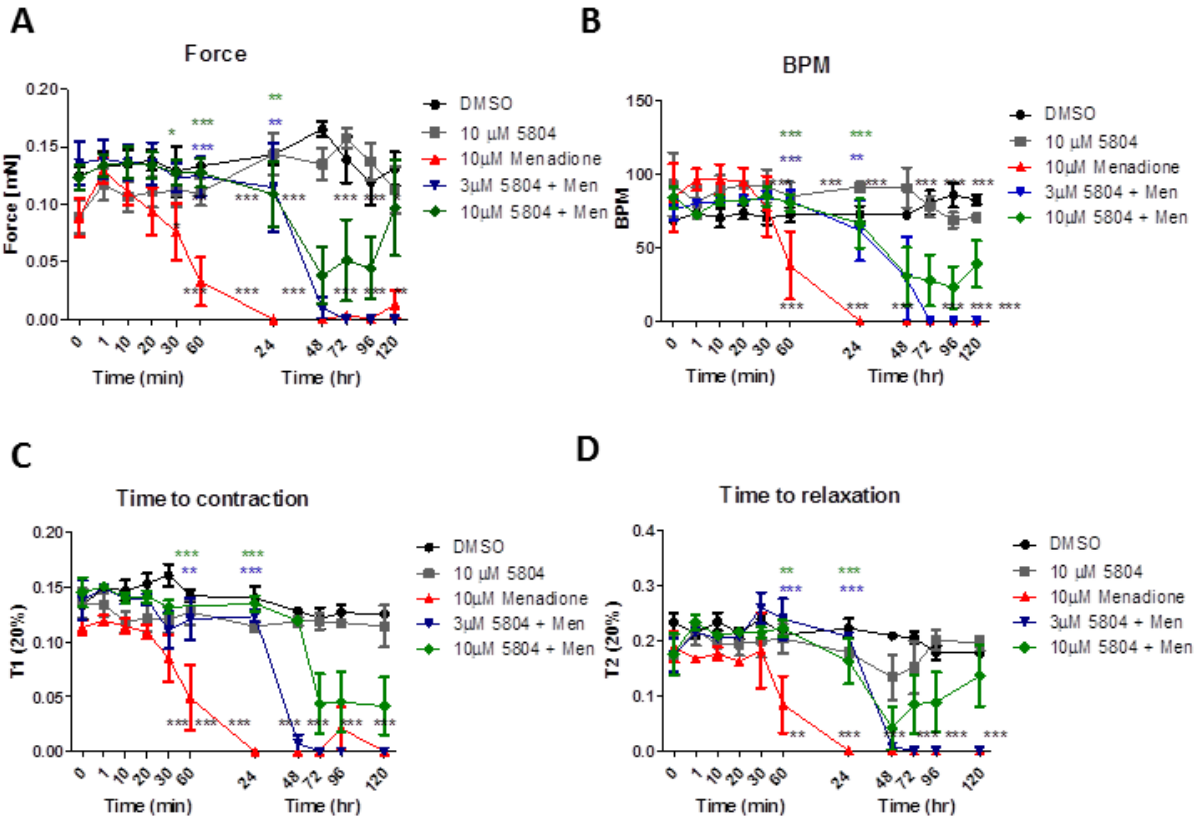


Figure 6.13 Contractility assessment of MAP4K4 inhibitor DMX-5804-treated CorV.4U-derived hEHT subjected to menadione. The effect of DMX-5804 (5804) in menadione-treated hEHT as measured by **(A)** force, **(B)** BPM, **(C)** time from 20% contraction to peak (T1 (20%)) and **(D)** time from peak to 20% relaxation (T2(20%)). Two-way ANOVA; N=5, *P < 0.05, **P < 0.01, ***P < 0.001.

6.7 Synopsis of main findings

Here we tested three inhibitors of MAP4K4, using hEHT generated from two hiPSC-CM cell lines. iCell hiPSC-CMs from Cellular Dynamics International were used in initial studies. However, issues were sometimes encountered with iCell in terms of batch to batch variation and cell quality, so an alternative source was sought. The more ventricularly enriched CorV.4U hiPSC-CMs from Axiogenesis were subsequently used, selected on the basis of higher physiological relevance and consistent cell quality.

Pharmacological inhibition of MAP4K4 using 3 different inhibitors did not adversely affect contractile function or beating rate of 3-dimensional models of human heart tissue in the two cell lines, and was at least partially protective against dysfunction by either exogenous or endogenous ROS.

We show that MAP4K4 inhibition by GNE-495 protects ventricularly enriched CorV4U derived hEHT from doxorubicin-induced loss of plasma membrane integrity and partially protects from contractile dysfunction. A second, later derivative of the in-house MAP4K4 inhibitor, DMX-5804, also protects from doxorubicin-induced loss of membrane integrity, partially protects from caspase-3 cleavage but does not rescue contractile dysfunction in iCell-derived hEHT. In CorV.4U-derived hEHT, DMX-5804, protected from menadione-induced cell death at 24 hr as measured by loss of plasma membrane integrity (AK activity) and preserved contractile properties in hEHT due to oxidative stress, under the conditions tested.

Taken together, these results suggest that pharmacological inhibition of MAP4K4 can protect against cell death and contractile dysfunction induced by acute exogenous or endogenous stress in human cardiac tissue.

6.8 Discussion

The presence of added fibroblasts in hEHT, although reported in some studies to improve mechanical function (Kensah et al. 2013; Liau et al. 2011; Liau et al. 2012), may have confounded the results observed and/or be masking the effect of compounds specifically on hiPSC-CMs. In particular, the best cell death assay in our hands (loss of membrane integrity measured by AK activity) is one which does not separate the contribution from these cell types, and immunohistochemistry was unreliable/ unsuccessful in attempting to dissect the contribution from each cell type in hEHT. As even cardiomyocyte-specific markers would not prove a functional impact via the myocyte, the main further refinement in terms of the model was aimed at addressing this point by generating fibroblast-free hEHT. Fibroblast-enriched EHT had been previously associated with increased force (possibly due to increased tonic tension) due to their contribution to development through paracrine and autocrine pathways and their contribution to ECM formation and alignment which translates into increased contractility (Wagoner Johnson & Harley 2011; Kensah et al. 2013; Tzatzalos et al. 2016). However, there is also evidence suggesting that over time the stiffness conferred by cumulative myofibroblasts ECM production, reduced degree of alignment and some level of distortion of excitatory conduction may account for decreased long term force (Wagoner Johnson & Harley 2011). This, in addition to the recent findings by the Eschenhagen lab showing that contraction amplitude and kinetics were more stable over time and less variable in hEHT that were not fibroblast-enriched (Mannhardt et al. 2017), served as the basis to optimise fibroblast-free fibrin-based hEHT in our lab using ventricularly enriched CorV.4U hiPSC-CMs. This cell line was selected to more uniformly represent the human left ventricle, the chamber in which cell death has the most significant impact (Harvey & Leinwand 2011; White & Chew 2008; Sabbah 2000). Force and BPM were not significantly different from hEHT co-cultured with fibroblasts, suggesting suitability for our further studies.

Comparison between inhibitors was not possible due to various limitations. Firstly, hiPSC-CMs cells are very expensive and 1 million cardiomyocytes are needed per construct, limiting the number of constructs available. Secondly, the platforms used only allow for one plate to be read at once at any given time for the automated assays, limiting direct comparison due to the inability to run experiments in parallel. In future, the use of multiple automated platforms at any given time would be beneficial to test all inhibitors alongside each other.

We were unable to provide siRNA data to validate our findings since we did not observe MAP4K4 knockdown when this experiment was attempted. Further, since previous members of the MAP4K4 team had successfully shown MAP4K4 knockdown using shRNAmir technology in iCell hiPSC-CM in 2D, we focused on trying to attain MAP4K4 knockdown by shRNA in 3D culture. Previously, MAP4K4 was knocked down followed by the induction of cell death by H_2O_2. A 2-fold reduction of cardiomyocyte death was observed compared to vehicle control, measured by loss of membrane integrity (DRAQ7 uptake) (Fiedler et. al, in revision). MAP4K4 mRNA expression after knockdown showed only low and insignificant levels of silencing (see Supplement). The EHT generation process relies on 100µL of cells, media and hydrogel mixture that sets around silicon posts to form a strip of tissue. It was decided not to exceed 30% of this in terms of increasing the volume that would go into the moulding cast, as this could affect the properties of the EHTs. Therefore, this was the limiting factor in term of the maximum MOI we were able to use for transduction. How this translated to knockdown at the protein level was not tested, and thus levels may be different to this. Further concentration of the virus by ultracentrifugation could increase knockdown levels. Alternatively, CRISPR-cas9 genome editing technology could have been used to knockdown gene expression, however, this would have constituted another PhD project in itself due to the sheer volume of work involved in developing, optimising and carrying out

such work and particularly, because at the time our work was carried out, CRISPR-cas9 was not performed in our lab.

Off-target effects may have influenced our results, although the unique P-loop-folded structure of MAP4K4 has been described to contribute to greater selectivity that might be expected for ATP-competitive inhibitors (Guimarães et al. 2011). The initial tool compound IC4-001 had off-target effects against 5 human protein kinases out of a screening panel of 140: MINK, MLK1, MLK3, NUAK1 and GCK (Fiedler et. al, in revision). The provisional lead compound, DMX-5804, also targets 5 related kinases; MINK1/MAP4K6, TNIK/MAP4K7, GCK/MAP4K2, GLK/MAP4K3 and KHS/MAP4K5. GEN-495 exhibits lesser selectivity with 7 off-target effects against 61 kinases; GCK, MLK1, Mer, MINK (MAP4K6), Rsk3, Rsk4 and PAK4 (Crawford et al. 2014). Given the homology, especially in the active site between MAP4K4 and its most closely related members, it was expected that GNE-495 inhibits the closely linked MINK (Vitorino et al. 2015). It is not possible to wholly exclude off-target effects as the cause for the effects reported in this study without carrying out complementary studies for each off-target kinase using alternative approaches such as shRNA mediated knockdown. Further, it is possible that high doses of the inhibitors might result in kinases that might only be partially inhibited at lower doses (such as those with a lower IC50 than MAP4K4), would likely also be inhibited in the presence of relatively high concentrations. However, putting into perspective the off-target hits obtained with DMX-5804, the concentrations required for half-maximal inhibition are 100- to 4000-fold higher than for MAP4K4, TNIK, and MINK1 (Fiedler et. al, in revision).

The concentrations of inhibitor used here were relatively high (10μM is towards the higher end of the spectrum). This was done to keep consistency across the MAP4K4 team, both in terms of previous data from the lab and data being generated alongside the work presented here. 10μM was the top concentration used for in-cell testing by other members of the MAP4K4 team (past and present) and the compounds were identified not to be toxic at this

concentration as assessed in H9C2 cells and iCell cardiomyocytes. It was appropriate to use this concentration in this setting, since our experiments aimed primarily at uncovering potential toxicity. After our initial studies, lower concentrations were introduced; however, the 'bandwidth' for our assays precluded us from testing more concentrations at once. In future, testing of a wider range of concentrations, particularly at lower concentrations would be beneficial and would contribute to strengthening these findings.

It is possible that the inhibitors may have some effect on cellular morphology. MAP4K4 possesses two consensus SH3 binding motifs which are involved in cytoskeleton regulation, mediating motility and shape (Yao et al. 1999). In addition, the MAP4K4 homozygous null mouse is embryonically lethal due to defective cell migration (Xue et al. 2001), suggesting that MAP4K4 inhibition might have been expected to have consequences for cell morphology. MAP4K4 has been shown to localise to CX43 positive gap junctions in 2D cultures of rat neonatal cardiomyocytes and is therefore likely to have an effect on the cytoskeleton (Lorna Fiedler, personal communication). In our study, we did not observe discernible deleterious effects on cytoskeletal dependent features qualitatively, although we did not quantify morphological aspects or cytoskeletal markers. However, pharmacological MAP4K4 inhibition has been observed to induce abnormal retinal vascular morphology in mice in vivo and delayed retinal vascular outgrow (Ndubaku et al. 2015). MAP4K4 has been implicated as an upstream regulator of proteins involved in cytoskeletal dynamics or adhesion such as Arp2 (LeClaire et al. 2015), Farp1 (Schwaid et al. 2015), moesin (Vitorino et al. 2015), IQSEC (Yue et al. 2014) and Pyk2 (Loftus et al. 2013). MAP4K4 deletion in endothelial cells caused reduced migration and disrupted angiogenesis (Vitorino et al. 2015). Therefore, in future, it would be interesting to test the effect of the inhibitors on cardiomyocyte morphology in the models used here.

Doxorubicin is a generator of extracellular ROS able to exert oxidative stress through a number of pathways (Burridge et al. 2016) and as such, the partial rescue observed by MAP4K4 inhibition might have been as a result of mitochondria-independent effects in the cell lines tested. In order to address potential mitochondria independent effects caused by doxorubicin, menadione, an endogenous generator of ROS (Loor et al. 2010; Criddle et al. 2006) was incorporated as the stress signal for subsequent experiments as both a more physiologically relevant signal and a more reductionist approach. This final refinement in terms of the stressor showed menadione to increase loss of membrane integrity and decreased force of contraction, as expected, consistent with doxorubicin findings. However, menadione decreased BPM even at 5 μM whereas doxorubicin did not.

DMX-5804 is the best compound tested here, as it possesses an improved potency, microsomal half-life, aqueous solubility and selectivity compared to IC4-001, protects against H_2O_2-induced oxidative stress (Imperial Innovations Limited, UP Patent Office Application GB1716867.5, MAP4K4 inhibitors, 13 October 2017, Fiedler et. al, in revision). Further, it has a structure which is completely different and unrelated from GNE-495, the published MAP4K4 inhibitor, allowing for it to evaluate its effects independently. Addition of DMX-5804 alone did not induce loss of membrane integrity, nor did it alter force or BPM, suggesting compound safety in either cell line. Further, it did not show any changes in the parameters measured in the presence or absence of fibroblasts. These findings are consistent across all three compounds as none of the inhibitors had adverse effects at the concentrations sufficient for cardioprotection, but a direct comparison between the inhibitors is needed to qualify this statement.

DMX-5804 was protective from cell death at 10 μM DMX-5804, 24 hr after menadione treatment in hiPSC-CM only hEHT. However, this effect was not sustained at later

timepoints, possibly due to little further loss in membrane integrity in the menadione-only group, rendering the later timepoints moot. In contrast, DMX-5804 was protective even 48 hr after doxorubicin treatment, suggesting that doxorubicin's cytotoxic effect is less acute and thus cells are still releasing AK into the media 48 hr after the insult. However, side-by-side comparisons of both compounds from both cell lines were not possible in our hands, for logistical reasons. Despite the differences in levels of protection between inhibitors and those differences observed in the stressor's response, it is clear that our data successfully shows MAP4K4 pharmacological inhibition to be safe from both cytotoxic and functional standpoints. In future, it would be important to test for the inhibitors' potential for hepatotoxicity, carcinogenic and mutagenic effects as well as reproductive toxicity studies.

Force after menadione treatment was preserved for 24 hr by low concentrations of the inhibitor and beating rate was preserved at both DMX-5804. The inhibitor did not rescue force or beating rate from doxorubicin-induced impairment, which points to the fact that MAP4K4 inhibition is likely to exert protection through an effect on endogenous ROS in the mitochondria. This notion is supported by the protection in cell death and contractile function seen by DMX-5804 when using menadione as the stressor. However, iCell were used in the doxorubicin studies, so differences in cell line may account for the discrepancies, especially iCell batches of poor quality were identified by us and others in 2D studies.

EHTs beat spontaneously, regulation of contractile function is less pronounced than in native tissue and no force-frequency relationship has been observed by us and others (Mannhardt et al. 2016). A possibility is that this due to the immaturity of t tubules and SR organisation since in native cardiomyocytes small differences in t tubule length and orientation are known to cause dysfunction of the calcium induce calcium release mechanism (Gómez et al. 1997). Further, native human heart tissue has primarily been studied under isometric conditions and EHT under physiological auxotonic conditions; whilst the impact has not been well described, auxotonic conditions have shown 50% lower forces than under isometric conditions in adult rat ventricular cardiomyocytes (Nishimura et al. 2004).

Forces on rat EHT were measured to be in the range of 2-4mN/mm^2, those for hESC and hiPSC EHT were 0.08-0.12 mN/mm^2 and intact hear muscle is in the range of 40-80 mN/mm^2 (Tulloch et al. 2011; Schaaf et al. 2011; van der Velden et al. 1998). The introduction of mechanical stretches has improved cardiac structure and force development (Fink et al. 2000). Adult human left ventricle myocardium has a conduction velocity of 0.3-1.0 meters/sec, whilst that of immature human heart has not been determined to our knowledge (Yang et al. 2014). Neonatal dog ventricular muscle has a propagation velocity of 0.33 meters/sec whilst adult tissue of 0.50 metres/sec (Spach et al. 2004). hiPSC derived EHT has been shown to have similar upstroke velocity as those values reported for non-failing hearts (Lemoine et al. 2017). This supports the validity of EHT culture of hiPSC-CMs as a means of studying electrophysiological and compound safety questions.

These results identify MAP4K4 as a pro-apoptotic mediator in menadione and doxorubicin induced cell death. MAP4K4 inhibition does not impair contractility, confirming suitability for further development, and inhibition partially rescues doxorubicin and menadione-induced contractile impairment.

These findings strengthen the usefulness of human stem cell-derived cardiomyocytes, both as part of patient-specific models of inherited disorder or, in this case, as a tool for target discovery and drug development. Despite their limitations, such as functional immaturity and lack of key cell-cell interactions, even in 2D human stem cell-derived cardiomyocytes have been reported to offer good predictive power (Burridge et al. 2014; Devalla et al. 2015; Gintant et al. 2016; Passier et al. 2016). The work hereby presented makes progress towards furthering the use of pluripotent stem cell-derived cardiomyocytes in organoids. Our results support both the use of human cardiomyocyte engineered heart tissue as a model to bridge the gap between animal models and human trials, and proposes MAP4K4 inhibition as a well-posed target for development towards cardioprotective treatment.

7. Discussion

7. Discussion

In this study, the hypothesis that MAP4K4 plays a pro-apoptotic role and drives dysfunction in human myocardium undergoing acute stress was tested. hiPSC-CMs were used as they provide an accessible human model with proven predictive power in cardiotoxicity pathways (Burridge et al. 2016).

MAP4K4 involvement in cardiomyocyte death and heart disease has been previously suggested using in vivo and in vitro approaches in rodent models. MAP4K4 is implicated in cardiomyocyte death in by a) activation in failing human hearts and pathological and genetic cell death mouse models, b) gain-of-function mutations potentiating cell death and failure in mouse hearts, and c) dominant-negative mutations and RNA interference in isolated rat cardiomyocytes being protective against cell death insults (Imperial Innovations Limited, UP Patent Office Application GB1716867.5, MAP4K4 inhibitors, 13 October 2017, Fiedler et. al, in revision). Importantly, in a human context, MAP4K4 was found to be activated in diseased human heart consistently across diverse etiologies relative to healthy donor hearts. MAP4K4 activation was consistently coupled to cell death as shown by increased levels of cleaved, activated caspase-3 and activation of TAK1 (Fiedler et al., in revision), a MAP3K intermediary able to drive cardiac cell death (Zhang et al. 2000).

However, by itself, analysis of end-stage heart failure does not determine whether MAP4K4 plays a pro-apoptotic role in diseased human myocardium, particularly in the setting of acute oxidative stress. This is of particular relevance since acute oxidative stress is an important feature during I/R injury. In addition, it is not known in any system whether MAP4K4 plays any role in cardiac metabolic or contractile function.

Using two different lines of human cardiomyocytes derived from pluripotent stem cells, human myocardium was modelled in both 2-dimensional (2D) and 3-dimensional (3D) culture, the latter being more representative of the intact heart. Involvement of MAP4K4 in

cell death, metabolism and contractile dysfunction induced by acute oxidative stress was tested using two pharmacological inhibitors developed in-house (IC4-001 and DMX-5804, Imperial Innovations Limited, UP Patent Office Application GB1716867.5, MAP4K4 inhibitors, 13 October 2017, Fiedler et. al, in revision), and one recently disclosed by Genentech, GNE-495 (Ndubaku et al. 2015). Here, we show that MAP4K4 promotes cell death and dysfunction in human cardiomyocytes and engineered heart tissue undergoing acute oxidative stress. Thus, pharmacological inhibition of MAP4K4 is not only cardioprotective, but is able to restore metabolic and contractile dysfunctions induced by stress. Furthermore, the inhibition of MAP4K4 by itself, does not adversely affect metabolism or contractile function. MAP4K4 is therefore a promising target for therapeutic intervention in ischemic human heart disease.

7.1 The role of MAP4K4 in human cardiomyocyte cell death

At present, the notion that MAP4K4 has a role in the heart has been suggested mainly by its pathobiological role linked to TAK1, JNK (Yao et al. 1999) and p38 (Zohn et al. 2006). These MAPKs are downstream of MAP4K4 and are known to be involved in cell death in cardiomyocytes (Fiedler et al., in revision; Rose et al. 2010).

Here we have successfully tested and demonstrated caspase-dependent apoptotic death through the assessment of cleaved caspase-3, and late apoptotic/necrotic death through the assessment of DRAQ7 staining profiles and the release of intracellular AK into cell culture supernatant. Previously, MAP4K4 shRNAmir mediated knockdown in hiPSC-CMs reduced H_2O_2-induced cell death measured by Draq7 uptake, further supporting a pro-apoptotic role for MAP4K4 in human cardiac muscle cells (Fiedler et. al., in revision). However, previous studies were conducted by knocking down MAP4K4 expression rather than pharmacological inhibition. The latter approach was favoured here since studying the effect of pharmacological inhibition is more relevant from a clinical perspective. Dissection of earlier stages in the death pathway would be a logical next step, particularly with regards to the potential contribution from the mitochondria.

Since our most convincing cell death data were those provided by the measurement of AK release, a marker of late stage apoptotic/necrotic events, it is also imperative to distinguish between the contribution to this response brought about by late apoptosis and necrosis, since this readout is unable to separate these. Firstly, apoptosis and necrosis can be dissected by analysis of morphology, flow cytometry and transmission electron microscopy. Biochemical techniques for this include DNA fragmentation by flow cytometry and cytochrome c release by western blotting. Primary and secondary necrosis can be dissected by analysis of caspases supernatant and chromatin protein high-mobility group b1 (HMGB1). HMGB1 release occurs at a late stage of death hence acting as a marker for secondary

necrosis and cyclophilin A is released during early stages (Christofferson & Yuan 2010). It is not simple to distinguish between late apoptosis and necrosis, but could be attempted through immunocytochemistry using Annexin V staining and propidium iodide (PI), since single PI staining suggests primary necrosis, single Annexin V staining suggests early apoptosis and double staining (Annexin V and PI) suggests secondary necrosis (Sawai & Domae 2011; Crowley et al. 2016). Ideally, this should be done using time-lapse microscopy to observe the markers as they appear. Alternatively, using antiapoptotic genes (Bcl-2) could help to distinguish between primary necrosis and secondary necrosis. In addition, it would be interesting to dissect the contribution by caspase-dependent and independent mechanisms, such as those form effectors like apoptosis-inducing factor (AIF), able to trigger caspase-independent apoptosis.

Necroptosis, ferroptosis and autophagic death and their potential involvement in the phenotypes observed, remain to be examined. Necroptosis is dependent on RIPK3 activation and takes place when caspase activation is blocked or insufficient (Yoon et al. 2016). It is important to distinguish cells undergoing apoptosis and necrosis from those undergoing necroptosis particularly as cells can shift from apoptosis to necroptosis and secondary necrosis and this often takes place in later stages of apoptosis (Yoon et al. 2016). As such, cell death detection should be complemented with real-time morphological approaches as well as with inhibition/knockdown approaches. Nuclei should be stained with PI as cells undergoing necroptosis have maintained chromatin structure and prominent nucleoli staining whilst apoptotic/necrotic cells present loss of chromatin structure (Yoon et al. 2016). Proteins central to the necroptotic pathway should be measured, such as RIPK3, RIPK1 and MLKL, using western blot, immunohistochemistry or flow cytometry. Ferroptosis is an iron-dependent form of death which results from lipid ROS production (Dixon et al. 2012). The presence of ferroptosis can be confirmed by measuring crucial proteins such as glutathione peroxidase 4 (GPX4), which presents reduced activity in ferroptosis, and glutathione which can be depleted during ferroptosis (Cao & Dixon 2016). In addition,

chemical inhibitors such as ferrostatin-1 and liproxstatin-1 can be used to confirm the presence of ferroptosis (Cao & Dixon 2016). Autophagy is a degradation system by the lysosome important under physiological and pathological conditions, however, monitoring autophagic activity are complex and difficult to interpret (Yoshii & Mizushima 2017). Assays capable of measuring autophagic flux quantitatively in live cells should be favoured, such as LC3 conjugation levels or through the use of Keima, a coral derived fluorescent protein that can be used to measure late stage autophagic flux by a cumulative readout of lysosomal fusion (Katayama et al. 2011).

H_2O_2-induced caspase-3 activation and initial loss of plasma membrane integrity in 2D cultures was found to be rescued by pharmacological inhibition of MAP4K4. These findings were also replicated in 3D tissue, where doxorubicin induced caspase-3 cleavage and MAP4K4 inhibition partially protected from this insult. Together with previous work in our lab showing a correlation between MAP4K4 activation and increased caspase-3 activity in human heart (Fiedler et al., manuscript in revision), these data indicate that MAP4K4 plays a pro-apoptotic role in human myocardium.

It should be noted that previous studies in the same cell type (iCell) did not show any induction of caspase-3 activity by H_2O_2 (Evie Maifoshie, PhD thesis, Imperial College London), likely explained by alternative methodological approaches: high-content, single-cell imaging versus caspase-3/-7 activity in whole well lysates, respectively. As such, confirmation using an alternative method such as the NucView caspase-3 substrate in the Cellomics platform and/or a caspase-3-YFP sensor driven by a cardiospecific promoter (Fujita et al. 2008) could be beneficial.

The findings in 3D culture showed that caspase-3 cleavage was induced due to doxorubicin-induced cytotoxicity, and that MAP4K4 inhibition partially protected from this. Others have also found that doxorubicin significantly upregulates the expression of death receptors (TNFR1, Fas, DR4 and DR5) in hiPSC-CMs at both protein and mRNA levels and that

cardiomyocytes undergo spontaneous apoptosis enhanced by TNF-related apoptosis inducing ligand (TRAIL) as well as decreased beating rate (Zhao & Zhang 2017; Zhang et al. 2015; Burridge et al. 2016; Gupta et al. 2018).

Inhibition of MAP4K4 however, was unable to sustain initial protection against loss of plasma membrane integrity (DRAQ7 in 2D studies) but it did sustain protection against activation of caspase-3 when only a single dose of compound was added. This might reflect concurrent caspase-3- (and MAP4K4-) independent mechanisms of cell death. However, when compound was replenished daily in later 3D culture experiments, loss of plasma membrane integrity (AK release) was able to sustain protection. In I/R injury and heart failure an increase in caspase-3 activation (as measured by protein levels of cleaved caspase 3) has been reported (Narula et al. 1999; Scheubel et al. 2002), however, caspase-independent apoptotic mechanisms could be involved, such as DNA fragmentation through Apoptosis Inducing Factor (AIF) release from apoptotic mitochondria (Bröker et al. 2005). Even the modest activity of caspase-3 remaining following MAP4K4 inhibition might be sufficient to cause cell death over extended periods of time, as suggested by evidence that minimally active caspase-8 in the heart resulted in failure due to ongoing, low levels of cell death (Wencker et al. 2003). In addition, differences in sensitivity to death signals is also dependent on the stage of differentiation (Mioulane et al. 2012). Whilst it could be argued that the hiPSC-CMs used here are immature, it should be noted that rat neonatal CMs, used previously in our lab (Xie et al. 2007) are also immature; in this system, MAP4K4 overexpression by viral-mediated gene transfer was sufficient to induce apoptosis, dissipate mitochondrial transmembrane potential, and activate caspase-3 and caspase-8, which is partly suppressed by Bcl-2 (Xie et al. 2007). Alternatively, toxicity (kinase- or non-kinase-related off-target effects) caused by the inhibitor could account at least in part for the effect seen; however, given the minimal adverse effect of the compounds given by themselves, it is more likely that incomplete inhibition of caspase-3 activity was insufficient to protect from

plasma membrane disruption. In future, gain-of-function experiments could be envisioned, using the hiPSC-CM models as the platform for death pathway dissection.

Since we only successfully tested mitochondrial function at sub-lethal concentrations of the stressors (to assess mitochondrial dysfunction rather than death), whether MAP4K4 is involved in apoptosis via the mitochondrial pathway remains to be elucidated. In the present study, MAP4K4 did not appear to be involved in BID cleavage, as a measure of mitochondria mediated cell death, although BID cleavage was successfully induced by H_2O_2. Although this suggests that MAP4K4 is not involved in apoptosis via mitochondrial pathways, there were a number of technical limitations affecting this particular assay and are therefore inconclusive.

A disparity observed as compared to the literature was the lack of p38 activation during oxidative stress. p38 inhibition has been found to be protective in other studies (Marber et al. 2011; Marber et al. 2010; Fryer et al. 2001; Denise Martin et al. 2012), but this is possibly due to effects on contractility or ECM remodelling rather than direct inhibition of cell death. JNK was not studied due to technical issues regarding the antibodies. We were not able to measure p38 activation by either MAP4K4 inhibition nor H_2O_2 treatment in our experiments, perhaps due to the fact that the antibody used was not isoform specific and could not detect any increases in β isoform (which has been specifically been found to be cardioprotective) (Liu et al. 2011). Alternatively, H_2O_2-induced cell death may be p38-independent in this cell type. The use of p38 inhibitors to test this would provide valuable insight. ERK1/2 activity was also unchanged by either H_2O_2 treatment and/or MAK4K4 inhibition in accordance with previous studies suggesting that it does not mediate cell death or dysfunction (Lu & Xu 2006). Earlier timepoints should be tested to rule out the possibility of having missed the activation window. Use of an additional hiPSC-CM cell line would be beneficial here to allow greater confidence in the results obtained. At this stage, however, the question as to which MAP4K4 effectors are at play in the systems tested remains unanswered.

Previous studies in mice showed that MAP4K4 (Myh6-MAP4K4) in combination with either pressure overload or genetic stimuli increases apoptosis (as measured by TUNEL staining and caspase-3 activation) and cardiac dysfunction (Fiedler et. al, in revision). More recently, other members of the MAP4K4 team used pharmacological inhibition by DMX-5804 in mice both pre- and post I/R injury and found that not only was infarct size reduced in both scenarios, but also cardiomyocyte apoptosis was also reduced in both cases, as measured by TUNEL staining. These findings in mice are in agreement with our findings with regards to MAP4K4 involvement in apoptosis in hiPSC-CMs both in 2D and 3D culture.

TAK1 is the best-characterised MAP4K4 effector, among number of the MAP3Ks (Yao et al. 1999; Zhang et al. 2000). TAK1 may link MAP4K4 and NFkB in the heart as TAK1 has been shown to activate cardiomyocyte cell death (Zhang et al. 2000) through JNK independent of its p38 activating function whilst TAK1 deficient cells undergo RIP1- mediated death after being exposed to TNF-α stimulation (Çöl Arslan & Scheidereit 2011). Cardiospecific ablation of TAK1 in mice led to remodelling and heart failure (Li et al. 2014), suggests a pro-survival role for TAK1. Since inhibition of MAP4K4, under oxidative stress conditions, causes the opposite effect than that observed in the cKO mice (i.e. protects from injury), our results support earlier evidence suggesting that TAK1 is involved in cardiomyocyte cell death. Increases in caspase-8 activity have been shown to activate NFkB (Hu et al. 2000) through TAK1 and TNFRI (Devin et al. 2001; Ea et al. 2006). As such, there is a possibility that TAK1 acts in two different ways; by binding MAP4K4 to trigger cell death or by associating with TNFR to signal survival. As such, it would be important to elucidate whether MAP4K4 binds and phosphorylates TAK1. Particularly since, TAK1 has been found to switch from apoptosis to necrosis through TNF stimulation with sustained activation leading to RIPK3 phosphorylation and necrosis, whilst deletion caused caspase-dependent apoptosis (Morioka et al. 2014). This suggests that TAK1 acts as a switch between apoptosis and necrosis.

7.2 The role of MAP4K4 in function in 2D culture

I/R injury exposes mitochondria to oxidative stress, such as the increased formation of ROS, causing damage and altering respiration rates, which directly impacts on cardiomyocyte contractility and survival. Maximal respiratory capacity is the maximum activity of electron transport and substrate oxidation achievable under specific conditions and suppression strongly indicates mitochondrial dysfunction (Brand & Nicholls 2011). Our most developed MAP4K4 inhibitor, DMX-5804, protected maximum respiratory capacity but not ECAR under conditions of endogenous stress, suggesting MAP4K4 involvement in regulating mitochondrial respiration but not glycolytic function. The mitochondrial 'reserve capacity' is depleted under conditions of stress such as pressure overload (Kingsley-Hickman et al. 1990) or ischemia (Gong et al. 2003), whereby cardiomyocytes develop an enhanced ability to consume oxygen, suggesting a mechanism for depletion of this reserve capacity in an environment in which oxygen availability is limited (Strauer 1987; Smith et al. 1996; Sako et al. 1988). As such, this reserve capacity is believed to be important, as when it is exceeded protein damage and cell death occur, in conjunction with decreased OCR (Hill et al. 2009). Spare respiratory capacity was restored to normal levels in the presence of the inhibitor alone on CorV.4U hiPSC-CMs although this was not the case on iCell hiPSC-CMs; suggesting that different mechanisms are at play in different cell lines and that changes to respiratory capacity may be involved as part of as a possible mechanism for MAP4K4-mediated protection. In addition, under the conditions chosen for these functional assays, no loss of membrane integrity was detected as measured by AK activity, suggesting that any effect observed was due to changes in mitochondrial function per se and not, indirectly, due to cell loss.

Overall findings in the alternative cell line (iCell) concurred, however, the individual components of mitochondrial respiration did not show protection, potentially due to a lack of power due to variability, alternative (and distinct) off-target effects between the inhibitors, greater heterogeneity of the iCell myocytes, lesser maturity, or a combination of these

factors. Off-target effects cannot be excluded in use of pharmacological approaches; however, we have mitigated this through the use of complementary compounds, overlapping exclusively in their effect on MAP4K4 and its relatives with an identical ATP-binding pocket. To resolve these, studies of each 'off-target' kinase would be needed using alternative approaches such as gene silencing by shRNA-mediated knockdown or CRISPR interference (Peretz et al. 2018; Boettcher & McManus 2015).

The significance of our findings regarding human cardiac mitochondrial function are three fold: results with the provisional lead compound DMX-5804 agree with findings using the earlier tool compound IC4-001, they illustrate the superiority of the CorV.4U line which allowed us to see protection at the level of the individual components of mitochondrial respiration, and, most importantly, both MAP4K4- dependent and -independent mechanisms may be at play. This implicates MAP4K4 in metabolic regulation in the heart, driving dysfunction in the setting of acute oxidative stress. Many studies have reported concurring findings reposting in the involvement of MAP4K4 in metabolism. MAP4K4 gene deletion or inhibition of kinase activity has been shown to reduce hyperglycemia in insulin resistant mice and plaque formation in atherosclerotic mice (Virbasius & Czech 2016). MAP4K4 deletion is able to suppresses insulin sensitivity and lipid synthesis (Danai et al. 2015) and to improve substrate uptake in skeletal muscle cells (Bouzakri & Zierath 2007). In addition, inducible endothelial cell MAP4K4 deletion in adult mice was able to ameliorate metabolic dysfunction in obesity (Roth Flach et al. 2017) and obesity induced hyperinsulinemia (Roth Flach et al. 2016). Animals lacking endothelial MAP4K4 were protected from skeletal muscle microvascular rarefaction in obesity and endothelial cells showed reduced senescence and increased metabolic capacity. Blood endothelial MAP4K4 promotes vascular dysfunction and impairs glucose homeostasis in mice whilst lymphatic endothelial MAP4K4 plays a role in lymphatic vascular integrity and immune cell traffic regulation in obesity (Roth Flach et al. 2017). This suggests that in endothelial cells, MAP4K4 has different functions in the blood and lymphatic endothelium.

Calcium cycling is important to contractile function and abnormal calcium dynamics feature in heart disease (Gorski et al. 2015). No effect was observed by DMX-5804 treatment on any of the calcium handling parameters. However, whilst we found that the amount of calcium cycling was highly sensitive to oxidative stress induced by menadione treatment (as measured by percentage of number of wells that exhibited calcium transients), but kinetics of calcium transient in cycling cultures were not. The concentrations at which calcium transients were lost correlated with those at which cell death was induced. DMX-5804 was able to rescue the number of wells engaging on calcium cycling but not the decrease in their amplitude, suggesting protection to be related to salvaging cell number rather than direct effects. This, however, should be confirmed by Western blotting and immunohistochemical analysis of contractile proteins. Particularly since, PKA-mediated phosphorylation of VDLC, RYR, SERCA2 and phospholamban allows for intracellular calcium transients with higher amplitude and faster reuptake into the SR (Armand & De Windt 2004) and therefore it is possible that these contractile proteins may have been affected. However, it is likely that these findings are the result of a failure to rescue automaticity, that is, the ability to spontaneously generate an electrical impulse. To test this, it would be crucial to utilise electrically paced cardiomyocytes or chronotropically stimulated ones. In future, confirmation on our 3D model as well as at the single cell level, a finer dose-response titration for menadione and establishing the time window in which to give DMX-5804 after ROS increase, would be useful next steps. However, these findings strongly suggest that the effect of MAP4K4 inhibition observed in contractility is due to increased cell survival.

7.3 Human engineered heart tissue as a platform for dissecting the role of MAP4K4 in the heart

We found our early, 2D, microscopy-based studies of cell death and MAP4K4 to be unreliable, particularly due to cell loss; however, we are unable to draw definitive conclusions as to whether this was a result of the techniques employed (DRAQ7 staining, immunofluorescence), high concentrations of the death agonist, or limitations of the iCell line, which was often found to look unhealthy and give variable results both by us and other members of the team. Apart from these initial exploratory experiments in which results were inconclusive (Chapter 3), we found that our 2D results in both cell lines were in general agreement with the 3D results obtained for the outputs tested. Particularly, AK activity, which was used in both 2D and 2D models, provided a direct means of comparison between both approaches for this study's most central end-point, cell death. However, it is not possible for technical reasons to measure metabolic parameters in 3D constructs using the mito stress test; ATP and ADP levels, ATP/ADP ratios and glycolytic intermediaries such as G6P (using tools such as metabolomics profiling) (Lucarelli et al. 2015) could be measured as a surrogate metabolic output for hEHT.

The generation of EHT that was not co-cultured with fibroblasts was a final refinement to the 3D model: this was done on the grounds of both producing superiorly performing EHT (as expected from the results obtained by the Eschenhagen lab) and bridging one of the main limitations which was the dissection of the contribution by each cell type to the responses observed. The latter was of particular importance, since even more selective assays than those used here, such as human cardiac troponin ELISA, the clinical 'gold standard' would not explicate the potential contribution of fibroblast death to the phenotype whilst other approaches were unavailable to us due to technical issues encountered by immunostaining (inconsistent results across the MAP4K4 team) as well as the limitation in terms of cost

regarding other potential techniques (i.e. western blotting requires large numbers of cells). It was recently found by the Eschenhagen lab that EHT can be generated using the two commercially available cell lines presented in this study (which are free from non-myocytes due to genetic selection), suggesting that previous findings relating to the mandatory need for 25% non-cardiomyocytes in collagen-derived EHTs (Naito et al. 2006) does not apply to human cardiac tissue produced using fibrin instead (Mannhardt et al. 2016). Notably, a recent study supports the notion that contraction amplitude and kinetics are more stable over time and less variable in hEHT that is not fibroblast-enriched (Mannhardt et al. 2017).

Comparison of EHT characteristics is troublesome due differences in preparations, conditions and the way in which parameters were measured. Our hEHT has a force of contraction ranging between 1-2mN/mm^2. The best performing hEHT in the field, to our knowledge, comprises hiPSC-CM cardiobundles which in dynamic culture have shown forces of 23.2 mN/mm^2 and for rat tissue 59.7 mN/mm^2, the first time matching those of adult rat ventricular myocardium (Jackman et al. 2016). More recently, large cardiac patches (1 cm x 1 cm) from neonatal rat ventricular cells have been generated, which are able to exhibit force of 18mN/mm^2 (Jackman et al. 2018). These studies use a force transducer to measure force of contraction which measures force directly, whereas our system takes indirect measurements through optical tracking; however, our system has the advantages of being sterile and non-invasive.

Whilst the tool compound IC4-001 showed rapid clearance and poor availability, making it unsuitable for animal testing, DMX-5804 has been able to reduce infarct size in mice even when administered an hour after reperfusion injury (Fiedler et al, manuscript under revision). Although its solubility and pharmacokinetic properties preclude it from becoming itself a candidate for human use, this compound has been particularly useful in this study for target validation in hiPSC-CMs. DMX-5804 alone did not induce loss of membrane integrity, nor changes to force or BPM, suggesting a profile suitable for use in terms of compound safety. These data are in agreement with our EHT studies using both CorV4U and iCell in

conjunction with fibroblast, and is encouraging from a safety standpoint. Further, this concurs with the findings using the Genentech compound GNE-495 (Ndubaku et al. 2015), which did not cause loss of plasma membrane integrity nor changes to contractile parameters. Taken together, these findings suggest that inhibition of MAP4K4 does not adversely affect contractile properties of human EHT.

Differences between endogenous and exogenous death stimuli were apparent. In this setting, menadione was able to increase loss of membrane integrity and decrease force of contraction, consistent with doxorubicin findings. DMX-5804 was protective from loss of membrane integrity 24 hr after menadione treatment in hiPSC-CM EHT but not at later timepoints, potentially due to all AK having already been released in the menadione only group. In contrast, DMX-5804 was protective even 48 hr after doxorubicin treatment, suggesting that cytotoxic effect exerted by doxorubicin is not as acute and as a result cells still release AK into the media even 48 hr after treatment with this death agonist.

Having a clear picture as to the effects of DMX-5804 in cell death in the 3D model was instrumental to the interpretation of the contractility analysis. It was found that force and beating rate after menadione treatment were preserved for 24 hr, whereas the inhibitor did not rescue force or beating rate from doxorubicin-induced impairment. However, the caveat is that iCell hiPSC-CMs were used in the doxorubicin studies, which are not directly comparable.

MAP4K4 knockdown (see **Supplement**) (or inhibition) by itself did not affect the contractile properties of hEHT. Only low and statistically insignificant levels of gene silencing were achieved. Potential explanations are viral titre, viral infectivity, and the conditions chosen for transduction in hEHT. Heterozygous null mice (incomplete knockdown) presumably do not exhibit motility defects at baseline during development since no discernible phenotype is present. No changes in chamber volume, diameter or function at baseline in heterozygous null mice compared to wildtype littermates were observed (Lorna Fiedler, personal communication). Consistent with the lack of phenotypes in heterozygous-null mice, no effect

was seen in EHTs' baseline mechanical performance. Though the efficacy of gene silencing was limited (or negligible), protection from oxidative stress was seen, as measured by membrane integrity and transient benefits in some contractile properties. Ways to reconcile these obvious discrepancies include errors in the estimation of knockdown efficiency, off-target effects as just one RNAi sequence was ultimately tested, and concordant errors in both the cell death and contractility assays. Of these, the first two are likeliest.

7.4 Technical limitations

Consistent technical limitations have been highlighted in this thesis, such as cell loss and inherent variability in quality of the iCell line of human cardiomyocytes. These were circumvented to some extent by introduction of an additional cell line, and more closely monitoring cell loss to determine whether this was a factor to be considered in interpreting results. However, wider limitations of the systems used in this study should be examined. The relevance of human cardiomyocytes in modelling disease is being recognised in terms of both mechanistic studies and in drug discovery pipelines particularly in the context of cardiac toxicity. In particular, hEHT is emerging as an important system in which to study cardiac signalling and test therapeutics in an environment that more closely recapitulates the intact human heart. The limitations of these systems should be acknowledged however and are discussed below.

The main limitation of our initial work was related to the quality of the cardiomyocytes. In some experiments in which we used the iCell line, the high variability could have been responsible for a lack of power and therefore confounded results. For example, in the metabolic data, while the overall effect of 4μM menadione was significant, the individual components of mitochondrial respiration did not show a significant effect. This illustrates why the optimisation and development of the assays using a) different cell line and b) a 3D model

were paramount. However, the use of only two lines may not be sufficient to ensure generality and thus the use of additional hiPSC-CM cell lines would be beneficial, whereby similar results would allow greater confidence from a clinical perspective, and strengthen our understanding of the role of MAP4K4 mediated signalling in cell death and human disease. Further, side-by-side comparison between the compounds in both cell lines, both systems (2D and 3D) and all death signals would be ideal although not possible in our hands due to logistical reasons.

General limitations of this study include culture limitations and the number of plates that could be run alongside at any given time for the automated assays. In the native heart, there are various interacting cell types present which contribute to normal function. In the models used here, there was a lack of fibroblasts and endothelial cells present in the preparations, and the presence of unknown components in the proprietary media. Further, limited 'bandwidth' for the metabolic and EHT experiments prevented the use of a larger range of compounds, with which to explore the structure-activity relationships and correlation between phenotypes and MAP4K4 inhibition. The Eschenhagen lab cultures EHT at 40% oxygen since cardiomyocytes are expected to require large quantities, however, our lab has shown that no changes to contractility parameters were observed as a result of culturing the constructs in 21% oxygen (Thomas Owen, PhD Thesis 2018, Imperial College London).

3D platforms have been able to improve upon the maturity of hiPSC-CMs. However, these do not produce fully mature cardiomyocytes. In general, the formation of T-tubules, the expression of a full array of sarcomeric proteins, physiological potassium ion channel densities and contraction forces have not matched values for fully mature human cardiomyocytes (Denning et al. 2016). More recently, attempts have been made to improve these parameters by electrical pacing and medium supplementation with adrenergic agonists, thyroid hormones and growth factors.

hiPSC-CMs are known to display heterogeneity from signal (action potential morphology) when it comes to measuring electrical activity, which means that action potential measurements (optical and patch clamp studies) are noisier than calcium measurements since calcium transients are slower (Verkerk et al. 2017; Denning et al. 2016). This led to the conclusion that concentrating on calcium transient measurements would be most appropriate in this setting. Further refinements for the calcium studies should include confirmation at the single cell level, a finer dose-response for menadione as well as investigation into the optimal time window in which to give DMX-5804 after ROS increase for cardioprotection purposes.

MAP4K4 mRNA expression after knockdown showed only low and insignificant levels of silencing (see Supplement). The EHT generation process relies on 100µL of cells, media and hydrogel mixture that sets around silicon posts to form the strip of tissue. It was decided not to exceed 30% of this in terms of increasing the volume that would go into the cast, as this could potentially affect the properties of the EHTs and as such, this was the limiting factor in term of the maximum MOI we were able to use for transduction. How this translated to knockdown at the protein level was not tested, and thus levels may be different to this. However, this amount of knockdown at the RNA level was sufficient to partially protect against deleterious effects caused by ROS production and therefore it is likely that further knockdown might confer increased protection (something that could be achieved by further concentration of the virus by ultracentrifugation).

Off-target effects may have had some influence on the results presented here, although the unique P-loop-folded structure of MAP4K4 contributes to greater selectivity that might be expected for ATP-competitive inhibitors. The initial tool compound IC4-001 had off-target effects against only 5 human protein kinases out of a screening panel of 140: MINK, MLK1, MLK3, NUAK1 and GCK (Imperial Innovations Limited, UP Patent Office Application GB1716867.5, MAP4K4 inhibitors, 13 October 2017, Fiedler et. al, in revision). The

provisional lead compound, DMX-5804, targets MINK1/MAP4K6, TNIK/MAP4K7, GCK/MAP4K2, GLK/MAP4K3 and KHS/MAP4K5. GEN-495 exhibits reasonable but lesser selectivity with 7 off-target effects against a panel of 61 kinases; GCK, MLK1, Mer, MINK (MAP4K6), Rsk3, Rsk4 and PAK4 (Crawford et al. 2014). Given the homology, especially in the active site between MAP4K4 and its most closely related members, it is not surprising that GNE-495 inhibits the closely linked kinase MINK (Vitorino et al. 2015). Off-target effects cannot be wholly excluded as the cause for the effects reported here without complementary studies for each off-target kinase using alternative approaches such as shRNA mediated knockdown. However, putting into perspective the off-target hits obtained with DMX-5804, the concentrations required for half-maximal inhibition are 100- to 4000-fold higher than for MAP4K4, TNIK, and MINK1 (Imperial Innovations Limited, UP Patent Office Application GB1716867.5, MAP4K4 inhibitors, 13 October 2017, Fiedler et. al, in revision).

H_2O_2 and menadione were used as inducer of oxidative stress and they model key aspects of ischemia-reperfusion (Brown & Griendling 2015). We found that menadione, the endogenous producer of ROS produced more consistent, less variable results. H_2O_2 was found to be particularly problematic when it came to dose-response experiments in our hand and by various members of the lab and thus, overtime it was decided to migrate to more reliable stressors. These are, however, reductionist approaches which by comparison to the native heart do not provide a complete picture of the landscape in vivo, particularly due to functional immaturity.

In future, protein levels should be confirmed by Western blotting or immunofluorescence, although this is currently limited by the quality of commercially available antibodies. Kinase activity assays on MAP4K4 from cell lysates have been problematic (Dorte Faust and Kathryn Chapman, personal communications), likely as a result of inadequate commercially available antibodies. In future, the use of a readout of MAP4K4 activity in human cardiomyocytes and hEHT will be essential, particularly for the confirmation of the results

presented in this study. As an alternative to immune complex kinase assays, one viable option could be the production of a phospho-specific antibody able to detect the phosphorylated active state of the enzyme, either a polyclonal or monoclonal antibody to a MAP4K4 phosphorylation site that reports on its activity.

7.5 Future directions

The improvement of maturation of hiPSC-CMs in EHT is paramount to the quality and performance of the tissue. Prolonged culture has been shown to increase maturation in ESC and hiPSC-CMs by studies assessing RNA expression and contractile properties (Babiarz et al. 2012; Lundy et al. 2013). The addition of T3 hormone (Burridge et al. 2015; Lee et al. 2010) or calsequestrin (CSQ; a calcium handling protein) overexpression (Dolnikov et al. 2006) also improve maturation, as does stretching and biochemical stimulation (redox signalling, VEGF, β-adrenergic) (Kolanowski et al. 2017). These are all strategies that could be advantageous in future studies. In addition, sustained electrical field stimulation has been proven to further improve EHT properties (Hirt et al. 2014). Chronic electrical stimulation of EHTs has been shown to double contractile force and elicit sarcomeric ultrastructure similar to myocardial tissue (Hirt et al. 2014), with force generated only a few fold inferior (4.4 mN/mm^2) to that in *in vivo* myocardium (Kensah et al. 2013). As such, in future EHTs might be paced from day one to more closely mimic conditions *in vivo* and provide a more mature platform (Liaw & Zimmermann 2015) to increase the model's predictive power.

hiPSC-CMs are a heterogeneous population which comprises both atrial and ventricular cardiomyocytes. This study mostly uses CorV.4U, a ventricularly enriched line. However, since the use of multiple lines will be required to ensure generality, the heterogeneity present in a most hiPSC lines, including iCell cardiomyocytes used here, will be an important point to address. In future, characterisation of these in both EHTs and 2D culture alongside each other, using markers such as MLC2v and MLC2a to discriminate between atrial and ventricular cardiomyocytes respectively as well as exploring the single cell landscape

through single cell qRT-PCR comparing cell types and 2D and 3D models side-by-side, provide a more complete picture as to the maturation of hiPSC-CMs in these settings and will help better understand how our models used here compare to native human cardiomyocytes.

Co-culture of cardiomyocytes with other cell types have been shown to improve functional features and engraftment compared to cardiomyocytes alone in an in vivo model of myocardial infarction (Sekine et al. 2008). Co-culturing of hiPSC-CMs, endothelial cells and fibroblasts at ratios similar to those present in vivo has shown to achieve cellular organisation, extracellular matrix and microvascular networks that mimic human native heart tissue (Polonchuk et al. 2017). Therefore, co-culture of hiPSC-CMs with fibroblasts and endothelial cells should also be explored, in order to more faithfully simulate the milieu of the multicellular heart. Further, this could also explain why some discrepancies exist between results obtained from rat neonatal ventricular cardiomyocytes and hiPSC-CMs (Chien et al. 2008).

Substrate preferences can predict metabolic properties and mechanisms. As such, testing additional substrates (or no substrate) would be interesting as this would provide an indication as to the mechanism for metabolic activity and further clarify the role of MAP4K4 signalling. In addition, measurements of changes in specific components such as ATP and lactate would be helpful in confirming current findings.

To further validate these studies *in vivo*, a mouse model of cardiac-specific inducible deletion of MAP4K4 has been generated by our lab. After confirming deletion by Western blotting, qRT-PCR and immunohistochemistry, mice will be subjected to I/R then non-invasive imaging, function *ex-vivo* and histology studies (infarct size/area at risk, apoptosis, and fibrosis). These data will be highly valuable in complementing these studies.

Overall, it will be interesting to determine the pathways involved as MAP4K4 targets in human cardiomyocytes, to delineate the mechanisms of MAP4K4 activation, and eventually

identify the acute and chronic cardiac disorders for which the inhibition of MAP4K4 could serve as potential therapy.

7. 6 Concluding remarks

At the beginning of this study we hypothesised that pharmacological inhibition of MAP4K4 protects against oxidative stress induced cell death, mitochondrial dysfunction and contractile dysfunction in human cardiac tissue.

We aimed to use novel and specific inhibitors of MAP4K4 to elucidate its role in cell death, mitochondrial function and contractility in human iPSC derived cardiomyocytes (hiPSC-CM) both in culture and in engineered heart tissue. MAP4K4 protects against oxidative stress induced cell death, mitochondrial dysfunction and contractile dysfunction in human cardiac tissue. Our findings support a pro-apoptotic role of MAP4K4 in cardiac human muscle and indicate that MAP4K4 may be involved in regulating metabolism in the heart and in particular, in driving dysfunction in the setting of acute oxidative stress. MAP4K4 is therefore a potential target for development of pharmacological inhibitors for cardioprotective treatment in the clinic.

A number of MAP kinases downstream of MAP4K4 have been pursued as targets for therapy in pre-clinical studies in cardiovascular disease. Perhaps the most iconic example is JNK, supported by both its role in I/R (Wei et al. 2011) and in neuronal injury, since inhibition of TAK1, JNK's upstream effector, was found to be protective in ischemic stroke (White et al. 2012). In addition, TNIK and MINK are the most closely related kinases to MAP4K4, and TNIK and MINK inhibition has recently been shown to confer benefits against neurodegeneration (Larhammar et al. 2017). However, the challenge faced by the translation of these pre-clinical findings to humans has not been easy to overcome. It has been problematic to achieve an increase of cardiac muscle cell survival using many other

potentially protective strategies in human clinical trials, with several conflicting results being reported and based only on non-human models (Hausenloy & Yellon 2015; Heusch 2013; Lincoff et al. 2014; Newby et al. 2014; Piot et al. 2008). Here, human cardiomyocytes have been employed as a strategy which has the potential to predict the clinical outcomes of the MAP4K4 inhibitors developed more accurately.

Our results further highlight the usefulness of human stem cell-derived cardiomyocytes, both as part of patient-specific models of inherited disorder or, in this case, as a helpful and reliable tool for target discovery and drug development. Human stem cell-derived cardiomyocytes have gained wide acceptance in the field of cardiotoxicity, particularly due to their performance when it comes to their predictive power, in spite of their limitations, which include aspects such as functional immaturity and cytoskeletal underdevelopment (Burridge et al. 2014; Devalla et al. 2015; Gintant et al. 2016; Passier et al. 2016). In addition, the use of 3D cultures as a means to evaluate functional parameters has increased the ability to model disease and native human settings more reliably and robustly (Lemoine et al. 2017).

Targets and interventions that have been validated not only in animal models but also in human cardiomyocytes and human engineered heart tissue are likely to prove worthy choices for development towards human trials in the near future. Our results support both, the use of human cardiomyocyte engineered heart tissue as a model to bridge the gap between animal models and human clinical studies, and propose MAP4K4 inhibition as a sensible, well-established and exciting target for development towards cardioprotective treatment.

8. References

References

Acehan, D. et al., 2002. Three-dimensional structure of the apoptosome: implications for assembly, procaspase-9 binding, and activation. *Molecular cell*, 9(2), pp.423–32. Available at: http://www.ncbi.nlm.nih.gov/pubmed/11864614 [Accessed November 2, 2017].

Adameova, A. et al., 2017. Evidence of necroptosis in hearts subjected to various forms of ischemic insults. *Canadian Journal of Physiology and Pharmacology*, 95(10), pp.1163–1169. Available at: http://www.ncbi.nlm.nih.gov/pubmed/28472590 [Accessed January 9, 2018].

Adameova, A. et al., 2016. Necroptotic cell death in failing heart: relevance and proposed mechanisms. *Heart Failure Reviews*, 21(2), pp.213–221. Available at: http://www.ncbi.nlm.nih.gov/pubmed/26872672 [Accessed January 9, 2018].

Akkina, R.K. et al., 1996. High-efficiency gene transfer into CD34+ cells with a human immunodeficiency virus type 1-based retroviral vector pseudotyped with vesicular stomatitis virus envelope glycoprotein G. *Journal of virology*, 70(4), pp.2581–5. Available at: http://www.ncbi.nlm.nih.gov/pubmed/8642689 [Accessed November 5, 2017].

Ammirati, M. et al., 2015. Discovery of an *in Vivo* Tool to Establish Proof-of-Concept for MAP4K4-Based Antidiabetic Treatment. *ACS Medicinal Chemistry Letters*, 6(11), pp.1128–1133. Available at: http://www.ncbi.nlm.nih.gov/pubmed/26617966 [Accessed January 15, 2018].

Anderson, M.E., Higgins, L.S. & Schulman, H., 2006. Disease mechanisms and emerging therapies: protein kinases and their inhibitors in myocardial disease. *Nature Clinical Practice Cardiovascular Medicine*, 3(8), pp.437–445. Available at: http://www.ncbi.nlm.nih.gov/pubmed/16874356 [Accessed November 3, 2017].

Antignani, A. & Youle, R.J., 2006. How do Bax and Bak lead to permeabilization of the outer mitochondrial membrane? *Current opinion in cell biology*, 18(6), pp.685–9. Available at: http://www.ncbi.nlm.nih.gov/pubmed/17046225 [Accessed January 10, 2018].

Aon, M.A. et al., 2006. Mitochondrial criticality: A new concept at the turning point of life or death. *Biochimica et Biophysica Acta (BBA) - Molecular Basis of Disease*, 1762(2), pp.232–240. Available at: http://www.ncbi.nlm.nih.gov/pubmed/16242921 [Accessed November 1, 2017].

Aon, M.A., Cortassa, S. & O'Rourke, B., 2010. Redox-optimized ROS balance: A unifying hypothesis. *Biochimica et Biophysica Acta (BBA) - Bioenergetics*, 1797(6–7), pp.865–877. Available at: http://www.ncbi.nlm.nih.gov/pubmed/20175987 [Accessed November 1, 2017].

Aouadi, M. et al., 2009. Orally delivered siRNA targeting macrophage Map4k4 suppresses systemic inflammation. *Nature*, 458(7242), pp.1180–4. Available at: http://www.pubmedcentral.nih.gov/articlerender.fcgi?artid=2879154&tool=pmcentrez&rendertype=abstract [Accessed September 15, 2015].

Aries, A. et al., 2004. Essential role of GATA-4 in cell survival and drug-induced cardiotoxicity. *Proceedings of the National Academy of Sciences of the United States of America*, 101(18), pp.6975–80. Available at: http://www.ncbi.nlm.nih.gov/pubmed/15100413 [Accessed January 15, 2018].

ARMAND, A. & De Windt, L.J., 2004. Calcium cycling in heart failure: how the fast became too furious. *Cardiovascular Research*, 62(3), pp.439–441. Available at: https://academic.oup.com/cardiovascres/article-lookup/doi/10.1016/j.cardiores.2004.03.022 [Accessed February 26, 2018].

Asrih, M. et al., 2013. Role of mitogen-activated protein kinase pathways in multifactorial adverse cardiac remodeling associated with metabolic syndrome. *Mediators of*

inflammation, 2013, p.367245. Available at: http://www.ncbi.nlm.nih.gov/pubmed/23365487 [Accessed November 3, 2017].

Auyeung, V.C. et al., 2013. Beyond Secondary Structure: Primary-Sequence Determinants License Pri-miRNA Hairpins for Processing. *Cell*, 152(4), pp.844–858. Available at: http://www.ncbi.nlm.nih.gov/pubmed/23415231 [Accessed October 11, 2017].

Babiarz, J.E. et al., 2012. Determination of the Human Cardiomyocyte mRNA and miRNA Differentiation Network by Fine-Scale Profiling. *Stem Cells and Development*, 21(11), pp.1956–1965. Available at: http://www.ncbi.nlm.nih.gov/pubmed/22050602 [Accessed November 5, 2017].

Bacman, S.R. et al., 2013. Specific elimination of mutant mitochondrial genomes in patient-derived cells by mitoTALENs. *Nature Medicine*, 19(9), pp.1111–1113. Available at: http://www.ncbi.nlm.nih.gov/pubmed/23913125 [Accessed November 1, 2017].

Baines, C.P. et al., 2005. Loss of cyclophilin D reveals a critical role for mitochondrial permeability transition in cell death. *Nature*, 434(7033), pp.658–662. Available at: http://www.ncbi.nlm.nih.gov/pubmed/15800627 [Accessed November 2, 2017].

Baines, C.P. et al., 2002. Mitochondrial PKCepsilon and MAPK form signaling modules in the murine heart: enhanced mitochondrial PKCepsilon-MAPK interactions and differential MAPK activation in PKCepsilon-induced cardioprotection. *Circulation research*, 90(4), pp.390–7. Available at: http://www.ncbi.nlm.nih.gov/pubmed/11884367 [Accessed January 15, 2018].

Baines, C.P., 2007. The mitochondrial permeability transition pore as a target of cardioprotective signaling. Available at: http://ajpheart.physiology.org/content/ajpheart/293/2/H903.full.pdf [Accessed November 2, 2017].

Baines, C.P. et al., 2007. Voltage-dependent anion channels are dispensable for

mitochondrial-dependent cell death. *Nature Cell Biology*, 9(5), pp.550–555. Available at: http://www.ncbi.nlm.nih.gov/pubmed/17417626 [Accessed November 2, 2017].

Balaban, R.S., 2002. Cardiac energy metabolism homeostasis: role of cytosolic calcium. *Journal of molecular and cellular cardiology*, 34(10), pp.1259–71. Available at: http://www.ncbi.nlm.nih.gov/pubmed/12392982 [Accessed November 1, 2017].

Balaban, R.S., 2009a. Domestication of the cardiac mitochondrion for energy conversion. *Journal of Molecular and Cellular Cardiology*, 46(6), pp.832–841. Available at: http://www.ncbi.nlm.nih.gov/pubmed/19265699 [Accessed November 1, 2017].

Balaban, R.S., 2009b. The role of Ca2+ signaling in the coordination of mitochondrial ATP production with cardiac work. *Biochimica et Biophysica Acta (BBA) - Bioenergetics*, 1787(11), pp.1334–1341. Available at: http://www.ncbi.nlm.nih.gov/pubmed/19481532 [Accessed November 1, 2017].

Bao, Q. & Shi, Y., 2007. Apoptosome: a platform for the activation of initiator caspases. *Cell Death and Differentiation*, 14(1), pp.56–65. Available at: http://www.ncbi.nlm.nih.gov/pubmed/16977332 [Accessed January 10, 2018].

Barth, E. et al., 1992. Ultrastructural quantitation of mitochondria and myofilaments in cardiac muscle from 10 different animal species including man. *Journal of molecular and cellular cardiology*, 24(7), pp.669–81. Available at: http://www.ncbi.nlm.nih.gov/pubmed/1404407 [Accessed November 1, 2017].

Bates, M.G.D. et al., 2012. Cardiac involvement in mitochondrial DNA disease: clinical spectrum, diagnosis, and management. *European Heart Journal*, 33(24), pp.3023–3033. Available at: http://www.ncbi.nlm.nih.gov/pubmed/22936362 [Accessed November 1, 2017].

Baumgartner, M. et al., 2006. The Nck-interacting kinase phosphorylates ERM proteins for formation of lamellipodium by growth factors. *Proceedings of the National Academy of*

Sciences, 103(36), pp.13391–13396. Available at: http://www.ncbi.nlm.nih.gov/pubmed/16938849 [Accessed January 15, 2018].

Belzacq, A.-S. et al., 2003. Bcl-2 and Bax modulate adenine nucleotide translocase activity. *Cancer research*, 63(2), pp.541–6. Available at: http://www.ncbi.nlm.nih.gov/pubmed/12543814 [Accessed November 2, 2017].

Benjamin, E.J., Blaha, M.J., Chiuve, S.E., Cushman, M., Das, S.R., Deo, R., de Ferranti, S.D., Floyd, J., Fornage, M., Gillespie, C., Isasi, C.R., Jiménez, M.C., Jordan, L.C., Judd, S.E., Lackland, D., Lichtman, J.H., Lisabeth, L., Liu, S., Longenecker, C.T., Mackey, R.H., Matsushita, K., Mozaffarian, D., Mussolino, M.E., Nasir, K., Neumar, R.W., Palaniappan, L., Pandey, D.K., Thiagarajan, R.R., Reeves, M.J., Ritchey, M., Rodriguez, C.J., Roth, G.A., Rosamond, W.D., Sasson, C., Towfighi, A., Tsao, C.W., Turner, M.B., Virani, S.S., Voeks, J.H., Willey, J.Z., Wilkins, J.T., Wu, J.H., Alger, H.M., Wong, S.S., Muntner, P. & American Heart Association Statistics Committee and Stroke Statistics Subcommittee, P., 2017. Heart Disease and Stroke Statistics-2017 Update: A Report From the American Heart Association. *Circulation*, 135(10), pp.e146–e603. Available at: http://www.ncbi.nlm.nih.gov/pubmed/28122885 [Accessed October 16, 2017].

Benjamin, E.J., Blaha, M.J., Chiuve, S.E., Cushman, M., Das, S.R., Deo, R., de Ferranti, S.D., Floyd, J., Fornage, M., Gillespie, C., Isasi, C.R., Jiménez, M.C., Jordan, L.C., Judd, S.E., Lackland, D., Lichtman, J.H., Lisabeth, L., Liu, S., Longenecker, C.T., Mackey, R.H., Matsushita, K., Mozaffarian, D., Mussolino, M.E., Nasir, K., Neumar, R.W., Palaniappan, L., Pandey, D.K., Thiagarajan, R.R., Reeves, M.J., Ritchey, M., Rodriguez, C.J., Roth, G.A., Rosamond, W.D., Sasson, C., Towfighi, A., Tsao, C.W., Turner, M.B., Virani, S.S., Voeks, J.H., Willey, J.Z., Wilkins, J.T., Wu, J.H., Alger, H.M., Wong, S.S., Muntner, P. & American Heart Association Statistics Committee and Stroke Statistics Subcommittee, O. behalf of the A.H.A.S.C. and S.S., 2017. Heart

Disease and Stroke Statistics-2017 Update: A Report From the American Heart Association. *Circulation*, 135(10), pp.e146–e603. Available at: http://www.ncbi.nlm.nih.gov/pubmed/28122885 [Accessed October 16, 2017].

van Berlo, J.H., Maillet, M. & Molkentin, J.D., 2013. Signaling effectors underlying pathologic growth and remodeling of the heart. *The Journal of clinical investigation*, 123(1), pp.37–45. Available at: http://www.pubmedcentral.nih.gov/articlerender.fcgi?artid=3533272&tool=pmcentrez&rendertype=abstract [Accessed September 3, 2015].

Bers, D.M., 2008. Calcium Cycling and Signaling in Cardiac Myocytes. *Annual Review of Physiology*, 70(1), pp.23–49. Available at: http://www.ncbi.nlm.nih.gov/pubmed/17988210 [Accessed November 26, 2017].

Bers, D.M., 2002. Cardiac excitation–contraction coupling. *Nature*, 415(6868), pp.198–205. Available at: http://www.nature.com/articles/415198a [Accessed February 27, 2018].

Bhuiyan, M.S. & Fukunaga, K., 2007. Inhibition of HtrA2/Omi ameliorates heart dysfunction following ischemia/reperfusion injury in rat heart in vivo. *European Journal of Pharmacology*, 557(2–3), pp.168–177. Available at: http://linkinghub.elsevier.com/retrieve/pii/S0014299906012799 [Accessed November 2, 2017].

Bienert, G.P., Schjoerring, J.K. & Jahn, T.P., 2006. Membrane transport of hydrogen peroxide. *Biochimica et Biophysica Acta (BBA) - Biomembranes*, 1758(8), pp.994–1003. Available at: http://www.ncbi.nlm.nih.gov/pubmed/16566894 [Accessed February 27, 2018].

Binah, O. et al., 2007. Functional and developmental properties of human embryonic stem cells–derived cardiomyocytes. *Journal of Electrocardiology*, 40(6), pp.S192–S196. Available at: http://www.ncbi.nlm.nih.gov/pubmed/17993321 [Accessed November 5,

2017].

Bing, O.H., 1994. Hypothesis: apoptosis may be a mechanism for the transition to heart failure with chronic pressure overload. *Journal of molecular and cellular cardiology*, 26(8), pp.943–8. Available at: http://www.ncbi.nlm.nih.gov/pubmed/7799449 [Accessed September 6, 2015].

Boatright, K.M. et al., 2003. A unified model for apical caspase activation. *Molecular cell*, 11(2), pp.529–41. Available at: http://www.ncbi.nlm.nih.gov/pubmed/12620239 [Accessed January 10, 2018].

Boettcher, M. & McManus, M.T., 2015. Choosing the Right Tool for the Job: RNAi, TALEN, or CRISPR. *Molecular cell*, 58(4), pp.575–85. Available at: http://www.ncbi.nlm.nih.gov/pubmed/26000843 [Accessed February 26, 2018].

Bogoyevitch, M.A. et al., 1996. Stimulation of the stress-activated mitogen-activated protein kinase subfamilies in perfused heart. p38/RK mitogen-activated protein kinases and c-Jun N-terminal kinases are activated by ischemia/reperfusion. *Circulation research*, 79(2), pp.162–73. Available at: http://www.ncbi.nlm.nih.gov/pubmed/8755992 [Accessed November 3, 2017].

Borlaug, B.A. & Paulus, W.J., 2011. Heart failure with preserved ejection fraction: pathophysiology, diagnosis, and treatment. *European heart journal*, 32(6), pp.670–9. Available at: http://www.ncbi.nlm.nih.gov/pubmed/21138935 [Accessed February 19, 2018].

Boudoulas, K.D. & Hatzopoulos, A.K., 2009. Cardiac repair and regeneration: the Rubik's cube of cell therapy for heart disease. *Disease Models & Mechanisms*, 2(7–8), pp.344–358. Available at: http://www.ncbi.nlm.nih.gov/pubmed/19553696 [Accessed October 17, 2017].

Bouzakri, K. et al., 2011. Bimodal effect on pancreatic β-cells of secretory products from

normal or insulin-resistant human skeletal muscle. *Diabetes*, 60(4), pp.1111–21. Available at: http://www.pubmedcentral.nih.gov/articlerender.fcgi?artid=3064085&tool=pmcentrez&rendertype=abstract [Accessed September 15, 2015].

Bouzakri, K. & Zierath, J.R., 2007. MAP4K4 Gene Silencing in Human Skeletal Muscle Prevents Tumor Necrosis Factor- -induced Insulin Resistance. *Journal of Biological Chemistry*, 282(11), pp.7783–7789. Available at: http://www.jbc.org/cgi/doi/10.1074/jbc.M608602200 [Accessed September 12, 2016].

Brady, C.A. et al., 2011. Distinct p53 Transcriptional Programs Dictate Acute DNA-Damage Responses and Tumor Suppression. *Cell*, 145(4), pp.571–583. Available at: http://www.ncbi.nlm.nih.gov/pubmed/21565614 [Accessed January 10, 2018].

Brand, M.D. & Nicholls, D.G., 2011. Assessing mitochondrial dysfunction in cells. *The Biochemical journal*, 435(2), pp.297–312. Available at: http://www.pubmedcentral.nih.gov/articlerender.fcgi?artid=3076726&tool=pmcentrez&rendertype=abstract [Accessed July 10, 2014].

Braunwald, E. & Bonow, R.O., 2012. *Braunwald's heart disease : a textbook of cardiovascular medicine*, Elsevier Saunders.

Breckwoldt, K. et al., 2017. Differentiation of cardiomyocytes and generation of human engineered heart tissue. *Nature Protocols*, 12(6), pp.1177–1197. Available at: http://www.nature.com/doifinder/10.1038/nprot.2017.033 [Accessed November 5, 2017].

Brener, S.J. et al., 2013. Relationship between myocardial reperfusion, infarct size, and mortality: the INFUSE-AMI (Intracoronary Abciximab and Aspiration Thrombectomy in Patients With Large Anterior Myocardial Infarction) trial. *JACC. Cardiovascular interventions*, 6(7), pp.718–24. Available at:

http://www.ncbi.nlm.nih.gov/pubmed/23866184 [Accessed September 6, 2015].

Brocheriou, V. et al., 2000. Cardiac functional improvement by a human Bcl-2 transgene in a mouse model of ischemia/reperfusion injury. *The Journal of Gene Medicine*, 2(5), pp.326–333. Available at: http://www.ncbi.nlm.nih.gov/pubmed/11045426 [Accessed November 2, 2017].

Brocheriou, V. et al., Cardiac functional improvement by a human Bcl-2 transgene in a mouse model of ischemia/reperfusion injury. *The journal of gene medicine*, 2(5), pp.326–33. Available at: http://www.ncbi.nlm.nih.gov/pubmed/11045426 [Accessed September 6, 2015].

Bröker, L.E., Kruyt, F.A.E. & Giaccone, G., 2005. Cell death independent of caspases: a review. *Clinical cancer research : an official journal of the American Association for Cancer Research*, 11(9), pp.3155–62. Available at: http://www.ncbi.nlm.nih.gov/pubmed/15867207 [Accessed September 6, 2015].

Brons, I.G.M. et al., 2007. Derivation of pluripotent epiblast stem cells from mammalian embryos. *Nature*, 448(7150), pp.191–195. Available at: http://www.nature.com/doifinder/10.1038/nature05950 [Accessed November 3, 2017].

Brown, D.A. et al., 2016. Expert consensus document: Mitochondrial function as a therapeutic target in heart failure. *Nature Reviews Cardiology*, 14(4), pp.238–250. Available at: http://www.nature.com/doifinder/10.1038/nrcardio.2016.203 [Accessed October 31, 2017].

Brown, D.I. & Griendling, K.K., 2015. Regulation of Signal Transduction by Reactive Oxygen Species in the Cardiovascular System. *Circulation Research*, 116(3), pp.531–549. Available at: http://www.ncbi.nlm.nih.gov/pubmed/25634975 [Accessed August 16, 2017].

Burridge, P.W. et al., 2014. Chemically defined generation of human cardiomyocytes. *Nature*

Methods, 11(8), pp.855–860. Available at: http://www.ncbi.nlm.nih.gov/pubmed/24930130 [Accessed August 16, 2017].

Burridge, P.W. et al., 2016. Human induced pluripotent stem cell–derived cardiomyocytes recapitulate the predilection of breast cancer patients to doxorubicin-induced cardiotoxicity. *Nature Medicine*, 22(5), pp.547–556. Available at: http://www.ncbi.nlm.nih.gov/pubmed/27089514 [Accessed August 16, 2017].

Burridge, P.W., Holmström, A. & Wu, J.C., 2015. Chemically Defined Culture and Cardiomyocyte Differentiation of Human Pluripotent Stem Cells. In *Current Protocols in Human Genetics*. Hoboken, NJ, USA: John Wiley & Sons, Inc., p. 21.3.1-21.3.15. Available at: http://www.ncbi.nlm.nih.gov/pubmed/26439715 [Accessed October 31, 2017].

Cao, J.Y. & Dixon, S.J., 2016. Mechanisms of ferroptosis. *Cellular and molecular life sciences : CMLS*, 73(11–12), pp.2195–209. Available at: http://www.ncbi.nlm.nih.gov/pubmed/27048822 [Accessed January 9, 2018].

Carrasco, A.J. et al., 2001. Adenylate kinase phosphotransfer communicates cellular energetic signals to ATP-sensitive potassium channels. *Proceedings of the National Academy of Sciences*, 98(13), pp.7623–7628. Available at: http://www.ncbi.nlm.nih.gov/pubmed/11390963 [Accessed November 1, 2017].

Chan, F.K.-M. et al., 2003. A role for tumor necrosis factor receptor-2 and receptor-interacting protein in programmed necrosis and antiviral responses. *The Journal of biological chemistry*, 278(51), pp.51613–21. Available at: http://www.ncbi.nlm.nih.gov/pubmed/14532286 [Accessed August 2, 2015].

Chang, C.-J. & Bouhassira, E.E., 2012. Zinc-finger nuclease-mediated correction of -thalassemia in iPS cells. *Blood*, 120(19), pp.3906–3914. Available at: http://www.ncbi.nlm.nih.gov/pubmed/23002118 [Accessed November 3, 2017].

Chang, J. et al., 2006. Activation of Rho-associated coiled-coil protein kinase 1 (ROCK-1) by caspase-3 cleavage plays an essential role in cardiac myocyte apoptosis. *Proceedings of the National Academy of Sciences*, 103(39), pp.14495–14500. Available at: http://www.ncbi.nlm.nih.gov/pubmed/16983089 [Accessed November 3, 2017].

Chang, L. & Karin, M., 2001. Mammalian MAP kinase signalling cascades. *Nature*, 410(6824), pp.37–40. Available at: http://www.ncbi.nlm.nih.gov/pubmed/11242034 [Accessed January 11, 2018].

Chang Liao, M.-L. et al., 2015. Sensing Cardiac Electrical Activity With a Cardiac Myocyte–Targeted Optogenetic Voltage IndicatorNovelty and Significance. *Circulation Research*, 117(5), pp.401–412. Available at: http://www.ncbi.nlm.nih.gov/pubmed/26078285 [Accessed February 27, 2018].

Chatzifrangkeskou, M. et al., 2016. ERK1/2 directly acts on CTGF/CCN2 expression to mediate myocardial fibrosis in cardiomyopathy caused by mutations in the lamin A/C gene. *Human Molecular Genetics*, 25(11), pp.2220–2233. Available at: http://www.ncbi.nlm.nih.gov/pubmed/27131347 [Accessed February 22, 2018].

Chen, J. et al., 2013. National Trends in Heart Failure Hospitalization After Acute Myocardial Infarction for Medicare Beneficiaries: 1998-2010. *Circulation*, 128(24), pp.2577–2584. Available at: http://www.ncbi.nlm.nih.gov/pubmed/24190958 [Accessed October 17, 2017].

Chen, J. et al., 2001. Raf-1 promotes cell survival by antagonizing apoptosis signal-regulating kinase 1 through a MEK-ERK independent mechanism. *Proceedings of the National Academy of Sciences*, 98(14), pp.7783–7788. Available at: http://www.ncbi.nlm.nih.gov/pubmed/11427728 [Accessed November 3, 2017].

Chen, Q.M. et al., 2000. Hydrogen Peroxide Dose Dependent Induction of Cell Death or Hypertrophy in Cardiomyocytes. *Archives of Biochemistry and Biophysics*, 373(1),

pp.242–248. Available at: http://www.ncbi.nlm.nih.gov/pubmed/10620344 [Accessed January 12, 2018].

Chen, S. et al., 2014. SOX2 regulates apoptosis through MAP4K4-survivin signaling pathway in human lung cancer cells. *Carcinogenesis*, 35(3), pp.613–23. Available at: http://www.ncbi.nlm.nih.gov/pubmed/24233838 [Accessed September 15, 2015].

Chen, W. et al., 2013. Diverse Sequence Determinants Control Human and Mouse Receptor Interacting Protein 3 (RIP3) and Mixed Lineage Kinase domain-Like (MLKL) Interaction in Necroptotic Signaling. *Journal of Biological Chemistry*, 288(23), pp.16247–16261. Available at: http://www.ncbi.nlm.nih.gov/pubmed/23612963 [Accessed December 5, 2017].

Chen, Z. et al., 2001. Overexpression of Bcl-2 attenuates apoptosis and protects against myocardial I/R injury in transgenic mice. *American journal of physiology. Heart and circulatory physiology*, 280(5), pp.H2313-20. Available at: http://www.ncbi.nlm.nih.gov/pubmed/11299236 [Accessed September 6, 2015].

Cheng, E.H.-Y. et al., 2003. VDAC2 Inhibits BAK Activation and Mitochondrial Apoptosis. *Science*, 301(5632), pp.513–517. Available at: http://www.ncbi.nlm.nih.gov/pubmed/12881569 [Accessed November 2, 2017].

Chien, K.R., 2000. Genomic circuits and the integrative biology of cardiac diseases. *Nature*, 407(6801), pp.227–232. Available at: http://www.nature.com/doifinder/10.1038/35025196 [Accessed October 17, 2017].

Chien, K.R., Domian, I.J. & Parker, K.K., 2008. Cardiogenesis and the complex biology of regenerative cardiovascular medicine. *Science (New York, N.Y.)*, 322(5907), pp.1494–7. Available at: http://www.sciencemag.org/content/322/5907/1494.full [Accessed September 29, 2015].

Chiong, M. et al., 2011. Cardiomyocyte death: mechanisms and translational implications.

Cell death & disease, 2(12), p.e244. Available at: http://www.ncbi.nlm.nih.gov/pubmed/22190003 [Accessed October 17, 2017].

Chipuk, J.E. et al., 2004. Direct Activation of Bax by p53 Mediates Mitochondrial Membrane Permeabilization and Apoptosis. *Science*, 303(5660), pp.1010–1014. Available at: http://www.ncbi.nlm.nih.gov/pubmed/14963330 [Accessed February 20, 2018].

Choi, T.G. et al., 2011. Apoptosis signal-regulating kinase 1 is an intracellular inducer of p38 MAPK-mediated myogenic signalling in cardiac myoblasts. *Biochimica et Biophysica Acta (BBA) - Molecular Cell Research*, 1813(8), pp.1412–1421. Available at: http://www.ncbi.nlm.nih.gov/pubmed/21530592 [Accessed October 30, 2017].

Christofferson, D.E. & Yuan, J., 2010. Cyclophilin A release as a biomarker of necrotic cell death. *Cell Death & Differentiation*, 17(12), pp.1942–1943. Available at: http://www.nature.com/articles/cdd2010123 [Accessed February 26, 2018].

Chuang, H.-C. et al., 2014. HGK/MAP4K4 deficiency induces TRAF2 stabilization and Th17 differentiation leading to insulin resistance. *Nature communications*, 5, p.4602. Available at: http://www.pubmedcentral.nih.gov/articlerender.fcgi?artid=4143962&tool=pmcentrez&rendertype=abstract [Accessed September 15, 2015].

Churchill, E.N. et al., 2005. Reperfusion-Induced Translocation of PKC to Cardiac Mitochondria Prevents Pyruvate Dehydrogenase Reactivation. *Circulation Research*, 97(1), pp.78–85. Available at: http://www.ncbi.nlm.nih.gov/pubmed/15961716 [Accessed November 3, 2017].

Cibelli, J. et al., 2013. Strategies for improving animal models for regenerative medicine. *Cell stem cell*, 12(3), pp.271–4. Available at: http://www.ncbi.nlm.nih.gov/pubmed/23472868 [Accessed January 15, 2018].

Çöl Arslan, S. & Scheidereit, C., 2011. The Prevalence of TNFα-Induced Necrosis over

Apoptosis Is Determined by TAK1-RIP1 Interplay W. S. El-Deiry, ed. *PLoS ONE*, 6(10), p.e26069. Available at: http://dx.plos.org/10.1371/journal.pone.0026069 [Accessed November 2, 2017].

Collins, C.S. et al., 2006. A small interfering RNA screen for modulators of tumor cell motility identifies MAP4K4 as a promigratory kinase. *Proceedings of the National Academy of Sciences of the United States of America*, 103(10), pp.3775–80. Available at: http://www.ncbi.nlm.nih.gov/pubmed/16537454 [Accessed January 15, 2018].

Crawford, T.D. et al., 2014. Discovery of Selective 4-Amino-pyridopyrimidine Inhibitors of MAP4K4 Using Fragment-Based Lead Identification and Optimization. *Journal of Medicinal Chemistry*, 57(8), pp.3484–3493. Available at: http://pubs.acs.org/doi/abs/10.1021/jm500155b [Accessed September 5, 2016].

Criddle, D.N. et al., 2006. Menadione-induced Reactive Oxygen Species Generation via Redox Cycling Promotes Apoptosis of Murine Pancreatic Acinar Cells. *Journal of Biological Chemistry*, 281(52), pp.40485–40492. Available at: http://www.ncbi.nlm.nih.gov/pubmed/17088248 [Accessed September 9, 2017].

Crow, M.T. et al., 2004. The Mitochondrial Death Pathway and Cardiac Myocyte Apoptosis. *Circulation Research*, 95(10), pp.957–970. Available at: http://www.ncbi.nlm.nih.gov/pubmed/15539639 [Accessed November 2, 2017].

Crowley, L.C. et al., 2016. Quantitation of Apoptosis and Necrosis by Annexin V Binding, Propidium Iodide Uptake, and Flow Cytometry. *Cold Spring Harbor Protocols*, 2016(11), p.pdb.prot087288. Available at: http://www.ncbi.nlm.nih.gov/pubmed/27803250 [Accessed February 26, 2018].

D'Angelo, D.D. et al., 1997. Transgenic Galphaq overexpression induces cardiac contractile failure in mice. *Proceedings of the National Academy of Sciences of the United States of America*, 94(15), pp.8121–6. Available at:

http://www.ncbi.nlm.nih.gov/pubmed/9223325 [Accessed November 2, 2017].

Dalloz, F., Osinska, H. & Robbins, J., 2001. Manipulating the Contractile Apparatus: Genetically Defined Animal Models of Cardiovascular Disease. *Journal of Molecular and Cellular Cardiology*, 33(1), pp.9–25. Available at: http://www.ncbi.nlm.nih.gov/pubmed/11133219 [Accessed October 17, 2017].

Danai, L. V et al., 2015. Inducible Deletion of Protein Kinase Map4k4 in Obese Mice Improves Insulin Sensitivity in Liver and Adipose Tissues. *Molecular and cellular biology*, 35(13), pp.2356–65. Available at: http://www.ncbi.nlm.nih.gov/pubmed/25918248 [Accessed September 11, 2016].

Danai, L. V. et al., 2013. Map4k4 suppresses Srebp-1 and adipocyte lipogenesis independent of JNK signaling. *The Journal of Lipid Research*, 54(10), pp.2697–2707. Available at: http://www.jlr.org/cgi/doi/10.1194/jlr.M038802 [Accessed September 11, 2016].

Danai, L. V. et al., 2013. Map4k4 suppresses Srebp-1 and adipocyte lipogenesis independent of JNK signaling. *Journal of Lipid Research*, 54(10), pp.2697–2707. Available at: http://www.ncbi.nlm.nih.gov/pubmed/23924694 [Accessed January 15, 2018].

Das, A., Xi, L. & Kukreja, R.C., 2008. Protein kinase G-dependent cardioprotective mechanism of phosphodiesterase-5 inhibition involves phosphorylation of ERK and GSK3beta. *The Journal of biological chemistry*, 283(43), pp.29572–85. Available at: http://www.ncbi.nlm.nih.gov/pubmed/18723505 [Accessed January 15, 2018].

Dassanayaka, S. & Jones, S.P., 2015. Recent Developments in Heart Failure. *Circulation research*, 117(7), pp.e58-63. Available at: http://www.ncbi.nlm.nih.gov/pubmed/26358111 [Accessed October 17, 2017].

Daugas, E. et al., 2000. Apoptosis-inducing factor (AIF): a ubiquitous mitochondrial

oxidoreductase involved in apoptosis. *FEBS letters*, 476(3), pp.118–23. Available at: http://www.ncbi.nlm.nih.gov/pubmed/10913597 [Accessed January 9, 2018].

Degterev, A. et al., 2005. Chemical inhibitor of nonapoptotic cell death with therapeutic potential for ischemic brain injury. *Nature Chemical Biology*, 1(2), pp.112–119. Available at: http://www.ncbi.nlm.nih.gov/pubmed/16408008 [Accessed October 18, 2017].

Delbridge, L.M.D. et al., 2017. Myocardial stress and autophagy: mechanisms and potential therapies. *Nature Reviews Cardiology*, 14(7), pp.412–425. Available at: http://www.nature.com/doifinder/10.1038/nrcardio.2017.35 [Accessed December 5, 2017].

Delgado, M.E. et al., 2014. Modulation of apoptosis sensitivity through the interplay with autophagic and proteasomal degradation pathways. *Cell death & disease*, 5, p.e1011. Available at: http://dx.doi.org/10.1038/cddis.2013.520 [Accessed August 13, 2015].

Delpire, E., 2009. The mammalian family of sterile 20p-like protein kinases. *Pflügers Archiv - European Journal of Physiology*, 458(5), pp.953–967. Available at: http://www.ncbi.nlm.nih.gov/pubmed/19399514 [Accessed January 11, 2018].

Denise Martin, E., De Nicola, G.F. & Marber, M.S., 2012. New therapeutic targets in cardiology: p38 alpha mitogen-activated protein kinase for ischemic heart disease. *Circulation*, 126(3), pp.357–68. Available at: http://www.ncbi.nlm.nih.gov/pubmed/22801653 [Accessed September 28, 2015].

Denning, C. et al., 2016. Cardiomyocytes from human pluripotent stem cells: From laboratory curiosity to industrial biomedical platform. *Biochimica et biophysica acta*, 1863(7 Pt B), pp.1728–48. Available at: http://www.ncbi.nlm.nih.gov/pubmed/26524115 [Accessed January 23, 2018].

Devalla, H.D. et al., 2015. Atrial-like cardiomyocytes from human pluripotent stem cells are a

robust preclinical model for assessing atrial-selective pharmacology. *EMBO Molecular Medicine*, 7(4), pp.394–410. Available at: http://www.ncbi.nlm.nih.gov/pubmed/25700171 [Accessed August 16, 2017].

Devin, A. et al., 2001. The and Subunits of I B Kinase (IKK) Mediate TRAF2-Dependent IKK Recruitment to Tumor Necrosis Factor (TNF) Receptor 1 in Response to TNF. *Molecular and Cellular Biology*, 21(12), pp.3986–3994. Available at: http://www.ncbi.nlm.nih.gov/pubmed/11359906 [Accessed January 24, 2018].

Dhingra, R., Ravandi, A. & Kirshenbaum, L.A., 2017. Ferroptosis: Beating on Death's Door. *American Journal of Physiology-Heart and Circulatory Physiology*, p.ajpheart.00692.2017. Available at: http://www.physiology.org/doi/10.1152/ajpheart.00692.2017 [Accessed January 9, 2018].

Dhingra, S. et al., 2009. IL-10 attenuates TNF- -induced NF B pathway activation and cardiomyocyte apoptosis. *Cardiovascular Research*, 82(1), pp.59–66. Available at: http://www.ncbi.nlm.nih.gov/pubmed/19181934 [Accessed January 15, 2018].

Dick, E. et al., 2011. Faster generation of hiPSCs by coupling high-titer lentivirus and column-based positive selection. *Nature Protocols*, 6(6), pp.701–714. Available at: http://www.ncbi.nlm.nih.gov/pubmed/21637193 [Accessed November 3, 2017].

Dimmeler, S., Zeiher, A.M. & Schneider, M.D., 2005. Unchain my heart: the scientific foundations of cardiac repair. *The Journal of clinical investigation*, 115(3), pp.572–83. Available at: http://www.pubmedcentral.nih.gov/articlerender.fcgi?artid=1052009&tool=pmcentrez&rendertype=abstract [Accessed July 22, 2015].

Diwan, A. et al., 2007. Inhibition of ischemic cardiomyocyte apoptosis through targeted ablation of Bnip3 restrains postinfarction remodeling in mice. *Journal of Clinical*

Investigation, 117(10), pp.2825–2833. Available at: http://www.ncbi.nlm.nih.gov/pubmed/17909626 [Accessed November 2, 2017].

Dixon, S.J. et al., 2012. Ferroptosis: an iron-dependent form of nonapoptotic cell death. *Cell*, 149(5), pp.1060–72. Available at: http://www.ncbi.nlm.nih.gov/pubmed/22632970 [Accessed February 26, 2018].

Dolnikov, K. et al., 2006. Functional Properties of Human Embryonic Stem Cell-Derived Cardiomyocytes: Intracellular Ca $^{2+}$ Handling and the Role of Sarcoplasmic Reticulum in the Contraction. *Stem Cells*, 24(2), pp.236–245. Available at: http://doi.wiley.com/10.1634/stemcells.2005-0036 [Accessed November 5, 2017].

Dorn, G.W. & Mochly-Rosen, D., 2002. Intracellular Transport Mechanisms of Signal Transducers. *Annual Review of Physiology*, 64(1), pp.407–429. Available at: http://www.ncbi.nlm.nih.gov/pubmed/11826274 [Accessed November 3, 2017].

Ea, C.-K. et al., 2006. Activation of IKK by TNFα Requires Site-Specific Ubiquitination of RIP1 and Polyubiquitin Binding by NEMO. *Molecular Cell*, 22(2), pp.245–257. Available at: http://www.ncbi.nlm.nih.gov/pubmed/16603398 [Accessed April 6, 2015].

Ebert, A.D., Liang, P. & Wu, J.C., 2012. Induced pluripotent stem cells as a disease modeling and drug screening platform. *Journal of cardiovascular pharmacology*, 60(4), pp.408–16. Available at: http://www.ncbi.nlm.nih.gov/pubmed/22240913 [Accessed January 15, 2018].

Eder, A. et al., 2014. Effects of proarrhythmic drugs on relaxation time and beating pattern in rat engineered heart tissue. *Basic Research in Cardiology*, 109(6). Available at: http://link.springer.com/10.1007/s00395-014-0436-7.

Eder, A. et al., 2015. Human engineered heart tissue as a model system for drug testing. *Advanced drug delivery reviews*. Available at: http://www.ncbi.nlm.nih.gov/pubmed/26026976 [Accessed June 1, 2015].

Eguchi, Y., Shimizu, S. & Tsujimoto, Y., 1997. Intracellular ATP levels determine cell death fate by apoptosis or necrosis. *Cancer research*, 57(10), pp.1835–40. Available at: http://www.ncbi.nlm.nih.gov/pubmed/9157970 [Accessed January 10, 2018].

Elbein, S.C. et al., 2009. Genome-wide linkage and admixture mapping of type 2 diabetes in African American families from the American Diabetes Association GENNID (Genetics of NIDDM) Study Cohort. *Diabetes*, 58(1), pp.268–74. Available at: http://www.pubmedcentral.nih.gov/articlerender.fcgi?artid=2606884&tool=pmcentrez&rendertype=abstract [Accessed September 6, 2015].

Engel, D. et al., 2004. Cardiac myocyte apoptosis provokes adverse cardiac remodeling in transgenic mice with targeted TNF overexpression. *American journal of physiology. Heart and circulatory physiology*, 287(3), pp.H1303-11. Available at: http://www.ncbi.nlm.nih.gov/pubmed/15317679 [Accessed September 6, 2015].

Engh, R.A. & Bossemeyer, D., 2002. Structural aspects of protein kinase control-role of conformational flexibility. *Pharmacology & therapeutics*, 93(2–3), pp.99–111. Available at: http://www.ncbi.nlm.nih.gov/pubmed/12191603 [Accessed November 3, 2017].

Eschenhagen, T. et al., 2012. Physiological aspects of cardiac tissue engineering. *AJP: Heart and Circulatory Physiology*, 303(2), pp.H133–H143. Available at: http://www.ncbi.nlm.nih.gov/pubmed/22582087 [Accessed October 31, 2017].

Eschenhagen, T. et al., 1997. Three-dimensional reconstitution of embryonic cardiomyocytes in a collagen matrix: a new heart muscle model system. *FASEB journal : official publication of the Federation of American Societies for Experimental Biology*, 11(8), pp.683–94. Available at: http://www.ncbi.nlm.nih.gov/pubmed/9240969 [Accessed September 9, 2017].

Fattah, C. et al., 2016. Gene Therapy With Angiotensin-(1-9) Preserves Left Ventricular Systolic Function After Myocardial Infarction. *Journal of the American College of*

Cardiology, 68(24), pp.2652–2666. Available at: http://www.ncbi.nlm.nih.gov/pubmed/27978950 [Accessed April 4, 2017].

Fearnley, C.J., Roderick, H.L. & Bootman, M.D., 2011. Calcium signaling in cardiac myocytes. *Cold Spring Harbor perspectives in biology*, 3(11), p.a004242. Available at: http://www.ncbi.nlm.nih.gov/pubmed/21875987 [Accessed February 27, 2018].

Ferrandi, C. et al., 2004. Inhibition of c-Jun N-terminal kinase decreases cardiomyocyte apoptosis and infarct size after myocardial ischemia and reperfusion in anaesthetized rats. *British journal of pharmacology*, 142(6), pp.953–60. Available at: http://www.ncbi.nlm.nih.gov/pubmed/15210584 [Accessed January 15, 2018].

Fiedler, L., Chapman, K., et al., 2014. 157 Approaches for Pharmacological Inhibition of Cardiac Cell Death: MAP4K4 as a Therapeutic Target. *Heart*, 100(Suppl 3), pp.A91–A91. Available at: http://heart.bmj.com/content/100/Suppl_3/A91.2.abstract [Accessed September 15, 2015].

Fiedler, L., Jenkins, M., et al., 2014. MAP4K4 MEDIATES CARDIOMYOCYTE CELL DEATH AND POTENTIATES A HEART FAILURE PHENOTYPE. *Heart*, 100(Suppl 4), pp.A20–A20. Available at: http://heart.bmj.com/content/100/Suppl_4/A20.2.abstract [Accessed September 15, 2015].

Fiedler, L.R. et al., 2014. 12 MAP4K4 as a Therapeutic Target in Cardiomyocyte Death: Novel inhibitors Identified through Pharmacophore Modelling and Virtual Screening. *Heart*, 100(Suppl 1), pp.A5–A5. Available at: http://heart.bmj.com/content/100/Suppl_1/A5.2.abstract [Accessed September 6, 2015].

Fink, C. et al., 2000. Chronic stretch of engineered heart tissue induces hypertrophy and functional improvement. *FASEB journal : official publication of the Federation of American Societies for Experimental Biology*, 14(5), pp.669–79. Available at: http://www.ncbi.nlm.nih.gov/pubmed/10744624 [Accessed January 22, 2018].

Fink, S.L. & Cookson, B.T., 2005. Apoptosis, pyroptosis, and necrosis: mechanistic description of dead and dying eukaryotic cells. *Infection and immunity*, 73(4), pp.1907–16. Available at: http://www.ncbi.nlm.nih.gov/pubmed/15784530 [Accessed January 9, 2018].

Foghsgaard, L. et al., 2001. Cathepsin B acts as a dominant execution protease in tumor cell apoptosis induced by tumor necrosis factor. *The Journal of cell biology*, 153(5), pp.999–1010. Available at: http://www.ncbi.nlm.nih.gov/pubmed/11381085 [Accessed January 9, 2018].

Francis, G.S. & Tang, W.H.W., 2003. Pathophysiology of congestive heart failure. *Reviews in cardiovascular medicine*, 4 Suppl 2, pp.S14-20. Available at: http://www.ncbi.nlm.nih.gov/pubmed/12776009 [Accessed October 17, 2017].

Friedrich, F.W. et al., 2014. FHL2 expression and variants in hypertrophic cardiomyopathy. *Basic Research in Cardiology*, 109(6), p.451. Available at: http://www.ncbi.nlm.nih.gov/pubmed/25358972 [Accessed September 12, 2017].

Fryer, R.M. et al., 2001. Stress-activated protein kinase phosphorylation during cardioprotection in the ischemic myocardium. *American journal of physiology. Heart and circulatory physiology*, 281(3), pp.H1184-92. Available at: http://www.ncbi.nlm.nih.gov/pubmed/11514286 [Accessed September 28, 2015].

Fujita, J. et al., 2008. Caspase activity mediates the differentiation of embryonic stem cells. *Cell stem cell*, 2(6), pp.595–601. Available at: http://www.pubmedcentral.nih.gov/articlerender.fcgi?artid=2494585&tool=pmcentrez&rendertype=abstract [Accessed September 28, 2015].

Gao, H. et al., 2016. Rho-Kinase inhibitor fasudil suppresses high glucose-induced H9c2 cell apoptosis through activation of autophagy. *Cardiovascular Therapeutics*, 34(5), pp.352–359. Available at: http://www.ncbi.nlm.nih.gov/pubmed/27333569 [Accessed

February 21, 2018].

Garrity, R. et al., 2015. Alteration of p-PKM2 by UV radiation and H2O2 in Human Keratinocytes. *FASEB J*, 29(1_Supplement), p.726.16-. Available at: http://www.fasebj.org/content/29/1_Supplement/726.16 [Accessed September 28, 2015].

Gille, J.J. & Joenje, H., 1992. Cell culture models for oxidative stress: superoxide and hydrogen peroxide versus normobaric hyperoxia. *Mutation research*, 275(3–6), pp.405–14. Available at: http://www.ncbi.nlm.nih.gov/pubmed/1383781 [Accessed February 27, 2018].

Gilmore, A.P., 2005. Anoikis. *Cell Death and Differentiation*, 12, pp.1473–1477. Available at: http://www.nature.com/doifinder/10.1038/sj.cdd.4401723 [Accessed January 9, 2018].

Gintant, G., Sager, P.T. & Stockbridge, N., 2016. Evolution of strategies to improve preclinical cardiac safety testing. *Nature Reviews Drug Discovery*, 15(7), pp.457–471. Available at: http://www.ncbi.nlm.nih.gov/pubmed/26893184 [Accessed August 16, 2017].

Goh, K.Y. et al., 2016. Impaired mitochondrial network excitability in failing guinea-pig cardiomyocytes. *Cardiovascular Research*, 109(1), pp.79–89. Available at: http://www.ncbi.nlm.nih.gov/pubmed/26433944 [Accessed November 1, 2017].

Gómez, A.M. et al., 1997. Defective excitation-contraction coupling in experimental cardiac hypertrophy and heart failure. *Science (New York, N.Y.)*, 276(5313), pp.800–6. Available at: http://www.ncbi.nlm.nih.gov/pubmed/9115206 [Accessed January 16, 2018].

Gong, G. et al., 2003. Oxidative capacity in failing hearts. *American Journal of Physiology - Heart and Circulatory Physiology*, 285(2), pp.H541–H548. Available at: http://www.ncbi.nlm.nih.gov/pubmed/12714322 [Accessed September 14, 2017].

Gorski, P.A., Ceholski, D.K. & Hajjar, R.J., 2015. Altered myocardial calcium cycling and energetics in heart failure--a rational approach for disease treatment. *Cell metabolism*, 21(2), pp.183–94. Available at: http://www.ncbi.nlm.nih.gov/pubmed/25651173 [Accessed August 16, 2017].

Gottlieb, R.A. & Mentzer, R.M., 2010. Autophagy during cardiac stress: joys and frustrations of autophagy. *Annual review of physiology*, 72, pp.45–59. Available at: http://www.pubmedcentral.nih.gov/articlerender.fcgi?artid=3682821&tool=pmcentrez&rendertype=abstract [Accessed September 6, 2015].

Grueneberg, D.A. et al., 2008. Kinase requirements in human cells: I. Comparing kinase requirements across various cell types. *Proceedings of the National Academy of Sciences of the United States of America*, 105(43), pp.16472–7. Available at: http://www.ncbi.nlm.nih.gov/pubmed/18948591 [Accessed November 3, 2017].

Guerra, S. et al., 1999. Myocyte death in the failing human heart is gender dependent. *Circulation research*, 85(9), pp.856–66. Available at: http://www.ncbi.nlm.nih.gov/pubmed/10532954 [Accessed November 3, 2017].

Guimarães, C.R.W. et al., 2011. Understanding the Impact of the P-loop Conformation on Kinase Selectivity. *Journal of Chemical Information and Modeling*, 51(6), pp.1199–1204. Available at: http://pubs.acs.org/doi/abs/10.1021/ci200153c [Accessed June 24, 2018].

Guntur, K.V.P. et al., 2010. *Map4k4* Negatively Regulates Peroxisome Proliferator-activated Receptor (PPAR) γ Protein Translation by Suppressing the Mammalian Target of Rapamycin (mTOR) Signaling Pathway in Cultured Adipocytes. *Journal of Biological Chemistry*, 285(9), pp.6595–6603. Available at: http://www.ncbi.nlm.nih.gov/pubmed/20038583 [Accessed January 15, 2018].

Gupta, S.K. et al., 2018. Quaking Inhibits Doxorubicin-Mediated Cardiotoxicity Through

Regulation of Cardiac Circular RNA ExpressionNovelty and Significance. *Circulation Research*, 122(2), pp.246–254. Available at: http://www.ncbi.nlm.nih.gov/pubmed/29133306 [Accessed February 26, 2018].

Gustafsson, A.B. & Gottlieb, R.A., 2007. Heart mitochondria: gates of life and death. *Cardiovascular Research*, 77(2), pp.334–343. Available at: http://www.ncbi.nlm.nih.gov/pubmed/18006487 [Accessed November 2, 2017].

Gutstein, D.E. et al., 2001. Conduction slowing and sudden arrhythmic death in mice with cardiac-restricted inactivation of connexin43. *Circulation research*, 88(3), pp.333–9. Available at: http://www.ncbi.nlm.nih.gov/pubmed/11179202 [Accessed February 27, 2018].

Hallows, K.R. et al., 2010. Role of the energy sensor AMP-activated protein kinase in renal physiology and disease. *American journal of physiology. Renal physiology*, 298(5), pp.F1067-77. Available at: http://www.ncbi.nlm.nih.gov/pubmed/20181668 [Accessed November 3, 2017].

Hamid, T. et al., 2009. Divergent Tumor Necrosis Factor Receptor-Related Remodeling Responses in Heart Failure: Role of Nuclear Factor- B and Inflammatory Activation. *Circulation*, 119(10), pp.1386–1397. Available at: http://www.ncbi.nlm.nih.gov/pubmed/19255345 [Accessed November 2, 2017].

Hanna, J. et al., 2007. Treatment of Sickle Cell Anemia Mouse Model with iPS Cells Generated from Autologous Skin. *Science*, 318(5858), pp.1920–1923. Available at: http://www.ncbi.nlm.nih.gov/pubmed/18063756 [Accessed November 3, 2017].

Hansen, A. et al., 2010. Development of a drug screening platform based on engineered heart tissue. *Circulation research*, 107(1), pp.35–44. Available at: http://www.ncbi.nlm.nih.gov/pubmed/20448218 [Accessed August 10, 2015].

Harvey, P.A. & Leinwand, L.A., 2011. Cellular mechanisms of cardiomyopathy. *The Journal*

of Cell Biology, 194(3), pp.355–365. Available at: http://www.ncbi.nlm.nih.gov/pubmed/21825071 [Accessed August 16, 2017].

Hausenloy, D.J. & Yellon, D.M., 2013. Myocardial ischemia-reperfusion injury: a neglected therapeutic target. *The Journal of clinical investigation*, 123(1), pp.92–100. Available at: http://www.pubmedcentral.nih.gov/articlerender.fcgi?artid=3533275&tool=pmcentrez&rendertype=abstract [Accessed September 14, 2015].

Hausenloy, D.J. & Yellon, D.M., 2015. Targeting Myocardial Reperfusion Injury — The Search Continues. *New England Journal of Medicine*, 373(11), pp.1073–1075. Available at: http://www.ncbi.nlm.nih.gov/pubmed/26321104 [Accessed November 23, 2017].

Hayakawa, Y. et al., 2003. Inhibition of cardiac myocyte apoptosis improves cardiac function and abolishes mortality in the peripartum cardiomyopathy of Galpha(q) transgenic mice. *Circulation*, 108(24), pp.3036–41. Available at: http://www.ncbi.nlm.nih.gov/pubmed/14638549 [Accessed September 6, 2015].

He, C. et al., 2012. Exercise-induced BCL2-regulated autophagy is required for muscle glucose homeostasis. *Nature*, 481(7382), pp.511–515. Available at: http://www.nature.com/doifinder/10.1038/nature10758 [Accessed November 2, 2017].

He, S. et al., 2009. Receptor interacting protein kinase-3 determines cellular necrotic response to TNF-alpha. *Cell*, 137(6), pp.1100–11. Available at: http://www.ncbi.nlm.nih.gov/pubmed/19524512 [Accessed September 6, 2015].

Heidenreich, P.A. et al., 2013. Forecasting the impact of heart failure in the United States: a policy statement from the American Heart Association. *Circulation. Heart failure*, 6(3), pp.606–19. Available at: http://www.pubmedcentral.nih.gov/articlerender.fcgi?artid=3908895&tool=pmcentrez&rendertype=abstract [Accessed April 1, 2015].

Hein, S. et al., 2003. Progression from compensated hypertrophy to failure in the pressure-overloaded human heart: structural deterioration and compensatory mechanisms. *Circulation*, 107(7), pp.984–91. Available at: http://www.ncbi.nlm.nih.gov/pubmed/12600911 [Accessed November 3, 2017].

Heusch, G., 2013. Cardioprotection: chances and challenges of its translation to the clinic. *Lancet (London, England)*, 381(9861), pp.166–75. Available at: http://www.ncbi.nlm.nih.gov/pubmed/23095318 [Accessed November 23, 2017].

Hill, B.G. et al., 2009. Importance of the bioenergetic reserve capacity in response to cardiomyocyte stress induced by 4-hydroxynonenal. *The Biochemical journal*, 424(1), pp.99–107. Available at: http://www.pubmedcentral.nih.gov/articlerender.fcgi?artid=2872628&tool=pmcentrez&rendertype=abstract [Accessed September 23, 2015].

Hirt, M.N. et al., 2014. Functional improvement and maturation of rat and human engineered heart tissue by chronic electrical stimulation. *Journal of Molecular and Cellular Cardiology*, 74, pp.151–161. Available at: http://dx.doi.org/10.1016/j.yjmcc.2014.05.009.

Hirt, M.N. et al., 2012. Increased afterload induces pathological cardiac hypertrophy: a new in vitro model. *Basic Research in Cardiology*, 107(6), p.307. Available at: http://www.ncbi.nlm.nih.gov/pubmed/23099820 [Accessed January 16, 2018].

Hirt, M.N., Hansen, A. & Eschenhagen, T., 2014. Cardiac Tissue Engineering: State of the Art. *Circulation Research*, 114(2), pp.354–367. Available at: http://www.ncbi.nlm.nih.gov/pubmed/24436431 [Accessed October 31, 2017].

Hochhauser, E. et al., 2003. Bax ablation protects against myocardial ischemia-reperfusion injury in transgenic mice. *American Journal of Physiology - Heart and Circulatory Physiology*, 284(6), pp.H2351–H2359. Available at: http://www.ncbi.nlm.nih.gov/pubmed/12742833 [Accessed October 20, 2017].

Holler, N. et al., 2000. Fas triggers an alternative, caspase-8-independent cell death pathway using the kinase RIP as effector molecule. *Nature Immunology*, 1(6), pp.489–495. Available at: http://www.ncbi.nlm.nih.gov/pubmed/11101870 [Accessed November 2, 2017].

Houser, S.R. et al., 2012. Animal Models of Heart Failure: A Scientific Statement From the American Heart Association. *Circulation Research*, 111(1), pp.131–150. Available at: http://www.ncbi.nlm.nih.gov/pubmed/22595296 [Accessed October 17, 2017].

Hu, W.H., Johnson, H. & Shu, H.B., 2000. Activation of NF-kappaB by FADD, Casper, and caspase-8. *The Journal of biological chemistry*, 275(15), pp.10838–44. Available at: http://www.ncbi.nlm.nih.gov/pubmed/10753878 [Accessed January 24, 2018].

Huang, H. et al., 2014. MAP4K4 deletion inhibits proliferation and activation of CD4+ T cell and promotes T regulatory cell generation in vitro. *Cellular Immunology*, 289(1–2), pp.15–20. Available at: http://www.ncbi.nlm.nih.gov/pubmed/24681727 [Accessed January 15, 2018].

Huang, J.Q. et al., 2000. In vivo myocardial infarct size reduction by a caspase inhibitor administered after the onset of ischemia. *European journal of pharmacology*, 402(1–2), pp.139–42. Available at: http://www.ncbi.nlm.nih.gov/pubmed/10940367 [Accessed September 6, 2015].

Huang, Y. et al., 2008. GATA4 is a survival factor in adult cardiac myocytes but is not required for alpha1A-adrenergic receptor survival signaling. *American journal of physiology. Heart and circulatory physiology*, 295(2), pp.H699-707. Available at: http://www.ncbi.nlm.nih.gov/pubmed/18552157 [Accessed January 15, 2018].

Hunt, S.A. et al., 2005. ACC/AHA 2005 Guideline Update for the Diagnosis and Management of Chronic Heart Failure in the Adult: A Report of the American College of Cardiology/American Heart Association Task Force on Practice Guidelines (Writing

Committee to Update the 2001 Guidelines for the Evaluation and Management of Heart Failure): Developed in Collaboration With the American College of Chest Physicians and the International Society for Heart and Lung Transplantation: Endorsed by the Heart Rhythm Society. *Circulation*, 112(12), pp.e154–e235. Available at: http://www.ncbi.nlm.nih.gov/pubmed/16160202 [Accessed October 17, 2017].

Hwang, H.S. et al., 2015. Comparable calcium handling of human iPSC-derived cardiomyocytes generated by multiple laboratories. *Journal of Molecular and Cellular Cardiology*, 85, pp.79–88. Available at: https://www.sciencedirect.com/science/article/pii/S0022282815001510 [Accessed January 23, 2018].

Ichijo, H. et al., 1997. Induction of apoptosis by ASK1, a mammalian MAPKKK that activates SAPK/JNK and p38 signaling pathways. *Science (New York, N.Y.)*, 275(5296), pp.90–4. Available at: http://www.ncbi.nlm.nih.gov/pubmed/8974401 [Accessed October 30, 2017].

Ide, T. et al., 1999. Mitochondrial electron transport complex I is a potential source of oxygen free radicals in the failing myocardium. *Circulation research*, 85(4), pp.357–63. Available at: http://www.ncbi.nlm.nih.gov/pubmed/10455064 [Accessed November 1, 2017].

Ieda, M. et al., 2009. Cardiac Fibroblasts Regulate Myocardial Proliferation through β1 Integrin Signaling. *Developmental Cell*, 16(2), pp.233–244. Available at: http://www.ncbi.nlm.nih.gov/pubmed/19217425 [Accessed November 3, 2017].

Imahashi, K. et al., 2004. Transgenic Expression of Bcl-2 Modulates Energy Metabolism, Prevents Cytosolic Acidification During Ischemia, and Reduces Ischemia/Reperfusion Injury. *Circulation Research*, 95(7), pp.734–741. Available at: http://www.ncbi.nlm.nih.gov/pubmed/15345651 [Accessed November 2, 2017].

Isakson, P. et al., 2009. Impaired preadipocyte differentiation in human abdominal obesity: role of Wnt, tumor necrosis factor-alpha, and inflammation. *Diabetes*, 58(7), pp.1550–7. Available at: http://www.pubmedcentral.nih.gov/articlerender.fcgi?artid=2699851&tool=pmcentrez&rendertype=abstract [Accessed September 6, 2015].

Jackman, C.P. et al., 2018. Engineered cardiac tissue patch maintains structural and electrical properties after epicardial implantation. *Biomaterials*, 159, pp.48–58. Available at: http://www.ncbi.nlm.nih.gov/pubmed/29309993 [Accessed January 23, 2018].

Jackman, C.P., Carlson, A.L. & Bursac, N., 2016. Dynamic culture yields engineered myocardium with near-adult functional output. *Biomaterials*, 111, pp.66–79. Available at: http://www.ncbi.nlm.nih.gov/pubmed/27723557 [Accessed January 23, 2018].

Jeremias, I. et al., 2000. Involvement of CD95/Apo1/Fas in cell death after myocardial ischemia. *Circulation*, 102(8), pp.915–20. Available at: http://www.ncbi.nlm.nih.gov/pubmed/10952962 [Accessed November 2, 2017].

Jin, M. et al., 2016. MAP4K4 deficiency in CD4 + T cells aggravates lung damage induced by ozone-oxidized black carbon particles. *Environmental Toxicology and Pharmacology*, 46, pp.246–254. Available at: http://www.ncbi.nlm.nih.gov/pubmed/27504712 [Accessed February 23, 2018].

Joglekar, M. V. et al., 2016. Human islet cells are killed by BID-independent mechanisms in response to FAS ligand. *Apoptosis*, 21(4), pp.379–389. Available at: http://www.ncbi.nlm.nih.gov/pubmed/26758067 [Accessed February 25, 2018].

Johnson, D.E., 2000. Noncaspase proteases in apoptosis. *Leukemia*, 14(9), pp.1695–703. Available at: http://www.ncbi.nlm.nih.gov/pubmed/10995018 [Accessed January 9, 2018].

Joza, N. et al., 2001. Essential role of the mitochondrial apoptosis-inducing factor in

programmed cell death. *Nature*, 410(6828), pp.549–554. Available at: http://www.ncbi.nlm.nih.gov/pubmed/11279485 [Accessed January 9, 2018].

Kaczara, P., Sarna, T. & Burke, J.M., 2010. Dynamics of H2O2 availability to ARPE-19 cultures in models of oxidative stress. *Free radical biology & medicine*, 48(8), pp.1064–70. Available at: http://www.ncbi.nlm.nih.gov/pubmed/20100568 [Accessed September 1, 2017].

Kaiser, R.A. et al., 2005. Genetic Inhibition or Activation of JNK1/2 Protects the Myocardium from Ischemia-Reperfusion-induced Cell Death *in Vivo*. *Journal of Biological Chemistry*, 280(38), pp.32602–32608. Available at: http://www.ncbi.nlm.nih.gov/pubmed/16043490 [Accessed January 15, 2018].

Kaiser, R.A. et al., 2004. Targeted inhibition of p38 mitogen-activated protein kinase antagonizes cardiac injury and cell death following ischemia-reperfusion in vivo. *The Journal of biological chemistry*, 279(15), pp.15524–30. Available at: http://www.ncbi.nlm.nih.gov/pubmed/14749328 [Accessed September 28, 2015].

Kaneko, S. et al., 2011. Smad inhibition by the Ste20 kinase Misshapen. *Proceedings of the National Academy of Sciences*, 108(27), pp.11127–11132. Available at: http://www.ncbi.nlm.nih.gov/pubmed/21690388 [Accessed November 3, 2017].

Kang, R. et al., 2011. The Beclin 1 network regulates autophagy and apoptosis. *Cell death and differentiation*, 18(4), pp.571–80. Available at: http://www.ncbi.nlm.nih.gov/pubmed/21311563 [Accessed November 2, 2017].

Karabekian, Z. et al., 2015. Downregulation of beta-microglobulin to diminish T-lymphocyte lysis of non-syngeneic cell sources of engineered heart tissue constructs. *Biomedical Materials*, 10(3), p.34101. Available at: http://www.ncbi.nlm.nih.gov/pubmed/25775354 [Accessed September 12, 2017].

Katayama, H. et al., 2011. A sensitive and quantitative technique for detecting autophagic

events based on lysosomal delivery. *Chemistry & biology*, 18(8), pp.1042–52. Available at: http://www.ncbi.nlm.nih.gov/pubmed/21867919 [Accessed September 6, 2015].

Kensah, G. et al., 2013. Murine and human pluripotent stem cell-derived cardiac bodies form contractile myocardial tissue in vitro. *European heart journal*, 34(15), pp.1134–46. Available at: http://www.ncbi.nlm.nih.gov/pubmed/23103664 [Accessed September 28, 2015].

Kerkelä, R. et al., 2006. Cardiotoxicity of the cancer therapeutic agent imatinib mesylate. *Nature Medicine*, 12(8), pp.908–916. Available at: http://www.ncbi.nlm.nih.gov/pubmed/16862153 [Accessed November 3, 2017].

Keshet, Y. & Seger, R., 2010. The MAP Kinase Signaling Cascades: A System of Hundreds of Components Regulates a Diverse Array of Physiological Functions. In *Methods in molecular biology (Clifton, N.J.)*. pp. 3–38. Available at: http://www.ncbi.nlm.nih.gov/pubmed/20811974 [Accessed January 11, 2018].

Kim, A.S. et al., 2011. A small molecule AMPK activator protects the heart against ischemia–reperfusion injury. *Journal of Molecular and Cellular Cardiology*, 51(1), pp.24–32. Available at: http://www.ncbi.nlm.nih.gov/pubmed/21402077 [Accessed November 3, 2017].

Kim, J.K. et al., 2006. Estrogen prevents cardiomyocyte apoptosis through inhibition of reactive oxygen species and differential regulation of p38 kinase isoforms. *The Journal of biological chemistry*, 281(10), pp.6760–7. Available at: http://www.ncbi.nlm.nih.gov/pubmed/16407188 [Accessed November 2, 2017].

Kim, S.-Y. et al., 2006. Doxorubicin-induced reactive oxygen species generation and intracellular Ca2+ increase are reciprocally modulated in rat cardiomyocytes. *Experimental & molecular medicine*, 38(5), pp.535–45. Available at: http://dx.doi.org/10.1038/emm.2006.63 [Accessed September 23, 2015].

Kingsley-Hickman, P.B. et al., 1990. 31P NMR measurement of mitochondrial uncoupling in isolated rat hearts. *The Journal of biological chemistry*, 265(3), pp.1545–50. Available at: http://www.ncbi.nlm.nih.gov/pubmed/2136855 [Accessed September 14, 2017].

Kinnula, V.L. et al., 1992. Regulation of hydrogen peroxide generation in cultured endothelial cells. *American journal of respiratory cell and molecular biology*, 6(2), pp.175–82. Available at: http://www.ncbi.nlm.nih.gov/pubmed/1540380 [Accessed September 11, 2016].

Kita-Matsuo, H. et al., 2009. Lentiviral vectors and protocols for creation of stable hESC lines for fluorescent tracking and drug resistance selection of cardiomyocytes. *PloS one*, 4(4), p.e5046. Available at: http://www.ncbi.nlm.nih.gov/pubmed/19352491 [Accessed November 5, 2017].

Klionsky, D.J., 2005. The molecular machinery of autophagy: unanswered questions. *Journal of cell science*, 118(Pt 1), pp.7–18. Available at: http://www.pubmedcentral.nih.gov/articlerender.fcgi?artid=1828869&tool=pmcentrez&rendertype=abstract [Accessed September 6, 2015].

Knaapen, M.W. et al., 2001. Apoptotic versus autophagic cell death in heart failure. *Cardiovascular research*, 51(2), pp.304–12. Available at: http://www.ncbi.nlm.nih.gov/pubmed/11470470 [Accessed September 6, 2015].

Kokoszka, J.E. et al., 2004. The ADP/ATP translocator is not essential for the mitochondrial permeability transition pore. *Nature*, 427(6973), pp.461–5. Available at: http://www.pubmedcentral.nih.gov/articlerender.fcgi?artid=3049806&tool=pmcentrez&rendertype=abstract [Accessed September 6, 2015].

Kolanowski, T.J., Antos, C.L. & Guan, K., 2017. Making human cardiomyocytes up to date: Derivation, maturation state and perspectives. *International Journal of Cardiology*, 241, pp.379–386. Available at: http://www.ncbi.nlm.nih.gov/pubmed/28377185 [Accessed

October 31, 2017].

Kompa, A.R., 2016. Do p38 mitogen-activated protein kinase inhibitors have a future for the treatment of cardiovascular disease? *Journal of thoracic disease*, 8(9), pp.E1068–E1071. Available at: http://www.ncbi.nlm.nih.gov/pubmed/27747066 [Accessed December 5, 2017].

Kostin, S. et al., 2003. Myocytes Die by Multiple Mechanisms in Failing Human Hearts. *Circulation Research*, 92(7), pp.715–724. Available at: http://www.ncbi.nlm.nih.gov/pubmed/12649263 [Accessed November 3, 2017].

Kostin, S. et al., 2003. Myocytes die by multiple mechanisms in failing human hearts. *Circulation research*, 92(7), pp.715–24. Available at: http://www.ncbi.nlm.nih.gov/pubmed/12649263 [Accessed August 13, 2015].

Koudstaal, S. et al., 2015. Necrostatin-1 alleviates reperfusion injury following acute myocardial infarction in pigs. *European Journal of Clinical Investigation*, 45(2), pp.150–159. Available at: http://www.ncbi.nlm.nih.gov/pubmed/25496079 [Accessed January 11, 2018].

Kuida, K. et al., 1998. Reduced apoptosis and cytochrome c-mediated caspase activation in mice lacking caspase 9. *Cell*, 94(3), pp.325–37. Available at: http://www.ncbi.nlm.nih.gov/pubmed/9708735 [Accessed November 2, 2017].

Kuppusamy, K.T. et al., 2015. Let-7 family of microRNA is required for maturation and adult-like metabolism in stem cell-derived cardiomyocytes. *Proceedings of the National Academy of Sciences*, 112(21), pp.E2785–E2794. Available at: http://www.ncbi.nlm.nih.gov/pubmed/25964336 [Accessed January 16, 2018].

Kurosawa, H., 2007. Methods for inducing embryoid body formation: in vitro differentiation system of embryonic stem cells. *Journal of Bioscience and Bioengineering*, 103(5), pp.389–398. Available at: http://www.ncbi.nlm.nih.gov/pubmed/17609152 [Accessed

October 31, 2017].

Kurrelmeyer, K.M. et al., 2000. Endogenous tumor necrosis factor protects the adult cardiac myocyte against ischemic-induced apoptosis in a murine model of acute myocardial infarction. *Proceedings of the National Academy of Sciences*, 97(10), pp.5456–5461. Available at: http://www.ncbi.nlm.nih.gov/pubmed/10779546 [Accessed November 2, 2017].

Kutner, R.H., Zhang, X.-Y. & Reiser, J., 2009. Production, concentration and titration of pseudotyped HIV-1-based lentiviral vectors. *Nature Protocols*, 4(4), pp.495–505. Available at: http://www.ncbi.nlm.nih.gov/pubmed/19300443 [Accessed November 5, 2017].

Kyriakis, J.M. & Avruch, J., 2012. Mammalian MAPK signal transduction pathways activated by stress and inflammation: a 10-year update. *Physiological reviews*, 92(2), pp.689–737. Available at: http://www.ncbi.nlm.nih.gov/pubmed/22535895 [Accessed May 29, 2015].

Kytö, V. et al., 2004. Apoptotic cardiomyocyte death in fatal myocarditis. *The American journal of cardiology*, 94(6), pp.746–50. Available at: http://www.ncbi.nlm.nih.gov/pubmed/15374778 [Accessed September 6, 2015].

Lai, L. et al., 2014. Energy Metabolic Reprogramming in the Hypertrophied and Early Stage Failing Heart: A Multisystems Approach. *Circulation: Heart Failure*, 7(6), pp.1022–1031. Available at: http://www.ncbi.nlm.nih.gov/pubmed/25236884 [Accessed November 1, 2017].

Lan, F. et al., 2013. Abnormal calcium handling properties underlie familial hypertrophic cardiomyopathy pathology in patient-specific induced pluripotent stem cells. *Cell stem cell*, 12(1), pp.101–13. Available at: http://www.ncbi.nlm.nih.gov/pubmed/23290139 [Accessed February 27, 2018].

Lanier, M. et al., 2017. Structure-Based Design of ASK1 Inhibitors as Potential Agents for Heart Failure. *ACS Medicinal Chemistry Letters*, 8(3), pp.316–320. Available at: http://www.ncbi.nlm.nih.gov/pubmed/28337323 [Accessed January 15, 2018].

Larhammar, M. et al., 2017. The Ste20 Family Kinases MAP4K4, MINK1, and TNIK Converge to Regulate Stress-Induced JNK Signaling in Neurons. *The Journal of Neuroscience*, 37(46), pp.11074–11084. Available at: http://www.ncbi.nlm.nih.gov/pubmed/28993483 [Accessed November 23, 2017].

Laurini, E. et al., 2018. Biomechanical defects and rescue of cardiomyocytes expressing pathologic nuclear lamins. *Cardiovascular Research*. Available at: http://www.ncbi.nlm.nih.gov/pubmed/29432544 [Accessed February 22, 2018].

LeClaire, L.L. et al., 2015. The Nck-interacting kinase NIK increases Arp2/3 complex activity by phosphorylating the Arp2 subunit. *The Journal of Cell Biology*, 208(2), pp.161–170. Available at: http://www.ncbi.nlm.nih.gov/pubmed/25601402 [Accessed January 15, 2018].

Lee, P. et al., 2003. Fas pathway is a critical mediator of cardiac myocyte death and MI during ischemia-reperfusion in vivo. *American journal of physiology. Heart and circulatory physiology*, 284(2), pp.H456-63. Available at: http://www.ncbi.nlm.nih.gov/pubmed/12414449 [Accessed September 6, 2015].

Lee, S. et al., 2015. Looking for Pyroptosis-Modulating miRNAs as a Therapeutic Target for Improving Myocardium Survival. *Mediators of Inflammation*, 2015, pp.1–8. Available at: http://www.hindawi.com/journals/mi/2015/254871/ [Accessed January 9, 2018].

Lee, Y.-K. et al., 2011. Calcium Homeostasis in Human Induced Pluripotent Stem Cell-Derived Cardiomyocytes. *Stem Cell Reviews and Reports*, 7(4), pp.976–986. Available at: http://link.springer.com/10.1007/s12015-011-9273-3 [Accessed February 27, 2018].

Lee, Y.-K. et al., 2010. Triiodothyronine Promotes Cardiac Differentiation and Maturation of

Embryonic Stem Cells via the Classical Genomic Pathway. *Molecular Endocrinology*, 24(9), pp.1728–1736. Available at: http://www.ncbi.nlm.nih.gov/pubmed/20667986 [Accessed November 5, 2017].

Lehman, J.J. & Kelly, D.P., 2002. Gene regulatory mechanisms governing energy metabolism during cardiac hypertrophic growth. *Heart failure reviews*, 7(2), pp.175–85. Available at: http://www.ncbi.nlm.nih.gov/pubmed/11988641 [Accessed November 1, 2017].

Lemieux, H. et al., 2011. Mitochondrial respiratory control and early defects of oxidative phosphorylation in the failing human heart. *The International Journal of Biochemistry & Cell Biology*, 43(12), pp.1729–1738. Available at: http://www.ncbi.nlm.nih.gov/pubmed/21871578 [Accessed November 1, 2017].

Lemoine, M.D. et al., 2017. Human iPSC-derived cardiomyocytes cultured in 3D engineered heart tissue show physiological upstroke velocity and sodium current density. *Scientific Reports*, 7(1), p.5464. Available at: http://www.ncbi.nlm.nih.gov/pubmed/28710467 [Accessed November 23, 2017].

Leyton-Mange, J.S. et al., 2014. Rapid cellular phenotyping of human pluripotent stem cell-derived cardiomyocytes using a genetically encoded fluorescent voltage sensor. *Stem cell reports*, 2(2), pp.163–70. Available at: http://www.ncbi.nlm.nih.gov/pubmed/24527390 [Accessed February 27, 2018].

Li, D. et al., 1999. Desmin mutation responsible for idiopathic dilated cardiomyopathy. *Circulation*, 100(5), pp.461–4. Available at: http://www.ncbi.nlm.nih.gov/pubmed/10430757 [Accessed October 17, 2017].

Li, H. et al., 1998. Cleavage of BID by caspase 8 mediates the mitochondrial damage in the Fas pathway of apoptosis. *Cell*, 94(4), pp.491–501. Available at: http://www.ncbi.nlm.nih.gov/pubmed/9727492 [Accessed January 9, 2018].

Li, L. et al., 2014. Transforming growth factor β-activated kinase 1 signaling pathway critically regulates myocardial survival and remodeling. *Circulation*, 130(24), pp.2162–72. Available at: http://www.ncbi.nlm.nih.gov/pubmed/25278099 [Accessed February 25, 2018].

Li, L.Y., Luo, X. & Wang, X., 2001. Endonuclease G is an apoptotic DNase when released from mitochondria. *Nature*, 412(6842), pp.95–99. Available at: http://www.ncbi.nlm.nih.gov/pubmed/11452314 [Accessed January 9, 2018].

Li, P. et al., 1997. Cytochrome c and dATP-dependent formation of Apaf-1/caspase-9 complex initiates an apoptotic protease cascade. *Cell*, 91(4), pp.479–89. Available at: http://www.ncbi.nlm.nih.gov/pubmed/9390557 [Accessed January 10, 2018].

Li, Y.Y. et al., 2000. Myocardial extracellular matrix remodeling in transgenic mice overexpressing tumor necrosis factor alpha can be modulated by anti-tumor necrosis factor alpha therapy. *Proceedings of the National Academy of Sciences of the United States of America*, 97(23), pp.12746–51. Available at: http://www.pubmedcentral.nih.gov/articlerender.fcgi?artid=18835&tool=pmcentrez&rendertype=abstract [Accessed September 6, 2015].

Lian, X. et al., 2012. Directed cardiomyocyte differentiation from human pluripotent stem cells by modulating Wnt/β-catenin signaling under fully defined conditions. *Nature Protocols*, 8(1), pp.162–175. Available at: http://www.ncbi.nlm.nih.gov/pubmed/23257984 [Accessed November 3, 2017].

Liang, P. et al., 2013. Drug Screening Using a Library of Human Induced Pluripotent Stem Cell-Derived Cardiomyocytes Reveals Disease-Specific Patterns of Cardiotoxicity. *Circulation*, 127(16), pp.1677–1691. Available at: http://www.ncbi.nlm.nih.gov/pubmed/23519760 [Accessed February 27, 2018].

Liang, Q. et al., 2001. The transcription factor GATA4 is activated by extracellular signal-

regulated kinase 1- and 2-mediated phosphorylation of serine 105 in cardiomyocytes. *Molecular and cellular biology*, 21(21), pp.7460–9. Available at: http://www.ncbi.nlm.nih.gov/pubmed/11585926 [Accessed January 15, 2018].

Liau, B. et al., 2011. Pluripotent stem cell-derived cardiac tissue patch with advanced structure and function. *Biomaterials*, 32(35), pp.9180–9187. Available at: http://www.ncbi.nlm.nih.gov/pubmed/21906802 [Accessed January 22, 2018].

Liau, B., Zhang, D. & Bursac, N., 2012. Functional cardiac tissue engineering. *Regenerative medicine*, 7(2), pp.187–206. Available at: http://www.ncbi.nlm.nih.gov/pubmed/22397609 [Accessed January 22, 2018].

Liaw, N.Y. & Zimmermann, W.-H., 2015. Mechanical stimulation in the engineering of heart muscle. *Advanced drug delivery reviews*. Available at: http://www.ncbi.nlm.nih.gov/pubmed/26362920 [Accessed September 24, 2015].

Lim, S.Y. et al., 2007. The Cardioprotective Effect of Necrostatin Requires the Cyclophilin-D Component of the Mitochondrial Permeability Transition Pore. *Cardiovascular Drugs and Therapy*, 21(6), pp.467–469. Available at: http://www.ncbi.nlm.nih.gov/pubmed/17965927 [Accessed November 3, 2017].

Lin, Y. et al., 1999. Cleavage of the death domain kinase RIP by caspase-8 prompts TNF-induced apoptosis. *Genes & development*, 13(19), pp.2514–26. Available at: http://www.pubmedcentral.nih.gov/articlerender.fcgi?artid=317073&tool=pmcentrez&rendertype=abstract [Accessed September 6, 2015].

Lincoff, A.M. et al., 2014. Inhibition of delta-protein kinase C by delcasertib as an adjunct to primary percutaneous coronary intervention for acute anterior ST-segment elevation myocardial infarction: results of the PROTECTION AMI Randomized Controlled Trial. *European Heart Journal*, 35(37), pp.2516–2523. Available at: http://www.ncbi.nlm.nih.gov/pubmed/24796339 [Accessed November 23, 2017].

Linkermann, A. & Green, D.R., 2014. Necroptosis. *The New England journal of medicine*, 370(5), pp.455–65. Available at: http://www.ncbi.nlm.nih.gov/pubmed/24476434 [Accessed January 9, 2018].

Lips, D.J. et al., 2004. MEK1-ERK2 Signaling Pathway Protects Myocardium From Ischemic Injury In Vivo. *Circulation*, 109(16), pp.1938–1941. Available at: http://www.ncbi.nlm.nih.gov/pubmed/15096454 [Accessed January 15, 2018].

Liu, A.-W. et al., 2011. ShRNA-targeted MAP4K4 inhibits hepatocellular carcinoma growth. *Clinical cancer research : an official journal of the American Association for Cancer Research*, 17(4), pp.710–20. Available at: http://www.ncbi.nlm.nih.gov/pubmed/21196414 [Accessed September 15, 2015].

Liu, H. et al., 1999. A Drosophila TNF-receptor-associated factor (TRAF) binds the ste20 kinase Misshapen and activates Jun kinase. *Current biology : CB*, 9(2), pp.101–4. Available at: http://www.ncbi.nlm.nih.gov/pubmed/10021364 [Accessed January 15, 2018].

Liu, H.-R. et al., 2005. Role of Omi/HtrA2 in Apoptotic Cell Death After Myocardial Ischemia and Reperfusion. *Circulation*, 111(1), pp.90–96. Available at: http://www.ncbi.nlm.nih.gov/pubmed/15611365 [Accessed November 2, 2017].

Liu, H., Pedram, A. & Kim, J.K., 2011. Oestrogen prevents cardiomyocyte apoptosis by suppressing p38α-mediated activation of p53 and by down-regulating p53 inhibition on p38β. *Cardiovascular research*, 89(1), pp.119–28. Available at: http://www.pubmedcentral.nih.gov/articlerender.fcgi?artid=3002868&tool=pmcentrez&rendertype=abstract [Accessed September 28, 2015].

Liu, Q. et al., 2009. ASK1 regulates cardiomyocyte death but not hypertrophy in transgenic mice. *Circulation research*, 105(11), pp.1110–7. Available at: http://www.ncbi.nlm.nih.gov/pubmed/19815822 [Accessed November 3, 2017].

Liu, W. et al., 2011. Pak1 as a Novel Therapeutic Target for Antihypertrophic Treatment in the Heart. *Circulation*, 124(24), pp.2702–2715. Available at: http://www.ncbi.nlm.nih.gov/pubmed/22082674 [Accessed November 3, 2017].

Loftus, J.C. et al., 2013. A Novel Interaction between Pyk2 and MAP4K4 Is Integrated with Glioma Cell Migration. *Journal of Signal Transduction*, 2013, pp.1–12. Available at: http://www.ncbi.nlm.nih.gov/pubmed/24163766 [Accessed January 15, 2018].

Loor, G. et al., 2010. Menadione triggers cell death through ROS-dependent mechanisms involving PARP activation without requiring apoptosis. *Free Radical Biology and Medicine*, 49(12), pp.1925–1936. Available at: http://www.ncbi.nlm.nih.gov/pubmed/20937380 [Accessed September 9, 2017].

Los, M. et al., 2002. Activation and caspase-mediated inhibition of PARP: a molecular switch between fibroblast necrosis and apoptosis in death receptor signaling. *Molecular biology of the cell*, 13(3), pp.978–88. Available at: http://www.ncbi.nlm.nih.gov/pubmed/11907276 [Accessed January 10, 2018].

Lu, J.T. et al., 2011. LMNA cardiomyopathy: cell biology and genetics meet clinical medicine. *Disease models & mechanisms*, 4(5), pp.562–8. Available at: http://www.ncbi.nlm.nih.gov/pubmed/21810905 [Accessed December 5, 2017].

Lu, Z. & Xu, S., 2006. ERK1/2 MAP kinases in cell survival and apoptosis. *IUBMB Life (International Union of Biochemistry and Molecular Biology: Life)*, 58(11), pp.621–631. Available at: http://doi.wiley.com/10.1080/15216540600957438 [Accessed December 4, 2017].

Luan, Z. et al., 2002. A novel GTP-binding protein hGBP3 interacts with NIK/HGK. *FEBS letters*, 530(1–3), pp.233–8. Available at: http://www.ncbi.nlm.nih.gov/pubmed/12387898 [Accessed January 15, 2018].

Lucarelli, G. et al., 2015. Metabolomic profile of glycolysis and the pentose phosphate

pathway identifies the central role of glucose-6-phosphate dehydrogenase in clear cell-renal cell carcinoma. *Oncotarget*, 6(15), pp.13371–86. Available at: http://www.ncbi.nlm.nih.gov/pubmed/25945836 [Accessed February 26, 2018].

Ludwig, T.E. et al., 2006. Feeder-independent culture of human embryonic stem cells. *Nature Methods*, 3(8), pp.637–646. Available at: http://www.ncbi.nlm.nih.gov/pubmed/16862139 [Accessed November 3, 2017].

Lundy, S.D. et al., 2013. Structural and Functional Maturation of Cardiomyocytes Derived from Human Pluripotent Stem Cells. *Stem Cells and Development*, 22(14), pp.1991–2002. Available at: http://www.ncbi.nlm.nih.gov/pubmed/23461462 [Accessed November 5, 2017].

Luo, X. et al., 1998. Bid, a Bcl2 interacting protein, mediates cytochrome c release from mitochondria in response to activation of cell surface death receptors. *Cell*, 94(4), pp.481–90. Available at: http://www.ncbi.nlm.nih.gov/pubmed/9727491 [Accessed January 9, 2018].

Ma, S. et al., 2015. The role of the autophagy in myocardial ischemia/reperfusion injury. *Biochimica et Biophysica Acta (BBA) - Molecular Basis of Disease*, 1852(2), pp.271–276. Available at: https://www.sciencedirect.com/science/article/pii/S0925443914001380 [Accessed December 5, 2017].

Ma, X. et al., 2012. Impaired autophagosome clearance contributes to cardiomyocyte death in ischemia/reperfusion injury. *Circulation*, 125(25), pp.3170–81. Available at: http://www.pubmedcentral.nih.gov/articlerender.fcgi?artid=3397471&tool=pmcentrez&rendertype=abstract [Accessed September 6, 2015].

Machida, N. et al., 2004. Mitogen-activated Protein Kinase Kinase Kinase Kinase 4 as a Putative Effector of Rap2 to Activate the c-Jun N-terminal Kinase. *Journal of Biological*

Chemistry, 279(16), pp.15711–15714. Available at: http://www.ncbi.nlm.nih.gov/pubmed/14966141 [Accessed November 3, 2017].

Mack, K.D. et al., 2005. Functional identification of kinases essential for T-cell activation through a genetic suppression screen. *Immunology letters*, 96(1), pp.129–45. Available at: http://www.ncbi.nlm.nih.gov/pubmed/15585316 [Accessed September 15, 2015].

Maiuri, M.C. et al., 2007. Functional and physical interaction between Bcl-X(L) and a BH3-like domain in Beclin-1. *The EMBO journal*, 26(10), pp.2527–39. Available at: http://www.pubmedcentral.nih.gov/articlerender.fcgi?artid=1868901&tool=pmcentrez&rendertype=abstract [Accessed September 6, 2015].

Maloyan, A. et al., 2010. Manipulation of Death Pathways in Desmin-Related Cardiomyopathy. *Circulation Research*, 106(9), pp.1524–1532. Available at: http://www.ncbi.nlm.nih.gov/pubmed/20360253 [Accessed November 14, 2017].

Mannhardt, I. et al., 2017. Blinded Contractility Analysis in hiPSC-Cardiomyocytes in Engineered Heart Tissue Format: Comparison With Human Atrial Trabeculae. *Toxicological Sciences*, 158(1), pp.164–175. Available at: http://www.ncbi.nlm.nih.gov/pubmed/28453742 [Accessed August 7, 2017].

Mannhardt, I. et al., 2016. Human Engineered Heart Tissue: Analysis of Contractile Force. *Stem cell reports*, 7(1), pp.29–42. Available at: http://www.ncbi.nlm.nih.gov/pubmed/27211213 [Accessed September 12, 2017].

Manning, G. et al., 2002. The Protein Kinase Complement of the Human Genome. *Science*, 298(5600), pp.1912–1934. Available at: http://www.ncbi.nlm.nih.gov/pubmed/12471243 [Accessed November 3, 2017].

Marber, M.S., Molkentin, J.D. & Force, T., 2010. Developing small molecules to inhibit kinases unkind to the heart: p38 MAPK as a case in point. *Drug discovery today. Disease mechanisms*, 7(2), pp.e123–e127. Available at:

http://www.ncbi.nlm.nih.gov/pubmed/21278838 [Accessed November 3, 2017].

Marber, M.S., Rose, B. & Wang, Y., 2011. The p38 mitogen-activated protein kinase pathway--a potential target for intervention in infarction, hypertrophy, and heart failure. *Journal of molecular and cellular cardiology*, 51(4), pp.485–90. Available at: http://www.pubmedcentral.nih.gov/articlerender.fcgi?artid=3061241&tool=pmcentrez&rendertype=abstract [Accessed July 27, 2015].

Margulis, L., 1975. Symbiotic theory of the origin of eukaryotic organelles; criteria for proof. *Symposia of the Society for Experimental Biology*, (29), pp.21–38. Available at: http://www.ncbi.nlm.nih.gov/pubmed/822529 [Accessed November 1, 2017].

Mariño, G. et al., 2014. Self-consumption: the interplay of autophagy and apoptosis. *Nature reviews. Molecular cell biology*, 15(2), pp.81–94. Available at: http://dx.doi.org/10.1038/nrm3735 [Accessed July 9, 2014].

Marks, A.R., 2013. Calcium cycling proteins and heart failure: mechanisms and therapeutics. *The Journal of clinical investigation*, 123(1), pp.46–52. Available at: http://www.ncbi.nlm.nih.gov/pubmed/23281409 [Accessed November 26, 2017].

Marzo, I. et al., 1998. Bax and adenine nucleotide translocator cooperate in the mitochondrial control of apoptosis. *Science (New York, N.Y.)*, 281(5385), pp.2027–31. Available at: http://www.ncbi.nlm.nih.gov/pubmed/9748162 [Accessed November 2, 2017].

Massey, A.C., Zhang, C. & Cuervo, A.M., 2006. Chaperone-mediated autophagy in aging and disease. *Current topics in developmental biology*, 73, pp.205–35. Available at: http://www.ncbi.nlm.nih.gov/pubmed/16782460 [Accessed September 6, 2015].

Matsui, Y. et al., 2007. Distinct roles of autophagy in the heart during ischemia and reperfusion: roles of AMP-activated protein kinase and Beclin 1 in mediating autophagy. *Circulation research*, 100(6), pp.914–22. Available at:

http://www.ncbi.nlm.nih.gov/pubmed/17332429 [Accessed September 6, 2015].

Matsumoto-Ida, M. et al., 2006. Activation of TGF-beta1-TAK1-p38 MAPK pathway in spared cardiomyocytes is involved in left ventricular remodeling after myocardial infarction in rats. *American journal of physiology. Heart and circulatory physiology*, 290(2), pp.H709-15. Available at: http://www.ncbi.nlm.nih.gov/pubmed/16183734 [Accessed November 3, 2017].

Mercola, M., Ruiz-Lozano, P. & Schneider, M.D., 2011. Cardiac muscle regeneration: lessons from development. *Genes & Development*, 25(4), pp.299–309. Available at: http://www.ncbi.nlm.nih.gov/pubmed/21325131 [Accessed October 17, 2017].

Merkle, S. et al., 2007. A Role for Caspase-1 in Heart Failure. *Circulation Research*, 100(5), pp.645–653. Available at: http://www.ncbi.nlm.nih.gov/pubmed/17303764 [Accessed November 2, 2017].

De Meyer, G.R.Y. & Martinet, W., 2009. Autophagy in the cardiovascular system. *Biochimica et Biophysica Acta (BBA) - Molecular Cell Research*, 1793(9), pp.1485–1495. Available at: http://www.ncbi.nlm.nih.gov/pubmed/19152812 [Accessed February 21, 2018].

Michel, J.-B., 2003. Anoikis in the Cardiovascular System: Known and Unknown Extracellular Mediators. *Arteriosclerosis, Thrombosis, and Vascular Biology*, 23(12), pp.2146–2154. Available at: http://www.ncbi.nlm.nih.gov/pubmed/14551156 [Accessed January 9, 2018].

Milano, G. et al., 2007. A peptide inhibitor of c-Jun NH2-terminal kinase reduces myocardial ischemia-reperfusion injury and infarct size in vivo. *American journal of physiology. Heart and circulatory physiology*, 292(4), pp.H1828-35. Available at: http://www.ncbi.nlm.nih.gov/pubmed/17158645 [Accessed September 28, 2015].

Miled, C. et al., 2005. A genomic map of p53 binding sites identifies novel p53 targets involved in an apoptotic network. *Cancer research*, 65(12), pp.5096–104. Available at:

http://www.ncbi.nlm.nih.gov/pubmed/15958553 [Accessed September 15, 2015].

Miller, T.D. et al., 1995. Infarct Size After Acute Myocardial Infarction Measured by Quantitative Tomographic 99mTc Sestamibi Imaging Predicts Subsequent Mortality. *Circulation*, 92(3), pp.334–341. Available at: http://circ.ahajournals.org/content/92/3/334.abstract [Accessed September 14, 2015].

Minamino, T. et al., 2002. MEKK1 is essential for cardiac hypertrophy and dysfunction induced by Gq. *Proceedings of the National Academy of Sciences of the United States of America*, 99(6), pp.3866–71. Available at: http://www.ncbi.nlm.nih.gov/pubmed/11891332 [Accessed January 12, 2018].

Mioulane, M. et al., 2012. Development of High Content Imaging Methods for Cell Death Detection in Human Pluripotent Stem Cell-Derived Cardiomyocytes. *Journal of Cardiovascular Translational Research*, 5(5), pp.593–604. Available at: http://www.ncbi.nlm.nih.gov/pubmed/22896035 [Accessed November 8, 2017].

Mitchell, P., 1961. Coupling of phosphorylation to electron and hydrogen transfer by a chemi-osmotic type of mechanism. *Nature*, 191, pp.144–8. Available at: http://www.ncbi.nlm.nih.gov/pubmed/13771349 [Accessed November 1, 2017].

Mizushima, N. et al., 2008. Autophagy fights disease through cellular self-digestion. *Nature*, 451(7182), pp.1069–75. Available at: http://www.pubmedcentral.nih.gov/articlerender.fcgi?artid=2670399&tool=pmcentrez&rendertype=abstract [Accessed July 10, 2014].

Morioka, S. et al., 2014. TAK1 kinase switches cell fate from apoptosis to necrosis following TNF stimulation. *The Journal of cell biology*, 204(4), pp.607–23. Available at: http://www.ncbi.nlm.nih.gov/pubmed/24535827 [Accessed February 26, 2018].

Morita, H., Seidman, J. & Seidman, C.E., 2005. Genetic causes of human heart failure. *Journal of Clinical Investigation*, 115(3), pp.518–526. Available at:

http://www.ncbi.nlm.nih.gov/pubmed/15765133 [Accessed October 17, 2017].

Moriwaki, K. & Chan, F.K.-M., 2013. RIP3: a molecular switch for necrosis and inflammation. *Genes & development*, 27(15), pp.1640–9. Available at: http://www.ncbi.nlm.nih.gov/pubmed/23913919 [Accessed December 5, 2017].

Morrison, D.K. & Davis, R.J., 2003. Regulation of MAP Kinase Signaling Modules by Scaffold Proteins in Mammals. *Annual Review of Cell and Developmental Biology*, 19(1), pp.91–118. Available at: http://www.ncbi.nlm.nih.gov/pubmed/14570565 [Accessed November 3, 2017].

Mummery, C.L. et al., 2012. Differentiation of Human Embryonic Stem Cells and Induced Pluripotent Stem Cells to Cardiomyocytes: A Methods Overview. *Circulation Research*, 111(3), pp.344–358. Available at: http://www.ncbi.nlm.nih.gov/pubmed/22821908 [Accessed November 3, 2017].

Muntean, D.M. et al., 2016. The Role of Mitochondrial Reactive Oxygen Species in Cardiovascular Injury and Protective Strategies. *Oxidative Medicine and Cellular Longevity*, 2016, pp.1–19. Available at: http://www.ncbi.nlm.nih.gov/pubmed/27200148 [Accessed September 9, 2017].

Murphy, E. & Steenbergen, C., 2008a. Ion Transport and Energetics During Cell Death and Protection. *Physiology*, 23(2), pp.115–123. Available at: http://www.ncbi.nlm.nih.gov/pubmed/18400694 [Accessed November 1, 2017].

Murphy, E. & Steenbergen, C., 2008b. Mechanisms Underlying Acute Protection From Cardiac Ischemia-Reperfusion Injury. *Physiological Reviews*, 88(2), pp.581–609. Available at: http://www.ncbi.nlm.nih.gov/pubmed/18391174 [Accessed November 1, 2017].

Murphy, M.P., 2009. How mitochondria produce reactive oxygen species. *Biochemical Journal*, 417(1), pp.1–13. Available at: http://www.ncbi.nlm.nih.gov/pubmed/19061483

[Accessed November 1, 2017].

Nabeebaccus, A., Zhang, M. & Shah, A.M., 2011. NADPH oxidases and cardiac remodelling. *Heart Failure Reviews*, 16(1), pp.5–12. Available at: http://www.ncbi.nlm.nih.gov/pubmed/20658317 [Accessed November 1, 2017].

Naito, H. et al., 2006. Optimizing engineered heart tissue for therapeutic applications as surrogate heart muscle. *Circulation*, 114(SUPPL. 1), pp.72–79.

Nakagawa, T. et al., 2005. Cyclophilin D-dependent mitochondrial permeability transition regulates some necrotic but not apoptotic cell death. *Nature*, 434(7033), pp.652–658. Available at: http://www.ncbi.nlm.nih.gov/pubmed/15800626 [Accessed November 2, 2017].

Nakai, A. et al., 2007. The role of autophagy in cardiomyocytes in the basal state and in response to hemodynamic stress. *Nature medicine*, 13(5), pp.619–24. Available at: http://www.ncbi.nlm.nih.gov/pubmed/17450150 [Accessed August 19, 2015].

Nakayama, H. et al., 2007. Ca2+- and mitochondrial-dependent cardiomyocyte necrosis as a primary mediator of heart failure. *Journal of Clinical Investigation*, 117(9), pp.2431–2444. Available at: http://www.ncbi.nlm.nih.gov/pubmed/17694179 [Accessed November 3, 2017].

Nam, Y.-J. et al., 2004. Inhibition of Both the Extrinsic and Intrinsic Death Pathways through Nonhomotypic Death-Fold Interactions. *Molecular Cell*, 15(6), pp.901–912. Available at: http://www.ncbi.nlm.nih.gov/pubmed/15383280 [Accessed November 2, 2017].

Narula, J. et al., 1999. Apoptosis in heart failure: release of cytochrome c from mitochondria and activation of caspase-3 in human cardiomyopathy. *Proceedings of the National Academy of Sciences of the United States of America*, 96(14), pp.8144–9. Available at: http://www.pubmedcentral.nih.gov/articlerender.fcgi?artid=22202&tool=pmcentrez&rendertype=abstract [Accessed September 6, 2015].

Narula, J. et al., 1996. Apoptosis in myocytes in end-stage heart failure. *The New England journal of medicine*, 335(16), pp.1182–9. Available at: http://www.ncbi.nlm.nih.gov/pubmed/8815940 [Accessed September 6, 2015].

Ndubaku, C.O. et al., 2015. Structure-Based Design of GNE-495, a Potent and Selective MAP4K4 Inhibitor with Efficacy in Retinal Angiogenesis. *ACS Medicinal Chemistry Letters*, 6(8), pp.913–918. Available at: http://pubs.acs.org/doi/abs/10.1021/acsmedchemlett.5b00174 [Accessed September 11, 2016].

Nechushtan, A. et al., 1999. Conformation of the Bax C-terminus regulates subcellular location and cell death. *The EMBO journal*, 18(9), pp.2330–41. Available at: http://www.ncbi.nlm.nih.gov/pubmed/10228148 [Accessed January 10, 2018].

Newby, L.K. et al., 2014. Losmapimod, a novel p38 mitogen-activated protein kinase inhibitor, in non-ST-segment elevation myocardial infarction: a randomised phase 2 trial. *The Lancet*, 384(9949), pp.1187–1195. Available at: http://www.ncbi.nlm.nih.gov/pubmed/24930728 [Accessed November 23, 2017].

Nicholls, D.G. et al., 2010. Bioenergetic profile experiment using C2C12 myoblast cells. *Journal of visualized experiments : JoVE*, (46). Available at: http://www.ncbi.nlm.nih.gov/pubmed/21189469 [Accessed September 12, 2016].

De Nicola, G.F. et al., 2013. Mechanism and consequence of the autoactivation of p38α mitogen-activated protein kinase promoted by TAB1. *Nature structural & molecular biology*, 20(10), pp.1182–90. Available at: http://www.pubmedcentral.nih.gov/articlerender.fcgi?artid=3822283&tool=pmcentrez&rendertype=abstract [Accessed September 14, 2015].

Nishida, K., 2016. Autophagy during cardiac remodeling. *Journal of Molecular and Cellular Cardiology*, 95, pp.11–18. Available at:

https://www.sciencedirect.com/science/article/pii/S0022282815301425 [Accessed December 6, 2017].

Nishida, K. et al., 2004. p38 Mitogen-Activated Protein Kinase Plays a Critical Role in Cardiomyocyte Survival but Not in Cardiac Hypertrophic Growth in Response to Pressure Overload. *Molecular and Cellular Biology*, 24(24), pp.10611–10620. Available at: http://www.ncbi.nlm.nih.gov/pubmed/15572667 [Accessed June 24, 2018].

Nishida, K. & Otsu, K., 2008. Cell death in heart failure. *Circulation journal : official journal of the Japanese Circulation Society*, 72 Suppl A, pp.A17-21. Available at: http://www.ncbi.nlm.nih.gov/pubmed/18772526 [Accessed February 20, 2018].

Nishida, K., Taneike, M. & Otsu, K., 2015. The role of autophagic degradation in the heart. *Journal of Molecular and Cellular Cardiology*, 78, pp.73–79. Available at: http://www.ncbi.nlm.nih.gov/pubmed/25300865 [Accessed December 6, 2017].

Nishida, K., Yamaguchi, O. & Otsu, K., 2008. Crosstalk between autophagy and apoptosis in heart disease. *Circulation research*, 103(4), pp.343–51. Available at: http://www.ncbi.nlm.nih.gov/pubmed/18703786 [Accessed September 6, 2015].

Nishimura, S. et al., 2004. Single cell mechanics of rat cardiomyocytes under isometric, unloaded, and physiologically loaded conditions. *American Journal of Physiology-Heart and Circulatory Physiology*, 287(1), pp.H196–H202. Available at: http://www.ncbi.nlm.nih.gov/pubmed/15001443 [Accessed January 16, 2018].

Nishitoh, H. et al., 1998. ASK1 is essential for JNK/SAPK activation by TRAF2. *Molecular cell*, 2(3), pp.389–95. Available at: http://www.ncbi.nlm.nih.gov/pubmed/9774977 [Accessed October 30, 2017].

Noguchi, T. et al., 2005. Recruitment of Tumor Necrosis Factor Receptor-associated Factor Family Proteins to Apoptosis Signal-regulating Kinase 1 Signalosome Is Essential for Oxidative Stress-induced Cell Death. *Journal of Biological Chemistry*, 280(44),

pp.37033–37040. Available at: http://www.ncbi.nlm.nih.gov/pubmed/16129676 [Accessed November 3, 2017].

Nunes, S.S. et al., 2013. Biowire: a platform for maturation of human pluripotent stem cell–derived cardiomyocytes. *Nature Methods*, 10(8), pp.781–787. Available at: http://www.ncbi.nlm.nih.gov/pubmed/23793239 [Accessed October 31, 2017].

O'Donoghue, M.L. et al., 2016. Effect of Losmapimod on Cardiovascular Outcomes in Patients Hospitalized With Acute Myocardial Infarction. *JAMA*, 315(15), p.1591. Available at: http://www.ncbi.nlm.nih.gov/pubmed/27043082 [Accessed December 5, 2017].

Oerlemans, M.I.F.J. et al., 2012. Inhibition of RIP1-dependent necrosis prevents adverse cardiac remodeling after myocardial ischemia–reperfusion in vivo. *Basic Research in Cardiology*, 107(4), p.270. Available at: http://www.ncbi.nlm.nih.gov/pubmed/22553001 [Accessed January 11, 2018].

Ogle, B.M. et al., 2016. Distilling complexity to advance cardiac tissue engineering. *Science translational medicine*, 8(342), p.342ps13. Available at: http://www.ncbi.nlm.nih.gov/pubmed/27280684 [Accessed January 15, 2018].

Olivetti, G. et al., 1997. Apoptosis in the failing human heart. *The New England journal of medicine*, 336(16), pp.1131–41. Available at: http://www.ncbi.nlm.nih.gov/pubmed/9099657 [Accessed September 6, 2015].

Olson, E.N., 2004. A decade of discoveries in cardiac biology. *Nature Medicine*, 10(5), pp.467–474. Available at: http://www.nature.com/doifinder/10.1038/nm0504-467 [Accessed October 17, 2017].

Olson, T.M. et al., 1998. Actin mutations in dilated cardiomyopathy, a heritable form of heart failure. *Science (New York, N.Y.)*, 280(5364), pp.750–2. Available at: http://www.ncbi.nlm.nih.gov/pubmed/9563954 [Accessed October 17, 2017].

Orr, A.L. et al., 2013. Inhibitors of ROS production by the ubiquinone-binding site of mitochondrial complex I identified by chemical screening. *Free Radical Biology and Medicine*, 65, pp.1047–1059. Available at: http://www.ncbi.nlm.nih.gov/pubmed/23994103 [Accessed November 1, 2017].

Palaniyandi, S.S. et al., 2008. Protein kinase C in heart failure: a therapeutic target? *Cardiovascular Research*, 82(2), pp.229–239. Available at: http://www.ncbi.nlm.nih.gov/pubmed/19168855 [Accessed November 3, 2017].

Pannekoek, W.-J. et al., 2013. Rap1 and Rap2 Antagonistically Control Endothelial Barrier Resistance C. Gottardi, ed. *PLoS ONE*, 8(2), p.e57903. Available at: http://www.ncbi.nlm.nih.gov/pubmed/23469100 [Accessed January 15, 2018].

Passier, R., Orlova, V. & Mummery, C., 2016. Complex Tissue and Disease Modeling using hiPSCs. *Cell Stem Cell*, 18(3), pp.309–321. Available at: http://linkinghub.elsevier.com/retrieve/pii/S1934590916000734 [Accessed August 16, 2017].

Pattingre, S. et al., 2005. Bcl-2 antiapoptotic proteins inhibit Beclin 1-dependent autophagy. *Cell*, 122(6), pp.927–39. Available at: http://www.ncbi.nlm.nih.gov/pubmed/16179260 [Accessed April 13, 2015].

Paull, D. et al., 2012. Nuclear genome transfer in human oocytes eliminates mitochondrial DNA variants. *Nature*, 493(7434), pp.632–637. Available at: http://www.ncbi.nlm.nih.gov/pubmed/23254936 [Accessed November 1, 2017].

Peretz, L. et al., 2018. Combined shRNA over CRISPR/cas9 as a methodology to detect off-target effects and a potential compensatory mechanism. *Scientific reports*, 8(1), p.93. Available at: http://www.ncbi.nlm.nih.gov/pubmed/29311693 [Accessed February 26, 2018].

Peter, M.E., 2004. The flip side of FLIP. *Biochemical Journal*, 382(2), p.e1. Available at:

http://www.ncbi.nlm.nih.gov/pubmed/15317488 [Accessed November 2, 2017].

Petrich, B.G. et al., 2004. Targeted activation of c-Jun N-terminal kinase in vivo induces restrictive cardiomyopathy and conduction defects. *The Journal of biological chemistry*, 279(15), pp.15330–8. Available at: http://www.ncbi.nlm.nih.gov/pubmed/14742426 [Accessed November 3, 2017].

Petrich, B.G., Molkentin, J.D. & Wang, Y., 2003. Temporal activation of c-Jun N-terminal kinase in adult transgenic heart via cre-loxP-mediated DNA recombination. *The FASEB Journal*, 17(6), pp.749–51. Available at: http://www.ncbi.nlm.nih.gov/pubmed/12594183 [Accessed November 3, 2017].

Piot, C. et al., 2008. Effect of Cyclosporine on Reperfusion Injury in Acute Myocardial Infarction. *New England Journal of Medicine*, 359(5), pp.473–481. Available at: http://www.ncbi.nlm.nih.gov/pubmed/18669426 [Accessed November 23, 2017].

Pizarro, M. et al., 2016. Basal autophagy protects cardiomyocytes from doxorubicin-induced toxicity. *Toxicology*, 370, pp.41–48. Available at: http://www.ncbi.nlm.nih.gov/pubmed/27666003 [Accessed February 21, 2018].

Polonchuk, L. et al., 2017. Cardiac spheroids as promising in vitro models to study the human heart microenvironment. *Scientific Reports*, 7(1), p.7005. Available at: http://www.nature.com/articles/s41598-017-06385-8 [Accessed February 25, 2018].

Potts, M.B. et al., 2005. Reduced Apaf-1 levels in cardiomyocytes engage strict regulation of apoptosis by endogenous XIAP. *The Journal of cell biology*, 171(6), pp.925–30. Available at: http://www.ncbi.nlm.nih.gov/pubmed/16344307 [Accessed November 2, 2017].

Pufall, M.A. & Graves, B.J., 2002. Autoinhibitory Domains: Modular Effectors of Cellular Regulation. *Annual Review of Cell and Developmental Biology*, 18(1), pp.421–462. Available at:

http://www.annualreviews.org/doi/10.1146/annurev.cellbio.18.031502.133614 [Accessed November 3, 2017].

Purcell, N.H. et al., 2007. Genetic inhibition of cardiac ERK1/2 promotes stress-induced apoptosis and heart failure but has no effect on hypertrophy in vivo. *Proceedings of the National Academy of Sciences of the United States of America*, 104(35), pp.14074–9. Available at: http://www.pubmedcentral.nih.gov/articlerender.fcgi?artid=1955824&tool=pmcentrez&rendertype=abstract [Accessed September 28, 2015].

Puri, V. et al., 2008. RNAi screens reveal novel metabolic regulators: RIP140, MAP4k4 and the lipid droplet associated fat specific protein (FSP) 27. *Acta physiologica (Oxford, England)*, 192(1), pp.103–15. Available at: http://www.pubmedcentral.nih.gov/articlerender.fcgi?artid=2880506&tool=pmcentrez&rendertype=abstract [Accessed September 15, 2015].

Qi, M. & Elion, E.A., 2005. MAP kinase pathways. *Journal of Cell Science*, 118(16), pp.3569–3572. Available at: http://www.ncbi.nlm.nih.gov/pubmed/16105880 [Accessed November 3, 2017].

Rais, Y. et al., 2013. Deterministic direct reprogramming of somatic cells to pluripotency. *Nature*, 502(7469), pp.65–70. Available at: http://www.ncbi.nlm.nih.gov/pubmed/24048479 [Accessed November 3, 2017].

Ramirez, M.T. et al., 1997. The MEKK-JNK pathway is stimulated by alpha1-adrenergic receptor and ras activation and is associated with in vitro and in vivo cardiac hypertrophy. *The Journal of biological chemistry*, 272(22), pp.14057–61. Available at: http://www.ncbi.nlm.nih.gov/pubmed/9162028 [Accessed November 3, 2017].

Ramos, J.W., 2008. The regulation of extracellular signal-regulated kinase (ERK) in mammalian cells. *The international journal of biochemistry & cell biology*, 40(12),

pp.2707–19. Available at: http://www.ncbi.nlm.nih.gov/pubmed/18562239 [Accessed September 28, 2015].

Readnower, R.D. et al., 2012. Standardized bioenergetic profiling of adult mouse cardiomyocytes. *Physiological genomics*, 44(24), pp.1208–13. Available at: http://www.ncbi.nlm.nih.gov/pubmed/23092951 [Accessed September 14, 2017].

Reiser, J. et al., 1996. Transduction of nondividing cells using pseudotyped defective high-titer HIV type 1 particles. *Proceedings of the National Academy of Sciences of the United States of America*, 93(26), pp.15266–71. Available at: http://www.ncbi.nlm.nih.gov/pubmed/8986799 [Accessed November 5, 2017].

Riley, T. et al., 2008. Transcriptional control of human p53-regulated genes. *Nature Reviews Molecular Cell Biology*, 9(5), pp.402–412. Available at: http://www.nature.com/articles/nrm2395 [Accessed January 10, 2018].

Rincón, M. & Davis, R.J., 2009. Regulation of the immune response by stress-activated protein kinases. *Immunological Reviews*, 228(1), pp.212–224. Available at: http://www.ncbi.nlm.nih.gov/pubmed/19290930 [Accessed January 11, 2018].

Robinton, D.A. & Daley, G.Q., 2012. The promise of induced pluripotent stem cells in research and therapy. *Nature*, 481(7381), pp.295–305. Available at: http://www.ncbi.nlm.nih.gov/pubmed/22258608 [Accessed November 3, 2017].

Rosca, M.G. & Hoppel, C.L., 2013. Mitochondrial dysfunction in heart failure. *Heart failure reviews*, 18(5), pp.607–22. Available at: http://www.ncbi.nlm.nih.gov/pubmed/22948484 [Accessed October 31, 2017].

Rose, B.A., Force, T. & Wang, Y., 2010. Mitogen-Activated Protein Kinase Signaling in the Heart: Angels Versus Demons in a Heart-Breaking Tale. *Physiological Reviews*, 90(4), pp.1507–1546. Available at: http://www.ncbi.nlm.nih.gov/pubmed/20959622 [Accessed November 3, 2017].

Roth Flach, R.J. et al., 2015. Endothelial protein kinase MAP4K4 promotes vascular inflammation and atherosclerosis. *Nature Communications*, 6, p.8995. Available at: http://www.ncbi.nlm.nih.gov/pubmed/26688060 [Accessed January 15, 2018].

Roth Flach, R.J. et al., 2017. Map4k4 impairs energy metabolism in endothelial cells and promotes insulin resistance in obesity. *American Journal of Physiology - Endocrinology And Metabolism*, 313(3), pp.E303–E313. Available at: http://www.ncbi.nlm.nih.gov/pubmed/28611026 [Accessed November 22, 2017].

Roth Flach, R.J. et al., 2016. Protein Kinase Mitogen-activated Protein Kinase Kinase Kinase Kinase 4 (MAP4K4) Promotes Obesity-induced Hyperinsulinemia. *The Journal of biological chemistry*, 291(31), pp.16221–30. Available at: http://www.ncbi.nlm.nih.gov/pubmed/27226575 [Accessed November 22, 2017].

Rothermel, B.A. & Hill, J.A., 2008. Autophagy in load-induced heart disease. *Circulation research*, 103(12), pp.1363–9. Available at: http://www.ncbi.nlm.nih.gov/pubmed/19059838 [Accessed October 17, 2017].

Rubinsztein, D.C., Shpilka, T. & Elazar, Z., 2012. Mechanisms of autophagosome biogenesis. *Current biology : CB*, 22(1), pp.R29-34. Available at: http://www.ncbi.nlm.nih.gov/pubmed/22240478 [Accessed August 17, 2015].

Sabbah, H., 2000. Apoptotic cell death in heart failure. *Cardiovascular Research*, 45(3), pp.704–712. Available at: https://academic.oup.com/cardiovascres/article-lookup/doi/10.1016/S0008-6363(99)00348-X [Accessed October 12, 2017].

Sabbah, H.N. et al., 1992. Mitochondrial abnormalities in myocardium of dogs with chronic heart failure. *Journal of molecular and cellular cardiology*, 24(11), pp.1333–47. Available at: http://www.ncbi.nlm.nih.gov/pubmed/1479624 [Accessed November 1, 2017].

Sadoshima, J. et al., 2002. The MEKK1-JNK pathway plays a protective role in pressure

overload but does not mediate cardiac hypertrophy. *The Journal of clinical investigation*, 110(2), pp.271–9. Available at: http://www.ncbi.nlm.nih.gov/pubmed/12122119 [Accessed January 12, 2018].

Sako, E.Y. et al., 1988. ATP synthesis kinetics and mitochondrial function in the postischemic myocardium as studied by 31P NMR. *The Journal of biological chemistry*, 263(22), pp.10600–7. Available at: http://www.ncbi.nlm.nih.gov/pubmed/3392029 [Accessed September 14, 2017].

Salmon, P. & Trono, D., 2007. Production and Titration of Lentiviral Vectors. In *Current Protocols in Human Genetics*. Hoboken, NJ, USA: John Wiley & Sons, Inc., p. Unit 12.10. Available at: http://www.ncbi.nlm.nih.gov/pubmed/18428406 [Accessed November 5, 2017].

Salmon, P. & Trono, D., 2006. Production and Titration of Lentiviral Vectors. In *Current Protocols in Neuroscience*. Hoboken, NJ, USA: John Wiley & Sons, Inc., p. Unit 4.21. Available at: http://www.ncbi.nlm.nih.gov/pubmed/18428637 [Accessed November 5, 2017].

Sánchez-Fernández, G. et al., 2014. Gαq signalling: The new and the old. *Cellular Signalling*, 26(5), pp.833–848. Available at: http://www.ncbi.nlm.nih.gov/pubmed/24440667 [Accessed October 20, 2017].

Sano, M. et al., 2004. Activation of cardiac Cdk9 represses PGC-1 and confers a predisposition to heart failure. *The EMBO journal*, 23(17), pp.3559–69. Available at: http://www.pubmedcentral.nih.gov/articlerender.fcgi?artid=516624&tool=pmcentrez&rendertype=abstract [Accessed September 6, 2015].

Sano, M. et al., 2007. p53-induced inhibition of Hif-1 causes cardiac dysfunction during pressure overload. *Nature*, 446(7134), pp.444–448. Available at: http://www.nature.com/doifinder/10.1038/nature05602 [Accessed October 17, 2017].

Sartorius, T. et al., 2012. Association of common genetic variants in the MAP4K4 locus with prediabetic traits in humans. *PloS one*, 7(10), p.e47647. Available at: http://www.pubmedcentral.nih.gov/articlerender.fcgi?artid=3475716&tool=pmcentrez&rendertype=abstract [Accessed September 6, 2015].

Sato, M. & Sato, K., 2013. Maternal inheritance of mitochondrial DNA by diverse mechanisms to eliminate paternal mitochondrial DNA. *Biochimica et Biophysica Acta (BBA) - Molecular Cell Research*, 1833(8), pp.1979–1984. Available at: http://www.ncbi.nlm.nih.gov/pubmed/23524114 [Accessed November 1, 2017].

Sawai, H. & Domae, N., 2011. Discrimination between primary necrosis and apoptosis by necrostatin-1 in Annexin V-positive/propidium iodide-negative cells. *Biochemical and Biophysical Research Communications*, 411(3), pp.569–573. Available at: http://www.ncbi.nlm.nih.gov/pubmed/21763280 [Accessed February 26, 2018].

Scarabelli, T. & Gottlieb, R., 2004. Functional and clinical repercussions of myocyte apoptosis in the multifaceted damage by ischemia/ reperfusion injury: old and new concepts after 10 years of contributions. *Cell Death and Differentiation*, 11, pp.144–152. Available at: https://www.nature.com/cdd/journal/v11/n2s/pdf/4401544a.pdf?origin=ppub [Accessed November 2, 2017].

Schaaf, S. et al., 2011. Human Engineered Heart Tissue as a Versatile Tool in Basic Research and Preclinical Toxicology L. J. de Windt, ed. *PLoS ONE*, 6(10), p.e26397. Available at: http://www.ncbi.nlm.nih.gov/pubmed/22028871 [Accessed October 31, 2017].

Schaper, J., Meiser, E. & Stämmler, G., 1985. Ultrastructural morphometric analysis of myocardium from dogs, rats, hamsters, mice, and from human hearts. *Circulation research*, 56(3), pp.377–91. Available at: http://www.ncbi.nlm.nih.gov/pubmed/3882260 [Accessed November 1, 2017].

Scherz-Shouval, R. et al., 2007. Reactive oxygen species are essential for autophagy and specifically regulate the activity of Atg4. *The EMBO Journal*, 26(7), pp.1749–1760. Available at: http://www.ncbi.nlm.nih.gov/pubmed/17347651 [Accessed February 21, 2018].

Scheubel, R.J. et al., 2002. Apoptotic pathway activation from mitochondria and death receptors without caspase-3 cleavage in failing human myocardium: fragile balance of myocyte survival? *Journal of the American College of Cardiology*, 39(3), pp.481–8. Available at: http://www.ncbi.nlm.nih.gov/pubmed/11823087 [Accessed September 6, 2015].

Schirone, L. et al., 2017. A Review of the Molecular Mechanisms Underlying the Development and Progression of Cardiac Remodeling. *Oxidative Medicine and Cellular Longevity*, 2017, pp.1–16. Available at: https://www.hindawi.com/journals/omcl/2017/3920195/ [Accessed October 17, 2017].

Schwaid, A.G. et al., 2015. MAP4K4 Is a Threonine Kinase That Phosphorylates FARP1. *ACS Chemical Biology*, 10(12), pp.2667–2671. Available at: http://www.ncbi.nlm.nih.gov/pubmed/26422651 [Accessed January 15, 2018].

Sciarretta, S. et al., 2011. Is autophagy in response to ischemia and reperfusion protective or detrimental for the heart? *Pediatric cardiology*, 32(3), pp.275–81. Available at: http://www.ncbi.nlm.nih.gov/pubmed/21170742 [Accessed December 5, 2017].

Sciarretta, S. et al., 2012. Pharmacological modulation of autophagy during cardiac stress. *Journal of cardiovascular pharmacology*, 60(3), pp.235–41. Available at: http://www.ncbi.nlm.nih.gov/pubmed/22710813 [Accessed December 5, 2017].

Sebastiani, M. et al., 2007. Induction of Mitochondrial Biogenesis Is a Maladaptive Mechanism in Mitochondrial Cardiomyopathies. *Journal of the American College of Cardiology*, 50(14), pp.1362–1369. Available at:

http://www.ncbi.nlm.nih.gov/pubmed/17903636 [Accessed November 1, 2017].

Segers, V.F.M. & Lee, R.T., 2008. Stem-cell therapy for cardiac disease. *Nature*, 451(7181), pp.937–942. Available at: http://www.nature.com/doifinder/10.1038/nature06800 [Accessed October 17, 2017].

Seidman, J.G. & Seidman, C., 2001. The genetic basis for cardiomyopathy: from mutation identification to mechanistic paradigms. *Cell*, 104(4), pp.557–67. Available at: http://www.ncbi.nlm.nih.gov/pubmed/11239412 [Accessed October 17, 2017].

Sekine, H. et al., 2008. Endothelial Cell Coculture Within Tissue-Engineered Cardiomyocyte Sheets Enhances Neovascularization and Improves Cardiac Function of Ischemic Hearts. *Circulation*, 118(14_suppl_1), pp.S145–S152. Available at: http://www.ncbi.nlm.nih.gov/pubmed/18824746 [Accessed February 25, 2018].

Selker, H.P. et al., 2017. Relationship between therapeutic effects on infarct size in acute myocardial infarction and therapeutic effects on 1-year outcomes: A patient-level analysis of randomized clinical trials. *American Heart Journal*, 188, pp.18–25. Available at: http://www.ncbi.nlm.nih.gov/pubmed/28577674 [Accessed February 20, 2018].

Shao, Z. et al., 2005. c-Jun N-Terminal Kinases Mediate Reactivation of Akt and Cardiomyocyte Survival After Hypoxic Injury In Vitro and In Vivo. *Circulation Research*, 98(1), pp.111–118. Available at: http://www.ncbi.nlm.nih.gov/pubmed/16306447 [Accessed January 15, 2018].

Sharrocks, A.D., Yang, S.H. & Galanis, A., 2000. Docking domains and substrate-specificity determination for MAP kinases. *Trends in biochemical sciences*, 25(9), pp.448–53. Available at: http://www.ncbi.nlm.nih.gov/pubmed/10973059 [Accessed November 3, 2017].

Shchemelinin, I., Sefc, L. & Necas, E., 2006. Protein kinases, their function and implication in cancer and other diseases. *Folia biologica*, 52(3), pp.81–100. Available at:

http://www.ncbi.nlm.nih.gov/pubmed/17089919 [Accessed November 3, 2017].

Shi, Y. et al., 2016. Induced pluripotent stem cell technology: a decade of progress. *Nature Reviews Drug Discovery*, 16(2), pp.115–130. Available at: http://www.nature.com/doifinder/10.1038/nrd.2016.245 [Accessed October 31, 2017].

Simoons, M.L. et al., 1986. Early thrombolysis in acute myocardial infarction: Limitation of infarct size and improved survival. *Journal of the American College of Cardiology*, 7(4), pp.717–728. Available at: http://content.onlinejacc.org/article.aspx?articleid=1111886 [Accessed September 14, 2015].

Sin, Y.Y. & Baillie, G.S., 2012. Protein kinase D in the hypertrophy pathway: Figure 1. *Biochemical Society Transactions*, 40(1), pp.287–289. Available at: http://www.ncbi.nlm.nih.gov/pubmed/22260707 [Accessed November 3, 2017].

Sinha, S. & Levine, B., 2008. The autophagy effector Beclin 1: a novel BH3-only protein. *Oncogene*, 27 Suppl 1, pp.S137-48. Available at: http://www.pubmedcentral.nih.gov/articlerender.fcgi?artid=2731580&tool=pmcentrez&rendertype=abstract [Accessed September 6, 2015].

Sivasubramanian, N. et al., 2001. Left ventricular remodeling in transgenic mice with cardiac restricted overexpression of tumor necrosis factor. *Circulation*, 104(7), pp.826–31. Available at: http://www.ncbi.nlm.nih.gov/pubmed/11502710 [Accessed September 6, 2015].

Slezak, J. et al., 1995. Hydrogen peroxide changes in ischemic and reperfused heart. Cytochemistry and biochemical and X-ray microanalysis. *The American journal of pathology*, 147(3), pp.772–81. Available at: http://www.pubmedcentral.nih.gov/articlerender.fcgi?artid=1870993&tool=pmcentrez&rendertype=abstract [Accessed September 28, 2015].

Smith, C.C.T. et al., 2007. Necrostatin: A Potentially Novel Cardioprotective Agent?

Cardiovascular Drugs and Therapy, 21(4), pp.227–233. Available at: http://www.ncbi.nlm.nih.gov/pubmed/17665295 [Accessed November 3, 2017].

Smith, D.R., Stone, D. & Darley-Usmar, V.M., 1996. Stimulation of mitochondrial oxygen consumption in isolated cardiomyocytes after hypoxia-reoxygenation. *Free radical research*, 24(3), pp.159–66. Available at: http://www.ncbi.nlm.nih.gov/pubmed/8728117 [Accessed September 14, 2017].

Somers, A. et al., 2010. Generation of Transgene-Free Lung Disease-Specific Human Induced Pluripotent Stem Cells Using a Single Excisable Lentiviral Stem Cell Cassette. *STEM CELLS*, 28(10), pp.1728–1740. Available at: http://www.ncbi.nlm.nih.gov/pubmed/20715179 [Accessed November 3, 2017].

Song, Z.-F. et al., 2008. Inhibition of the activity of poly (ADP-ribose) polymerase reduces heart ischaemia/reperfusion injury via suppressing JNK-mediated AIF translocation. *Journal of cellular and molecular medicine*, 12(4), pp.1220–8. Available at: http://www.ncbi.nlm.nih.gov/pubmed/18782186 [Accessed January 15, 2018].

Spach, M.S. et al., 2004. Cell size and communication: Role in structural and electrical development and remodeling of the heart. *Heart Rhythm*, 1(4), pp.500–515. Available at: http://www.ncbi.nlm.nih.gov/pubmed/15851207 [Accessed January 22, 2018].

Stein, G.Y. et al., 2014. Type-II myocardial infarction--patient characteristics, management and outcomes. *PloS one*, 9(1), p.e84285. Available at: http://www.ncbi.nlm.nih.gov/pubmed/24392121 [Accessed November 14, 2017].

Stoehr, A. et al., 2014. Automated analysis of contractile force and Ca2+ transients in engineered heart tissue. *AJP: Heart and Circulatory Physiology*, 306(9), pp.H1353–H1363. Available at: http://www.ncbi.nlm.nih.gov/pubmed/24585781 [Accessed September 9, 2017].

Stoka, V. et al., 2001. Lysosomal Protease Pathways to Apoptosis. *Journal of Biological*

Chemistry, 276(5), pp.3149–3157. Available at: http://www.ncbi.nlm.nih.gov/pubmed/11073962 [Accessed January 9, 2018].

Stone, G.W. et al., 2016. Relationship Between Infarct Size and Outcomes Following Primary PCI. *Journal of the American College of Cardiology*, 67(14), pp.1674–1683. Available at: http://www.ncbi.nlm.nih.gov/pubmed/27056772 [Accessed February 20, 2018].

Stosiek, C. et al., 2003. In vivo two-photon calcium imaging of neuronal networks. *Proceedings of the National Academy of Sciences*, 100(12), pp.7319–7324. Available at: http://www.ncbi.nlm.nih.gov/pubmed/12777621 [Accessed February 27, 2018].

Strauer, B.E., 1987. Cardiac energetics in clinical heart disease. *Basic research in cardiology*, 82 Suppl 2, pp.389–402. Available at: http://www.ncbi.nlm.nih.gov/pubmed/2959264 [Accessed September 14, 2017].

Strömbäck, U. et al., 2017. The second myocardial infarction: Higher risk factor burden and earlier second myocardial infarction in women compared with men. The Northern Sweden MONICA study. *European Journal of Cardiovascular Nursing*, 16(5), pp.418–424. Available at: http://journals.sagepub.com/doi/10.1177/1474515116686229 [Accessed November 14, 2017].

Strzyz, P., 2017. Cell death: Pulling the apoptotic trigger for necrosis. *Nature Reviews Molecular Cell Biology*, 18(2), pp.72–72. Available at: http://www.nature.com/doifinder/10.1038/nrm.2017.1 [Accessed December 5, 2017].

Su, Y.C. et al., 1997. NIK is a new Ste20-related kinase that binds NCK and MEKK1 and activates the SAPK/JNK cascade via a conserved regulatory domain. *The EMBO journal*, 16(6), pp.1279–90. Available at: http://www.ncbi.nlm.nih.gov/pubmed/9135144 [Accessed January 15, 2018].

Suliman, H.B. & Piantadosi, C.A., 2015. Mitochondrial Quality Control as a Therapeutic

Target. *Pharmacological Reviews*, 68(1), pp.20–48. Available at: http://www.ncbi.nlm.nih.gov/pubmed/26589414 [Accessed November 1, 2017].

Sun, L. et al., 2012. Mixed Lineage Kinase Domain-like Protein Mediates Necrosis Signaling Downstream of RIP3 Kinase. *Cell*, 148(1–2), pp.213–227. Available at: http://www.ncbi.nlm.nih.gov/pubmed/22265413 [Accessed December 5, 2017].

Susin, S.A. et al., 1999. Molecular characterization of mitochondrial apoptosis-inducing factor. *Nature*, 397(6718), pp.441–446. Available at: http://www.ncbi.nlm.nih.gov/pubmed/9989411 [Accessed January 9, 2018].

Susin, S.A. et al., 2000. Two distinct pathways leading to nuclear apoptosis. *The Journal of experimental medicine*, 192(4), pp.571–80. Available at: http://www.ncbi.nlm.nih.gov/pubmed/10952727 [Accessed January 9, 2018].

Suzuki, M., Youle, R.J. & Tjandra, N., 2000. Structure of Bax: coregulation of dimer formation and intracellular localization. *Cell*, 103(4), pp.645–54. Available at: http://www.ncbi.nlm.nih.gov/pubmed/11106734 [Accessed November 2, 2017].

Suzuki, Y. et al., 2001. A serine protease, HtrA2, is released from the mitochondria and interacts with XIAP, inducing cell death. *Molecular cell*, 8(3), pp.613–21. Available at: http://www.ncbi.nlm.nih.gov/pubmed/11583623 [Accessed January 9, 2018].

Suzuki, Y., Nakabayashi, Y. & Takahashi, R., 2001. Ubiquitin-protein ligase activity of X-linked inhibitor of apoptosis protein promotes proteasomal degradation of caspase-3 and enhances its anti-apoptotic effect in Fas-induced cell death. *Proceedings of the National Academy of Sciences*, 98(15), pp.8662–8667. Available at: http://www.ncbi.nlm.nih.gov/pubmed/11447297 [Accessed January 10, 2018].

Sy, J.C. et al., 2008. Sustained release of a p38 inhibitor from non-inflammatory microspheres inhibits cardiac dysfunction. *Nature materials*, 7(11), pp.863–8. Available at:

http://www.pubmedcentral.nih.gov/articlerender.fcgi?artid=2705946&tool=pmcentrez&rendertype=abstract [Accessed September 28, 2015].

Szobi, A. et al., 2017. Analysis of necroptotic proteins in failing human hearts. *Journal of translational medicine*, 15(1), p.86. Available at: http://www.ncbi.nlm.nih.gov/pubmed/28454582 [Accessed January 9, 2018].

Taabazuing, C.Y., Okondo, M.C. & Bachovchin, D.A., 2017. Pyroptosis and Apoptosis Pathways Engage in Bidirectional Crosstalk in Monocytes and Macrophages. *Cell chemical biology*, 24(4), p.507–514.e4. Available at: http://www.ncbi.nlm.nih.gov/pubmed/28392147 [Accessed January 9, 2018].

Tachibana, H. et al., 2006. JNK1 is required to preserve cardiac function in the early response to pressure overload. *Biochemical and Biophysical Research Communications*, 343(4), pp.1060–1066. Available at: http://www.ncbi.nlm.nih.gov/pubmed/16579967 [Accessed January 15, 2018].

Takahashi, K. et al., 2007. Induction of Pluripotent Stem Cells from Adult Human Fibroblasts by Defined Factors. *Cell*, 131(5), pp.861–872. Available at: http://www.ncbi.nlm.nih.gov/pubmed/18035408 [Accessed October 31, 2017].

Takahashi, K. & Yamanaka, S., 2006. Induction of Pluripotent Stem Cells from Mouse Embryonic and Adult Fibroblast Cultures by Defined Factors. *Cell*, 126(4), pp.663–676. Available at: http://www.ncbi.nlm.nih.gov/pubmed/16904174 [Accessed November 3, 2017].

Tang, X. et al., 2006. An RNA interference-based screen identifies MAP4K4/NIK as a negative regulator of PPAR , adipogenesis, and insulin-responsive hexose transport. *Proceedings of the National Academy of Sciences*, 103(7), pp.2087–2092. Available at: http://www.ncbi.nlm.nih.gov/pubmed/16461467 [Accessed January 15, 2018].

Tannous, P. et al., 2008. Autophagy is an adaptive response in desmin-related

cardiomyopathy. *Proceedings of the National Academy of Sciences of the United States of America*, 105(28), pp.9745–50. Available at: http://www.pnas.org/content/105/28/9745 [Accessed September 6, 2015].

Teekakirikul, P. et al., 2010. Cardiac fibrosis in mice with hypertrophic cardiomyopathy is mediated by non-myocyte proliferation and requires Tgf-β. *Journal of Clinical Investigation*, 120(10), pp.3520–3529. Available at: http://www.ncbi.nlm.nih.gov/pubmed/20811150 [Accessed November 3, 2017].

Thavandiran, N. et al., 2013. Design and formulation of functional pluripotent stem cell-derived cardiac microtissues. *Proceedings of the National Academy of Sciences*, 110(49), pp.E4698–E4707. Available at: http://www.ncbi.nlm.nih.gov/pubmed/24255110 [Accessed October 31, 2017].

Thomas, R.L. & Gustafsson, A.B., 2013. Mitochondrial autophagy--an essential quality control mechanism for myocardial homeostasis. *Circulation journal : official journal of the Japanese Circulation Society*, 77(10), pp.2449–54. Available at: http://www.ncbi.nlm.nih.gov/pubmed/23985961 [Accessed November 1, 2017].

Townsend, N. et al., 2016. Cardiovascular disease in Europe: epidemiological update 2016. *European Heart Journal*, 37(42), pp.3232–3245. Available at: https://academic.oup.com/eurheartj/article-lookup/doi/10.1093/eurheartj/ehw334 [Accessed October 16, 2017].

Tsujimoto, Y. et al., 1999. Bcl-2 family proteins regulate the release of apoptogenic cytochrome c by the mitochondrial channel VDAC. *Nature*, 399(6735), pp.483–487. Available at: http://www.nature.com/doifinder/10.1038/20959 [Accessed November 2, 2017].

Tulloch, N.L. et al., 2011. Growth of Engineered Human Myocardium With Mechanical Loading and Vascular Coculture. *Circulation Research*, 109(1), pp.47–59. Available at:

http://www.ncbi.nlm.nih.gov/pubmed/21597009 [Accessed October 31, 2017].

Tzatzalos, E. et al., 2016. Engineered heart tissues and induced pluripotent stem cells: Macro- and microstructures for disease modeling, drug screening, and translational studies. *Advanced Drug Delivery Reviews*, 96, pp.234–244. Available at: http://www.ncbi.nlm.nih.gov/pubmed/26428619 [Accessed August 7, 2017].

Ursitti, J.A. et al., 2007. Role of an alternatively spliced form of alphaII-spectrin in localization of connexin 43 in cardiomyocytes and regulation by stress-activated protein kinase. *Journal of molecular and cellular cardiology*, 42(3), pp.572–81. Available at: http://www.ncbi.nlm.nih.gov/pubmed/17276456 [Accessed November 3, 2017].

Uzun, A.U. et al., 2016. Ca2+-Currents in Human Induced Pluripotent Stem Cell-Derived Cardiomyocytes Effects of Two Different Culture Conditions. *Frontiers in Pharmacology*, 7, p.300. Available at: http://www.ncbi.nlm.nih.gov/pubmed/27672365 [Accessed October 31, 2017].

Vandenburgh, H. et al., 2008. Drug-screening platform based on the contractility of tissue-engineered muscle. *Muscle & Nerve*, 37(4), pp.438–447. Available at: http://www.ncbi.nlm.nih.gov/pubmed/18236465 [Accessed November 6, 2017].

Varfolomeev, E.E. et al., 1998. Targeted disruption of the mouse Caspase 8 gene ablates cell death induction by the TNF receptors, Fas/Apo1, and DR3 and is lethal prenatally. *Immunity*, 9(2), pp.267–76. Available at: http://www.ncbi.nlm.nih.gov/pubmed/9729047 [Accessed November 2, 2017].

Vaseva, A.V. et al., 2012. p53 Opens the Mitochondrial Permeability Transition Pore to Trigger Necrosis. *Cell*, 149(7), pp.1536–1548. Available at: http://www.ncbi.nlm.nih.gov/pubmed/22726440 [Accessed January 10, 2018].

van der Velden, J. et al., 1998. Force production in mechanically isolated cardiac myocytes from human ventricular muscle tissue. *Cardiovascular research*, 38(2), pp.414–23.

Available at: http://www.ncbi.nlm.nih.gov/pubmed/9709402 [Accessed January 22, 2018].

Verkerk, A.O. et al., 2017. Patch-Clamp Recording from Human Induced Pluripotent Stem Cell-Derived Cardiomyocytes: Improving Action Potential Characteristics through Dynamic Clamp. *International journal of molecular sciences*, 18(9). Available at: http://www.ncbi.nlm.nih.gov/pubmed/28867785 [Accessed November 8, 2017].

Virbasius, J. V & Czech, M.P., 2016. Map4k4 Signaling Nodes in Metabolic and Cardiovascular Diseases. *Trends in endocrinology and metabolism: TEM*, 27(7), pp.484–92. Available at: http://www.ncbi.nlm.nih.gov/pubmed/27160798 [Accessed September 11, 2016].

Vitorino, P. et al., 2015. MAP4K4 regulates integrin-FERM binding to control endothelial cell motility. *Nature*, 519(7544), pp.425–430. Available at: http://www.ncbi.nlm.nih.gov/pubmed/25799996 [Accessed January 15, 2018].

Wagoner Johnson, A. & Harley, B.A., 2011. *Mechanobiology of cell-cell and cell-matrix interactions*, Springer. Available at: https://books.google.co.uk/books?id=UH_PAFlbF9sC&pg=PA95&dq=fibroblast+in+eht&hl=en&sa=X&ved=0ahUKEwje4PXJ4cXVAhWsKsAKHSsVAu4Q6AEIKDAA#v=onepage&q=fibroblast in eht&f=false [Accessed August 7, 2017].

Wan, Y.Y. et al., 2006. The kinase TAK1 integrates antigen and cytokine receptor signaling for T cell development, survival and function. *Nature Immunology*, 7(8), pp.851–858. Available at: http://www.ncbi.nlm.nih.gov/pubmed/16799562 [Accessed November 3, 2017].

Wang, H. et al., 2016. Global, regional, and national life expectancy, all-cause mortality, and cause-specific mortality for 249 causes of death, 1980–2015: a systematic analysis for the Global Burden of Disease Study 2015. *The Lancet*, 388(10053), pp.1459–1544.

Available at: http://www.ncbi.nlm.nih.gov/pubmed/27733281 [Accessed November 14, 2017].

Wang, J. & Lenardo, M.J., 2000. Roles of caspases in apoptosis, development, and cytokine maturation revealed by homozygous gene deficiencies. *Journal of cell science*, 113 (Pt 5), pp.753–7. Available at: http://www.ncbi.nlm.nih.gov/pubmed/10671365 [Accessed November 2, 2017].

Wang, L., Du, F. & Wang, X., 2008. TNF-alpha induces two distinct caspase-8 activation pathways. *Cell*, 133(4), pp.693–703. Available at: http://www.ncbi.nlm.nih.gov/pubmed/18485876 [Accessed April 20, 2015].

Wang, M. et al., 2013. Identification of Map4k4 as a Novel Suppressor of Skeletal Muscle Differentiation. *Molecular and Cellular Biology*, 33(4), pp.678–687. Available at: http://www.ncbi.nlm.nih.gov/pubmed/23207904 [Accessed January 15, 2018].

Wang, Y. et al., 1998. Cardiac hypertrophy induced by mitogen-activated protein kinase kinase 7, a specific activator for c-Jun NH2-terminal kinase in ventricular muscle cells. *The Journal of biological chemistry*, 273(10), pp.5423–6. Available at: http://www.ncbi.nlm.nih.gov/pubmed/9488659 [Accessed November 3, 2017].

Wang, Y. et al., 2012. Genetic correction of β-thalassemia patient-specific iPS cells and its use in improving hemoglobin production in irradiated SCID mice. *Cell Research*, 22(4), pp.637–648. Available at: http://www.nature.com/doifinder/10.1038/cr.2012.23 [Accessed November 3, 2017].

Wang, Y., 2007. Mitogen-Activated Protein Kinases in Heart Development and Diseases. *Circulation*, 116(12), pp.1413–1423. Available at: http://www.ncbi.nlm.nih.gov/pubmed/17875982 [Accessed November 3, 2017].

Wei, J. et al., 2011. c-Jun N-terminal Kinase (JNK-1) Confers Protection against Brief but Not Extended Ischemia during Acute Myocardial Infarction. *Journal of Biological*

Chemistry, 286(16), pp.13995–14006. Available at: http://www.ncbi.nlm.nih.gov/pubmed/21324895 [Accessed January 15, 2018].

Wei, M.C. et al., 2000. tBID, a membrane-targeted death ligand, oligomerizes BAK to release cytochrome c. *Genes & development*, 14(16), pp.2060–71. Available at: http://www.ncbi.nlm.nih.gov/pubmed/10950869 [Accessed November 2, 2017].

Wencker, D. et al., 2003. A mechanistic role for cardiac myocyte apoptosis in heart failure. *The Journal of clinical investigation*, 111(10), pp.1497–504. Available at: http://www.ncbi.nlm.nih.gov/pubmed/12750399 [Accessed November 2, 2017].

Whelan, R.S., Kaplinskiy, V. & Kitsis, R.N., 2010. Cell death in the pathogenesis of heart disease: mechanisms and significance. *Annual review of physiology*, 72, pp.19–44.

White, B.J. et al., 2012. Protection from cerebral ischemia by inhibition of TGFβ-activated kinase. *Experimental neurology*, 237(1), pp.238–45. Available at: http://www.ncbi.nlm.nih.gov/pubmed/22683931 [Accessed November 23, 2017].

White, H.D. & Chew, D.P., 2008. Acute myocardial infarction. *Lancet*, 372(9638), pp.570–84. Available at: http://www.ncbi.nlm.nih.gov/pubmed/18707987 [Accessed May 13, 2015].

Wilkins E, Wilson L, Wickramasinghe K, Bhatnagar P, Leal J, Luengo-Fernandez R, Burns R, Rayner M, T.N., 2017. *CVD Statistics*, Available at: http://www.ehnheart.org/cvd-statistics.html [Accessed October 16, 2017].

Willems, E., Bushway, P.J. & Mercola, M., 2009. Natural and synthetic regulators of embryonic stem cell cardiogenesis. *Pediatric cardiology*, 30(5), pp.635–42. Available at: http://www.ncbi.nlm.nih.gov/pubmed/19319460 [Accessed November 5, 2017].

Wlodkowic, D. et al., 2013. Kinetic viability assays using DRAQ7 probe. *Current protocols in cytometry / editorial board, J. Paul Robinson, managing editor ... [et al.]*, Chapter 9, p.Unit 9.41. Available at:

http://www.pubmedcentral.nih.gov/articlerender.fcgi?artid=3873765&tool=pmcentrez&rendertype=abstract [Accessed September 16, 2015].

Wright, J.H. et al., 2003. The STE20 kinase HGK is broadly expressed in human tumor cells and can modulate cellular transformation, invasion, and adhesion. *Molecular and cellular biology*, 23(6), pp.2068–82. Available at: http://www.ncbi.nlm.nih.gov/pubmed/12612079 [Accessed January 15, 2018].

Wu, W. et al., 2011. Mitogen-Activated Protein Kinase Inhibitors Improve Heart Function and Prevent Fibrosis in Cardiomyopathy Caused by Mutation in Lamin A/C Gene. *Circulation*, 123(1), pp.53–61. Available at: http://www.ncbi.nlm.nih.gov/pubmed/21173351 [Accessed February 22, 2018].

Xia, X. et al., 2007. Transgenes Delivered by Lentiviral Vector are Suppressed in Human Embryonic Stem Cells in A Promoter-Dependent Manner. *Stem Cells and Development*, 16(1), pp.167–176. Available at: http://www.ncbi.nlm.nih.gov/pubmed/17348812 [Accessed September 12, 2017].

Xie, M. et al., 2007. Abstract 1949: The Protein Kinase MAP4K4 Is Activated in Failing Human Hearts and Mediates Cardiomyocyte Apoptosis in Experimental Models, in vitro and in vivo. *Circulation*, 116(Suppl 16). Available at: http://circ.ahajournals.org/content/116/Suppl_16/II_420.1 [Accessed November 2, 2017].

Xie, M., Burchfield, J.S. & Hill, J.A., 2013. Pathological ventricular remodeling: mechanisms: part 1 of 2. *Circulation*, 128(4), pp.388–400. Available at: http://www.ncbi.nlm.nih.gov/pubmed/23877061 [Accessed December 5, 2017].

Xie, Y. et al., 2016. Ferroptosis: process and function. *Cell Death & Differentiation*, 23(3), pp.369–379. Available at: http://www.ncbi.nlm.nih.gov/pubmed/26794443 [Accessed January 9, 2018].

Xue, Y. et al., 2001. Mesodermal patterning defect in mice lacking the Ste20 NCK interacting kinase (NIK). *Development (Cambridge, England)*, 128(9), pp.1559–72. Available at: http://www.ncbi.nlm.nih.gov/pubmed/11290295 [Accessed September 15, 2015].

Yamada, M. et al., 2016. Genetic Drift Can Compromise Mitochondrial Replacement by Nuclear Transfer in Human Oocytes. *Cell Stem Cell*, 18(6), pp.749–754. Available at: http://www.ncbi.nlm.nih.gov/pubmed/27212703 [Accessed December 5, 2017].

Yamaguchi, O. et al., 2004. Cardiac-specific disruption of the c-raf-1 gene induces cardiac dysfunction and apoptosis. *Journal of Clinical Investigation*, 114(7), pp.937–943. Available at: http://www.ncbi.nlm.nih.gov/pubmed/15467832 [Accessed November 3, 2017].

Yamaguchi, O. et al., 2003. Targeted deletion of apoptosis signal-regulating kinase 1 attenuates left ventricular remodeling. *Proceedings of the National Academy of Sciences*, 100(26), pp.15883–15888. Available at: http://www.ncbi.nlm.nih.gov/pubmed/14665690 [Accessed June 24, 2018].

Yan, W. et al., 2001. The Nck-interacting Kinase (NIK) Phosphorylates the Na^+-H^+ Exchanger NHE1 and Regulates NHE1 Activation by Platelet-derived Growth Factor. *Journal of Biological Chemistry*, 276(33), pp.31349–31356. Available at: http://www.ncbi.nlm.nih.gov/pubmed/11369779 [Accessed January 15, 2018].

Yang, L. et al., 2008. Human cardiovascular progenitor cells develop from a KDR+ embryonic-stem-cell-derived population. *Nature*, 453(7194), pp.524–528. Available at: http://www.ncbi.nlm.nih.gov/pubmed/18432194 [Accessed November 3, 2017].

Yang, W. et al., 2003. MX1013, a dipeptide caspase inhibitor with potent in vivo antiapoptotic activity. *British journal of pharmacology*, 140(2), pp.402–12. Available at: http://www.pubmedcentral.nih.gov/articlerender.fcgi?artid=1574042&tool=pmcentrez&rendertype=abstract [Accessed September 6, 2015].

Yang, X., Pabon, L. & Murry, C.E., 2014. Engineering Adolescence: Maturation of Human Pluripotent Stem Cell-Derived Cardiomyocytes. *Circulation Research*, 114(3), pp.511–523. Available at: http://www.ncbi.nlm.nih.gov/pubmed/24481842 [Accessed January 16, 2018].

Yang, Y. et al., 2000. Ubiquitin protein ligase activity of IAPs and their degradation in proteasomes in response to apoptotic stimuli. *Science (New York, N.Y.)*, 288(5467), pp.874–7. Available at: http://www.ncbi.nlm.nih.gov/pubmed/10797013 [Accessed January 10, 2018].

Yao, S. et al., 2006. Long-term self-renewal and directed differentiation of human embryonic stem cells in chemically defined conditions. *Proceedings of the National Academy of Sciences*, 103(18), pp.6907–6912. Available at: http://www.ncbi.nlm.nih.gov/pubmed/16632596 [Accessed November 3, 2017].

Yao, Z. et al., 1999. A novel human STE20-related protein kinase, HGK, that specifically activates the c-Jun N-terminal kinase signaling pathway. *The Journal of biological chemistry*, 274(4), pp.2118–25. Available at: http://www.ncbi.nlm.nih.gov/pubmed/9890973 [Accessed September 28, 2015].

Yaoita, H. et al., 1998. Attenuation of ischemia/reperfusion injury in rats by a caspase inhibitor. *Circulation*, 97(3), pp.276–81. Available at: http://www.ncbi.nlm.nih.gov/pubmed/9462530 [Accessed September 6, 2015].

Yoon, S. et al., 2016. Necroptosis is preceded by nuclear translocation of the signaling proteins that induce it. *Cell Death & Differentiation*, 23(2), pp.253–260. Available at: http://www.nature.com/articles/cdd201592 [Accessed February 26, 2018].

Yoshii, S.R. & Mizushima, N., 2017. Monitoring and Measuring Autophagy. *International journal of molecular sciences*, 18(9). Available at: http://www.ncbi.nlm.nih.gov/pubmed/28846632 [Accessed February 26, 2018].

Youle, R.J. & Strasser, A., 2008. The BCL-2 protein family: opposing activities that mediate cell death. *Nature Reviews Molecular Cell Biology*, 9(1), pp.47–59. Available at: http://www.ncbi.nlm.nih.gov/pubmed/18097445 [Accessed January 10, 2018].

Yu, J. et al., 2011. Efficient Feeder-Free Episomal Reprogramming with Small Molecules M. Pera, ed. *PLoS ONE*, 6(3), p.e17557. Available at: http://dx.plos.org/10.1371/journal.pone.0017557 [Accessed November 3, 2017].

Yu, J. et al., 2007. Induced Pluripotent Stem Cell Lines Derived from Human Somatic Cells. *Science*, 318(5858), pp.1917–1920. Available at: http://www.ncbi.nlm.nih.gov/pubmed/18029452 [Accessed October 31, 2017].

Yu, X. et al., 2005. A Structure of the Human Apoptosome at 12.8 Å Resolution Provides Insights into This Cell Death Platform. *Structure*, 13(11), pp.1725–1735. Available at: http://www.ncbi.nlm.nih.gov/pubmed/16271896 [Accessed November 2, 2017].

Yu, Y. et al., 2008. Phosphorylation of Thr-178 and Thr-184 in the TAK1 T-loop Is Required for Interleukin (IL)-1-mediated Optimal NFκB and AP-1 Activation as Well as IL-6 Gene Expression. *Journal of Biological Chemistry*, 283(36), pp.24497–24505. Available at: http://www.ncbi.nlm.nih.gov/pubmed/18617512 [Accessed November 3, 2017].

Yue, J. et al., 2014. Microtubules regulate focal adhesion dynamics through MAP4K4. *Developmental cell*, 31(5), pp.572–85. Available at: http://www.cell.com/article/S1534580714006911/fulltext [Accessed September 29, 2015].

Yussman, M.G. et al., 2002. Mitochondrial death protein Nix is induced in cardiac hypertrophy and triggers apoptotic cardiomyopathy. *Nature medicine*, 8(7), pp.725–30. Available at: http://www.ncbi.nlm.nih.gov/pubmed/12053174 [Accessed September 6, 2015].

Zavada, J., 1982. The Pseudotypic Paradox. *J. gen. Virol*, 63, pp.15–24. Available at:

http://www.microbiologyresearch.org/docserver/fulltext/jgv/63/1/JV0630010015.pdf?expires=1509903021&id=id&accname=guest&checksum=5F876AC6DC00DB44083A38EA2DC02D46 [Accessed November 5, 2017].

Zhang, D. et al., 2000. TAK1 is activated in the myocardium after pressure overload and is sufficient to provoke heart failure in transgenic mice. *Nature medicine*, 6(5), pp.556–63. Available at: http://www.ncbi.nlm.nih.gov/pubmed/10802712 [Accessed September 6, 2015].

Zhang, D. et al., 2013. Tissue-engineered cardiac patch for advanced functional maturation of human ESC-derived cardiomyocytes. *Biomaterials*, 34(23), pp.5813–5820. Available at: http://www.ncbi.nlm.nih.gov/pubmed/23642535 [Accessed January 16, 2018].

Zhang, J. et al., 2009. Functional Cardiomyocytes Derived From Human Induced Pluripotent Stem Cells. *Circulation Research*, 104(4), pp.e30–e41. Available at: http://www.ncbi.nlm.nih.gov/pubmed/19213953 [Accessed November 5, 2017].

Zhang, J. et al., 2009. Inhibition of the activity of Rho-kinase reduces cardiomyocyte apoptosis in heart ischemia/reperfusion via suppressing JNK-mediated AIF translocation. *Clinica Chimica Acta*, 401(1–2), pp.76–80. Available at: http://www.ncbi.nlm.nih.gov/pubmed/19061880 [Accessed January 15, 2018].

Zhang, Y. et al., 2015. Potent Paracrine Effects of human induced Pluripotent Stem Cell-derived Mesenchymal Stem Cells Attenuate Doxorubicin-induced Cardiomyopathy. *Scientific Reports*, 5(1), p.11235. Available at: http://www.ncbi.nlm.nih.gov/pubmed/26057572 [Accessed February 26, 2018].

Zhao, J. et al., 2012. Mixed lineage kinase domain-like is a key receptor interacting protein 3 downstream component of TNF-induced necrosis. *Proceedings of the National Academy of Sciences of the United States of America*, 109(14), pp.5322–7. Available at: http://www.ncbi.nlm.nih.gov/pubmed/22421439 [Accessed December 5, 2017].

Zhao, L. & Zhang, B., 2017. Doxorubicin induces cardiotoxicity through upregulation of death receptors mediated apoptosis in cardiomyocytes. *Scientific Reports*, 7, p.44735. Available at: http://www.ncbi.nlm.nih.gov/pubmed/28300219 [Accessed March 23, 2017].

Zheng, Y. et al., 2015. Identification of Happyhour/MAP4K as Alternative Hpo/Mst-like Kinases in the Hippo Kinase Cascade. *Developmental Cell*, 34(6), pp.642–655. Available at: http://www.ncbi.nlm.nih.gov/pubmed/26364751 [Accessed January 15, 2018].

Zhu, H. et al., 2007. Cardiac autophagy is a maladaptive response to hemodynamic stress. *The Journal of clinical investigation*, 117(7), pp.1782–93. Available at: http://www.pubmedcentral.nih.gov/articlerender.fcgi?artid=1890995&tool=pmcentrez&rendertype=abstract [Accessed September 6, 2015].

Zimmermann, W.-H. et al., 2002. Tissue engineering of a differentiated cardiac muscle construct. *Circulation research*, 90(2), pp.223–30. Available at: http://www.ncbi.nlm.nih.gov/pubmed/11834716 [Accessed September 9, 2017].

Zimmermann, W.H. et al., 2000. Three-dimensional engineered heart tissue from neonatal rat cardiac myocytes. *Biotechnology and bioengineering*, 68(1), pp.106–14. Available at: http://www.ncbi.nlm.nih.gov/pubmed/10699878 [Accessed September 9, 2017].

Zohn, I.E. et al., 2006. p38 and a p38-Interacting Protein Are Critical for Downregulation of E-Cadherin during Mouse Gastrulation. *Cell*, 125(5), pp.957–969. Available at: http://www.ncbi.nlm.nih.gov/pubmed/16751104 [Accessed January 15, 2018].

Zorov, D.B., Juhaszova, M. & Sollott, S.J., 2006. Mitochondrial ROS-induced ROS release: An update and review. *Biochimica et Biophysica Acta (BBA) - Bioenergetics*, 1757(5–6), pp.509–517. Available at: http://www.ncbi.nlm.nih.gov/pubmed/16829228 [Accessed November 1, 2017].

9. Supplement

Knockdown strategies as a tool to explore the role of MAP4K4 in cell death and contractility in hEHT.

Our group previously used shRNAmir-based technology to knockdown expression of MAP4K4 in iCell hiPSC-CM in 2-dimensional cultures in order to study the role of MAP4K4 in human cardiac muscle cell death. MAP4K4 was knocked down followed by the induction of cell death by administering 250 μM H_2O_2. A 2-fold reduction of cardiomyocyte death was observed compared to vehicle control, measured by loss of membrane integrity (DRAQ7 uptake). This suggests that MAP4K4 plays a pro-apoptotic role in human cardiomyocytes upon oxidative stress, and that inhibiting its activity therefore, would be cardioprotective in the human heart (Imperial Innovations Limited, UP Patent Office Application GB1716867.5, MAP4K4 inhibitors, 13 October 2017, Fiedler et. al, in revision).

In previous Chapters we have used inhibitors of MAP4K4 which have shown protection in cell death assays, consistent with this hypothesis. However, by comparison to the proof-of-principle study by gene silencing, these employed different cell sources and functional assays, as well as 3D systems. Therefore, a genetic loss-of-function study in hEHT would be of interest. Using knockdown and inhibitors of MAP4K4 combined to probe off-target effects could be a way to obtain more robust data on whether the effects of MAP4K4 are specific. We therefore aimed to further expand previous findings using knockdown approaches, using genetic knockdown strategies in hEHT. DMX-5804 (DMX-5804), was also assessed alongside MAP4K4 knockdown, as a potential way to screen for potential compound off-target effects.

EHT were generated in the absence of fibroblasts to permit assessment of cardiomyocyte cell death (adenylate kinase release) specifically. In addition, the Eschenhagen lab has shown that contraction amplitude and kinetics were more stable over time and less variable

in hEHT that was not fibroblast-enriched (Mannhardt et al. 2017). It might be expected that 3D tissue would be more difficult to manipulate genetically but, importantly, shRNA mediated inhibition of beta-2-microglobulin expression has been used in murine EHT (Karabekian et al. 2015) and overexpression of FHL2 in neonatal rat cardiomyocytes derived EHT has been achieved (Friedrich et al. 2014). Here we attempted genetic knockdown in human-derived EHT.

9.1 Optimisation of Lentiviral trandsduction in 293 FT HEKS

To validate transduction efficacy of shRNA mediated knockdown on MAP4K4 RNA expression after virus production, 293 FT HEK cells were transduced in culture for 48 hr with lentivirus containing shRNA constructs. Undiluted virus was added over a dilution series from 1:20 to 1:12,500. For the knockdown of MAP4K4, we used shERWOOD-UltramiR short hairpin RNA (shRNA) in lentiviral ZIP-hEF1-alpha vectors that co-express the fluorescent reporter ZsGreen, to aid the monitoring of transfection and transduction efficacy. These constructs feature a new generation design with an optimised microRNA scaffold 'UltramiR' for optimal primary microRNA processing shown to achieve more potent and consistent knockdown than existing shRNA reagents (Auyeung et al. 2013).

3 shRNAs against MAP4K4 (3415338, 3415336, 3415333; product code TLHSU1400-9448) were tested at concentrations ranging from 1:20 to 1:12500, with all concentrations showing detectable ZsGreen expression. However, neither quantification nor comparison with a non-targeting control (NTC) construct was possible due to considerable cell detachment. Based on qualitative observations, efficient transduction efficacy is achievable up to 1:12,500 dilution using these constructs (Fig. **9.1A**), therefore proposing the shRNA constructs as workable candidates for transduction optimisation in the costly hiPSC-CMs.

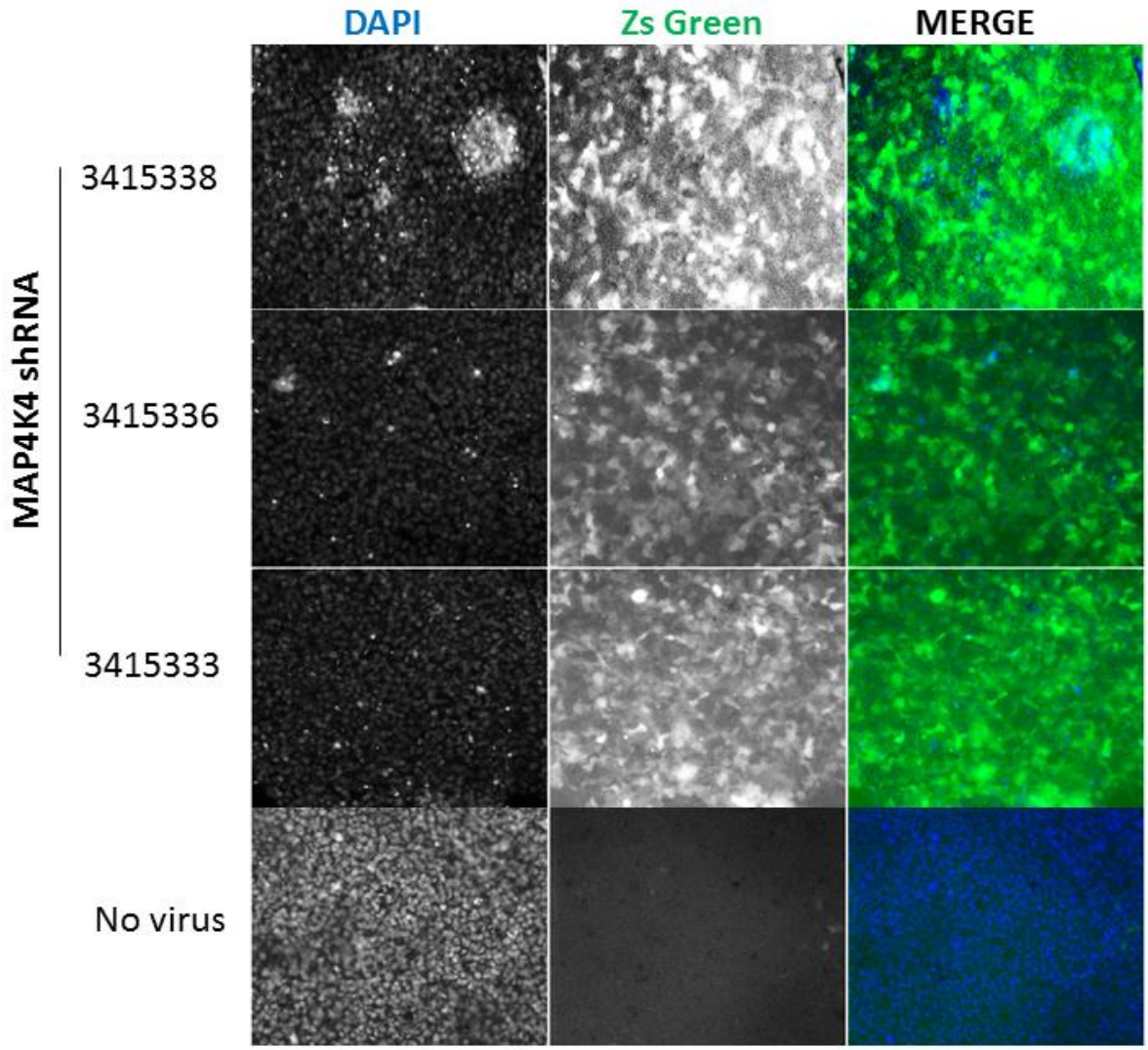


Figure 9.1 MAP4K4 shRNA transduction in 293 FT HEK. 293 FT HEKS were transduced with shRNA in culture for 48 hours. 3 shRNA against MAP4K4 (Lentivirus 3415338, 3415336, 3415333) were tested. A) A representative field, from wells of transduced 293 FT HEK, 1:100 dilution is shown for each condition. Each field shows ZsGreen and DAPI (nuclear stain). Images were captured using Cellomics, 20X magnification. 2 biological replicates (3 replicates per experiment).

9.2 Optimisation of Lentiviral transduction in hiPSC-CMs

To validate transduction efficacy of shERWOOD-UltramiR short hairpin RNA (shRNA) on MAP4K4 in hiPSC-CMs in culture after virus production, hiPSC-CMs were transduced for 48 hr. Virus was added over a 5-fold dilution series from 1:20 to 1:12500. 3 shRNA against

MAP4K4 (3415338, 3415336, 3415333) and a non-targeting control (NTC) construct which targets GFP were tested at concentrations ranging from 1:20 to 1:12500. For all constructs, over 80% of cells were ZsGreen-positive at concentrations 1:20 and 1:100, and over 70% of cells were ZsGreen-positive at concentrations 1:500 and 1:2500. However, for the lowest concentration (1:12500), the percentage of ZsGreen positive cells was more variable, ranging from 70 to 40% (Fig. **9.2A, B**). This suggests consistent and sufficiently high transduction efficacy can be achieved from 1:20 and 1:100 dilution in the human cardiomyocytes. One construct was taken forward for testing in EHT systems due to the high cost involved. The most consistently performing construct was taken forward – 3415336 (Fig. **9.2A, B**).

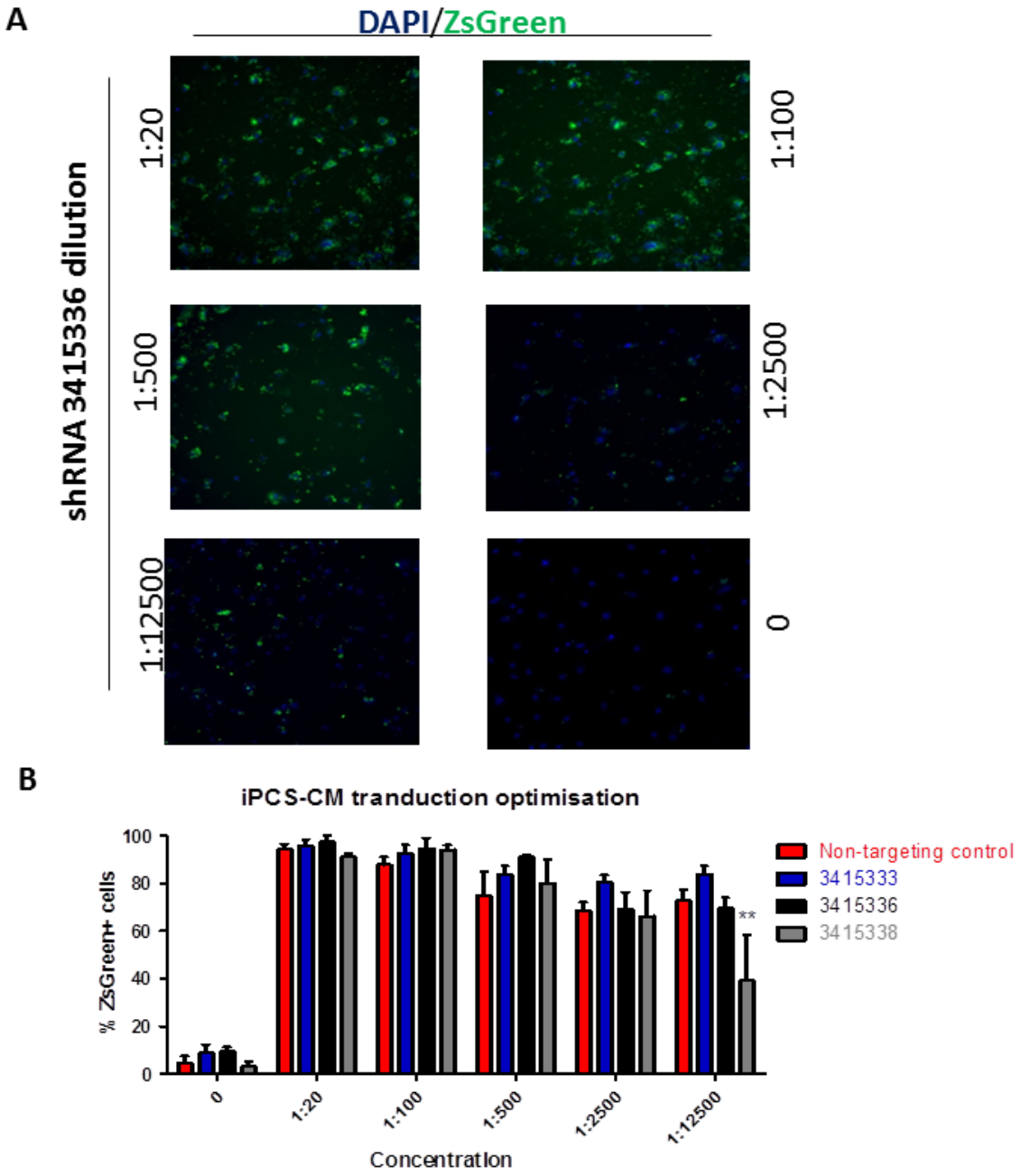


Figure 9.2 MAP4K4 shRNA transduction in hiPSC-CMs. hiPSC-CMs were transduced in culture for 48 hours over a 5-fold dilution series. 3 shRNA against MAP4K4 (3415338, 3415336, 3415333) and a non-targeting control (NTC) construct. A) Representative fieldsfrom wells of transduced hiPSC-CMs, 1:100 dilution. B) Quantification of ZsGreen positive cells in MAP4K4 transduced hiPSC-CMs. Images were captured using Widefield Zeiss AxioObserver, 20X magnification. 3 biological replicates (3 replicates per experiment). Two-way ANOVA; **P < 0.01 for non-targeting control vs 3415338.

9.3 Optimisation of Lentiviral transduction in hEHT

To validate transduction efficacy of the shERWOOD-UltramiR short hairpin RNA (shRNA) on MAP4K4 in EHT, fibrin-based human engineered heart tissue was generated in 24-well format between flexible silicone posts under auxotonic stretching conditions as previously described (Hansen et al, 2010). CorV.4U EHT was transduced for 24 hr from 0.12 to $8.3x10^{-3}$ MOI and cultured for 12 days. The chosen shRNA against MAP4K4 (3415336) based on studies in 2-dimensional cultures of these cells, and a non-targeting control (NTC) construct which targets GFP were tested. EHTs were ZsGreen positive after 12 days in culture for the two highest concentrations of 3415336 (MOI 0.12 and 0.024) for NTC (MOI $8.3x10^{-3}$) (Fig. **9.3A**). Quantification was not possible however, due to the high number of nuclei present and their intensity which did not permit accurate object segmentation/definition. Based on qualitative observations, the highest concentration of 3415336 was chosen for further experiments. Assessment of MAP4K4 mRNA expression showed no reduction despite the high efficiency of transduction as assessed by ZsGreen expression (Fig. **9.3B**). Sub-optimal knockdown however, permits combinatorial studies using both reduction in overall expression and inhibition of activity and was thus used as an opportunity to investigate the specificity of the MAP4K4 pharmacological inhibitor DMX-5804.

Whether virus transduction by itself, or sub-optimal knockdown of MAP4K4 had any effect on EHT function was first assessed. Neither virus transduction by itself (NTC control) nor knockdown of MAP4K4 influenced force, BPM, time to relaxation or time to contraction by 14 days following transfection (Fig. **9.4**).

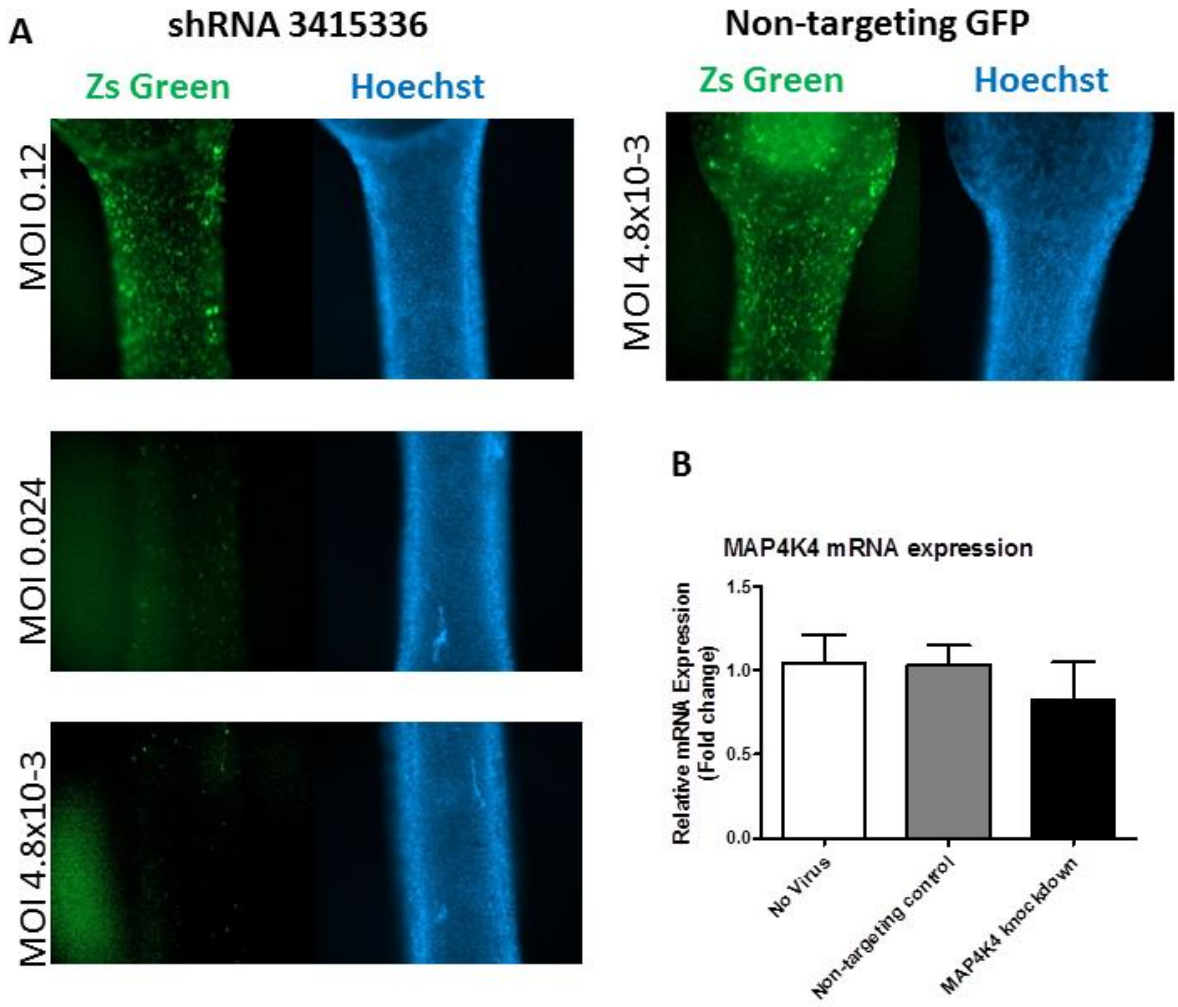


Figure 9.3 MAP4K4 shRNA transduction in CorV.4U-derived hEHT. EHTs transduced for 24 hours in 5-fold dilutions (MOI from 0.12 to $8.3x10^{-3}$) and kept in culture for 14 days. One shRNA against MAP4K4 (3415336) and a non-targeting control (NTC) construct which targets GFP were tested. A) Representative images of transduced hEHTs. Images were captured using Widefield Zeiss AxioObserver, 20X magnification. 3 biological replicates (3 replicates per experiment). B) Quantification of relative mRNA Expression in MAP4K4 transduced hEHT. 2 independent biological replicates (3 replicates per experiment). NSD by repeated measures ANOVA.

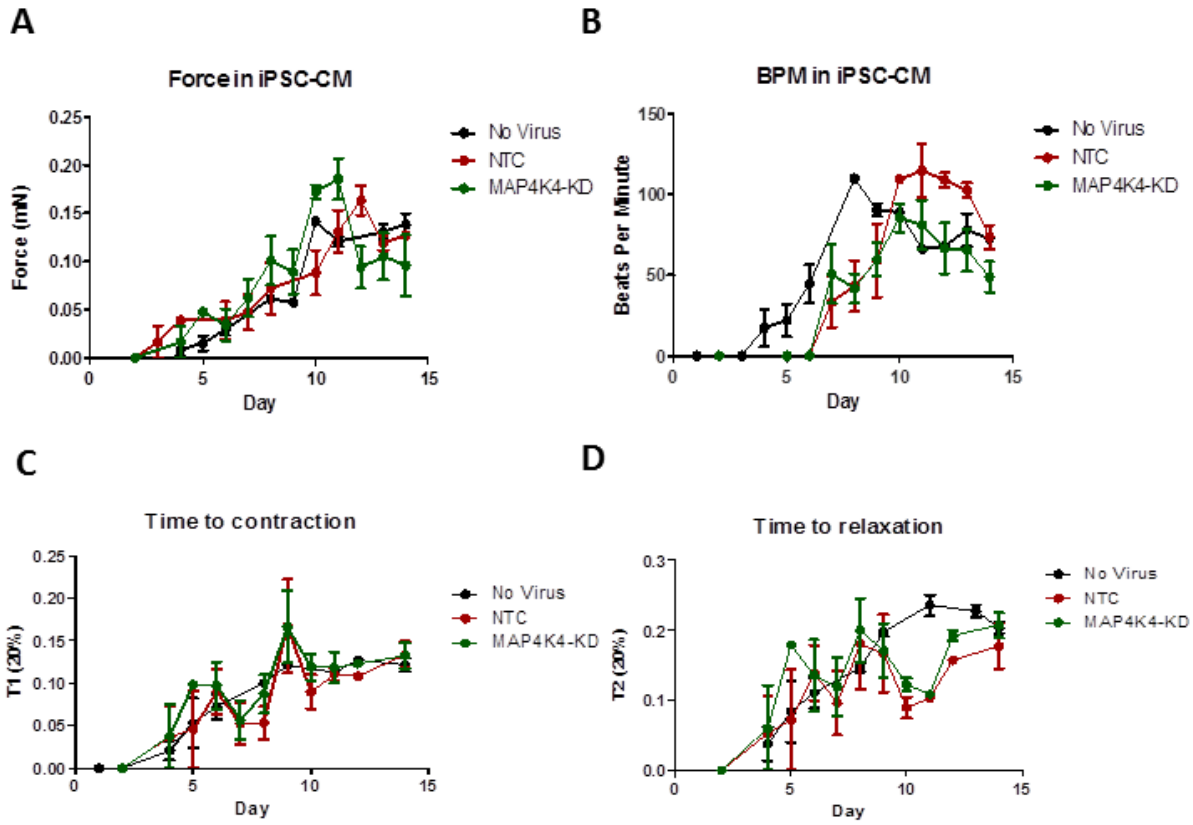


Figure 9.4 Contractile profile of CorV.4U-derived hEHT after lentiviral transfection. 3415336 and non-targeting control (NTC) (24 hr transfection). Contractility analysis was performed using video optical recording to measure force and other contractile parameters in real-time over 14 days. **A)** Force generation (mN). **B)** BPM. **C)** Time to contraction (T1(20%)). **D)** Time to relaxation (T2(20%)). Two-way ANOVA, NSD, N=4-8.

9.4 MAP4K4 knockdown followed by menadione treatment – cell death and contractile response

To evaluate the effect of MAP4K4 knockdown on oxidative stress, MAP4K4 and NTC transduced hEHT were treated with menadione after 12 days in culture following transduction. Menadione induces loss of membrane integrity and decreases force of contraction and BPM in a dose dependent manner (Chapter 6). As expected, menadione compared to vehicle control (using previously optimised conditions, Chapter 6) induced loss of membrane integrity at 24 hr, 48 and 72 hr by 79-, 46- and 29-fold respectively (Fig. **9.5A**).

MAP4K4 knockdown rescued menadione-induced loss of plasma membrane integrity to around 20% of NTC menadione-treated control at 24 hr (Fig. **9.5A**). At 48 hr, there was a 77% reduction of menadione-induced loss of plasma membrane integrity compared to menadione only control (Fig. **9.5A**). There was no protection observed at 72 hr which may reflect that AK was already maximal since levels were low in all groups (Fig. **9.5A**).

In terms of the contractile assessment, MAP4K4 knockdown did not preserve force impairment induced by menadione (Fig. **9.6A**). Beating rate (BPM) showed no sustained effect (Fig. **9.6B**), with no changes observed on time to contraction and relaxation (Fig. **9.7A, B**). However, the variation between EHTs was larger for functional studies than for AK release, limiting our ability to resolve consistent differences.

In summary, MAP4K4 knockdown protects from menadione–induced cell death as measured by loss of cell membrane integrity (AK activity), with at best minor effects on contractile properties.

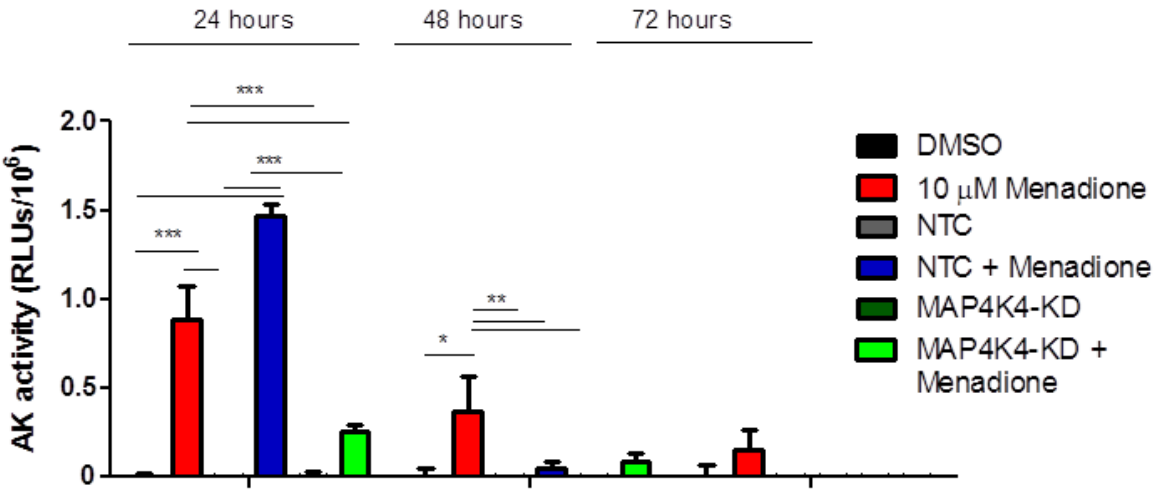


Figure 9.5 Plasma membrane integrity assessment of MAP4K4 shRNA-treated CorV.4U-derived hEHT subjected to menadione. shRNA against MAP4K4 (3415336) and a non-targeting control (NTC) for 24 hours transfection. A**)** The effect of MAP4K4 shRNA in menadione-induced cell death at 24, 48 and 72 hours as measured by loss of cell membrane integrity (AK activity). Two-way ANOVA; N=4, *P < 0.05, **P < 0.01, ***P < 0.001

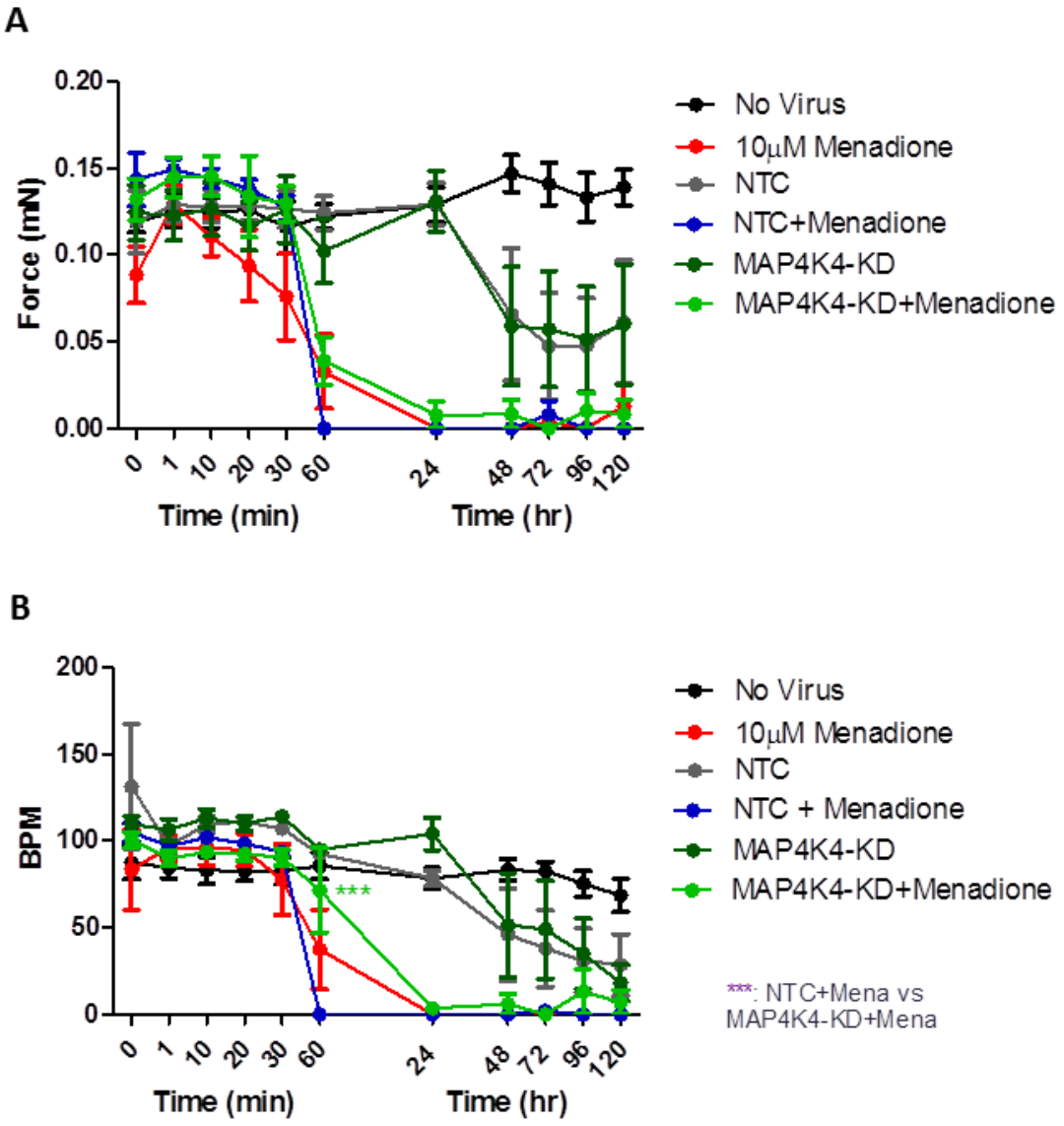


Figure 9.6 Contractility assessment of MAP4K4 shRNA-treated CorV.4U-derived hEHT subjected to menadione. shRNA against MAP4K4 (3415336) and non-targeting control (NTC) construct. **A)** Force generation (mN) in CorV.4U derived hEHT **B)** BPM in CorV.4U-derived hEHT. Two-way ANOVA, N=4, ***P < 0.001

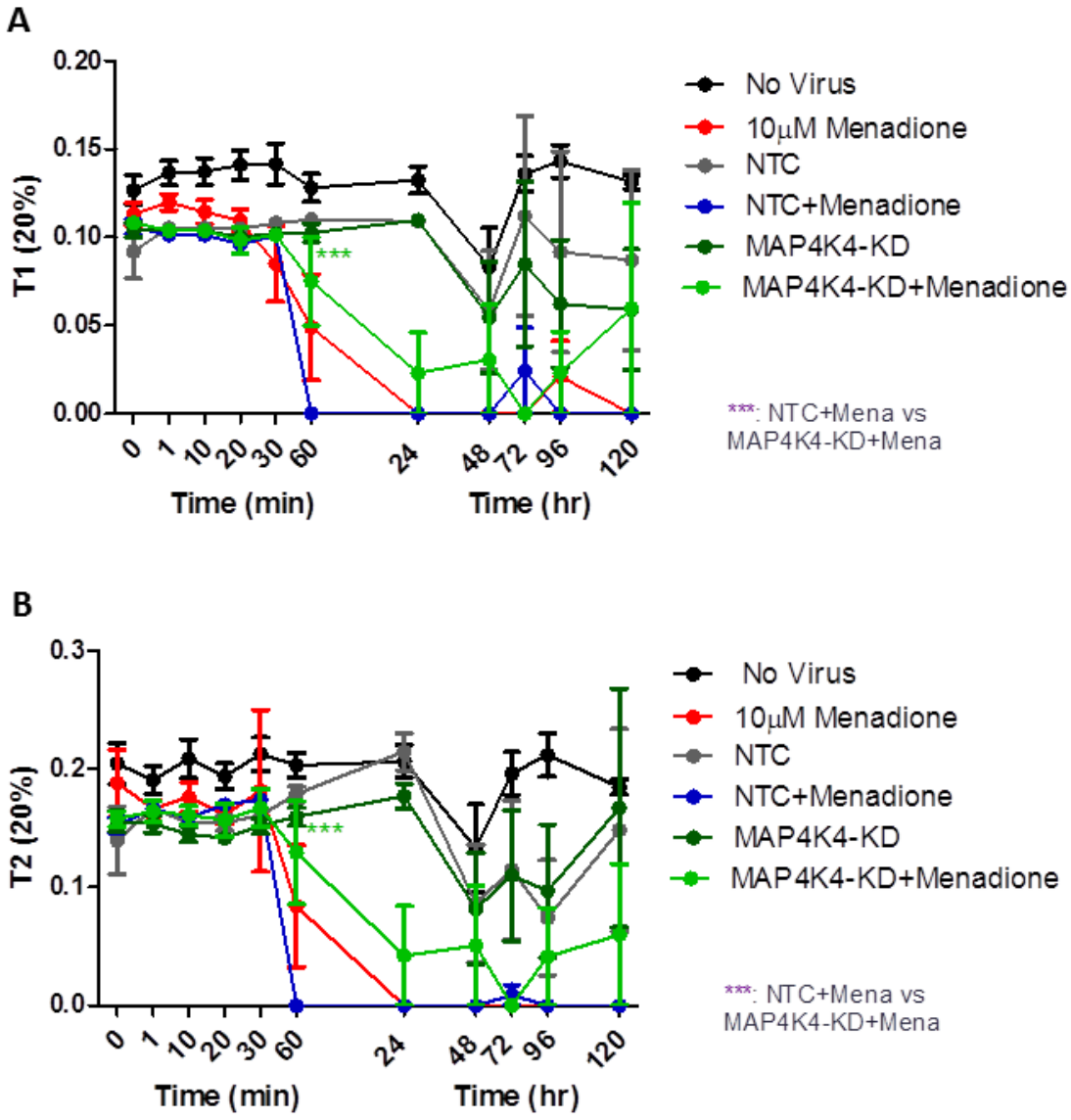


Figure 9.7 Assessment of systolic and diastolic function in MAP4K4 shRNA-treated CorV.4U-derived hEHT subjected to menadione. shRNA against MAP4K4 (3415336) and non-targeting control (NTC) construct. **A)** Time to contraction (T1(20%). **B)** Time to relaxation (T2(20%)). Two-way ANOVA, N=4, ***P < 0.001

9.5 MAP4K4 knockdown followed by DMX-5804 and menadione treatment – cell death and contractile response

Although we have previously seen preservation of force due to MAP4K4 pharmacological inhibition (ATP competing compound at the kinase active site), the response to menadione in terms of force was completely unaffected by MAP4K4 knockdown. However, knockdown was protective to some extent in other contexts, most notably cell death in the hEHT. Our system therefore presents a tool for addressing whether the positive effects seen by pharmacological inhibition previously is due to MAP4K4 inhibition specifically or off-target inhibition of a related kinase (there are 5 kinases known to also be targeted). DMX-5804 was added to MAP4K4 shRNA transduced hEHT and compared to NTC transduced hEHT treated with DMX-5804.

At 24 hr, both DMX-5804 and MAP4K4 knockdown individually reduced the release of AK elicited by menadione (Fig **9.8**). The combination of MAP4K4 knockdown and DMX-5804 in hEHT showed a further reduction in AK after menadione treatment, significant compared to DMX-5804 but not to MAP4K4 knockdown only (Fig. **9.8D**).

In terms of impaired contractile assessment induced by menadione, pharmacological inhibition and MAPK4 shRNA combined did not cause statistically significant changes to either force or beating rate compared to either alone (Fig. **9.9-9.10**).

Therefore, loss of MAP4K4 had larger effects than inhibition of MAP4K4 activity, under the conditions tested, consistent with a potential requirement for kinase-independent functions of the protein (Fiedler et. al., in revision). This preliminary data proposes this new method of transfecting hEHT as a tool for studying in-cell selectivity and specificity when using standard techniques may have been unsuccessful or not possible.

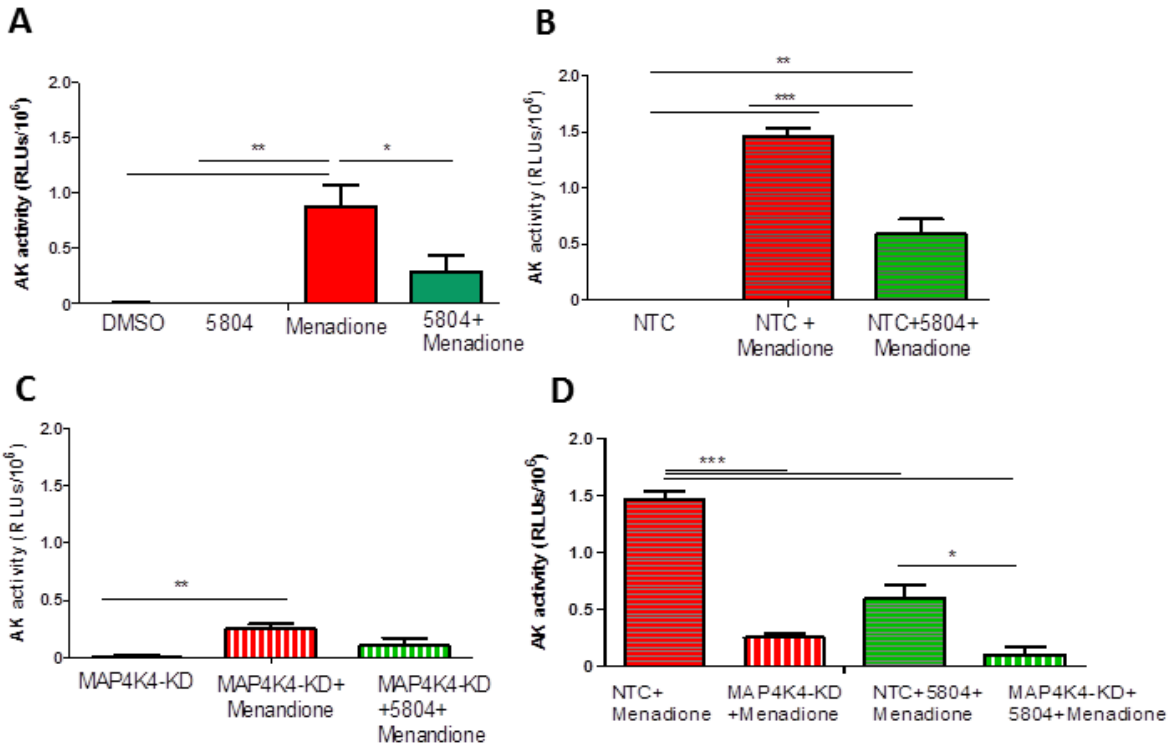


Figure 9.8 Plasma membrane integrity assessment of MAP4K4 shRNA-treated CorV.4U-derived hEHT subjected to 10µM menadione in conjunction with 10µM DMX-5804. A) Untreated cells; **B)** Non-targeting control; **C)** MAP4K4-knockdown; **D)** Direct comparison of MAP4K4-knockdown and DMX-5804 (5804) after Menadione. Two-way ANOVA; N=4-5 for all group apart from N=2 for MAP4K4 + 5804+Menadione and NTC + 5804+Menadione groups, *P < 0.05, **P < 0.01, ***P < 0.001

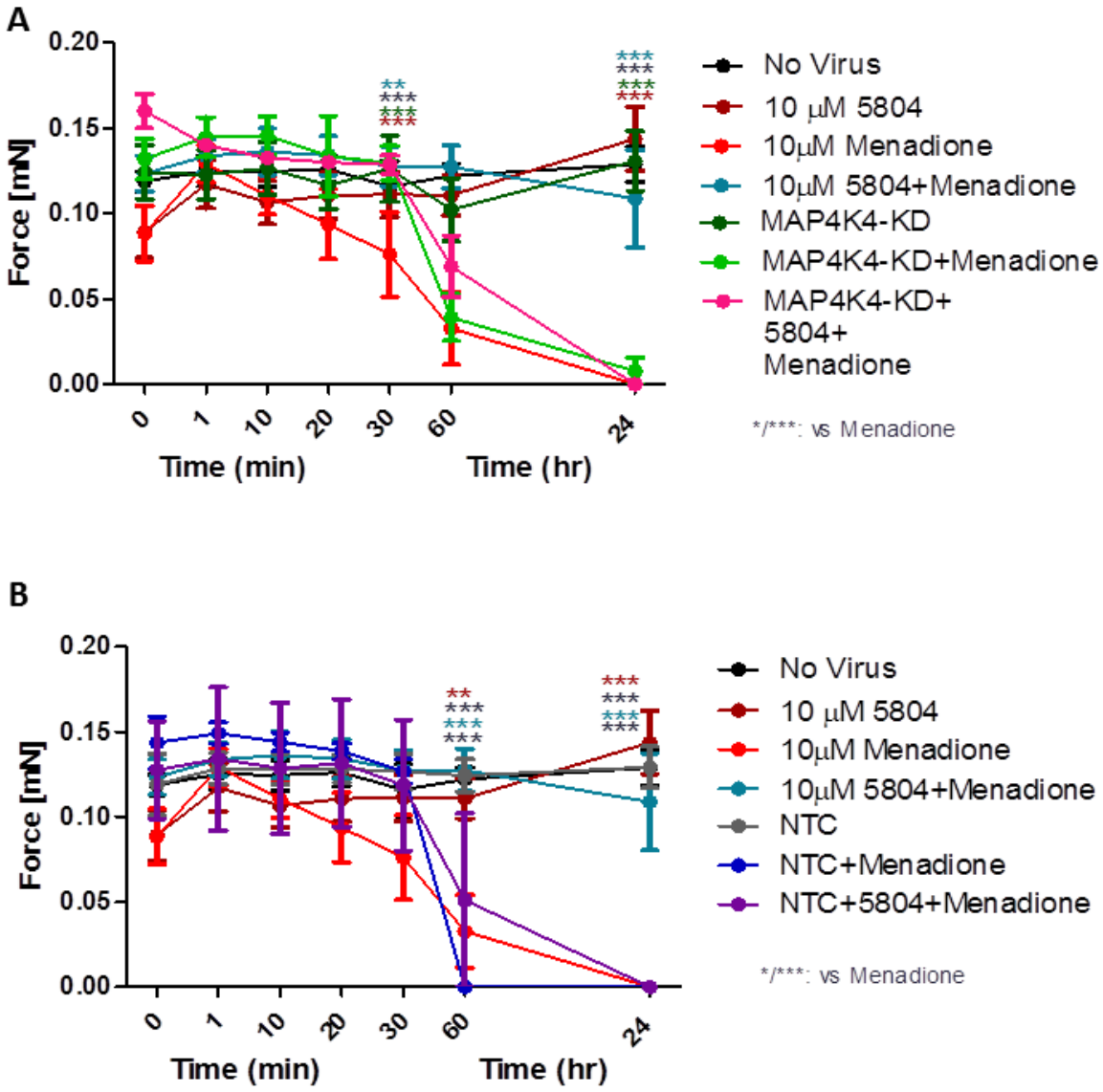


Figure 9.9 Preliminary assessment of force in MAP4K4 shRNA-treated CorV.4U-derived hEHT subjected to 10μM menadione in conjunction with 10μM DMX-5804. A) Force generation (mN) in MAP4K4 shRNA transduced CorV.4U-derived hEHT treated with 5804 and menadione. **B)** Force generation (mN) in non-targeting control (NTC) shRNA-transduced CorV.4U-derived hEHT treated with 5804 and Menadione. Two-way ANOVA; N=4-5 for all group apart from N=2 for MAP4K4 + 5804 + Menadione and NTC + 5804 + Menadione groups, *P < 0.05, **P < 0.01, ***P < 0.001

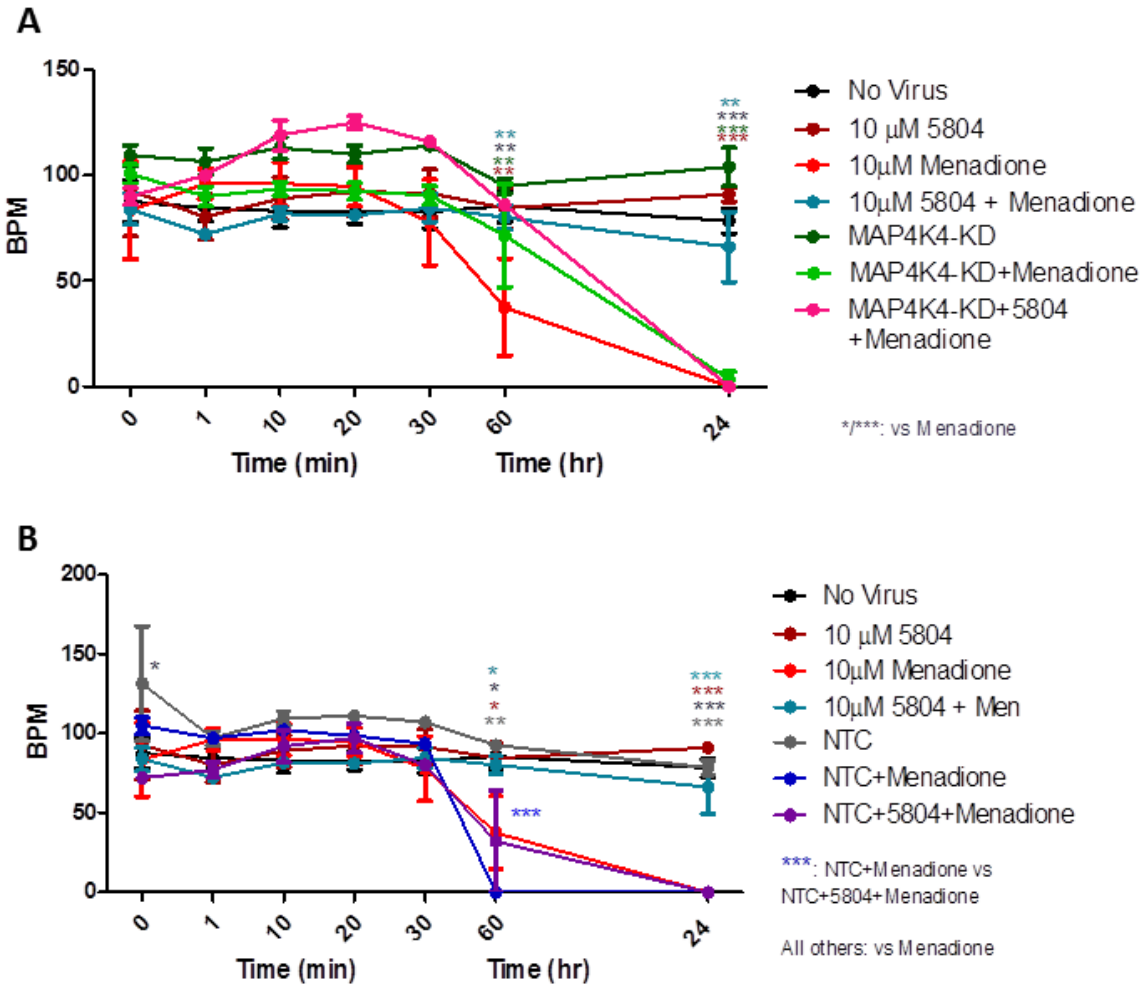


Figure 9.10 Preliminary assessment of BPM in MAP4K4 shRNA-treated CorV.4U-derived hEHT subjected to 10µM menadione in conjunction with 10µM DMX-5804. A) BPM in MAP4K4 shRNA transduced CorV.4U-derived hEHT treated with 5804 and menadione. **B)** BPM in non-targeting control (NTC) shRNA-transduced CorV.4U-derived hEHT treated with 5804 and Menadione. Two-way ANOVA; N=4-5 for all group apart from N=2 for MAP4K4 + 5804 + Menadione and NTC + 5804 + Menadione groups, *P < 0.05, **P < 0.01, ***P < 0.001

9.6 Synopsis of main findings

Here we expanded on previous findings shown in Chapter 6, where pharmacological inhibition of MAP4K4 was found to be protective against deleterious effects of ROS induction in human engineered heart tissue. We tested whether inhibition of MAP4K4 activity by knockdown would similarly be protective. In addition, a combination of pharmacological and genetic inhibition was explored to test whether protection by either alone could be enhanced by using alternative modes of inhibition. Further, this approach can be used to assess whether the protection previously seen from compounds is likely to be due to MAP4K4 inhibition or off-target effects.

The shERWOOD-UltramiR short hairpin RNA (shRNA) displayed efficient transduction in hiPSC-CMs in 3D culture. 3 shRNA against MAP4K4 and a non-targeting control (NTC) construct targeting GFP were tested. Over 80% of cells were ZsGreen positive for the higher concentrations and over 70% of cells were ZsGreen positive for the intermediate concentrations. This confirms that hiPSC-CMs are readily modifiable by the vector system used. This suggests high transfection and transduction efficacy, and as such, our next step was to use these shRNA constructs for transduction in hEHT, with just one construct deployed due to the costly nature of these studies. EHTs were ZsGreen positive after 12 days in culture for the two highest shRNA concentrations tested and for NTC.

Neither lentiviral shRNA transduction by itself nor MAP4K4 knockdown affects the contractile properties of hEHT. MAP4K4 knockdown protects from menadione–induced cell death at 24 and 48 hr as measured by loss of cell membrane integrity (AK activity). However, the response to menadione in terms of force was unaffected by MAP4K4 knockdown. MAP4K4 knockdown did not protect from menadione-induced force impairment; however, beating rate, time to contraction and relaxation at 60 min were rescued.

Addition of DMX-5804 to MAP4K4 knockdown enhances the protective effects of either alone in terms of cell death and initially preserves beating rate. In the context of cell death and contractility measurements and the effects of menadione, this combination was not additive compared to knockdown alone, but was able to enhance the effects of pharmacological inhibition alone.

9.7 Discussion

Lentiviral shRNA was selected rather than siRNA for stable, long-term knockdown, since hEHTs require 12 days in culture to reach maturity, as defined by force during spontaneous contraction. The shERWOOD-UltramiR short hairpin RNA possesses an optimised microRNA scaffold 'UltramiR' for optimal primary microRNA processing (avoids alterations in conserved regions of the flanking sequences thought to reduce knockdown efficiency due to disruption to processing) shown to achieve more potent and consistent knockdown than existing shRNA reagents (Auyeung et al. 2013). The shRNA in lentiviral ZIP-hEF1-alpha vectors that co-express the fluorescent reporter ZsGreen were used. Importantly, the promoter present here, (hEF1-alpha) is not affected by silencing that can arise from embryonic components in immature cells such as the case when using others such as CMV (Xia et al. 2007).

Despite high efficiency of transduction when assessed by reporter expression, no significant levels of knockdown at the mRNA level was achieved. However, the results show this is sufficient to cause changes under the conditions tested. This suggests that protein expression is sufficiently lowered to permit further studies under these conditions. In addition the sub-optimal reduction in protein expression was permissive for exploring the specificity of pharmacological approaches. Combined effects using both approaches to impair MAP4K4

activity (directly, and through loss of protein itself) could therefore be assessed within this range, whereby an increase or decrease would be detectable.

How this translated to knockdown at the protein level was not tested however, and levels may be different to those at the level of transcription. Nonetheless, the results show that this amount of knockdown at the RNA level is sufficient to at least partially protect against deleterious effects caused by ROS production and it is possible that further enhancing knockdown might confer further protection. In future, protein levels should be confirmed by Western blotting or immunofluorescence. Exploration of this however, is currently limited by the quality of available antibodies. Kinase assays on MAP4K4 extracted from cell have not easily reported on the level of activity of the enzyme (Dorte Faust, personal communication), possibly due to the dilution of the inhibitor on cell breakage after lysis and/or the unreliability of the commercially available antibodies against MAP4K4. In future, a reporter of MAP4K4 activity in cells will be crucial, especially in order to confirm the findings hereby presented. A good option could be the production of a phospho-specific antibody that detects the phosphorylated active state of the enzyme; either a polyclonal or monoclonal antibody to a MAP4K4 phosphorylation site that reports on its activity.

It was found that neither shRNA transduction nor MAP4K4 knockdown by itself affects the contractile properties of hEHT. This was an unexpected result since MAP4K4 has been shown to localise to CX43 positive gap junctions and is therefore likely to have an effect on contractility (Lorna Fiedler, personal communication). However, this was tested in 2D cultures of rat neonatal cardiomyocytes, rather than in 3D environment where gap junctions would be in a more native state. MAP4K4 possesses two consensus SH3 binding motifs which are involved in cytoskeleton regulation, mediating motility and shape (Yao et al. 1999). In addition, the MAP4K4 homozygous null mouse is embryonically lethal due to defective cell migration (Xue et al. 2001), suggesting that MAP4K4 knockdown might have been expected to have consequences for contractility either at baseline, or in response to exogenous modulating factors. However, this was not the case. This may be explained by the different

levels of knockdown; in the mouse being complete (null) and in our system, incomplete. Further heterozygous null mice (incomplete knockdown) presumably do not exhibit similar motility defects at baseline during development since no discernible phenotype is present. Measurements of basic echocardiography parameters did not show any changes in chamber volume, diameter or function at baseline in heterozygous null mice compared to wildtype littermates (Lorna Fiedler, personal communication). In our study, knockdown is similarly incomplete and does not produce discernible deleterious effects on cytoskeletal dependent features.

MAP4K4 knockdown protected against ROS induced cell death but not impaired force while both were preserved by pharmacological inhibition. This could be an indication of off-target (but still protective) effects of DMX-5804. It could also be related to levels of knockdown, with more complete removal of MAP4K4 activity needed to protect force. The relationship between cell death and observed force reduction in the 3D EHT is not known and may well not be linear. For example 30% loss of cells might or might not eliminate the contractile activity of the whole EHT, depending on whether this was concentrated in one area (and so disrupted the end-to-end connectivity) or diffuse.

Another possibility is that it is the kinase activity of MAP4K4 that contributes to regulation of force (inhibitable by pharmacological compounds), while the physical presence of the protein itself with associated binding partners, might be more relevant for eliciting cell death responses. Inhibition of MAP4K4 at the active site might also affect phosphorylation/autophosphorylation states and the composition of associated complexes thus the inhibitors will affect both force generation and cell death. This system we have designed could have significant utility as a tool for addressing whether the protection seen from the compounds previously is due to MAP4K4 inhibition or due to off-target effects as well as the relative importance of kinase activity compared to the loss of protein.

Taken together, these findings support a pro-apoptotic role of MAP4K4 in cardiac human muscle. MAP4K4 is therefore a potential target for development of pharmacological inhibitors for cardioprotective treatment in the clinic.

9.8 Methods

9.8.1 HEK293T culture

HEK293T cell line (Clontech 632180) was used for transfection and virus production. Lenti-X HEK293T cells were kept in DMEM (Life Technologies 61965-026) supplemented with 10% FBS (growth media) at approximately 80% confluency. 2ml 0.25% Trypsin/EDTA (Life Technologies 25200056s) per 75cm^2 was employed and incubated at 37^{o}C for 2min. Trypsin was inactivated by addition of 8ml growth media and collected by centrifugation at 250g for 5min. Cells were suspended in 10ml fresh growth media, from which the cell suspension was divided into vented T75 (Corning® 430641) or T150 (Corning® 430825) cell culture flasks and, made up to 12ml and 25ml final volume respectively.

9.8.2 Lentiviral vector production, transduction and titration

The 2nd generation packaging system developed by Didier Trono's laboratory at the University of Geneva, Switzerland (Salmon & Trono 2007; Salmon & Trono 2006) was used. Lenti-X 293T cells were transfected with the shRNA lentiviral vector, the packaging vector (psPAX2; Addgene 12260) and the envelope vector (pMD2.G; Addgene 12259) to produce viral particles that were then harvested in the cell culture supernatant (Kutner et al. 2009). The lentiviral particles generated are encapsidated with the envelope of the vesicular stomatitis virus (envelope glycoprotein; VSV-G) (Zavada 1982) which is able to infect a wide

range of cells types independent of the cell surface receptor expression (Akkina et al. 1996; Reiser et al. 1996).

9. 8. 2.1 Bacterial Culture and DNA purification

The ZIP Lentiviral shRNA (TransOMIC technologies, TLHSU1400-9448) for MAP4K4 and non-targeting control (Fig. **9.12**) were purchased as a stock of transformed E.coli cryopreserved in glycerol and stored at -80˚C (Table **9.1**). Individual constructs were amplified by scraping the stocks and placing them in LB Lennox (low salt) broth (EMD Millipore 71751) supplemented with 100µg/mL amplicillin (Sigma-Aldrich A9393) antibiotics. Cultures were grown at 30˚C and continuously shaken at 220rpm for 30 hr. DNA plasmids were purified by collecting bacterial cultures by centrifugation at 4000g for 10 min and using the Plasmid Maxi kit (Qiagen 12163) as per manufacturer's instructions. DNA was quantified using NanoDrop 1000 Spectrophotometer (Thermo Scientific) and used for transfection and virus production.

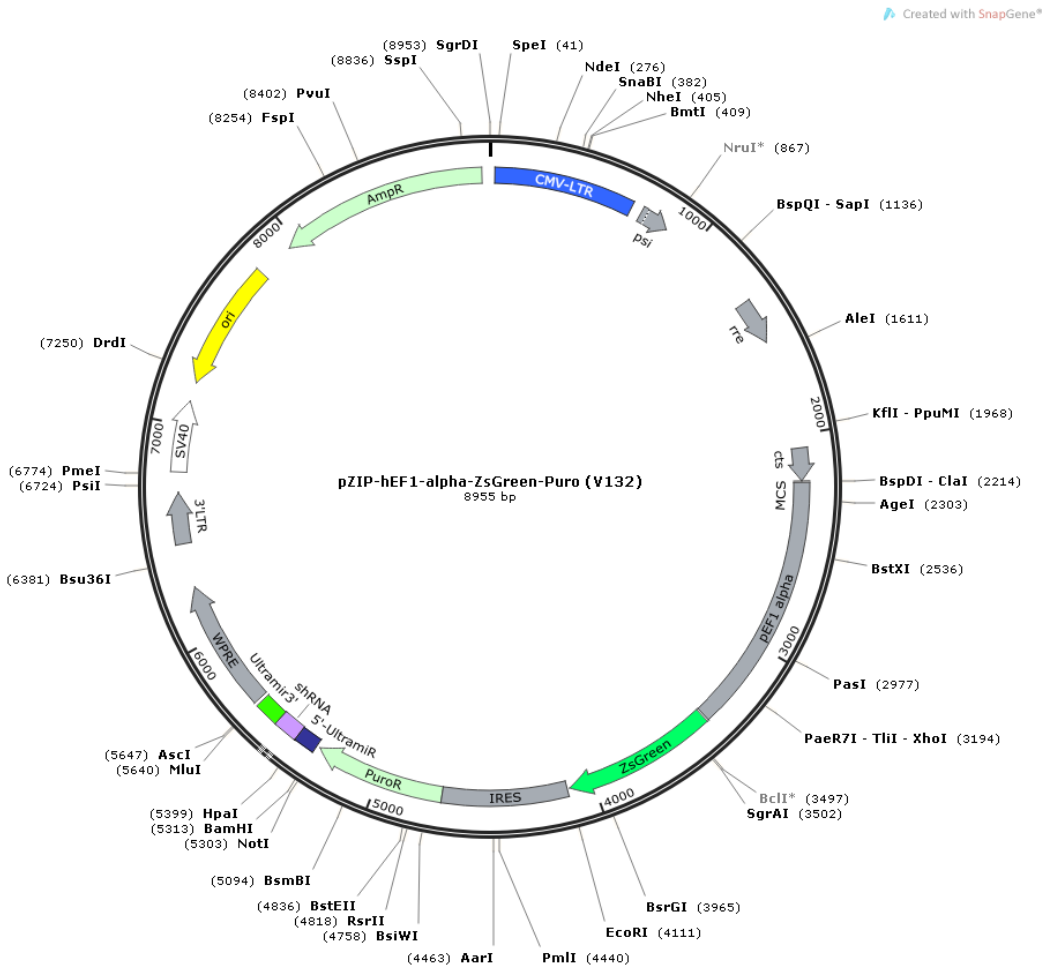


Figure 9.12 Schematic representation of the pZIP lentiviral shRNA vector, its features and elements (TransOMIC technologies manual, TLHSU1400-9448).

Clone id	Gene	Species	Sequence
ULTRA-3415336	MAP4K4	Homo sapiens	TGCTGTTGACAGTGAGCGCGCTTTTGAAACATCCTTTTAATAGTGAAGCCACAGATGTATTAAAAGGATG TTTCAAAAGCTTGCCTACTGCCTCGGA
ULTRA-3415333	MAP4K4	Homo sapiens	TGCTGTTGACAGTGAGCGCACCGAAGACGATTTCAACAAATAGTGAAGCCACAGATGTATTTGTTGAAA TCGTCTTCGGTTTGCCTACTGCCTCGGA
ULTRA-3415338	MAP4K4	Homo sapiens	TGCTGTTGACAGTGAGCGCTGGCACCTATGGACAAGTCTATAGTGAAGCCACAGATGTATAGACTTGTC CATAGGTGCCATTGCCTACTGCCTCGGA
ULTRA-NT#4	EGFP	Homo sapiens	TGCTGTTGACAGTGAGCGAAGGCAGAAGTATGCAAAGCATTAGTGAAGCCACAGATGTAATGCTTTGCA TACTTCTGCCTGTGCCTACTGCCTCGGA

Table 9.1 pZIP shRNA sequences

9.8.2.2 Lentiviral vector production and concentration

The protocol performed is based on Kutner et al. (Kutner et al. 2009). Lenti-X 293T cells were used as packaging cells and plated at 60000 cells/cm^2 in 10 cm^2 cell culture dishes (4 per lentiviral vector). Transfection took place 24 hr after seeding using 6µg of the shRNA lentiviral vector, 4.5 µg psPAX2, 3µg of pMD2.G and transfection reagent FuGENE 6 (Promega, E2691) at a 1:3 ratio (1 µg DNA to 3 µL FuGENE 6) in serum free DMEM. 12 hr post-transfection the medium was replaced with 10ml DMEM per dish. 36 hr post-transfection the viral supernatant was collected, filtered using a 0.45µm polyethersulfone low protein-binding filter (Whatman, 6780-2504) and kept at 4 °C. 10ml DMEM was added for a second viral supernatant collection 48 hr later as above. Supernatant was cooled and centrifuged on a 20% sucrose cushion (see below for details) in an Optima XPN100 ultracentrifuge and SW32.Ti swinging bucket rotor (Beckman Coulter) at 82,700x g for 2 hr at 4 °C. Supernatant was then discarded and the pellet containing the lentiviral particles was carefully dried for 3 min at room temperature (RT) using pipettes to aim the process. The pellet was then re-suspended for 2 hr in 200 µL PBS and vortexed every 20 min. The preparation was aliquoted and stored at -80°C.

20% Sucrose cushion: 20g sucrose (BD Biosciences, 354236), 100 mM NaCl (Thermo Fisher, A/0400/PB17), 20 mM HEPES (Life Technologies, 15630106), 1 mM EDTA (Sigma, 03690) and distilled water (Life Technologies, 15230162).

9.8.2.3 Lentiviral vector titration

The titre is the number of transducing units (TU) per ml and this was determined for each lentiviral vector preparation using the florescent proteins encoded by them. The shRNA in lentiviral ZIP-hEF1-alpha vectors used co-express the fluorescent reporter ZsGreen. To determine the titre of each lentiviral vector preparation directly in the target cells, hiPSC-CMs

were utilised as well as HEK293T cells as a positive control (seeded 24 hr prior to transduction). The lentiviral preparations were added at 5-fold dilutions ranging from 1:20 to 1:12500 to the cells in serum free media containing 8µg/ml polybrene (Merck Millipore, TR-1003-G) and after 24 hr, media was changed to complete media. Cell were transduced for 48 hr and images were captured using Widefield Zeiss AxioObserver, 20X magnification or using Cellomics ArrayScan VTI high content screening instrument and ArrayScan image acquisition software (Thermo Fisher, UK).

The biological titre (TU/ml or transducing units) of each lentiviral vector preparation was calculated as:

$$\frac{TU}{ml} = \frac{(F * N * D * 1000)}{V}$$

Where:

F = % fluorescent cells

N = number of cells at time of transduction

D = Fold dilution of lentiviral vector sample used for transduction

V = Volume of diluted lentiviral vector sample added into each well for transduction (ml)

9.8.2.4 Viral transduction of hEHTs

For the transduction of hEHT, the amount of lentiviral vector sample which could be added to each EHT during the generation step was limited by the fact that the mixture which then sets in each mould amounts to 100 µl. This is a protocol that has proven to be very sensitive and therefore changing the volumes and proportions of this mixture could affect the properties of the EHT or even cause for the constructs not to set or attach to the posts. It was therefore

decided that exceeding 30% of this final 100 µl volume and hence diluting the mixture further would not be wise and thus the highest MOI (virus particles per cell) tested was MOI 0.12 which amounted to 30 µl of lentiviral vector preparation. Using that as the highest MOI, two further 1 in 5 dilutions were also tested (MOI 0.024 and $8.3x10^{-3}$), although the highest concentration achieved the most efficient transduction and was used for experiments. Transduction was carried out by adding the lentiviral vector sample containing 8µg/ml polybrene (Merck Millipore TR-1003-G) to the EHT mixture during master mix preparation (see hEHT generation section). EHTs were cultured and treated in the same way as untransduced EHTs.

9.8.3 RNA Extraction (EHTs)

RNA was extracted from each EHT by placing each in 350µl TRIzol (ThermoFisher A33251). EHTs were then homogenised by hand using a sterile pestle until cells were mostly in solution. RNA was then extracted from EHT samples via the Qiagen RNA Easy protocol as per manufacturer's instructions. RNA quality and quantity were assessed using a NanoDrop 1000 spectrometer (ThermoFisher ND-1000).

9.8.4 Gene expression analysis

RNA concentrations were normalised and cDNA was made by reverse transcription (Applied Biosystems 1308188) as per the manufacturer's protocol. In brief, RNA was converted to cDNA (High Capacity cDNA transcription kit (ABI)) using 100 ng of RNA in 20µL final volume. qRT-PCR was performed as per the manufacturer's protocol with TaqMan Gene Expression Assays (see Table **9.2**), 2X TaqMan Gene Expression Master Mix (Life Technologies) and 10 ng cDNA, final volume 20 µL. Applied Biosystems (ABI) 7500 Real-Time PCR System was used at 50˚C for 2 min, 95 ˚C for 10 min, 40 cycles at 25˚C for 15

sec and 60˚C for 1 min. All samples were run with and normalised to UBC. Delta cycle threshold was calculated as cycle threshold of the gene of interest minus UBC cycle threshold. Delta delta cycle threshold was calculated as delta cycle threshold minus control delta cycle threshold. Fold change was calculated by averaging minus delta delta cycle threshold values squared.

qRT-PCR primers	Provider	Assay ID
human MAP4K4	Thermo Fisher Scientific	Hs00377415_m1
human UBC	Thermo Fisher Scientific	Hs00824723_m1

Table 9.2 qRT-PCR primers